



Universitat de Lleida

## Cell Stress and RNA Splicing in Amyotrophic Lateral Sclerosis: Novel Opportunities for Therapeutic Development

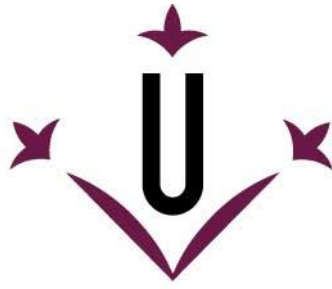
Pascual Torres Cabestany

<http://hdl.handle.net/10803/671440>

**ADVERTIMENT.** L'accés als continguts d'aquesta tesi doctoral i la seva utilització ha de respectar els drets de la persona autora. Pot ser utilitzada per a consulta o estudi personal, així com en activitats o materials d'investigació i docència en els termes establerts a l'art. 32 del Text Refós de la Llei de Propietat Intel·lectual (RDL 1/1996). Per altres utilitzacions es requereix l'autorització prèvia i expressa de la persona autora. En qualsevol cas, en la utilització dels seus continguts caldrà indicar de forma clara el nom i cognoms de la persona autora i el títol de la tesi doctoral. No s'autoritza la seva reproducció o altres formes d'explotació efectuades amb finalitats de lucre ni la seva comunicació pública des d'un lloc aliè al servei TDX. Tampoc s'autoritza la presentació del seu contingut en una finestra o marc aliè a TDX (framing). Aquesta reserva de drets afecta tant als continguts de la tesi com als seus resums i índexs.

**ADVERTENCIA.** El acceso a los contenidos de esta tesis doctoral y su utilización debe respetar los derechos de la persona autora. Puede ser utilizada para consulta o estudio personal, así como en actividades o materiales de investigación y docencia en los términos establecidos en el art. 32 del Texto Refundido de la Ley de Propiedad Intelectual (RDL 1/1996). Para otros usos se requiere la autorización previa y expresa de la persona autora. En cualquier caso, en la utilización de sus contenidos se deberá indicar de forma clara el nombre y apellidos de la persona autora y el título de la tesis doctoral. No se autoriza su reproducción u otras formas de explotación efectuadas con fines lucrativos ni su comunicación pública desde un sitio ajeno al servicio TDR. Tampoco se autoriza la presentación de su contenido en una ventana o marco ajeno a TDR (framing). Esta reserva de derechos afecta tanto al contenido de la tesis como a sus resúmenes e índices.

**WARNING.** Access to the contents of this doctoral thesis and its use must respect the rights of the author. It can be used for reference or private study, as well as research and learning activities or materials in the terms established by the 32nd article of the Spanish Consolidated Copyright Act (RDL 1/1996). Express and previous authorization of the author is required for any other uses. In any case, when using its content, full name of the author and title of the thesis must be clearly indicated. Reproduction or other forms of for profit use or public communication from outside TDX service is not allowed. Presentation of its content in a window or frame external to TDX (framing) is not authorized either. These rights affect both the content of the thesis and its abstracts and indexes.



**Universitat de Lleida**

**TESI DOCTORAL**

**Cell Stress and RNA Splicing in Amyotrophic Lateral  
Sclerosis: Novel Opportunities for Therapeutic  
Development**

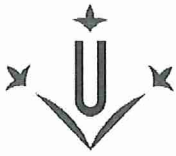
Pascual Torres Cabestany

Memòria presentada per optar al grau de Doctor per la Universitat de Lleida  
Programa de Doctorat en Salut

Director/a  
Dr. Manuel Portero Otín  
Dr. Reinald Pamplona Gras

Tutor/a  
Manuel Portero Otín





Universitat de Lleida  
Departament de Medicina Experimental

Av. Alcalde Rovira Roure, 80  
E-25198 LLEIDA (Catalunya)  
Telf. +34 (9) 73 702442

En **REINALD PAMPLONA GRAS**, Doctor en Medicina i Catedràtic de Fisiologia de la Universitat de Lleida, i en **MANUEL PORTERO OTIN**, Doctor en Medicina i Professor de Fisiologia de la Universitat de Lleida,

CERTIFIQUEN:

Que el treball de recerca titulat: '**Cell Stress and RNA Splicing in Amyotrophic Lateral Sclerosis: Novel Opportunities for Therapeutic Development**' desenvolupat pel Sr Pascual Torres Cabestany, per a optar al grau de Doctor per la Universitat de Lleida, i que ha estat realitzada sota la nostra direcció i supervisió, es troba en condicions de ser defensada davant el tribunal corresponent designat per la Universitat de Lleida.

I signem la present als efectes oportuns a Lleida, 21 d'Octubre de 2020.

Signat: Reinald Pamplona Gras

Manuel Portero Otin

# Abstract

ALS is a multifactorial neurodegenerative disease. As it is currently an incurable disease without a known cause, the efforts in discovering novel targets are well justified. Available evidence indicates that ALS pathophysiology can be partially comprised of interactions between lipid alterations, oxidative stress, TDP-43 mislocalization, and RNA metabolism. In order to explore the impact of TDP-43 mislocalization, we quantified for the first time the cryptic exon splicing derived from TDP-43 dysfunction in human tissue, cell models, and mice. Cryptic exons are candidate biomarkers in ALS, and we quantified them in other pathologies related to TDP-43 disturbances, such as the Alzheimer-LATE type dementia. One of the TDP-43 controlled mRNAs is coding for ATG4B, an essential protein at the build-up of autophagy's membranal machinery. On the other hand, the central nervous system membranes are enriched in polyunsaturated fatty acids (PUFAs), which are very sensitive to oxidative stress. The group's previous publications indicated a decrease in docosahexaenoic acid (DHA) -a PUFA- in ALS donors' spinal cord. DHA is a crucial regulator of inflammation and has been implicated in age-related neurodegenerative diseases. This thesis shows that dietary intervention can effectively increase DHA content of the spinal cord by using a DHA enriched diet, which has a beneficial effect on male survival time. This improvement was associated with decreased inflammatory and DNA damage markers. Because a similar DNA damage and cytokine release profile are seen in senescence-associated secretory profile (SASP) in neuroinflammation, we also examined the potential role of senescence in ALS. We detected increased levels of SASP markers and signs of cell senescence (increased expression of p16-INK and p21) in pre- and symptomatic stages in the hSOD1-G93A ALS spinal cord. However, a senolytic treatment with Navitoclax (a Bcl-2 inhibitor) did not offer any benefit in mice survival nor a decreased level of cell senescence and SASP markers. We also demonstrate that cryptic exon splicing is increased in the hSOD1-G93A ALS model at the end-stage, and it is correlated with senescence marker p16-INK mRNA. Finally, to enhance transference potential, we explored both metabolomic and cryptic exon splicing alterations in peripheral biomarkers. Unfortunately, cryptic exons measured in nervous tissue are not expressed in peripheral blood mononuclear cells. Notwithstanding, platelet metabolome analyses revealed significant changes in case-control and prognostic approaches. Globally, this thesis highlights novel findings related to potential dietary interventions, open the door for new therapeutic agents such as senolytic drugs and propose new metabolomics and transcriptomic biomarkers.

# Resum

L'ELA és una malaltia neurodegenerativa multifactorial. Atès que actualment és una malaltia incurable sense una causa coneguda, els esforços per descobrir noves dianes terapèutiques estan ben justificats. L'evidència disponible indica que la fisiopatologia de l'ELA pot estar composta parcialment d'interaccions entre alteracions de lípids, estrès oxidatiu, deslocalització de TDP-43 i metabolisme de l'ARN. Per explorar l'impacte de la deslocalització de TDP-43, quantifiquem per primera vegada l'*splicing* críptic derivat de la disfunció de TDP-43 en teixit humà, models cel·lulars i ratolins. Els exons críptics són candidats a biomarcadors en l'ELA, i els quantifiquem en altres patologies relacionades amb alteracions de TDP-43, com la demència tipus Alzheimer-LATE. Un dels ARNm controlats per TDP-43 codifica per ATG4B, una proteïna essencial en la formació de la maquinària de membrana de l'autofàgia. D'altra banda, les membranes de el sistema nerviós central estan enriquides en àcids grassos poliinsaturats (PUFA), molt sensibles a l'estrès oxidatiu. Les publicacions anteriors de el grup demostren una disminució en l'àcid docosahexaenoic (DHA) -un PUFA- a la medul·la espinal dels donants d'ELA. El DHA és un regulador crucial de la inflamació i s'ha relacionat amb malalties neurodegeneratives relacionades amb l'edat. Aquesta tesi mostra que la intervenció dietètica pot augmentar eficaçment el contingut de DHA de la medul·la espinal mitjançant l'ús d'una dieta enriquida amb DHA, que té un efecte beneficiós en la supervivència dels ratolins transgènics mascles. Aquesta millora es va associar amb una disminució dels marcadors inflamatoris i de dany de l'ADN. A causa de que s'observa un dany en l'ADN similar i un perfil d'alliberament de citocines en el perfil secretor associat a la senescència (SASP) en la neuroinflamació, també examinem el paper potencial de la senescència en l'ELA. Vam detectar nivells augmentats de marcadors SASP i signes de senescència cel·lular (expressió augmentada de p16-INK i p21) en etapes presintomàtiques i simptomàtiques en la medul·la espinal dels ratolins hSOD1-G93A. No obstant això, el tractament senolític amb Navitoclax (un inhibidor de Bcl-2) no va oferir cap benefici en la supervivència dels ratolins ni una disminució dels nivells d'expressió de gens de senescència cel·lular i marcadors SASP. També vam demostrar que l'*splicing* críptic augmenta en ratolins hSOD1-G93A en l'etapa final i es correlaciona amb el marcador de senescència p16-INK. Finalment, per millorar el potencial de transferència, vam explorar les alteracions de l'*splicing* críptic i canvis metabolòmics com a potencials biomarcadors perifèrics. Desafortunadament, els exons críptics mesurats en teixit nerviós no s'expressen en cèl·lules mononuclears de sang perifèrica. No obstant això, les anàlisis del metaboloma plaquetari van revelar canvis significatius en els enfocaments de casos-controls i de pronòstic. En conclusió, aquesta tesi destaca les noves troballes relacionades amb possibles intervencions dietètiques, obre

la porta a nous agents terapèutics com els senolítics, i proposa nous biomarcadors metabolòmics i transcriptòmics.

# Resumen

La ELA es una enfermedad neurodegenerativa multifactorial. Dado que actualmente es una enfermedad incurable sin una causa conocida, los esfuerzos para descubrir nuevas dianas terapéuticas están bien justificados. La evidencia disponible indica que la fisiopatología de la ELA puede estar compuesta parcialmente de interacciones entre alteraciones de lípidos, estrés oxidativo, deslocalización de TDP-43 y metabolismo del ARN. Para explorar el impacto de la deslocalización de TDP-43, cuantificamos por primera vez el *splicing* críptico derivado de la disfunción de TDP-43 en tejido humano, modelos celulares y ratones. Los exones crípticos son candidatos a biomarcadores en la ELA, y los cuantificamos en otras patologías relacionadas con alteraciones de TDP-43, como la demencia tipo Alzheimer-LATE. Uno de los ARNm controlados por TDP-43 codifica para ATG4B, una proteína esencial en la formación de la maquinaria de membrana de la autofagia. Por otro lado, las membranas del sistema nervioso central están enriquecidas en ácidos grasos poliinsaturados (PUFA), muy sensibles al estrés oxidativo. Las publicaciones anteriores del grupo demuestran una disminución en el ácido docosahexaenoico (DHA) -un PUFA- en la médula espinal de los donantes de ELA. El DHA es un regulador crucial de la inflamación y se ha relacionado con enfermedades neurodegenerativas relacionadas con la edad. Esta tesis muestra que la intervención dietética puede aumentar eficazmente el contenido de DHA de la médula espinal mediante el uso de una dieta enriquecida con DHA, que tiene un efecto beneficioso en la supervivencia de los ratones transgénicos machos. Esta mejora se asoció con una disminución de los marcadores inflamatorios y de daño del ADN. Debido a que se observa un daño en el ADN similar y un perfil de liberación de citocinas en el perfil secretor asociado a la senescencia (SASP) en la neuroinflamación, también examinamos el papel potencial de la senescencia en la ELA. Detectamos niveles aumentados de marcadores SASP y signos de senescencia celular (expresión aumentada de p16-INK y p21) en etapas presintomáticas y sintomáticas en la médula espinal de los ratones hSOD1-G93A. Sin embargo, el tratamiento senolítico con Navitoclax (un inhibidor de Bcl-2) no ofreció ningún beneficio en la supervivencia de los ratones ni una disminución de los niveles de expresión de genes de senescencia celular y marcadores SASP. También demostramos que el *splicing* críptico aumenta en ratones hSOD1-G93A en la etapa final y se correlaciona con el marcador de senescencia p16-INK. Por último, para mejorar el potencial de transferencia, exploramos las alteraciones del *splicing* críptico y cambios metabólicos como potenciales biomarcadores periféricos. Desafortunadamente, los exones crípticos medidos en tejido nervioso no se expresan en células mononucleares de sangre periférica. No obstante, los análisis del metaboloma plaquetario revelaron cambios significativos en los enfoques de casos-contróles y de pronóstico. En conclusión, esta tesis destaca los hallazgos novedosos relacionados con posibles intervenciones dietéticas, abre la puerta a nuevos agentes



terapéuticos como los senolíticos, y propone nuevos biomarcadores metabolómicos y transcriptómicos.

## INDEX

<b>1</b>	<b>INTRODUCTION</b>	<b>15</b>
1.1	Epidemiology and genetics of ALS	16
1.1.1	ALS: a complex disease	16
1.1.2	<i>SOD1</i> mutations	19
1.1.3	<i>C9ORF72</i> hexanucleotide repeat expansion	21
1.1.4	<i>TARDBP</i> mutations	22
1.2	A clinical overview of ALS	25
1.3	Pathogenic mechanisms in ALS	28
1.3.1	Excitotoxicity	28
1.3.2	Protein oxidative damage	29
1.3.3	DNA oxidative damage	32
1.3.4	Protein aggregation:	34
1.3.5	Autophagy dysregulation	38
1.3.6	Nucleocytoplasmic transport impairment	42
1.3.7	Cryptic exon transcriptopathy	45
1.3.8	Neuroinflammation and aging	48
1.4	TDP-43 pathology in AD-LATE	55
1.5	Confidential part	
1.6	ALS biomarkers	62
1.6.1	General concepts	62
1.6.2	Targeted strategies	63
1.6.3	Non-targeted approaches	65
<b>2</b>	<b>HYPOTHESIS</b>	<b>69</b>
<b>3</b>	<b>OBJECTIVES</b>	<b>71</b>
<b>4</b>	<b>MATERIALS AND METHODS</b>	<b>74</b>
<b>5</b>	<b>ARTICLES</b>	<b>86</b>
5.1	Article 1	87
5.2	Article 2	95
5.3	Article 3	114
5.4	Article 4	132
5.5	Article 5	146
5.6	Article 6	167
<b>6</b>	<b>DISCUSSION</b>	<b>191</b>
<b>7</b>	<b>CONCLUSIONS</b>	<b>199</b>
<b>8</b>	<b>REFERENCES</b>	<b>201</b>

**List of Abbreviations**

1H-NMR	Proton Nuclear Magnetic resonance
2'-MOE	2'-O-methoxy-ethyl
2'-Ome	2'-O-Methyl
3-DG	3-deoxyglucosone
8-oxo-dG	8-Oxo-2'-deoxyguanosine
ABCC9	ATP Binding Cassette Subfamily C Member 9
AD	Alzheimer's Disease
AD-NC	Alzheimer's Disease-Neuropathological Change
AGE	Advanced Glycation End-product
ALE	Advanced Lipoxidation End-product
ALS	Amyotrophic Lateral Sclerosis
ALS2	Amyotrophic Lateral Sclerosis 2
ALSFRS	Amyotrophic Lateral Sclerosis Functional Rating Scale
ALSFRS-R	Revised Amyotrophic Lateral Sclerosis Functional Rating Scale
APG5	Autophagy Protein 5
APOE4	Apolipoprotein E4
ARA	Arachidonic Acid
ATG	Autophagy-related
ATM	Ataxia Telangiectasia Mutated
ATP	Adenosine Triphosphate
ATXN2	Ataxin 2
AUC	Area Under the Curve
BCL-xL	B-Cell CLL/Lymphoma xL
BER	Base Excision Repair
BMAA	$\beta$ -Methylamino-l-alanine
BMI	Body Mass Index
Ca	Calcium
CCS	Copper Chaperone for Superoxide
CEL	N $\epsilon$ -carboxyethyl-lysine
CHK1	Checkpoint Kinase 1
CHK2	Checkpoint Kinase 2
CML	N $\epsilon$ -carboxymethyl-lysine
CNS	Central Nervous System
COX	Cyclooxygenase
CSF	Cerebrospinal Fluid
CXCL1	C-X-C Motif Chemokine Ligand 1
DBI	Double Bound Index
DCTN1	Dynactin Subunit 1
DDR	Deoxyribonucleic Acid Damage Response
DENN	differentially expressed in normal and neoplastic cells
DHA	Docosahexaenoic Acid
DNA	Deoxyribonucleic Acid
DNA-PK	Deoxyribonucleic Acid-dependent Protein Kinase
DNP	2,4-Dinitrophenol
DPA	Docosapentaenoic Acid
DPR	Dipeptide Repeat
EAAT2	Excitatory Amino Acid Transporter 2
EFNB1	Ephrin B1

## List of Abbreviations

EPA	Eicosapentaenoic Acid
ETC	Electron Transport Chain
FA	Fatty Acid
fALS	familial Amyotrophic Lateral Sclerosis
FDA	Food and Drug Administration
FDR	False Discovery Rate
FG-Nup	phenylalanine-glycine-Nucleoporin
FIG4	FIG4 Phosphoinositide 5-Phosphatase
FTD	Frontotemporal Dementia
FUS	Fused in Sarcoma
GC/MS	Gas Chromatography/Mass Spectrometry
GDP	Guanosine diphosphate
GLE1	GLE1 RNA Export Mediator
GLT1	Glutamate Transporter 1
GRN	Granulin
GTP	Guanosine Triphosphate
H2AX	H2A histone family member X
HNE	4-hydroxy-2-nonenal
hnRNP	heterogeneous nuclear Ribonucleoprotein
HRE	Hexanucleotide Repeat Expansion
hSOD1	human Superoxide Dismutase 1
IL	Interleukin
KCNMB2	Potassium Calcium-Activated Channel Subfamily M Regulatory Beta Subunit 2
KD	Knock-down
KI	Knock-In
KO	Knock-Out
LATE	Limbic-predominate Age-related TDP-43 Encephalopathy
LATE-NC	Limbic-predominate Age-related TDP-43 Encephalopathy-Neuropathological Change
LC3	Microtubule-associated protein 1A/1B-light chain 3
LCCS1	Lethal Congenital Contracture Syndrome 1
LCD	Low Complex Domani
LLPS	Liquid-Liquid Phase Separation
LMN	Lower Motor Neuron
LNA	Locked Nucleic Acid
MDAL	N $\epsilon$ -malondialdehyde-lysine
MFN2	Mitofusin 2
MN	Motor Neuron
mRNA	messenger Ribonucleic Acid
mRNP	messenger Ribonucleoprotein
mtDNA	mitochondrial Deoxyribonucleic Acid
mTOR	mammalian Target Of Rapamycin
MUFA	Monounsaturated Fatty Acid
ND3	NADH Dehydrogenase 3
ND6	NADH Dehydrogenase 6
NES	Nuclear Export Signal
Nfl	Neurofilament light chain
NFT	Neurofibrillary Tangles
NGS	Next-Generation Sequencing
NLS	Nuclear Localization Signal
NOX2	NADPH Oxidase 2

## *List of Abbreviations*

NPC	Nuclear Pore Complex
NPV	Negative Predictive Value
OPTN	Optineurin
PAI-2	Plasminogen Activator Inhibitor, Type II
PBMC	Peripheral Blood Mononuclear Cell
PC	Phosphatidyl Choline
PCA	Principal Component Analysis
PCD	Programmed Cell Death
PD	Parkinson's Disease
PE	Phosphatidylethanolamine
PFN1	Profilin 1
PHB2	Prohibitin 2
PI	Peroxidability Index
PI3KCD	Phosphatidylinositol 4,5-bisphosphate 3-kinase catalytic subunit delta isoform
PK	Pharmacokinetics
PLS-DA	Partial Least Squares-Discriminant Analysis
PMN	Polymorphonuclear
PMO	Phosphorodiamidate Morpholino Oligomers
PNA	Peptide Nucleic Acid
pNfH	phosphorylated Neurofilament Heavy
poly-GA	poly-Glycine Alanine
poly-GP	poly-Glycine Proline
poly-GR	poly-Glycine Arginine
poly-PA	Poly-Proline Alanine
poly-PR	poly-Proline Arginine
PPV	Positive Predictive Value
pre-mRNA	pre-messenger Ribonucleic Acid
PS	Phosphorothioate
PUFA	Polyunsaturated Fatty Acid
Q-SNARE	Q-soluble N-ethylmaleimide-sensitive factor-attachment protein (SNAP) receptor
Rab-GEF	Rab-Guanine nucleotide Exchange Factor
RCT	Randomised Clinical Trial
riRNA	ribosomal Ribonucleic Acid
RNA	Ribonucleic Acid
RNP	Ribonucleoprotein
ROC	Rceiver Operating Characteristic
ROS	Reactive Oxygen Species
sALS	sporadic Amyotrophic Lateral Sclerosis
SASP	Senescence-Associated Secretory Phenotype
SFA	Saturated Fatty Acid
SG	Stress Granule
siRNA	silencing Ribonucleic Acid
SOD1	Superoxide Dismutase 1
SPM	Specialized Pro-resolving Mediators
SQSTM1	Sequestrosome 1
STX17	Syntaxin 17
SV	Structural Variant
TARDBP	TAR DNA-Binding Protein 43
TBK	TANK Binding Kinase 1
tcDNA	Tricyclo-Deoxyribonucleic Acid
TDP-43	TAR DNA-Binding Protein 43

### *List of Abbreviations*

TG	Thymidine Guanidine
TMEM106B	Transmembrane Protein 106B
TNF-alpha	Tumor Necrosis Factor-alpha
UBQLN2	Ubiquilin 2
UFA	Unsaturated Fatty Acid
UG	Uridine Guanidine
UMN	Upper Motor Neuron
UPRmt	mitochondrial Unfolded Protein Response
VAPB	VAMP Associated Protein B
VCP	Valosin Containing Protein
VSP	Voltage Sensitive Phosphatases
WGS	Whole-Genome Sequencing
WT	Wild Type

List of Figures

Figure 1. Genetics of ALS.....	17
Figure 2. Gene discovery in ALS.....	19
Figure 3. SOD1 mutational landscape.....	20
Figure 4. C9orf72 toxic mechanisms.....	22
Figure 5. TDP-43 functions.....	23
Figure 6. TARDBP mutational landscape.....	24
Figure 7. Anatomy of the motor system.....	26
Figure 8. Glutamate excitotoxicity .....	29
Figure 9. Molecular effectors of oxidative damage .....	31
Figure 10. Possible outcomes after the DDR .....	33
Figure 11. Prion-like theory.....	37
Figure 12. Autophagy dysregulation in ALS .....	41
Figure 13. NPC structure .....	44
Figure 14. Splicing regulatory elements.....	46
Figure 15. Senescence and SASP pathway .....	52
Figure 16. Acute inflammation and resolution .....	54
Figure 17. LATE-NC and ADNC estimated prevalence .....	56
Figure 20. Omics sciences overview .....	66

*List of Tables*

**List of Tables**

<b>Table 1. LATE-NC Stages according to TDP-43 pathology extent.....</b>	<b>55</b>
<b>Table 2. Antibody dilutions.....</b>	<b>77</b>
<b>Table 3. Sequence of RT-qPCR oligos .....</b>	<b>78</b>



# **1 INTRODUCTION**

## **1.1 Epidemiology and genetics of ALS**

### **1.1.1 ALS: a complex disease**

Amyotrophic lateral sclerosis (ALS) was first described in 1869 by French neurologist Jean-Martin Charcot in a group of patients with progressive paralysis. He correlated the symptoms with a loss of grey matter in the ventral horn (corresponding to motor neurons) and damaged lateral tract (sclerosis).

ALS is the most incident motor neuron disease in adulthood. One to two of 100.000 people is diagnosed with ALS worldwide every year with a man: woman ratio of 3:2 (Kiernan et al., 2011). Notably, in Spain, the incidence is 1.4 per 100.000 people/year. Worldwide prevalence is 2-5 per 100.000, whereas prevalence in the Spanish population is especially higher (5.4 per 100.000 people), probably due to the proportion of the aged population (Camacho, Esteban, & Paradas, 2018).

ALS is characterized by the loss of upper and lower motor neurons, leading to progressive paralysis and death in 2-5 years. Interestingly, the peak of onset of this disease is 58-63 years. This fact has a profound impact not only on a personal level but also on a social level. This disabling disease affects the active population and dramatically shortens the lifespan of the patients. Moreover, the incidence of ALS is expected to increase by 69% in 2040, especially in developing countries. This fact is a consequence of a higher life span and the aging of the population. Nevertheless, the improvement in ALS managing and research may lower the impact of this prediction (Arthur et al., 2016).

ALS is typically classified into two groups depending on genetic association: sporadic ALS (sALS) without other diseased relatives, and familial ALS (fALS) with Mendelian inheritance. The first one represents 95% of the cases and does not have any known cause. On the other hand, several genes are linked to fALS in an autosomal dominant inheritance (**Figure 1**).

Twin data from sALS patients have shown an approximately 60% of heritability (Al-Chalabi et al., 2010). However, 80-90% of the genetic component of sALS is still unknown (Gibson et al., 2017; Zou et al., 2017). This data demonstrates a high heritability component in sALS, where genetic variants that confer moderate risk of sALS play an essential and largely unknown role. Rare variants are predicted to be the primary source of the heritability of sALS. Nevertheless, the low number of people sharing the same genetic rare variant constrains the statistical analyses. To overcome this problem, MinE Project is collecting and analyzing by Next Generation Sequencing (NGS) technology

## Introduction

15000 DNA samples from people with sALS and 7500 control subjects to analyze full DNA profiles and find enriched rare variants in this large sALS cohort (Van Rheenen, Pulit, et al., 2018).



**Figure 1. Genetics of ALS.** Representation of the most relevant genes linked to ALS in European and Asian populations. Half of the genetic component in fALS and more than 90% in sALS remains unknown (Mejzini R. et al 2019).

The genetic architecture of sALS is complex and sequencing probably is not enough to understand it. Four primary sources of confounding factors could interfere with the dissection of Whole Genome Sequence (WGS) data: i) oligogenic inheritance (when one genetic variant is not enough to cause the disease, although it increases the risk), ii) pleiotropy (the same genetic variant can cause different disease), iii) age-dependent and incomplete penetrance (a genetic variant could increase the risk of the disease in age-dependent or incomplete manner), and iv) somatic mosaicism (a mutation can occur after mitotic division and found only in specific cells). Identifying truly genetic variants in sALS is just the first step to disentangle the genetic component(s) of the disease. The effects of genetic variants in non-coding regions (99% of the genome) are not easy to predict. Some authors claim that structural variants (SVs), composed by insertion, deletions, inversions, and microsatellites, could have an underestimated impact on the genetics of sALS. SVs are generally found in non-coding regions but have a higher impact on gene expression than single nucleotide

## Introduction

variants (SNVs) (Chiang et al., 2017). NGS platforms and exome sequencing are not able to find most of SVs due to the nature of this repetitive and variable elements and the location in non-coding regions. However, SVs like *C9ORF72* repeat expansion (the most common gene variant in fALS and sALS) and *ATXN2* repeat expansion are described in ALS, and maybe other SVs can explain part of the missing genetic component of ALS (Theunissen et al., 2020). Also, SV can be relevant in oligogenic inheritance. As an example, *SQSTM1* SV is associated with some *SOD1* fALS families, and it may explain an incomplete penetrance (Pytte et al., 2020). Understanding the genetics of the disease will open the door for precision medicine, gene therapy, and genetic counseling.

The first mutation associated with fALS was discovered in the *SOD1* gene in 1993 (Rosen et al., 1993). Since then, 29 genes have been associated with fALS and sALS (**Figure 2**). Most of them are involved in RNA processing, protein homeostasis, and the cytoskeleton. In the case of fALS, approximately half of genetic variants have been discovered, with significant differences regarding the frequencies of significant mutations between Asian and European cohorts (Zou et al., 2017). (Figure 1 from PMID: 31866818). The known mutations in ALS correspond to *SOD1*, *C9ORF72*, and *TARDBP*.

On the other hand, 40% of the variance of developing ALS is associated with environmental factors. According to a mathematical model based on the comparison of the incidence rate and age of onset, only six steps leads to the onset of ALS (Al-Chalabi et al., 2014). Knowing each of these steps would result in effective prevention of the disease. Nevertheless, environmental studies are challenging to perform due to its dynamic nature and gene-environment interactions, in contrast to genetics. Moreover, ALS clinical onset could be a result of years of pre-clinical stage, where molecular events could lead to the disease manifestation. The only proven environmental risk factor of ALS is smoking through an unknown mechanism, and some authors hypothesize a link with oxidative stress (Armon, 2009). Besides, male gender and age are also risk factors. Vivekananda and collaborators performed a case-control study measuring the ratio of the index to ring finger length (2D:4D ratio) as a surrogate marker of prenatal testosterone exposure. They found that the ALS cohort had a lower 2D:4D ratio, indicating a higher prenatal testosterone exposure that could increase the vulnerability of motor neurons to death (Vivekananda et al., 2011). Sexual dimorphism is also present in mouse models in a similar way. The female mouse model of fALS overexpressing a mutated h*SOD1* (G93A) transgene has more prolonged survival and a delayed onset compared to male mouse (Gurney et al., 1994). In our laboratory, we demonstrated the role of estrogen preventing oxidative stress-mediated by the overexpression of mutated h*SOD1* *in vitro* (Cacabelos, Ramírez-Núñez, et al., 2016). Additionally, controversial evidence points to physical activity (Hamidou et al., 2014; Huisman et al., 2013) and military service in the US (Beard & Kamel, 2015) as risk factors of ALS. Another probable (yet not confirmed) risk factor is the exposure to neurotoxins like lead (M.-D. Wang, Gomes,

## Introduction

Cashman, Little, & Krewski, 2014), some pesticides (Malek, Barchowsky, Bowser, Youk, & Talbott, 2012) and  $\beta$ -Methylamino-L-alanine (BMAA) (Masseret et al., 2013).

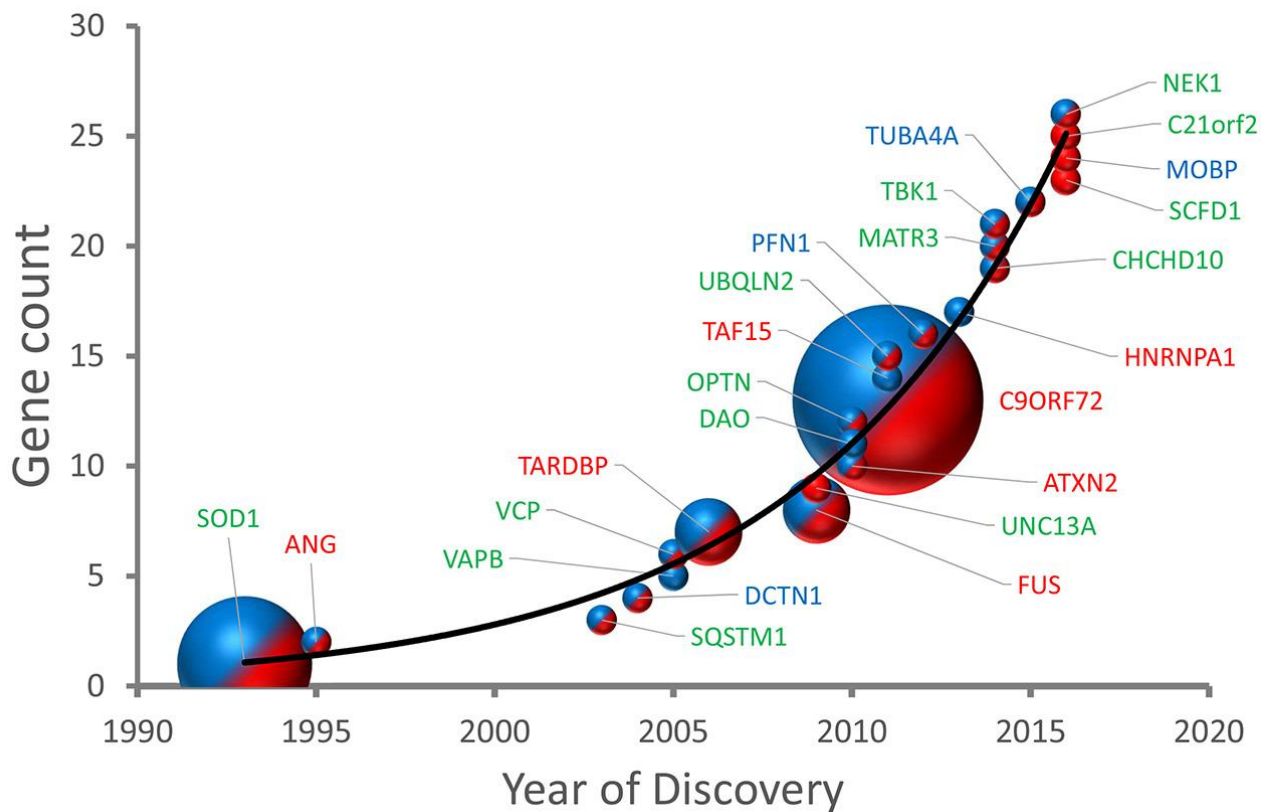


**Figure 2. Gene discovery in ALS.** The number of mutated genes associated with ALS is exponentially increasing. The mutation found in sALS is colored in red and those linked to fALS in blue. Blue and red circles indicate the mutation found in fALS and sALS (Brown RH and Al-Chalabi A 2017).

### 1.1.2 SOD1 mutations

Cu/Zn Superoxide Dismutase (SOD1) is an enzyme localized in the cytosol and the intermembrane space of mitochondria, which catalyzes the dismutation of superoxide radical, mainly produced during cellular respiration, into oxygen and hydrogen peroxide (McCord & Fridovich, 1969). This activity plays an important antioxidant role in preventing the oxidation of lipids, proteins, and carbohydrates. According to the oxidative stress theory of aging postulated in 1956 by Denham Harman, superoxide radical is the primary source of damage to macromolecules (HARMAN, 1956).



## Introduction

Moreover, the random insertion of the transgene may alter other genes in SOD1-G93A strains (De Giorgio, Maduro, Fisher, & Acevedo-Arozena, 2019). Nonetheless, SOD1 overexpression mouse models have been the only pre-clinical model for drug testing before starting a Randomized Clinical Trials (RCT). This fact is probably the main reason for the failure of 22 of 24 compounds tested in RCT for ALS. Only Riluzole (tested before mutant SOD1 mouse models) and Edaravone have a mild effect increasing the survival for a few months (Petrov, Mansfield, Moussy, & Hermine, 2017).

### 1.1.3 C9ORF72 hexanucleotide repeat expansion

In 2011, two independent groups discovered the most common gene variant in fALS: GGGGCC Hexanucleotide Repeat Expansion (HRE) in *C9ORF72* (DeJesus-Hernandez et al., 2011; Renton et al., 2011). This polymorphic SV forms extremely stable structures (100% G-C content) termed G4-quadruplexes in the DNA and RNA (Fratta et al., 2012). As happen with other repetitive structures or microsatellites, there are often expansions and retraction after DNA replication, leading to genetic mosaicism in somatic cells. Therefore, the number of repeat expansions is variable between tissues (Nordin et al., 2015) and can modify the disease penetrance (Murphy et al., 2017). For example, a 70-repeat allele from an unaffected father can be expanded to 1750-repeat in ALS affected children (McGoldrick et al., 2018). The correlation with disease phenotype/risk factor and repeat number expansion are not clear (Gami et al., 2015; Van Mossevelde, van der Zee, Cruts, & Van Broeckhoven, 2017), and other variables such as promoter methylation can also modulate disease progression (E. Y. Liu et al., 2014). Three disease mechanisms are proposed for *C9ORF72* pathogenesis (**Figure 4**) (Kumar, Hasan, & Hassan, 2017):

-RNA toxicity: When GGGGCC is transcribed in both sense and antisense way, it also folds into stable quaternary structures in pre-mRNA and sequester different RNA Binding Proteins (RBPs) leading to impairment in RNA biology, including splicing, translation, and transport. Moreover, the antisense RNA foci, but not the sense foci, correlates with the mislocalization of TDP-43 by unknown mechanisms (Cooper-Knock et al., 2015).

-Dipeptide Repeat (DPR) inclusion: Both sense and antisense *C9ORF72* mRNA containing HRE can produce proteins (DPR) by unconventional non-AUG (RAN) translation. DPR are found aggregated in *C9ORF72* ALS patients. DPRs can alter nucleocytoplasmic transport, splicing, and liquid-liquid phase separation (Freibaum & Taylor, 2017).

-Haploinsufficiency: *C9ORF72* protein is structurally related to DENN Rab-GEFs. It has been involved in membrane trafficking and autophagy (Sellier et al., 2016). However, *C9orf72* deletion alone does not lead to motor neuron disease (Lagier-Tourenne et al., 2013; O'Rourke et al., 2016).

## Introduction

Interestingly, the combination of RNA and DPR toxicity, together with *C9ORF72* deletion, exacerbates axonal trafficking defects *in vitro* (Abo-Rady et al., 2020).

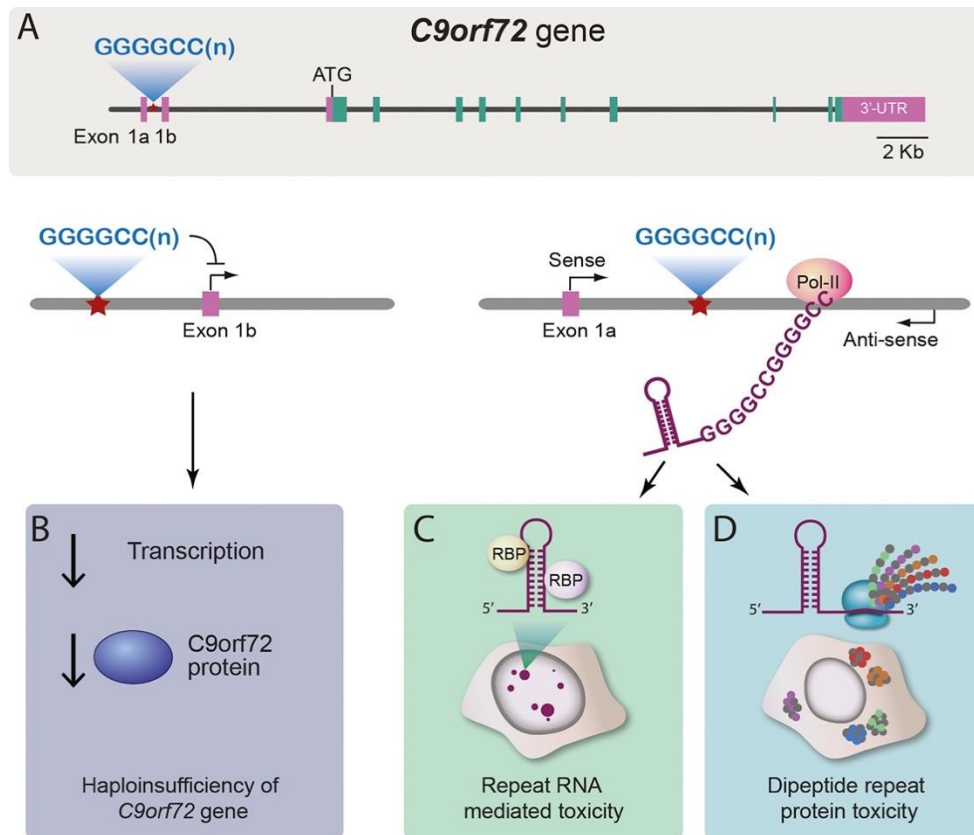


**Figure 4. *C9orf72* toxic mechanisms.** Three possible toxic mechanisms are proposed for *C9orf72* HRE (A). The downregulation of the protein product by haploinsufficiency of the gene, leading to its loss of functions (B). RBP sequestration in the RNA foci (B). Protein aggregation of DPRs derived from HRE RAN (non-AUG) translation (Gitler AD and Tsuiji H 2016).

There are several *C9ORF72* mouse models commercially available in The Jackson Laboratory. These models differ in the number of GGGGCC repeats and mouse strains. However, any of them develop the ALS paralytic phenotype. It is curious the case of *C9orf72* 500 repeats mouse (Stock No: 029099, The Jackson Laboratory) because the original article reported paralysis and gait abnormalities (Yuanjing Liu et al., 2016) that were not reproduced in The Jackson Laboratory facilities. Nevertheless, some of these *C9ORF72* mouse models display behavioral impairments and anxiety that resemble Frontotemporal Dementia phenotype, also linked to *C9ORF72* HRE).

### 1.1.4 *TARDBP* mutations

TDP-43 is the protein product of the TAR DNA-Binding Protein 43 (*TARDBP*) gene. TDP-43 was discovered in 1995 as a binding protein of the HIV-1 trans-activation response (TAR) element. Tat



## Introduction

HIV protein binds to the TAR element to promote viral transcription. TDP-43 can prevent Tat binding, thus inhibiting viral replication (Ou, Wu, Harrich, García-Martínez, & Gaynor, 1995). Additionally, TDP-43 can prevent the alternative splicing of CFTR's exon 9 by binding to a polymorphic UG repeat region in the pre-mRNA (Buratti et al., 2001). Further studies elucidated multiple functions of this protein in RNA metabolism, regulating transcription, mRNA transport, stress granule formation, and splicing (**Figure 5**) (Cohen, Lee, & Trojanowski, 2011).

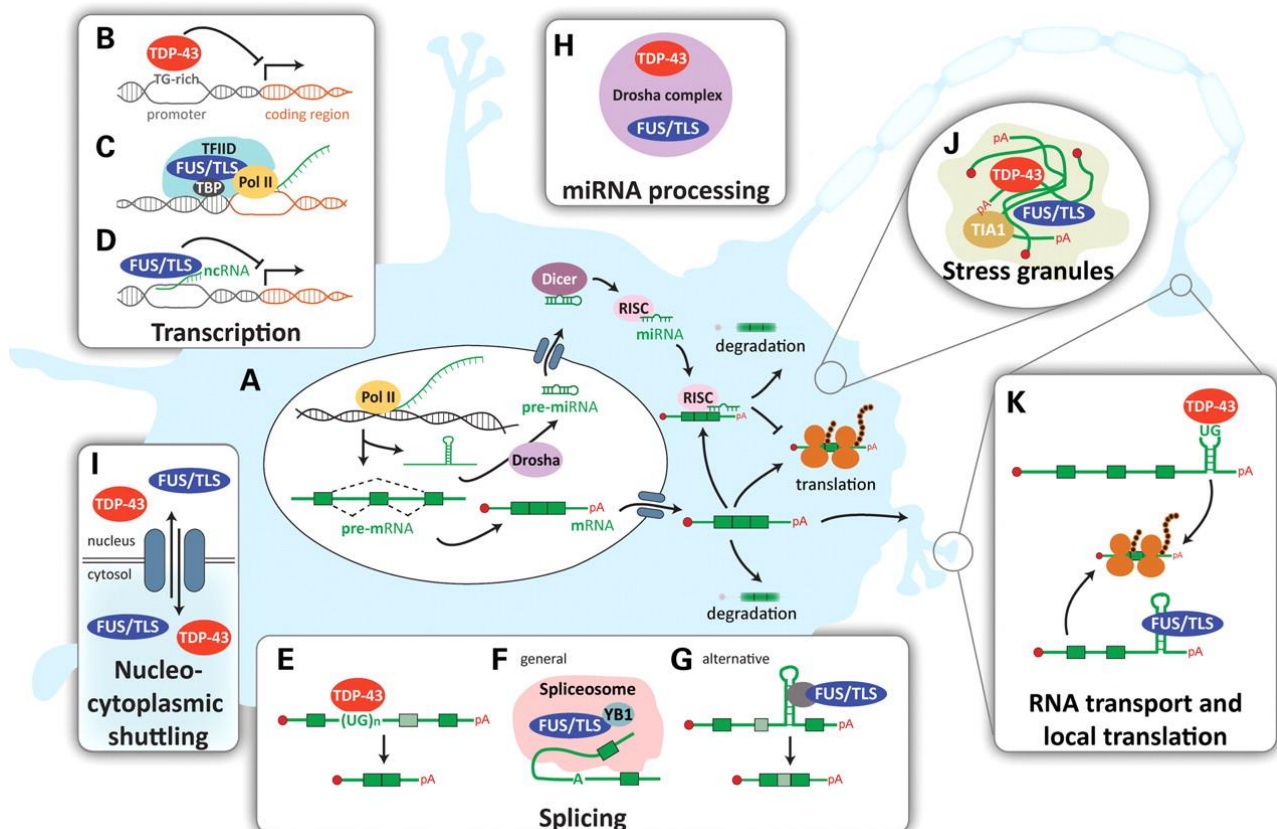


**Figure 5. TDP-43 functions.** TDP-43 is a multifunctional protein involved in several processes of RNA biology (A-I) (Lagier-Tourenne et al 2010).

*TARDBP* is highly conserved in evolution (H. Y. Wang, Wang, Bose, & Shen, 2004) and is a member of the heterogeneous nuclear ribonucleoproteins (hnRNPs) family. Structurally, TDP-43 is formed by two tandem RNA Recognition Motifs (RRM1 and RRM2) with two highly conserved hexameric and octameric segments denoted respectively as ribonucleoprotein 2 (RNP2) and ribonucleoprotein 1 (RNP1); and a C-terminal composed by a glycine-rich domain. RRM motifs are essential for DNA/RNA binding to TG/UG abundant sequences, and the C-terminal domain is relevant for protein interaction and dimerization (Kuo, Doudeva, Wang, Shen, & Yuan, 2009). About fifty missense mutations in *TARDBP* have been found in ALS. Most of the *TARDBP* mutations are found in the C-terminal domain (**Figure 6**). Mutations induce changes in the solubility and eventually trigger nuclear export and cytoplasmic aggregation. Whether cytoplasmic aggregation (Neumann et al., 2006) or

## Introduction

nuclear clearance (Nana et al., 2019) or combined, are the main contributor to pathogenesis is still under debate.

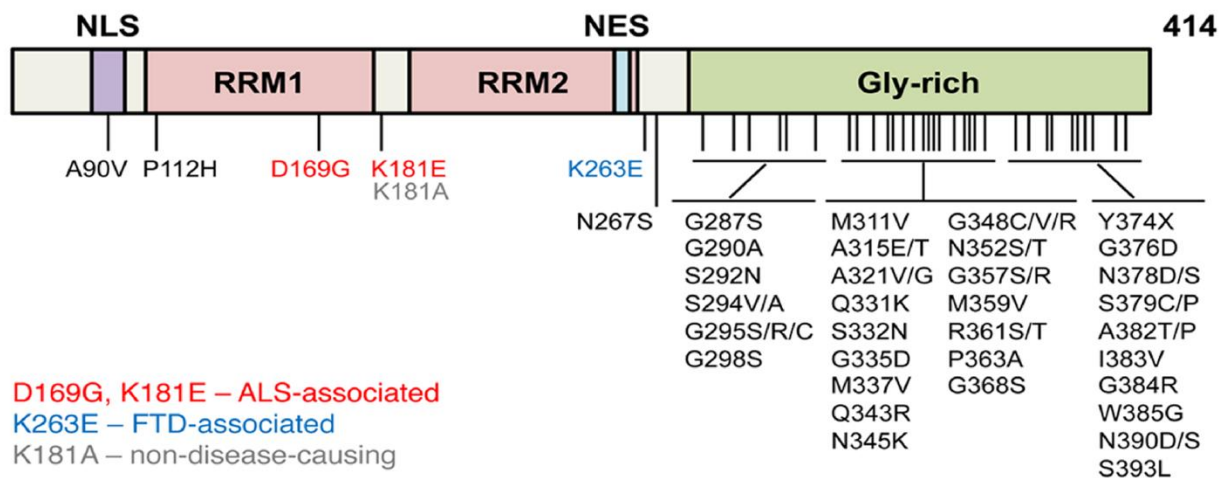


**Figure 6. *TARDBP* mutational landscape.** In contrast to *SOD1* mutations, those found in *TARDBP* are concentrated in C-terminal (Gly-rich) Domain (Chen H-J et al 2019)

There are several animal models for TDP-43 pathology. However, any of them reproduce all the features of the disease but can be useful to study different aspects of the disease (De Giorgio et al., 2019). Transgenic mice carrying a variable copy number of mutated *TARDBP* are the most used. The pathology and the phenotype of these models are mostly dependent on copy number, promoter, genetic background, and mutation. Some of them reproduce TDP-43 aggregation, phosphorylation, or ubiquitination. One of the pitfalls of these models is the overexpression expression of *TARDBP*, random insertion (potentially mutagenic) of the transgene, and sometimes the lack of loss of function of the endogenous TDP-43. Another strategy is the mutation of the genomic *TARDBP* to generate knock-in (KI) mice with average expression levels. However, even closer to human fALS mouse models, they do not develop the disease. KI mice carrying mutations in RRM2 exhibit splicing defects and are an excellent model to study this specific disease mechanism. The last TDP-43 mouse model is conditional KO. *TARDBP* is essential for embryonic development (Sephton et al., 2010), but specific motor neuron *TARDBP* KO causes slow-progressive motor neuron degeneration (Iguchi et al., n.d.). They are useful to study TDP-43 functions in specific cell types *in vivo* (Jeong et al., 2017).

On the one hand, transgene models, although they reproduce some features of the disease, are not likely to share a common disease mechanism with human patients. On the other hand, physiological KI models do not reproduce the disease. A possible reason for the lack of symptoms in KI models is the underestimated oligogenic inheritance (Van Blitterswijk et al., 2012). The breeding of distinct KI mouse could be useful to obtain proper combinations which develop an oligogenic fALS. The improvement of reliable preclinical models is critical to improving drug discovery for RCTs.

## 1.2 A clinical overview of ALS

From a clinical point of view, ALS can be classified as a group of different conditions that share the neurodegeneration of both upper and lower motor neurons (UMN and LMN, respectively) (**Figure 7**). ALS diagnostic is based on El Escorial Criteria (Brooks, Miller, Swash, & Munsat, 2000), which requires “(A) the presence of

-(A:1) Evidence of lower motor neuron (LMN) degeneration by clinical, neuropathological, or electrophysiologic examination.

-(A:2) Evidence of upper motor neuron (UMN) degeneration by clinical examination, and

-(A:3) Progressive spread of symptoms or signs within a region or to other regions, as determined by the history of examination,

together with:

(B) the absence of

-(B:1) Electrophysiological or pathological evidence of other disease processes that might explain the signs of LMN and UMN degeneration, and

-(B:2) Neuroimaging evidence of other disease processes that might explain the observed clinical and electrophysiological signs.”

The lack of specific biomarkers hinders the diagnostic, which often is not definitive or misdiagnosed in 10% of the cases with ALS mimic syndromes (Traynor et al., 2000). Therefore, El Escorial Criteria also divides the ALS diagnostic according to the confidence level:

“-Clinically definite ALS

UMN and LMN clinical signs or electrophysiological evidence in three regions

Clinically definite ALS-laboratory supported

UMN and LMN clinical signs in one region and the patient is a carrier of a pathogenic SOD1-gene mutation

-Clinically probable ALS

UMN and LMN clinical or electrophysiological evidence by LMN and UMN signs in two regions with some UMN signs rostral to the LMN signs

-Clinically possible ALS

UMN and LMN clinical or electrophysiological signs in one region only, or

UMN signs in at least two regions, or

UMN and LMN signs in two regions with no UMN signs rostral to LMN signs. Neuroimaging and laboratory studies have excluded other diagnoses.”

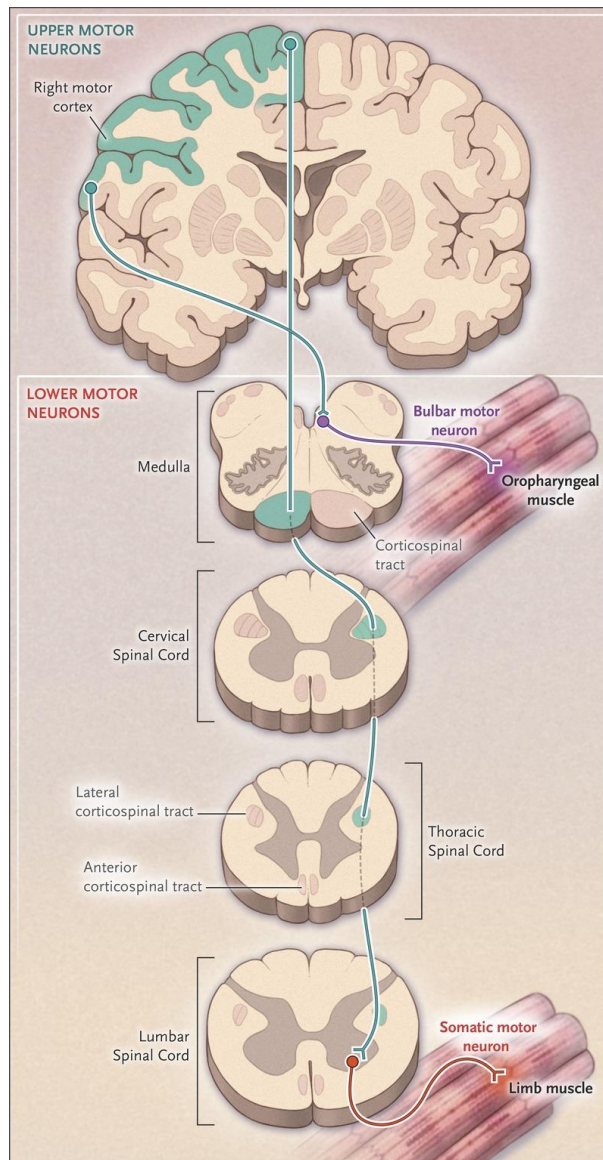


**Figure 7. Anatomy of the motor system.** The motor system is the main affected in ALS. It is composed of UMNs in the frontal cortex traveling through the corticospinal tract to synapse with LMNs. LMNs are located in the ventral horn of the spinal cord and control the voluntary movements of limbs. UMNs can also synapse with bulbar motor neurons that control facial muscles (Brown RH and Al-Chalabi A 2017).

ALS can be stratified by the clinical onset of the patients. On the one hand, when the signs and symptoms are related to motor neurons located in the brainstem, it is classified as bulbar ALS. This specific bulbar phenotype corresponds to 25% of the patients, and the symptomatology includes sialorrhea, facial weakness, gait abnormalities, dysphagia, and speech disturbances. On the other hand, when the signs and symptoms start in the limbs, it is referred to as spinal ALS, and it is the most common phenotype (75% of the cases). The symptomatology includes weakness and progressive spastic limb paralysis.

## *Introduction*

Additionally, progressive paralysis can be more spastic (UMN degeneration predominance) or more flaccid (LMN degeneration predominance). In general, bulbar onset survival is shorter due to the proximity of disease onset to vital motor neuron nuclei innervating respiratory muscles (Kiernan et al., 2011). The median survival of ALS is 15.3 months for spinal onset and 13.1 months for bulbar onset, although other variables such as age on onset, lag from onset to the first visit, Body Mass Index (BMI) < 18.5, and respiratory capacity negatively influence on survival time (Traxinger, Kelly, Johnson, Lyles, & Glass, 2013).

The ALS Functional Rating Scale-Revised (ALSFRS-R) is a validated instrument for monitoring the disability of ALS patients. It takes into account the degree of disability in executing several functions and symptoms, including speech, salivation, swallowing, handwriting, patients with gastrostomy and >50% daily nutrition intake via G-tube (Yes/No), cutting food and handling utensils, dressing and hygiene, turning in bed and adjusting bedclothes, walking, climbing stairs, dyspnea, orthopnea, and respiratory insufficiency. Average ability to do these tasks are scored by 4 points, and 0 points if the person is unable to do it (Cedarbaum et al., 1999). Moreover, the decline in ALSFRS-R score (measured by ALSFRS-R slope) is useful to estimate the disease progression and the efficacy of a given treatment in Randomized Clinical Trials (RCT) (Castrillo-Viguera, Grasso, Simpson, Shefner, & Cudkowicz, 2010).

According to a mathematical model, the main contributors to disease prognosis are the clinical onset and the diagnostic delay (the time between the first symptoms and the diagnostic). Using these two variables, ALS patients can be divided into five clusters with non-overlapping survival duration. Curiously, 1200 of the 1467 patients of this study are grouped into two groups, suggesting a more homogenous disease than expected (Ganesalingam et al., 2009). Similar results were obtained in a recent study with a larger cohort and a more significant number of clinical and biochemical variables (Kueffner et al., 2019).

Regarding clinical managing, a multidisciplinary clinic approach improves survival in ALS (Rooney et al., 2015). Patients develop multiple complications that need integrative healthcare. ALS patients in this multidisciplinary clinic approach are seen by a neurologist with specialist expertise in ALS, a specialist ALS nurse, and a neuromuscular multidisciplinary team, including a physiotherapist, occupational therapist, speech, and swallow therapist, and dietician, and given direct next-day access to Respiratory Medicine where indicated. Meetings of these healthcare professionals are necessary to implement a personalized intervention. One of the elements to consider is an appropriate diet. Muscular atrophy is a catabolic process that ultimately kills the patient when it occurs in respiratory muscles

## *Introduction*

Moreover, 50% of ALS patients are hypermetabolic, and it is associated with a faster progression (Bouteloup et al., 2009). A premorbid BMI is a protective factor of ALS (O'Reilly et al., 2013), whereas a low BMI is associated with a poor outcome (Barone et al., 2019). Dietary intervention with a high caloric diet should be taken into account according to preliminary evidence in an RCT to prevent a low BMI (Wills et al., 2014). Therefore, other dietary interventions could be low-cost and low-risk treatments for ALS.

## **1.3 Pathogenic mechanisms in ALS**

### **1.3.1 Excitotoxicity**

Glutamate is an excitatory neurotransmitter widely used in the central nervous system (CNS). When an excessive release or a lack of clearance occurs, it remains in the synaptic cleft prolonging the excitation of postsynaptic receptors with toxic effects (**Figure 8**) (P. Van Damme, Dewil, Robberecht, & Van Den Bosch, 2006). In 1992, Rothstein et al. observed a defect in glutamate transport in ALS patients that could lead to neurotoxic extracellular levels of this neurotransmitter (Jeffrey D. Rothstein, Martin, & Kuncl, 1992). This finding was the rationale for a Randomized Clinical Trial (RCT) of a supposed anti-excitotoxicity molecule (Riluzole®), which reported a benefit extending the survival for 2-3 months (Bensimon, Lacomblez, & Meininger, 1994). However, this mild effect is driven from the extension of the late stage of the disease, extending the worst phase for the patients in which respiratory or nutritional intervention is determined as clinically necessary (Fang et al., 2018). Riluzole was the only FDA approved drug for ALS until 2016.

At a molecular level, there is a loss of astroglia Glutamate Transporter 1 (GLT1 or EAAT2) in the motor cortex and spinal cord (the central affected CNS regions in the disease) in ALS patients (Jeffrey D. Rothstein, Van Kammen, Levey, Martin, & Kuncl, 1995). Loss of GLT1 is also confirmed in the G93A SOD1 mouse model during the neurodegeneration but not before onset and without altering glutamate concentration in cerebrospinal fluid (CSF) (Bendotti et al., 2001). However, GLT1 overexpression in G93A mouse delays grip strength decline but does not extend life span, suggesting a modest role of this glutamate transport in the disease (H. Guo et al., 2003). Although excitotoxicity has been widely reported in several ALS models and electrophysiological studies are included in the clinical diagnosis of ALS (Brooks et al., 2000), the cause of this alteration remains elusive (King, Woodhouse, Kirkcaldie, & Vickers, 2016).

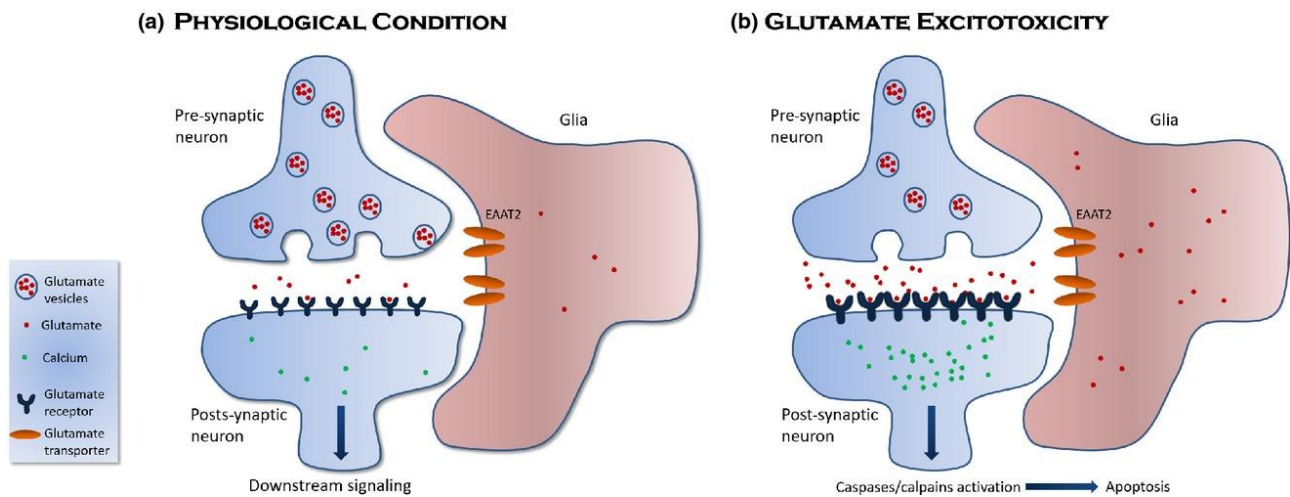


**Figure 8. Glutamate excitotoxicity.** Glial cells remove the glutamate from the synaptic cleft to limit the effects of this neurotransmitter. EAAT2 is a glutamate transporter involved in this process and is downregulated in ALS. Therefore, glutamate can exert its functions for a longer time and triggers the apoptosis of overexposed neurons (Fotana ACK 2015).

### 1.3.2 Protein oxidative damage

Reactive Oxygen Species (ROS) are generated by a leak of electron flow through the Electron Transport Chain (ETC) in mitochondria. An electron can reduce the  $O_2$  into a high reactive  $O_2^{\bullet-}$  (superoxide). Complex I and III are the primary source of ROS, and its efficiency is critical to prevent and imbalance increasing ROS production (Q. Chen, Vazquez, Moghaddas, Hoppel, & Lesnefsky, 2003; Herrero & Barja, 2000). The lower content of oxidable amino acid methionine and the adaptation of cell membranes contribute to preventing oxidative damage and age-related events (Pamplona, Portero-Otín, et al., 2005).

ROS modify macromolecules via non-enzymatic reactions, altering the physicochemical properties. The most common form of protein oxidation implies third-party molecules derived from the oxidation of carbohydrates (glycoxidation) and lipids (lipoxidation) (John W Baynes, 2003; Requena et al., 1997). Superoxide is produced after the reduction of  $O_2$  and has a short half-life (microseconds) and rapidly reacts within surrounding molecules near of complex I in the mitochondrial inner membrane. SOD enzymes can catalyze the dismutation of  $O_2^{\bullet-}$  into  $O_2$  and  $H_2O_2$ , preventing the oxidizing damage of superoxide. However, hydrogen peroxide can react with  $Fe^{2+}$  producing  $OH^{\bullet}$  (Hydroxyl radical) +  $OH^-$  and  $Fe^{3+}$  (metal-catalyzed oxidation named Fenton reaction) (Hayyan, Hashim, & Alnashef, 2016). When ROS, like superoxide or hydroxyl radical, oxidize carbohydrates or lipids generate relatively stable intermediates that can spread across the cell modifying proteins and altering its functions (Singh, Barden, Mori, & Beilin, 2001). Glycoxidation and lipoxidation of proteins result in Advanced Glycation End-products (AGEs) and Advanced lipidation end-products (ALEs). In

## Introduction

the case of AGEs formation, the spreading intermediates are glyoxal, methylglyoxal, and 3-deoxyglucosone (3-DG), derived from glycolysis (**Figure 9**) (Thornalley, Langborg, & Minhas, 1999).

On the other hand, principal substrates for the generation of ALEs are fatty acids (FAs) from cell membranes. FAs are formed by a carboxylic group and an aliphatic chain with a variable number of carbons and unsaturations (carbon-carbon double bond). FAs can be classified by the number of unsaturations of the aliphatic chain. Saturated fatty acid (SFA) lacks double bonds, monounsaturated fatty acids (MUFAs) contain one double bond, and polyunsaturated fatty acids (PUFAs) have multiple double bonds. The carbon from the carboxylic group is named alpha, and the opposite of the aliphatic chain is omega. Hence, n or  $\omega$ -3 FAs means that the first unsaturation is located in the third carbon from the omega terminal. The number of carbons and unsaturation from the aliphatic chain is also crucial for the nomenclature, i. e., C22:6n3 is interpreted as an aliphatic chain of 22 carbons, six unsaturations and the first of them is in the third carbon from the omega terminal. Additionally, FAs unsaturation can be *cis*, if the adjacent hydrogens of the double bond are on the same side, or *trans* if they are on the opposite side.

The characteristics mentioned above of FAs determine the physicochemical properties of the molecule. The number of unsaturations and *cis* configuration are both negatively correlated with melting temperature. A side effect of increasing the number of unsaturations, also known as Double Bond Index (DBI), is an exponential increase of the sensitivity to oxidation or Peroxidability Index (PI) (Bielski, Arudi, & Sutherland, 1983). Non-enzymatic oxidation of PUFAs results in chain breakdown and the formation of reactive aldehyde intermediates, like hydroxynonenal and malondialdehyde. These short molecules propagate across the cell, oxidizing other biomolecules like proteins (Schopfer, Cipollina, & Freeman, 2011).

Both ALEs and AGEs are formed by carbonyl adducts with proteins, such as N $\epsilon$ -carboxymethyl-lysine (CML), N $\epsilon$ -carboxyethyl-lysine (CEL) and N $\epsilon$ -malondialdehyde-lysine (MDAL), which can be measured by Gas Chromatography/Mass Spectrometry (GC/MS) techniques (J W Baynes & Thorpe, 2000). The high content of lipids, especially PUFAs with high PI and elevated oxygen consumption in CNS, make this tissue highly susceptible to oxidative damage (O'Brien & Sampson, 1965; Sastry, 1985; Schopfer et al., 2011). In the case of ALS, several fatty acids are altered in the spinal cord. Interestingly, docosahexaenoic acid (DHA, C22:6n3) together with PI are markedly decreased in the spinal cord of ALS donors, whereas frontal cortex DHA and PI are slightly increased. However, in both tissue, there is an increase in AGEs and ALEs measured by GC/MS and western blot analyses of carbonylated proteins. In this line, a suboptimal assembly of Complex I and Complex III could be responsible for a higher ROS production promoting AGEs and ALEs accumulation in the spinal cord of ALS patients (Ilieva et al., 2007). A plausible hypothesis for the reduction of DHA content is a faster consumption to counteract the neuroinflammation in the spinal cord. Although DHA has a high



## Introduction

PI, it is also implicated in the resolution of the neuroinflammation (Hong, Gronert, Devchand, Moussignac, & Serhan, 2003) and excitotoxicity (Högyes et al., 2003). In the same work, under a paradigm of an early stage of excitotoxicity in organotypic spinal cord cultures, DHA, PI, and protein oxidation are increased similarly to the frontal cortex. The authors attributed these changes to events before motor neuron death, followed by DHA consumption to mitigate detrimental insults.

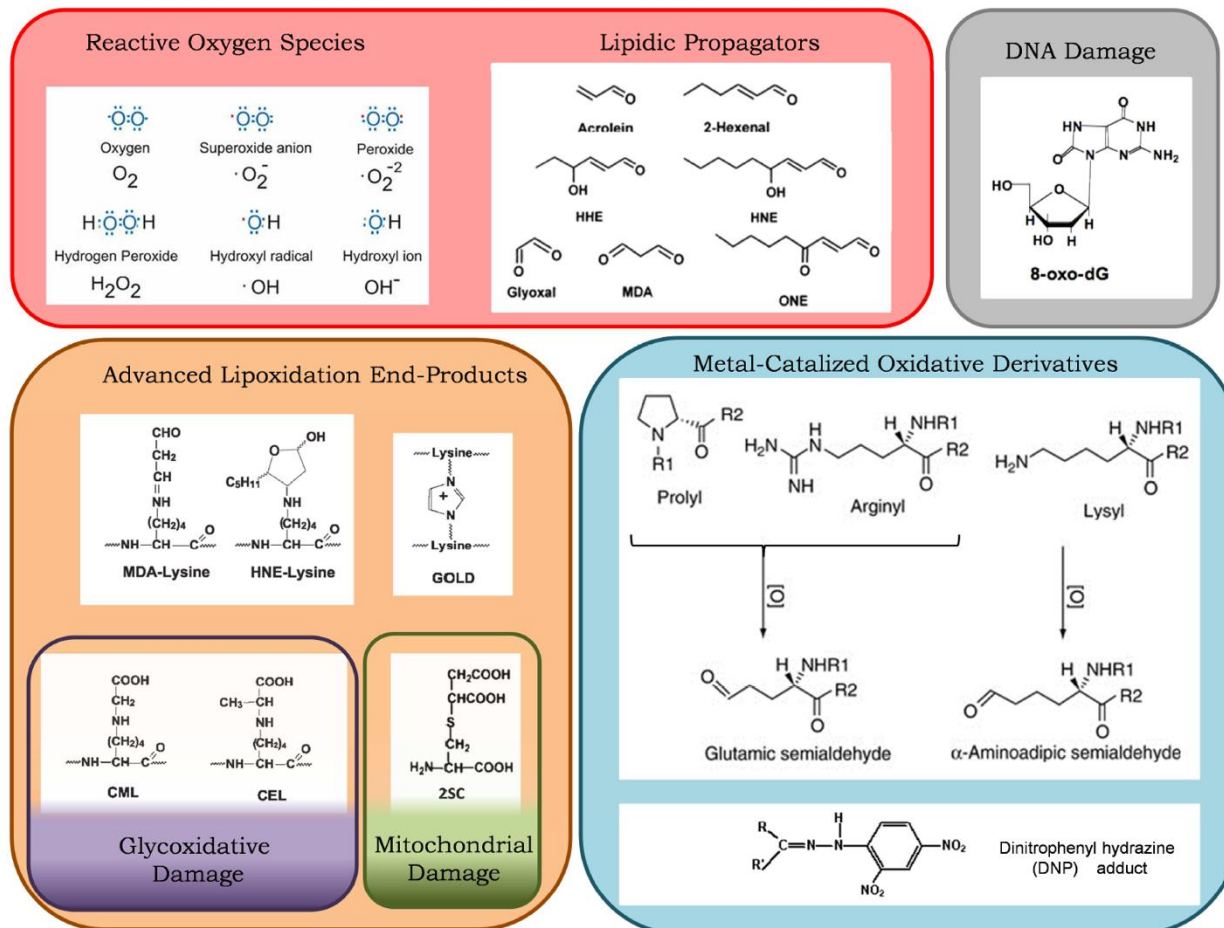


**Figure 9. Molecular effectors of oxidative damage.** ROS can modify lipids to form reactive carbonyl molecules (lipidic propagators). These molecules form stable adducts with proteins (AGEs and ALEs). Depending on the source of the oxidative damage, the products can be classified in glycoxidative damage, lipoxidative damage, mitochondrial damage, metal-catalyzed oxidative derivatives, and DNA damage (Cacabelos D 2014).

Studies of oxidative stress in the hSOD1-G93A mouse model are controversial due to the overexpression of mutant SOD1, an antioxidant enzyme, which does not entirely lose its activity. Regarding cellular respiratory function, hSOD1-G93A mice have a lower  $O_2$  in the spinal cord only at a late stage, probably due to general atrophy status. However, females hSOD1-G93A mice have a higher Complex I  $O_2$  than transgenic males, suggesting a mechanism for female ALS resilient. In the case of oxidative stress protein damage, the results in the mouse model do not reproduce the human ones, probably due to the antioxidant effect of hSOD1 overexpression. Notably, DHA content

in the mouse model has a strong interaction with transgene expression, age, and gender. Female transgenic mice have a higher content of DHA in the early stages, which is likely to exert a gender-specific neuroprotective role. Nevertheless, in the late stages of the disease in the mouse model, DHA content in the spinal cord is lower than the early stages (Cacabelos, Ramírez-Núñez, et al., 2016), similar to the human disease.

### **1.3.3 DNA oxidative damage**

ROS can also modify DNA generating 8-Oxo-2'-deoxyguanosine (8-oxo-dG) as one of the most known products. Mitochondrial DNA (mtDNA), due to the proximity of the ROS source in the ETC, contains 2-3 times more oxidized bases than nuclear DNA. This phenomenon has been proposed as a contributor to mitochondrial dysfunction in age-related processes (Hudson et al., 1998). Oxidation of DNA bases has a mutagenic effect, prokaryotes and eukaryotes have evolved to repair this damage. Base Excision Repair (BER) is the central system to correct the oxidized base in mammalian cells (Dempfle & Harrison, 1994; Dianov, Bischoff, Piotrowski, Vilhelm, & Bohr, 1998).

However, BER is not 100% efficient, and mutations eventually occur. Cells have evolved to detect and respond when genome integrity is compromised to prevent the inheritance of potentially oncogenic mutations. *P53* is a master regulator of the signaling pathway of oxidative damage in DNA. This gene is deleted in several cancers (S. J. Baker et al., 1989; Mowat, Cheng, Kimura, Bernstein, & Benchimol, 1985; Takahashi et al., 1989) and is an important tumor suppressor. However, this protein has been proposed as a pro-aging factor and inductor of senescence (Rodier, Campisi, & Bhaumik, 2007). This gene has a crucial role in the DNA Damage Response (DDR). When BER is deficient, oxidation of the base can derive in DNA Double-Strand Break (DSB). ATM is a serine/threonine kinase that is recruited to DSB and initiate DDR (Lee & Paull, 2007). ATM phosphorylates p53 and Checkpoint Kinase 2 (CHK2), which in turn also phosphorylates p53 (Pluquet & Hainaut, 2001). ATM and other DDR related kinases (ATR, DNA-PK, CHK1, CHK2) phosphorylate histone gamma-H2AX. Phosphorylation of this histone is critical for the assembly of DNA-repair complexes of DSB (Celeste et al., 2002; Rogakou, Pilch, Orr, Ivanova, & Bonner, 1998). Phosphorylation of p53 reduces the interaction with the ubiquitin ligase MDM2, enhancing its stabilization to function as a transcription factor of many genes (Lavin & Gueven, 2006).

In an initial stage of the DDR, p53 is localized in the focus of DNA damage promoting DNA repair (Al Rashid et al., 2005) and upregulates the expression of the cyclin-dependent kinase inhibitor p21 (Guillouf et al., 1995). Cell fate after DDR is driven by the degree of p53 activation and can result in four possible outcomes (**Figure 10**) (Rodier et al., 2007):

## Introduction

- i) A proper repair and the return to cell homeostasis when the damage is not severe.
- ii) A defective repair and a premature re-entry in the cell cycle could derive in the accumulation of mutation and carcinogenesis.
- iii) When the damage is severe, p53 can induce apoptosis to prevent potential carcinogenesis.
- iv) Cellular senescence, a permanent cell cycle arrest, can be derived from severe DNA damage in a cell type and physiological dependent manner.

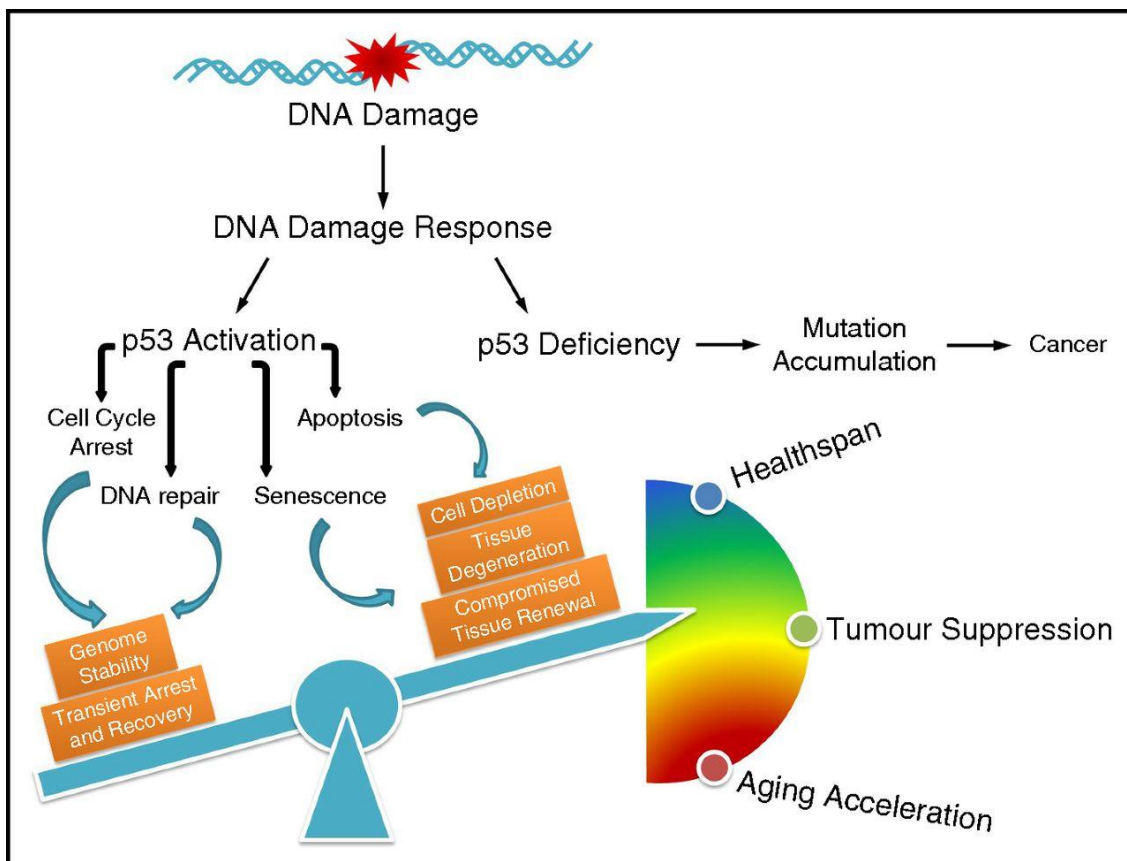


**Figure 10. Possible outcomes after the DDR.** DDR is engaged after DNA oxidation. Depending on the magnitude of the stress and the cell type, it can result in distinct cell fates. The protein p53 regulates these outcomes (cell cycle arrest, DNA repair, senescence, and apoptosis) and has profound implications in healthspan, tumor suppression, and aging (Ou H-L and Schumacher B 2018).

Neurons are particularly prone to DNA damage due to high oxygen consumption and transcriptional rate (open chromatin and free vulnerable DNA). DNA damage is notably higher in neurodegenerative diseases, including ALS (Coppedè & Migliore, 2015). 8-oxo-dG concentration is elevated in both sALS and fALS CNS (Ferrante et al., 2002) and G93A mouse model at the early pre-symptomatic stage (Aguirre, Beal, Matson, & Bogdanov, 2005; Warita, Hayashi, Murakami, Manabe, & Abe, 2001). Moreover, urinary 8-oxo-dG is associated with disease severity, suggesting a role as a biomarker (Bogdanov et al., 2000). In 1982, Bradley and Krasin formulated a hypothesis in which

## *Introduction*

the primary abnormality in ALS is an accumulation of DNA damage in motor neurons, which compromises gene transcription in these cells, probably due to a deficiency of DNA repair enzyme (Walter G. Bradley & Krasin, 1982). In this line, some mutations and polymorphisms in DNA repair enzymes have been associated with sALS and fALS (Y.-Z. Chen et al., 2004; Coppedè et al., 2007; Olkowski, 1998).

Additionally, other genes linked to ALS can induce or impair DDR in neurons (Higelin et al., 2018; Konopka & Atkin, 2018). Moreover, different pieces of evidence show lower expression of different DNA repair enzymes in both nucleus and mitochondria in sALS and fALS CNS, cell and animal models, pointing to an early event in the disease before motor neuron death (W G Bradley, Robison, & Tandan, 1987; Kikuchi et al., 2002; Kisby, Milne, & Sweatt, 1997; Manabe et al., 2001; Murakami et al., 2007; Shaikh & Martin, 2002; Tandan, Robison, Munzer, & Bradley, 1987). Nevertheless, a new study of laser capture microdissection of motor neurons shows a hypomethylation of several DDR enzymes promoters and a higher expression in ALS patients. The authors concluded that vulnerable neurons in ALS have higher levels of DNA damage, but they can engage a DDR (Kim, Jeong, Wong, & Martin, 2020).

Oxidative stress and mitochondrial dysfunction have been studied in ALS since a long time ago. The relative impact and whether they are the primary cause of ALS remains elusive. FDA approved the use of a ROS scavenger (antioxidant drug) Edaravone to treat ALS. However, this drug is only valid when it is administered in an early stage with a definite or probable diagnosis of ALS, defined by the revised El Escorial criteria. Phase III RCT demonstrated a 33% protection on ALSFRS-R decline only in participants who met these inclusion criteria (Abe et al., 2017).

### **1.3.4 Protein aggregation:**

Protein aggregates are a hallmark of ALS. Different mutated genes are frequently found aggregated in fALS but also without the mutation in sALS. These aggregates are formed by large insoluble cytoplasmic inclusions and are often polyubiquitinated and phosphorylated. However, the origin of this aggregation is mostly unknown. A recent study indicates that ALS vulnerable motor neurons have a supersaturated proteome compared to other resistant neurons. This characteristic could compromise the solubility of the proteins and the promotion towards aggregation (Yerbury et al., 2019). Other authors point to higher proteasomal activity in the resistant neurons as a defense mechanism to maintain the protein homeostasis (proteostasis) (An et al., 2019).

The most common protein aggregate in ALS is named either Lewy body-like hyaline inclusions or skein-like inclusions. In 2006, Neumann M. et al. identified hyperphosphorylated, ubiquitinated, and cleaved TDP-43 as the protein which conforms cytoplasmic inclusions in ALS and Frontotemporal Dementia (FTD-TDP) (Neumann et al., 2006). TDP-43 aggregates are found in 97% of sALS patients

## Introduction

in spinal cord and fALS negative-SOD1 patients (Mackenzie et al., 2007; C.-F. Tan et al., 2007). These cytoplasmic inclusions are found in degenerating motor neurons in the spinal cord and the surrounding oligodendroglia but also hippocampal and frontal cortex neurons. Ultrastructural analyses reveal that the typical conformation of TDP-43 aggregates is 10–20 nm diameter straight filaments of dense granular material. These aggregates are usually found in the cytoplasm but also in the nucleus and neurites of degenerating neurons (Lin & Dickson, 2008).

TDP-43 has a glycine-rich region in its C-terminal domain, which is critical and sufficient for aggregation. Interestingly, mutations associated with TDP-43 found in fALS are concentrated in this region, promoting its aggregation (B. S. Johnson et al., 2009). However, toxic effects TDP-43 aggregation are under debate due to the disparity of models and methods to evaluate the cytotoxicity (Hergesheimer et al., 2019).

An initial step for TDP-43 aggregation is an intermediate oligomerization. In this phase, the interaction with specific UG enriched RNA regions is critical to prevent the TDP-43 self-assembly into intermediate oligomers (French et al., 2019). Moreover, the addition of UG-rich oligonucleotides increases TDP-43 solubility and prevents its self-assembly (Zacco et al., 2019). Although the vast majority of mutations in *TARDBP* are found in the C-terminal domain, those mutations nearby RRM1 disturb RNA and ATP interaction, lower its solubility, and promote self-assembly and aggregation (Dang & Song, 2020). Several stressors found in ALS, such as oxidative stress, endoplasmic reticulum stress, chronic excitotoxicity, and proteasomal stress, can also induce the aggregation of TDP-43 (V. Ayala et al., 2011).

Due to the ability of TDP-43 to self-assembly and neuroanatomical progression of ALS, some authors have postulated the Prion-Like theory (**Figure 11**). Prions are misfolded and aggregation-prone proteins capable of transmitting this state to other normal-folded proteins. Classical prion diseases in humans cause neurodegeneration with a genetic cause (Prusiner, 1991) or zoonotic infection (Ironside, 2012). Prions are infectious agents and can cause epidemic diseases (Aguzzi, Sigurdson, & Heikenwaelder, 2008; Gajdusek, Gibbs, & Alpers, 1966; Prusiner, 1982). However, ALS is not classified as an infectious disease, and the transmissibility of TDP-43 proteinopathy in humans has not been demonstrated. Strictly, ALS cannot be defined as a prion disease, but TDP-43 seeding, self-template oligomerization, and cell transmissibility are demonstrated *in vitro* (Furukawa, Kaneko, Watanabe, Yamanaka, & Nukina, 2011; Nonaka et al., 2013; Porta et al., 2018).

The aggregation-prone domain of TDP-43 has been conserved, even its potential toxicity. One of the reasons seems to be the regulation of Stress Granules (SGs) formation. SGs are large structures conformed of proteins and RNA. These structures formed during cell stress are dynamic and reversible. Although the functions of SGs have not been fully elucidated, the most accepted theory

## *Introduction*

is the protection of the RNA during cell stress (Kedersha & Anderson, 2002; Nover, Scharf, & Neumann, 1989). TDP-43 is localized in SGs during stress, and it is essential for their assembly due to its RNA interaction, highlighting that TDP-43 self-assembly has a protective role against cell stress (McDonald et al., 2011).

Further structural studies demonstrated the capacity of TDP-43 to undergo a reversible phase transition mediated by its low complexity (LC) domain. This phase transition is based on the capacity of forming hydrogel particles from soluble proteins through polymerization (Kato et al., 2012). This physical phenomenon is called liquid-liquid phase separation (LLPS). It allows increasing a specific protein concentration at a particular cellular location, a fact particularly relevant for RNA Binding Protein (RBP) (Hyman, Weber, & Jülicher, 2014). It may be evolutionarily advantageous to concentrate TDP-43 where RNA is processed (Conicella et al., 2020).

As stated above, the toxic properties of aggregated TDP-43 are under debate. There is a manifest presence of TDP-43 aggregates in neurodegenerating neurons, but whether it is a cause or consequence and the biological effects remain unknown. Additionally, a high-throughput mutational screening in yeast demonstrated higher toxicity of TDP-43 mutations, which enhance its phase transition. They also observed a decreased toxicity in TDP-43 aggregation-prone mutation. The authors concluded that TDP-43 aggregation is a protective mechanism to prevent toxic phase transition (Bolognesi et al., 2019). However, this paradigm is demonstrated in yeast and with an exogenous TDP-43 overexpression. Therefore, the specific vulnerability of motor neurons and regular TDP-43 expression has not been taken into account.

SOD1 is also an aggregation-prone protein. It is misfolded and aggregated in fALS SOD1 linked patients. SOD1 aggregation may occur in sALS (Forsberg et al., 2010) and other fALS (Forsberg et al., 2019), although it is controversial (Da Cruz et al., 2017) and could be related to oligogenic forms (Kuuluvainen et al., 2019).

A proper formation of SOD1 functional and stable homodimers requires the presence of a zinc ion, a copper ion, and an intramolecular disulfide bond. At its turn, the addition of the copper ion requires a copper chaperone (CCS). Interestingly, some fALS mutations render a defective interaction between SOD1 and CCS (Wright, Antonyuk, & Hasnain, 2016). The absence of copper and reduced cysteines in the enzyme create an unstable hydrophobic motif. As a consequence, unstructured toxic apo-SOD1 oligomers are formed (Luchinat et al., 2014). Oligomers tend to form large aggregates, mainly in the proximal axons of motor neurons. These aggregates are interwoven intermediate filaments of 10-15 nm in diameter, resembling Lewi Bodies. A smaller proportion of aggregates appears as a granular, amorphous vesicular material. Aggregation of ubiquitinated apo-SOD1 starts at the pre-symptomatic stage in mice, increases in time, and probably disturbs axonal transport

## Introduction

(Bourassa, Brown, Borchelt, Vogt, & Miller, 2014; Jonsson et al., 2006; Sasaki et al., 2005). Enhancing SOD1 metal stabilization within CCS activity in transgenic mice has a considerable increase in survival (Williams et al., 2016). This fact reflects the importance of SOD1 maturation in the aggregation process and pathology.

SOD1 aggregation has been linked to the prion-like hypothesis. As in the case of TDP-43, there is no evidence for SOD1 infectious disease with human to human or zoonotic spreading. However, several *in vitro* and *in vivo* evidence for seeding and transmissibility have been reported (Ayers et al., 2014; Chattopadhyay et al., 2015; Chia et al., 2010; Ekhtiari Bidhendi et al., 2018; Grad et al., 2014; Christian Münch, O'Brien, & Bertolotti, 2011; Pokrishevsky, Hong, Mackenzie, & Cashman, 2017). In the case of SOD1, but not in TDP-43, animal to animal propagation has been established. Nevertheless, the authors suggested animal-animal transmission through indirect evidence using an uncommon model. They just see a faster disease of G85R-YFP fused mice when they injected spinal cord homogenates (not only SOD1 oligomers) from paralyzed G93A strain. Other strain combinations failed to worsen the disease, generating doubts about *in vivo* properties of prion-like propagators (Ayers et al., 2014).

C9ORF72 repeat expansion translation produces DPRs (poly-GR, poly-GP, poly-GA, poly-PR, and poly-PA), which can also form cytoplasmic aggregates (Mori et al., 2013). Poly-GA DPR is the most common DPR in C9ORF72-ALS (Mackenzie et al., 2015). Ultrastructural analysis reveals that poly-GA DPR is formed by large aggregates of 3  $\mu$ m in diameter of dense polymorphic ribbons (Q. Guo et al., 2018). Prion-like properties are less studied in DPRs, but they can be transmitted cell-to-cell and can induce TDP-43 aggregation (Khosravi et al., 2020; Westergard et al., 2016).

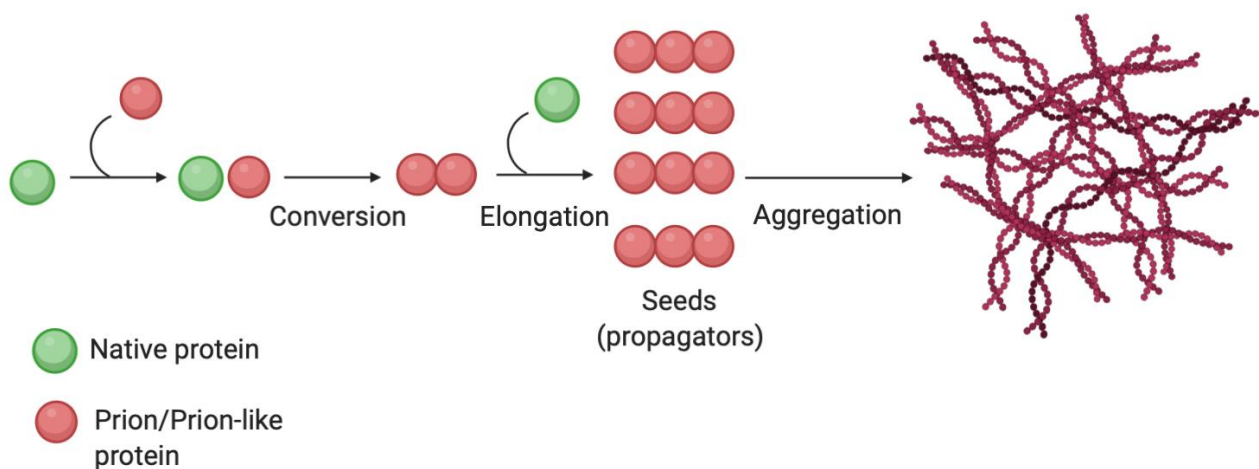


**Figure 11. Prion-like theory.** A prion is a misfolded protein with the ability to convert other native-folded forms of the same protein to prions. Prions can self-assemble to form seeds that are

## *Introduction*

propagated within the surrounding tissue. These seeds are eventually condensed in large aggregates (Composite using Biorender).

### **1.3.5 Autophagy dysregulation**

Autophagy was discovered in 1967 as an observation of liver mitochondria self-degradation within large lysosomes in rats (Deter & De Duve, 1967). However, it was in the early 1990s when Yoshinori Ohsumi and colleagues began to characterize the molecular effectors of the autophagy. In 1996 Ohsumi clones the first autophagy-related gene, APG5 (ATG5), in yeast (Kametaka, Matsuura, Wada, & Ohsumi, 1996). The work of Ohsumi and other researchers boost the knowledge of autophagy, and he won the Nobel Prize in 2016. The molecular mechanism of autophagy is exceptionally conserved across every eukaryote. However, it has not been described in prokaryotes. *Saccharomyces cerevisiae* genome encodes for 32 autophagy-related genes (Nakatogawa, Suzuki, Kamada, & Ohsumi, 2009) highly conserved in mammals. For a unified nomenclature, the use of ATG or Atg (autophagy-related) follow by a number is widely used in the literature (Klionsky et al., 2003).

Autophagy is thought to be a survival mechanism of the cell under stress situation. It can provide energy during starvation and remove damaged or aggregated proteins or organelle. However, it has been related to cell death (Kroemer & Levine, 2008), senescence (Young et al., 2009), and carcinogenesis (Mathew, Karantza-Wadsworth, & White, 2007), highlighting a complex and context-dependent role in cell fate. Autophagy can be divided into two groups: selective or non-selective. The first one consists of the degradation of misfolded or aggregated protein, damaged or over-abundant organelles, and invading pathogens. The recognition of cargo material within the receptors is crucial for this purpose.

On the other hand, non-selective autophagy occurs under starvation or cell stress in which cells catabolize some cell structures to obtain energy and overcome this situation. Mechanistically, there are three types of autophagy: macroautophagy, microautophagy, and chaperone-mediated autophagy. In macro-autophagy, a double-membrane structure engulfs the cargo (proteins and organelles) and forms the autophagosome. Autophagosome is fused with lysosomes to form autophagolysosomes to degrade the cargo. In microautophagy, the lysosome membrane is invaginated to take up the cargo. In chaperone-mediated autophagy, proteins are delivered to lysosomes through chaperones (like Hsc-70) and recognized by lysosomal receptor LAMP-2A. Macroautophagy (from now on, autophagy) is the most studied type and has been associated with several diseases.



## Introduction

In the first step of autophagy, mTOR complex initiates the formation of an isolated membrane from unknown origin (Díaz-Troya, Pérez-Pérez, Florencio, & Crespo, 2008). This complex integrates several inputs and regulates cell metabolism (Goberdhan, Wilson, & Harris, 2016). Nutrient starvation is a paradigm to study non-selective autophagy and the activation of mTOR. Selective autophagy is essential to maintain cell homeostasis (Dikic & Elazar, 2018). Depending on the severity of the stress, the number of the autophagosome and the size will be different. mTOR phosphorylates PI3KC3 Complex I and generates phosphatidylinositol 3-phosphate (PtdIns3P). At the initiation point, ATG8 must be cleaved by ATG4. After ATG8 cleavage, a glycine is exposed at the C-terminus. A ubiquitin-like system composed of ATG3 (E1) and ATG7 (E2) recognizes C-terminal glycine. PtdIns3P activates WIPI2b, which recruits ATG8 to the autophagosome within ATG16L1 of the ATG12–ATG5–ATG16L1 (E3) complex and conjugates cleaved ATG8 (LC3) with phosphatidylethanolamine (PE) (Dooley et al., 2014).

The next phase of autophagy is the elongation (maturation). In this step, the amount of phosphatidylethanolamine (PE)-conjugated ATG8 (LC3) determines the size of the autophagosome (Z. Xie, Nair, & Klionsky, 2008). Moreover, ATG8 confers the selectivity of the cargos (Turco & Martens, 2016). ATG4 catalyzes the ATG8-PE deconjugation. This step is critical to recycle ATG8 and allows the elongation (Hirata, Ohya, & Suzuki, 2017; Nakatogawa, Ishii, Asai, & Ohsumi, 2012). ATG4 has four family members (ATG4A, ATG4B, ATG4C, and ATG4D). ATG4 homologs differ in their activity and affinity. For example, ATG4B activity of processing ATG8 (LC3B) is 1500-fold higher than the other homologs. ATG4A prefers GABARAP-L2 to LC3B, whereas ATG4B processes all ATG8 homologs. ATG4C and ATG4D protease activity are shallow (Li et al., 2011; Tanida et al., 2004). ATG4B activity is regulated by post-translational modification, inhibited by oxidation (Scherz-Shouval et al., 2007), and activated by phosphorylation (Yang et al., 2015) and O-GlcNAcylation (Jo et al., 2016). ATG4B protein levels are regulated by ubiquitination and miRNAs, thus controlling basal autophagy and stress response (Kuang et al., 2012; Y. Wu et al., 2017). The dual role of ATG4 promoting PE conjugation and deconjugation of ATG8 makes it difficult to predict the final effect on ATG8-PE abundance. Elongation of autophagosome is also mediated by phospholipid transfer from the endoplasmic reticulum (ER) by Atg2 (Osawa et al., 2019). Although the lipid composition of autophagosome is poorly understood, different classes of phospholipids modify its physicochemical properties, modifying the shape, size, and mediating the cargo delivery (de la Ballina, Munson, & Simonsen, 2020).

The growing autophagosome engulfment of cargoes can be selective or non-selective. The *selective* form is based on the receptor ATG8, which recognizes adaptor molecules attached to the target. The most studied system is the p62/SQSTM1 adaptor. This protein adaptor recognizes poly-ubiquitinated cargos (like protein aggregates) and tethers them to autophagosome (Pankiv et al., 2007). SQSTM1 accumulates in the cytosol when autophagy is inhibited and is often used for its

## *Introduction*

monitoring (Bjørkøy et al., 2009). Cargoes can be misfolded proteins, mitochondrial (mitophagy), lysosomes (lysophagy), ER (ERphagy), peroxisomes (pexophagy), and nucleus (nucleophagy) (Anding & Baehrecke, 2017).

When autophagosome is finally closed, it is fused to the lysosome to form autophagolysosome. Autophagosomes are transported to the lysosomes through the microtubules-dynein system (Jahreiss, Menzies, & Rubinsztein, 2008). HOPS is a protein complex of vacuolar protein sorting 11 (VPS11), Vps16, VPS18, Vps33A, VPS39, and Vps41. It regulates the tethering of autophagosomes and lysosomes in yeast and mammals (Balderhaar & Ungermann, 2013; Solinger & Spang, 2013). Q-SNARE STX17 is a protein that interacts with the HOPS complex to induce the formation of autophagolysosomes (P. Jiang et al., 2014). The lysosome requires V-ATPase and the counterion transporter to generate an internal pH= 4.5-5 optimal hydrolytic enzymes (Mindell, 2012) in order to degrade its cargo.

A prominent feature of autophagy imbalance in ALS is the presence of cytoplasmic poly-ubiquitinated aggregated proteins. All forms of sALS and fALS are characterized by cytoplasmic inclusion, suggesting the autophagy dysregulation as a common disease mechanism. Most of the protein aggregates in ALS are ubiquitinated and positive for SQSTM1, indicating an initial but inefficient autophagic degradation (Brady, Meng, Zheng, Mao, & Hu, 2011; Gal et al., 2009). Moreover, mutations in several genes involved in autophagy, like *SQSTM1*, *UBQLN2*, *DCTN1*, *OPTN*, *PFN1*, *FIG4*, *C9ORF72*, *TBK1*, *VAPB*, *ALS2*, and *VCP* are found in fALS and sALS (H.-J. Chen et al., 2010; C. Y. Chow et al., 2009; Cirulli et al., 2015; DeJesus-Hernandez et al., 2011; Fecto et al., 2011; Hadano et al., 2001; J. O. Johnson et al., 2010; Maruyama et al., 2010; Christoph Münch et al., 2004; Osaka, Ito, & Suzuki, 2016; C.-H. Wu et al., 2012). These genes participate in different steps of autophagy (**Figure 12**).

## Introduction

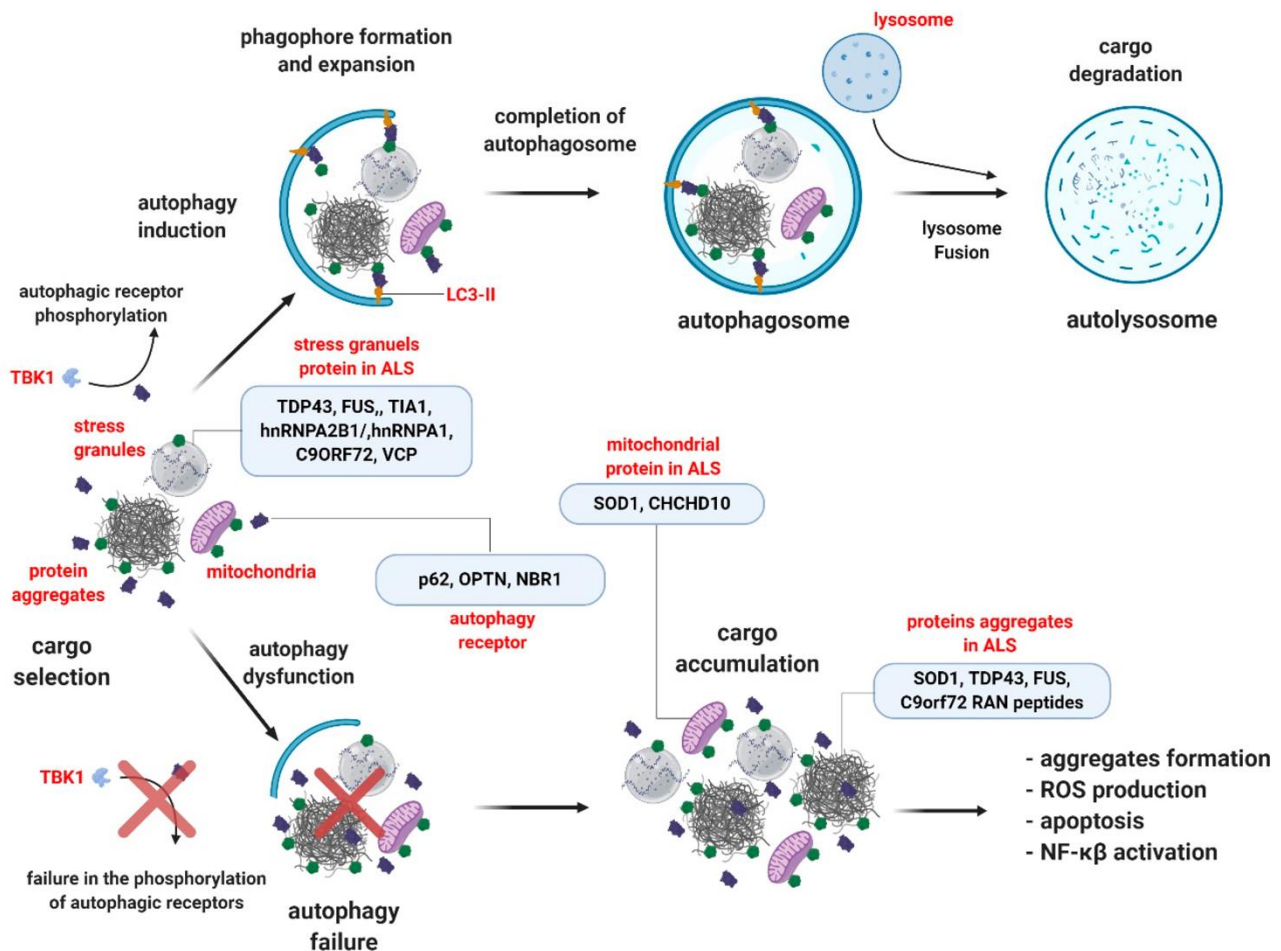


**Figure 12. Autophagy dysregulation in ALS.** Selective macroautophagy is a process in which the target proteins or organelles are degraded. This process starts with the phagophore formation engulfing the cargoes and finishes with the lysosome fusion and cargo degradation in autolysosomes. Several genes and molecular structures involved in autophagy (in red) are mutated or altered in ALS (Vicencio E et al 2020).

Neurons are mainly dependent on autophagy for proteostasis because they cannot dilute the toxic misfolded proteins and dysfunctional organelles by cell division (M. Damme, Suntio, Saftig, & Eskelinen, 2015). Motor neurons, due to its complex morphology and functions, are highly dependent on energy supply and vesicular transport. These cells need an efficient organelle quality control, like mitophagy, to remove damaged mitochondria to maintain a proper energetic metabolism (Palikaras, Lionaki, & Tavernarakis, 2015). Protein aggregates can compromise vesicular transport, necessary for autophagosome and lysosome function, and also axonal transport (F. Zhang et al., 2007).

However, we can only analyze and static final stage in the human disease. Different animal and cell models are used. To study this dynamic process, The abovementioned mutations in fALS and sALS are predicted to have some opposite effects in autophagy regulation (Nguyen, Thombre, & Wang, 2019). It could mean that either an overactivated or defective autophagy can be related to motor

## Introduction

neuron death. It also complicates possible therapies targeting autophagy. For example, rapamycin (an mTOR inhibitor) is a standard inductor of autophagy. Rapamycin has a protective role in *Tardbp* mutant mice (I.-F. Wang et al., 2012), whereas it exacerbates disease progression in *SOD1* mutant mice (X. Zhang et al., 2011). According to a study performed in *SOD1* mutant mice, autophagy may have a dual role in ALS depending on disease stage and cell type. Authors conclude that autophagy in motor neurons is required to prevent muscular denervation in the early stages, but it has a detrimental role late in the disease in a non-cell-autonomous manner (Rudnick et al., 2017).

Autophagy disturbances are implicated in ALS pathogenicity. There are several molecules and therapeutic interventions to enhance or inhibit autophagy in every step. However, how and when target autophagy in ALS is under debate.

### 1.3.6 Nucleocytoplasmic transport impairment

Nucleocytoplasmic transport is a regulated connection between the nucleoplasm and the cytoplasm. This connection is mainly driven by the Nuclear Pore Complex (NPC). NPC is a large complex of approximately 110 MDa (Hoelz, Glavy, & Beck, 2016), and it is formed by high conserved proteins termed Nups. Structurally, Nups are divided into seven groups: cytoplasmic filament Nups, nucleoplasmic and cytoplasmic ring Nups, inner ring complex Nups, transmembrane Nups, central Nups containing phenylalanine-glycine (FG) repeats, nuclear basket Nups, and adaptor Nups.

NPC is formed by a scaffold structure consisting of symmetrical nucleoplasmic and cytoplasmic ring, and the inner ring complex between them. These parts of the NPC contain hundreds of copies of the same protein. FG-Nups project their intrinsically disordered Low Complex Domain (LCD) of phenylalanine, and glycine repeats into the center of the channel (**Figure 13**). Some authors postulate that FG-Nups create a selective barrier by phase separation of hydrogel properties of LCD. It allows the free transport of less than 40 KDa molecules and active transport for larger molecules (Hoelz, Debler, & Blobel, 2011).

Nucleocytoplasmic transport is carried out by exportins and importins proteins. This active transport consists of a differential gradient of Ran-GTP (enriched in the nucleoplasm) and Ran-GDP (enriched in the cytoplasm). Importins usually couple the Nuclear Localization Signal (NLS)-containing cargo with the RanGTP-RanGDP gradient to import proteins to the nucleus. Exportins recognize Nuclear Export Signal (NES)-containing cargo and couple de RanGTP gradient with the nuclear export (Cautain, Hill, De Pedro, & Link, 2015). Other molecules, including tRNA, miRNA, snRNA, and ribosomal RNA export, are also coupled with the RanGDP-RanGTP gradient. However, mRNA export does not depend on this gradient. The mRNP complex binds to nascent pre-mRNA, and, after maturation, it is recognized by NXF1-NXT1 and TREX that mediate the export. (Köhler & Hurt,

## Introduction

2007). Once in the cytoplasm, some mRNPs are modified to preclude the return to the nucleus, ensuring unidirectional mRNA transport (Ma et al., 2013).

Homozygous recessive mutations in a gene encoding for mRNA export regulator *GLE1* is linked to Lethal congenital contracture syndrome 1 (LCCS1). LCCS1 is often lethal in the fetal period. When the carriers are born, they develop the most severe form of arthrogyrosis in children. This disease is characterized by the loss of spinal motor neurons (Vuopala, Ignatius, & Herva, 1995). Interestingly, heterozygous deleterious mutations in *GLE1* are associated with adult-onset ALS, suggesting a haploinsufficiency mechanism (Kanab et al., 2015). This phenomenon highlights the specific vulnerability of motor neurons to mRNA transport disturbances.

Moreover, *C9ORF72* HRE also leads to mRNA export and NPC structural disturbances. *C9ORF72* HRE toxicity is enhanced by additional mutations in several mRNA export modulators (Freibaum et al., 2015; Y. J. Zhang et al., 2016). Another proposed toxic mechanism for nucleocytoplasmic transport impairment is related to protein aggregation. TDP-43 pathological aggregates in human samples contain components of nucleocytoplasmic transport pathways. FG-Nups, due to their LCD (a Prion-like domain), are aggregation-prone components. FG-Nup aggregation leads to the nuclear envelope and NPC assembly defects. Consequently, it impairs protein and RNA nucleocytoplasmic transport (Chou et al., 2018). Furthermore, importin mislocalization is also present in ALS, and it has been associated with DPR pathology and TDP-43 mislocalization (Aizawa, Yamashita, Kato, Kimura, & Kwak, 2019; Solomon et al., 2018).

One of the mechanisms for ensuring a proper protein location is the presence of NLS. Mutations in NLS of *FUS* and *HNRNPA1*, RNA binding proteins, are linked to ALS (Gal et al., 2011; Q. Liu et al., 2016). Although, any *TARDBP* mutation in NLS has not been determined in ALS. *TARDBP*  $\Delta$ NLS expression has been used to reproduce TDP-43 pathology in animal and cellular models (Che, Jiang, Xie, Jiang, & Hu, 2011; L.-L. Jiang et al., 2017; Walker et al., 2015). TDP-43 is a predominately nuclear protein. However, it is shuttled continuously to the cytoplasm in a transcription-dependent manner (Y. M. Ayala et al., 2008). Nuclear import of TDP-43 is an active transport mediated by Importin- $\alpha$ , whereas nuclear export is a passive mechanism (Pinarbasi et al., 2018). Nuclear clearance of TDP-43 is likely to be an early event in human diseases. Neurons that display TDP-43 nuclear loss exhibit atrophic phenotype independently of TDP-43 cytoplasmic inclusions (Nana et al., 2019). When TDP-43 cannot bind to pre-mRNA in the nucleus, hundreds of genes are dysregulated. This situation can be defined as a “transcriptomopathy”, affecting several molecular pathways (L.-S. Wu et al., 2019).

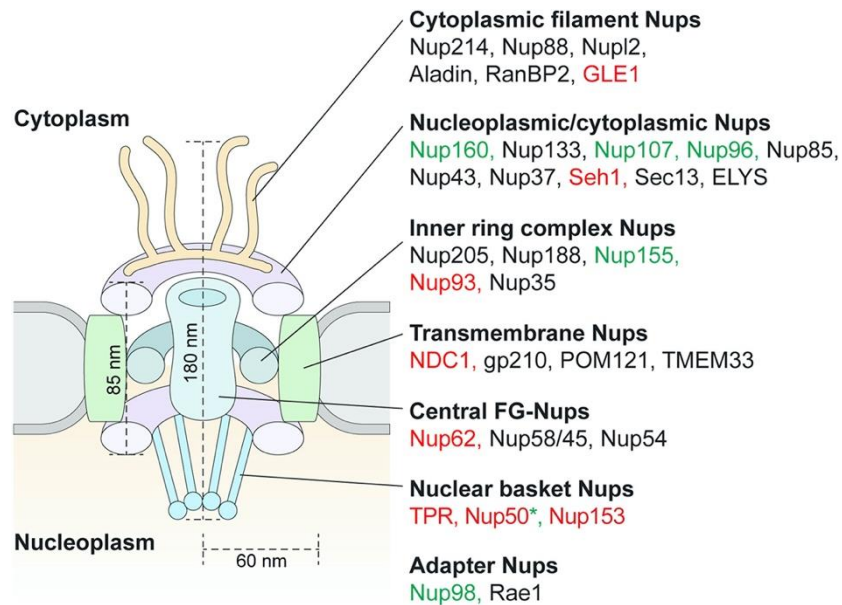


**Figure 13. NPC structure.** NPC is a large complex formed by Nups. Nups are divided into seven groups according to their relative position in NPC. Components in which loss of function (LOF) suppresses or in which gain of function (GOF) enhances degeneration in yeast and flies C9ORF72 HRE models are labeled green, whereas components in which LOF enhances or GOF suppresses degeneration are colored in red (Kim HJ and Taylor JP 2017).

The product of the *TARDBP* gene (TDP-43) can also be located in mitochondria. The role of mitochondrial TDP-43 has not been fully elucidated since it is a relatively recent discovery (W. Wang et al., 2016). In a normal situation, TDP-43 is located in mitochondria in selected neuronal populations in both young and aged mice (Termsarasab et al., 2020), indicating that TDP-43 is a physiologically neuronal mitochondrial protein. Soluble TDP-43 is present in the mitochondrial matrix and it has a specific sequence for its insertion to this organelle. In mitochondria, TDP-43 negatively regulates the respiratory subunit of complex I *ND3* and *ND6* mRNA by binding to UG repeats. In ALS subjects, mitochondrial TDP-43 amount is higher than control ones, compromising Complex I assembly and bioenergetic metabolism (W. Wang et al., 2016). Mitochondrial TDP-43 location is regulated by its expression and by the mitochondrial Unfolded Protein Response (UPR<sup>mt</sup>), the quality control system for mitochondrial proteins. LonP1 protease is a member of UPR<sup>mt</sup> and mediates TDP-43 mitochondrial degradation. Both wild type TDP-43 and A315T mutant TDP-43 overexpression lead to mitochondrial dysfunction (complex I disassembly and ROS production), partially prevented by UPR<sup>mt</sup> (P. Wang et al., 2019). Other TDP-43 functions in this organelle are both the mitochondrial biogenesis and the mitophagy by interacting with MFN2 and PHB2. Interestingly, there are low levels of full-length TDP-43 and higher levels of N-terminal 27 KDa and C-terminal 30 KDa fragments in mitochondria. These fragments can be produced by the mitochondrial peptidase PMPCA (Davis et al., 2018). These facts highlight the role of peptidases for TDP-43 mitochondrial location linked to toxic effects in ALS and to possible new targets for drug discovery.

### 1.3.7 Cryptic exon transcriptomopathy

Splicing can be defined as the process of joining two coding regions of pre-mRNA (the product of the transcription by RNA polymerase II) denominated exons, and the removal of non-coding sequences, termed introns (Berget, Moore, & Sharp, 1977; L. T. Chow, Gelinis, Broker, & Roberts, 1977). This process is conserved in all eukaryotes and appeared early in evolution. Splicing is necessary to prevent intron translation that would lead to aberrant protein synthesis. Introns are highly variable, dynamic, and poorly conserved in the mRNA of eukaryotes (Mlguyera, 2005). There are some points in evolution that have triggered a massive intron gain, being mammals and birds the eukaryotic lineage with a higher intron per gene ratio (Mlguyera, 2005). The origin of introns and splicing remains controversial, although there are some plausible explanations like the 'intron invasion' theory. In this theory, the primitive mitochondrial endosymbiont introduced group II retroelements with the capacity to auto-insert in the host cell genome (the precursor of the nuclear genome). This invasion gave rise to selective pressure for the nuclear compartmentalization to separate nuclear unspliced RNA (which would lead to aberrant polypeptides) from cytosolic ribosomes (Martin & Koonin, 2006).

Splicing can be classified into two types according to the frequency of a given splicing event. Constitutive splicing comprises the changes impinged to a set of exons that are included in all mRNA isoforms of the gene. On the other hand, Alternative Splicing (AS) of a gene can produce distinct mRNAs depending on the included exons. It allows a great increase in the proteome complexity (Yansheng Liu et al., 2017), AS being regulated by *cis*- and *trans*-acting elements (**Figure 14**). These elements regulate the recognition of the exon by the spliceosome, the protein complex that removes the introns and joins exons. Spliceosome joins the 5' splice site (5' ss) with the 3' splice site (3' ss) of the following exon. Branch point and polypyrimidine tract are conserved elements necessary to spliceosome assembly. *Cis*-acting elements are sequences in exonic or intronic regions that promote or repress exon splicing. *Trans*-acting elements are proteins that bind to *cis*-acting elements and interact with spliceosome. Serine-Rich (SR) proteins bind to pre-mRNA *cis*-acting elements Exon Splicing Enhancers (ESE) and Intron Splicing Enhancers (ISE) to promote the splicing. On the other hand, heterogeneous nuclear ribonucleoproteins (hnRNPs) bind to Intron Splicing Silencers (ISS) and Exon Splicing Silencers (ESS) to inhibit the splicing. All these elements form the splicing code (**Figure 14**) (Matlin, Clark, & Smith, 2005).

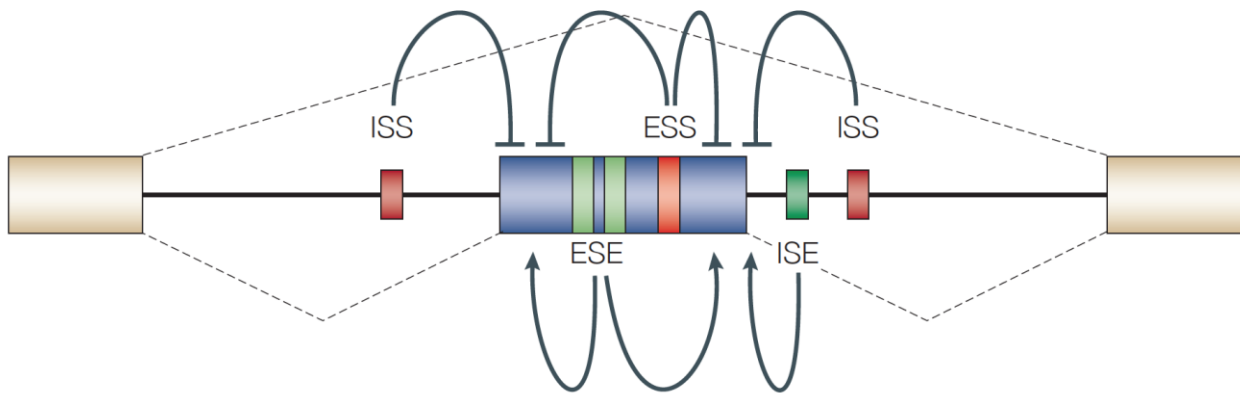


**Figure 14. Splicing regulatory elements.** The splicing decision depends on cis- and trans-elements. SR proteins bind to ESE and ISE to enhance the splicing, whereas hnRNPs bind to ESS and ISS to repress it (Matlin AJ et al 2005).

Cryptic splicing is a specific form of AS that leads to the inclusion of a deleterious sequence in the mRNA. It is constantly taking place in cells but usually at a low rate (Kapustin et al., n.d.). In cryptic splicing, the spliceosome complex recognizes a wide range of (degenerate) splice sites, branch point and polypyrimidine tract. Therefore, there are numerous cryptic splice sites (Faustino & Cooper, 2003). Cryptic splicing alteration can be activated within *cis*-acting element mutations and are often associated with human diseases (Cartegni, Chew, & Krainer, 2002). Moreover, hnRNPs can also prevent the use of cryptic splice sites. This is the case of TDP-43 cryptic exon repression (J. P. Ling, Pletnikova, Troncoso, & Wong, 2015).

Nevertheless, cryptic exons can lead to the formation of new (premature) exons (Sorek, 2007), as a part of evolution. Assuming, that evolution depends on genetic variation, variants that contribute to a better adaptation to the environment will be fixed (i.e. selected), whereas those which cause a deleterious effect tends to be removed. Thus, it is considered that one of the processes that generate genetic variation is the exonization of an intron using a cryptic splice site. However, it often drives to a random sequence introduced in the mRNA and potentially to an aberrant protein (Sorek, 2007).

The mechanism of the cell to control the impact of these novel exons in the proteome is the alternative splicing coupled with the surveillance of aberrant mRNAs. These transcripts frequently contain a Premature Termination Codon (PTC), which are removed by Non-sense mRNA Mediated Decay (NMD) (McGlinicy & Smith, 2008). The AS process, coupled with NMD, allows a higher variability in the transcriptome to be tested by evolutionary forces without compromising the integrity and the functionality of the proteome (Sorek, 2007). 74% of human genes contain one or more alternative exon (J. M. Johnson et al., 2003), with approximately 35% of these contain a PTC predicted to be removed by NMD, and just 5.8% of the proteins derived from PTC-containing mRNA



## *Introduction*

are translated (Hillman, Green, & Brenner, 2004). Nevertheless, experimental data shows that upper frameshift protein 1 (UPF1), the supposed principal regulator of NMD, just regulates a small extent of PTC-containing mRNAs (Pan et al., 2006), suggesting a tight control at the splicing level.

To maintain a low inclusion ratio of new exonized sequences in mRNA, hnRNPs prevent their splicing (Z. Wang & Burge, 2008). TDP-43 is a member of this gene family (Buratti & Baralle, 2008), showing a high affinity for UG dinucleotide repeats. TDP-43 is bound to UG repeats through its RRM1 and RRM2 motifs and it is able to regulate (either repress or enhance) the inclusion of exon enriched in UG repeats (Buratti et al., 2001). The binding TDP-43 to its target pre-mRNA prevents the inclusion of a large number of non-conserved (cryptic) exons (new exonized sequences) that contains a UG tract close to 3' splicing site (SS) or/and 5'SS (J. P. Ling et al., 2015). The repression of cryptic splicing is shared with other hnRNPs, as PTBP1 and PTBP2, which also repress cryptic exons with CU repeats (Jonathan P. Ling et al., 2016), hnRNP L affecting those exons with CA repeat (McClory, Lynch, & Ling, 2018) and hnRNP C inhibits the exonization of Alu elements (Zarnack et al., 2013). Specifically, UG repeats form a secondary structure that enhances the splicing depending on the number of repeats and the propension to hairpin formation (Hefferon, Groman, Yurk, & Cutting, 2004). However, the importance of the secondary structure on splicing (Jin, Yang, & Zhang, 2011) and the difficulty to predict the folding of pre-mRNA, hinder the anticipation of the TDP-43 effect on the splicing. TDP-43 can either promote or repress the splicing of a given target, so we could only indicate the final effect (inclusion or exclusion) based on experimental data at today's date (Passoni, De Conti, Baralle, & Buratti, 2012). Noteworthy, the position of UG tract near 3'SS or 5'SS and the distance from the polyA site (Rot et al., 2017) influence the splicing activity of TDP-43, but not in all cases. Usually, known cryptic exons are all repressed by TDP-43, contain the UG tract upstream and/or downstream of 3'SS and 5'SS, being located at different distances from the polyA site (J. P. Ling et al., 2015).

The origin of UGs in the pre-mRNA is the simple sequence repeat (SSR) or microsatellite 'AC' in the genome. This SSR is the most common dinucleotide repetition in the human genome (Tóth, Gáspári, & Jurka, 2000), accounting for 0.25% of the whole sequence (Lander et al., 2001). For this reason, they have a higher probability to reside in a proper location to act as a splicing modulator. Moreover, repetition motifs are polymorphic both between different species and in the same specie (Tóth et al., 2000) due to the replication slippage (Ellegren, 2004). This phenomenon can explain the low conservation of cryptic exons. Replication slippage of AC repeats depends on the length and the purity (Ellegren, 2004; Vergnaud & Denoeud, 2000). A mutation that disrupts the purity of the repetition can stabilize the SSR. Interestingly, the most frequent number of repetitions of TDP-43-regulated cryptic exons is just two UG, which implies a low number of repetitions needed to exonize a sequence via UG repeats. It gives rise to a potentially large number of genes containing cryptic exons (predicted to be more than 1000 genes) (Q. Tan et al., 2016). TDP-43 also regulates

## Introduction

conserved exons (Hefferon et al., 2004) within the same mechanism but in a lower proportion (J. P. Ling et al., 2015). Interestingly, UGUGU and GUGUG motifs are enriched beside 5'ss in conserved exons and potentially could serve as a 'genetic buffer'. Genetic buffers allow changes of nucleotides in the 5' ss that otherwise will diminish the splicing of the exon. It is important to increase the variability of sequences (and amino acids) in 5' ss (Xiao et al., 2009).

Therefore, cryptic exons are random sequences inserted in mRNA and are not derived from transposable elements. These cryptic exons contain weak splicing signals (acceptor and donor), slightly different from the consensus (Humphrey, Emmett, Fratta, Isaacs, & Plagnol, 2017). TDP-43 does not act alone in splicing and other *cis*- and *trans*-acting elements can be present in TDP-43-regulated genes. An example of this complex regulation is the splicing of the constitutive apoA-II exon 3. In this context, TDP-43 (splicing repressor), an ESE and an ISE play a role in the splicing outcome. The ESE is located in exon 3. It is highly conserved and essential for the inclusion of the exon. However, a long and poor conserved UG tract is present only in humans (16 UG repeats) and chimpanzees (17 UG repeats) but absent in mice. This UG tract acts as a *de novo* binding site for TDP-43 which represses the splicing in humans and chimpanzees. TDP-43 splicing repression is balanced with an ISE in both species. Moreover, TDP-43 depletion is enough to induce the splicing, even without the ESE and the ISE (Mercado, Ayala, Romano, Buratti, & Baralle, 2005). It suggests that an unbound UG tract can promote exonization. Therefore, TDP-43 and other hnRNPs can be considered as the guardians of the transcriptome since they prevent cryptic exon transcriptomopathy. In this sense, cryptic exon transcriptomopathy (e.g. induced by TDP-43 dysfunction) could result in an asymmetric impact in affected transcripts, depending on the inclusion rate and the position. The possible outcomes are NMD (downregulation), in-frame insertion (extra sequence) or upregulation (J. P. Ling et al., 2015). Moreover, TDP-43 sensitive cryptic exons are highly variable between cell types (Jeong et al., 2017).

The fact that rodents do not exhibit these characteristics is still unknown. The presence of TDP-43 pathology is controversial in SOD1 forms of fALS (G. S. Jeon et al., 2019; Mackenzie et al., 2007; Shan, Voadlo, & Krieger, 2009; Zeineddine, Farrarwell, Lambert-Smith, & Yerbury, 2017). In this thesis, we evaluated TDP-43 loss of function and the extent of cryptic splicing in this model. Finding commonalities could help in the understanding of the disease and the discovery of better targets for therapy.

### 1.3.8 Neuroinflammation and aging

Inflammation is a physiological response to harmful conditions, such as tissue injury or invading pathogens. In an acute phase, inflammation has a beneficial role, promoting tissue remodeling and pathogen elimination. However, chronic inflammation can be detrimental, and it is associated to age-

## Introduction

related diseases. Inflammatory cells produce cytotoxic molecules, which normally kill pathogens or infected cells, but side effects include tissue damage.

One of the characteristics of aging is a sterile chronic mild-inflammation dubbed inflammaging (Franceschi & Campisi, 2014). In inflammaging, aging cells accumulate damaged organelles and macromolecules which can induce an inflammatory response which consists of the release of intracellular components (ATP, peroxidized fatty acids, cardiolipin, etc.) , that would trigger an activation of immune (or inflammatory) cells (Franceschi & Campisi, 2014). Moreover, damaged mitochondria generate oxidative stress, increasing molecular damage. These signals are integrated into the NLRP3 inflammasome pathway, which promotes caspase-1 activation and IL-1 $\beta$  pro-inflammatory cytokine secretion. Mitochondrial derived molecules, due to its bacterial origin, are the main source of inflammasome activation (Q. Zhang et al., 2010).

Another link between inflammation and aging is the cellular senescence. This process was first described by Leonard Hayflick as a limit to the replication of diploid cells *in vitro* (Hayflick, 1965). Senescent cells become larger, flatten out, increase their granularity and the borders tend to vanish (Schmitt, 2007). Moreover, an increase in Senescence-Associated  $\beta$ -galactosidase (SA- $\beta$ -gal) activity, related to a higher content of lysosomes, is also a common marker in senescent cells (Kurz, Decary, Hong, & Erusalimsky, 2000). Apart from a physiological limitation derived from the telomere shortening after mitotic division, cellular senescence participates in pathological processes. In 1997, Serrano et al., discovered the molecular effectors of cellular senescence. They highlight for the first time that cellular senescence is also an antitumoral mechanism. When an oncogenic gene (*ras*) is overactivated in primary cells, it induces cell cycle arrest with a senescent phenotype mediated by p53 and cell cycle inhibitors p16<sup>INK4a</sup> and p21<sup>CIP1</sup> (Serrano, Lin, McCurrach, Beach, & Lowe, 1997). In this line, different types of cell stress, including oxidative stress, can induce DNA damage and potentially generate detrimental mutations and carcinogenesis. To prevent the transmission of these mutations, cells can undergo senescence. However, the cellular senescence process is highly variable between cell types and its definition is currently under debate (Hernandez-Segura, Nehme, & Demaria, 2018). Senescent cells are dysfunctional and normally secrete different pro-inflammatory paracrine cytokines to trigger tissue remodeling. This secretory phenotype is known as Senescence-Associated Secretory Phenotype (SASP) (**Figure 15**) (Coppé et al., 2008).

Although SASP can be considered a physiological response to repair the tissue after injury or stress, it may have detrimental effects such as promoting chronic inflammation. Cellular senescence and SASP has been linked to several age-related diseases, such as cancer, Type-2 diabetes, atherosclerosis, among other SASP is composed of a myriad of secreted molecules. Although it is highly variable depending on cell type, SASP normally includes interleukins (IL-1 $\alpha$ , IL-1  $\beta$ , IL-6) and chemokines (IL-8, CXCL1), among other molecules to orchestrate an inflammatory response (He &

## Introduction

Sharpless, 2017). Indeed, senescent glial cells and SASP have been recently observed in Alzheimer (AD) (Musi et al., 2018; P. Zhang et al., 2019) and Parkinson's Disease (PD) (Chinta et al., 2018) animal models, suggesting an unanticipated role in neurodegeneration. Whether these changes are also present in ALS is still unknown but as happens in other molecular changes (protein aggregation, oxidative stress, neuroinflammation...), senescence and SASP could happen in ALS.

The benefits of eliminating senescence cells (*senolysis*) was first described in animal models genetically altered. The addition of a suicide gene under p16 promoter induces apoptosis in senescent cells and prevents age-related disorder in a progeroid mouse model (D. J. Baker et al., 2011). Moreover, clearance of senescence cells also increases lifespan and decreases age-related pathologies (including cancer, kidney dysfunction and cardiomyocyte hypertrophy) in mouse physiological aging (D. J. Baker et al., 2016). Other examples of the senolysis benefits are found in post-traumatic osteoarthritis (O. H. Jeon et al., 2017), acute myeloid leukemia (Abdul-Aziz et al., 2019), age-associated intervertebral disc degeneration (Patil et al., 2019), obesity-related anxiety (Ogrodnik et al., 2019) and Alzheimer (Musi et al., 2018; P. Zhang et al., 2019). However, these examples of senolysis were driven by transgene expression of a suicide gene, without a clear translation to the clinic. The emergence of specific drugs that selectively kill senescent cells (senolytics) has recently revolutionized this field. In 2013, the Kirkland group speculated with the feasibility of using senolytics to treat age-related human diseases based on the distinct morphology, secreted protein patterns, and gene expression profiles of senescent cells (Tchkonia, Zhu, Van Deursen, Campisi, & Kirkland, 2013). Although exhibiting an active DDR, a high concentration of pro-apoptotic cytokines and other toxic factors, senescent cells do not undergo apoptosis by itself and must be killed by immune cells (Xue et al., 2007). Apoptosis is a type of Programmed Cell Death (PCD) executed by caspases and triggered by mitochondrial depolarization (intrinsic pathway) or external receptors (extrinsic pathway). Kirkland group analyzed transcriptomic changes behind senescent cells and found an increase in anti-apoptotic genes. Based on that, they screened several drugs and found that the apoptosis inhibitors Dasatinib and Quercetin were able to specifically kill senescent cell *in vivo* and *in vitro* (Zhu et al., 2015). Additionally, the same article described the use of senolytic siRNAs targeting EFNB1 or 3, PI3KCD, p21, BCL-xL, and PAI-2. Moreover, Dasatinib and/or Quercetin also had a modest effect in increasing healthspan in progeroid mouse (Zhu et al., 2015). Another inhibitor of an anti-apoptotic pathway, ABT-263 (Navitoclax), also kills senescent cells specifically. This drug is a Bcl-2 family member inhibitor and its senolytic effect depends on the expression of its targets (Zhu et al., 2016). Due to the variability of genes that are required for a specific cell type senescence, senolytics do not eliminate all senescent cells (Zhu et al., 2015). The use of senolytics in age-related chronic disease could mean an extremely long-term RCTs due to human longevity. Additionally, its use may also have side-effects inhibiting the physiological roles of senescence (Demaria et al., 2014).

## *Introduction*

The first hypothesis of the cellular senescence as a major pathological mechanism in neurodegenerative disorders was postulated in 2009 (Golde & Miller, 2009). In this article, the authors proposed a positive feedback loop between proteinopathy, chronic inflammation and senescence in AD. Interestingly, they speculated that astroglia, microglia and neurons could be senescent. Neuronal senescence is somehow contradictory since these cells are normally post-mitotic. However, like many other cells, they can harbor senescence markers, including changes in morphology, lipofuscin granules and expression senescence and SASP genes (F. C. C. Tan, Hutchison, Eitan, & Mattson, 2014). Important evidence supporting this hypothesis is the amelioration of animal models of PD and AD after a senolytic treatment (Chinta et al., 2018; Musi et al., 2018; P. Zhang et al., 2019).

Microglia is the specialized monocyte in nervous tissue and the main regulator of neuroinflammation. However, these cells have multiple physiological and pathological roles (Prinz & Priller, 2014). They can proliferate and change their phenotype when an insult occurs. Protein aggregates and cell debris release trigger a change from the M2 anti-inflammatory microglia phenotype to the M1 (activated) cytotoxic microglia. M1 microglia can release pro-inflammatory cytokines (IL-6, TNF $\alpha$ , IL-1 $\beta$ , among others), ROS and mediate neuronal phagocytosis, thus damaging motor neurons in ALS and exacerbating the inflammation (Henkel, Beers, Zhao, & Appel, 2009). Moreover, the degree of microglial activation is associated with the disease progression in ALS patients and mouse models (Gargiulo et al., 2016; M. R. Turner et al., 2004). Interestingly, microglia can be senescent. This process takes place in the aging brain. Senescent microglia display morphological changes and an increase in SASP cytokine (TNF $\alpha$ , IL-1 $\beta$ , IL-6) release (Sierra, Gottfried-Blackmore, McEwen, & Bulloch, 2007).

Besides microglia, other cell could be involved in central nervous system potential senescent changes. Astrocytes are the main support cells for neurons but, similarly to microglia, they also have a double edge sword role in ALS. In a normal situation, astrocytes metabolically sustain motor neurons and uptake Ca<sup>2+</sup> excess from synapses. However, some ALS astrocytes become cytotoxic and stop metabolic support and Ca<sup>2+</sup> uptake (Nagai et al., 2007; Jeffrey D. Rothstein et al., 1995). Toxic effects from mutated cells to other non-mutated cells are termed non-cell autonomous. Non-cell autonomous effects are present in ALS (Nagai et al., 2007), and different mutations in a specific cell type can lead to opposite effects in a complex oligogenic manner (Germino et al., 2020). Astrocytes from ALS donors and mouse models express higher levels of pro-inflammatory mediators (prostaglandin E2, leukotriene B4, nitric oxide, and NOX2), thus contributing to neuroinflammation (Haidet-Phillips et al., 2011; Hensley et al., 2006; Marchetto et al., 2008). There is an increase of senescent astrocytes in AD, probably induced by the exposure of extracellular aggregates. These cells secrete pro-inflammatory IL-6 cytokine, a component of SASP (Bhat et al., 2012).

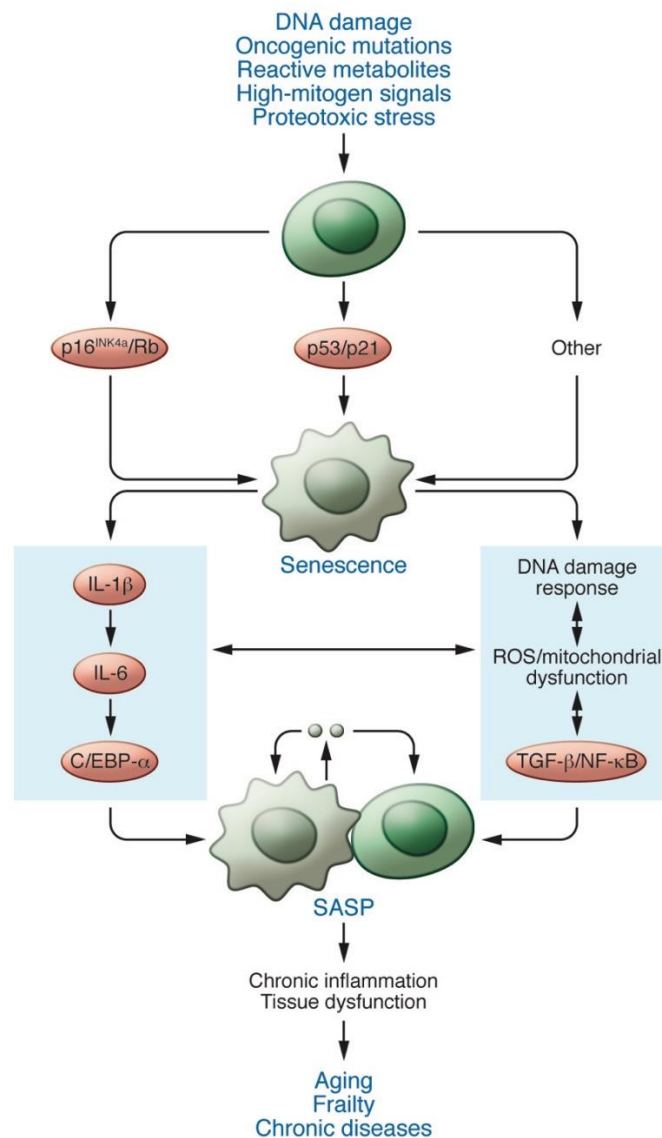


**Figure 15. Senescence and SASP pathway.** Different cell stressors damage DNA and induce cellular senescence activating p53/p21 and p16/Rb cell cycle inhibitors. Senescent cells secrete several pro-inflammatory molecules (SASP) with paracrine effects. SASP promotes chronic inflammation and is associated with age-related diseases (Tchkonia T et al 2013).

Anti-inflammatory agents have been widely used since centuries ago to stop the detrimental effects of inflammation. These drugs target initial pro-inflammatory pathways, preventing leukocyte infiltration and blocking the release of cytotoxic molecules. For example, aspirin and other NSAIDs, inhibit the production of prostaglandins, pro-inflammatory lipid mediators derived from n-6 PUFA arachidonic acid by COX enzyme catalysis (Poorani, Bhatt, Dwarakanath, & Das, 2016). However, the resolution of inflammation is not a passive process. Antagonizing key pro-inflammatory mediators does not lead to a permanent resolution. Resolution implies the clearance of apoptotic cells and microbes from inflamed tissue, which is not achieved by inhibiting inflammation (Serhan et al., 2007). The discovery of n-3 PUFA DHA and eicosapentaenoic acid (EPA) derived pro-resolution molecules

## *Introduction*

has opened a new window to manage inflammatory diseases (Schwab, Chiang, Arita, & Serhan, 2007). These molecules are often termed Specialized Pro-resolving Mediators (SPMs).

There are four classes of SPMs: resolvins, protectins and maresins. SPMs are synthesized from n-3 PUFAS DHA (D-series resolvins and protectins), EPA (E-series resolvins) and docosapentaenoic acid (DPA) (D-series resolvins and maresins) and lipoxins (arachidonic acid). The main source of these FAs is the dietary intake (fish oil) or supplementation, besides endogenous synthesis from dietary available precursors (Calder, 2015). SPMs synthesis requires several steps mediated by LOX and acetylated COX-2 and has biological effects even at pico-nanograms in tissue (Serhan et al., 2002). Their actions include cessation of polymorphonuclear cell (PMNs) infiltration, enhancement of macrophage phagocytosis of apoptotic PMNs, cells debris and microbes, as well as transcriptional and translational changes, shortening of time to resolution and reduction of pain (Serhan & Levy, 2018).

SPMs have demonstrated benefits in hepatobiliary surgery, coronary artery disease, traumatic brain injury and cancer-associated inflammation (Serhan & Levy, 2018). Moreover, recent studies reveal decreased levels of resolvins in neurodegenerative diseases and a positive effect of resolvins treatment in animal models of AD and PD (Kantarci et al., 2018; Krashia et al., 2019). Regarding ALS, DHA levels are decreased in the spinal cord of patients, suggesting an impaired metabolism (Ilieva et al., 2007). Also, a population-based case-control study found elevated fish consumption, the main source of n-3 PUFAs, associated with a lower risk of ALS (Filippini et al., 2020). Furthermore, DHA and especially Resolvin D1 (1100 times greater potency than DHA) prevent cytokine pro-inflammatory (IL-6 and TNF- $\alpha$ ) production from ALS macrophages and neuronal death (G. Liu et al., 2012).

Whether DHA supply is able to modulate ALS damage in experimental models is still unknown. Previous publications of the group revealed that a high polyunsaturated fatty acid content in diet accelerate the disease in hSOD1-G93A male mice. Nevertheless, antagonistic effects of n-6 and n-3 PUFA was not addressed in this work. Although DHA is a pro-resolvin molecule, it is also high susceptible to be oxidized. Hence, the potential role in ALS is ambiguous.

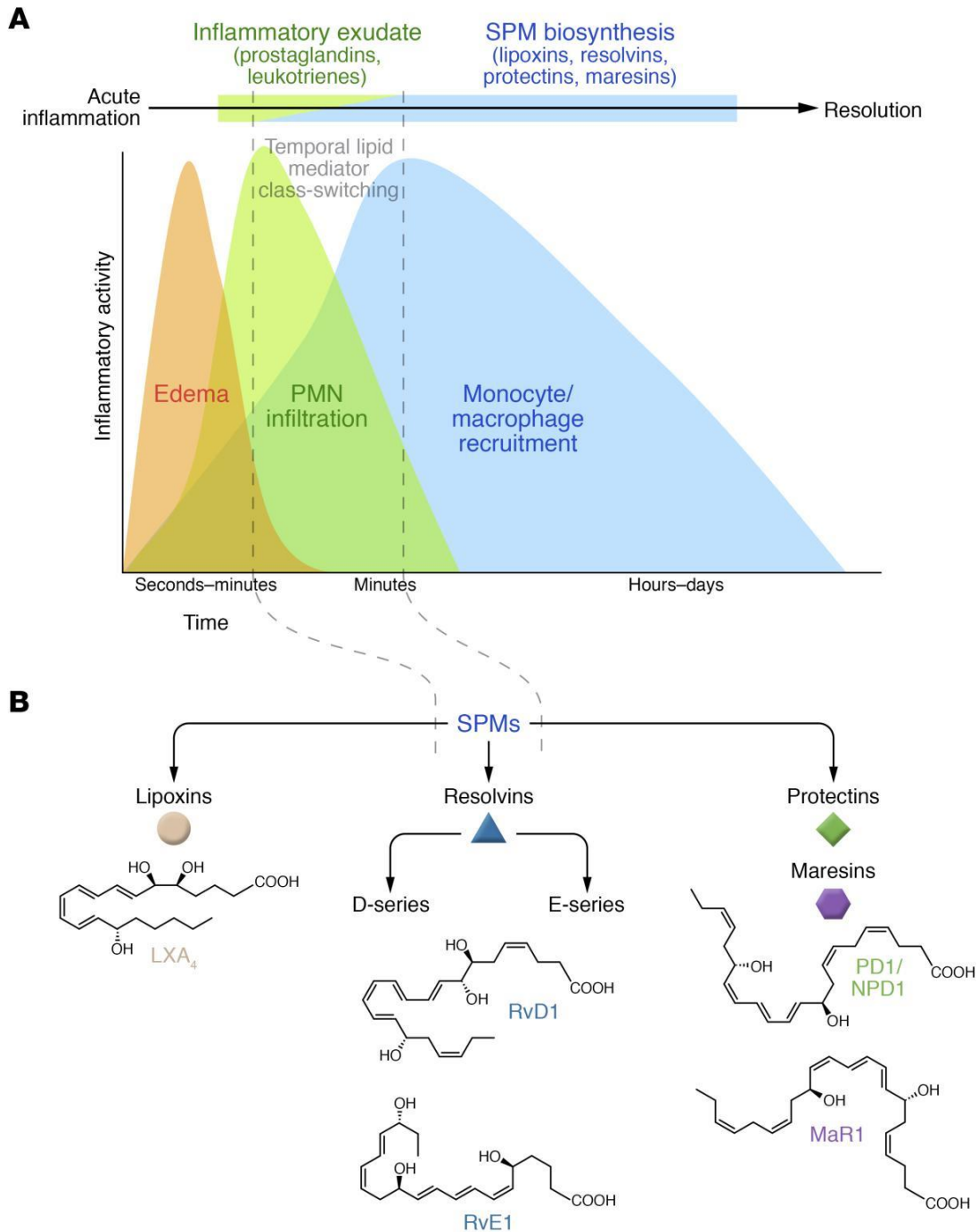


**Figure 16. Acute inflammation and resolution.** There are temporally defined steps during acute inflammation. The synthesis of SPMs initiates the resolution phase that finishes with the elimination of the insult and immune cells from the tissue (A). SPMs are a family of lipidic molecules derived from n-6 FAs (lipoxins) and n-3 FAs (resolvins, protectins and maresins) (B) (Serhan CN and Levy BD 2018).



## 1.4 TDP-43 pathology in AD-LATE

AD is the most frequent form of dementia worldwide, strongly associated with age (Livingston et al., 2020). The prevalence of AD is extremely high (3% of people age 65-74, 17% of people age 75-84 and 32% of people older than 85) and is expected to increase the next years (Hebert, Weuve, Scherr, & Evans, 2013). The affected brain exhibits cortex atrophy, neuronal loss and deposition of two different aggregates: extracellular amyloid fibrils composed of the amyloid  $\beta$  ( $A\beta$ ) peptide and intracellular neurofibrillary tangles (NFTs) composed by hyperphosphorylated neurofilament tau (Wilcock & Esiri, 1982).

The disease begins with the neurodegeneration of memory circuits of the hippocampus and entorhinal cortex (structures of the limbic system). Neurodegeneration gradually extends within other cortical regions and leads to language, reasoning and social-behavioral impairments (Braak & Braak, 1991). Aimed by the toxic properties of amyloid fibrils, some authors have postulated the amyloid hypothesis as a major disease mechanism in AD (Hardy & Allsop, 1991). However, phase III clinical trials with monoclonal antibodies targeting amyloid fibrils only have moderate effect slowing cognitive decline in mild subjects (Selkoe & Hardy, 2016). Other authors hypothesize that NFTs are responsible for the progress of the disease, not amyloid fibrils (Kametani & Hasegawa, 2018). Nevertheless, a drug targeting NFTs aggregation failed to demonstrate a benefit for AD patients in a clinical trial (Gauthier et al., 2016). Hence, AD etiology, as well as patient stratification for clinical trials, should be reconsidered. With this purpose, in 2019 Nelson et al., defined a new disease entity termed Limbic-predominant Age-related TDP-43 Encephalopathy (LATE) which was previously diagnosed as AD (Nelson et al., 2019), involving dementia with TDP-43 intracellular inclusions. Neuropathological staging of AD neuropathological changes (AD-NC) (Braak stage) is based on NFTs distribution. Stages I-IV correspond to mild to severe entorhinal cortex affection, whereas cortical regions are also affected in stages V-VI (Braak & Braak, 1991). To help individualization of patients, LATE neuropathological changes (LATE-NC) stages are classified by TDP-43 pathology extent (**Table 1**)

**Table 1. LATE-NC Stages according to TDP-43 pathology extent (modified from Nelson PT et al 2019).**

LATE-NC Stage	TDP-43 pathology
0	None
1	Amygdala
2	Hippocampus
3	Middle frontal gyrus (MFG)

## Introduction

However, both amyloid and tau aggregates are also found in LATE-NC. LATE is associated with the oldest individuals with a severe cognitive impairment, previously classified in advanced Braak stage. Pure LATE-NC subjects have a more gradual decline than LATE/AD-NC mixed pathology, suggesting a synergistic effect. Authors estimate that >20% of brain autopsies from >80 years old people probably have LATE-NC (Nelson et al., 2019) and 25-50% of those with AD-NC (Wilson, Dugger, Dickson, & Wang, 2011) (**Figure 17**). A plausible explanation is the interaction of TDP-43 and A $\beta$  processing. For instance, A $\beta$  aggregation triggers TDP-43 pathology, independently of NFTs, in animal models (Herman, Khandelwal, Stanczyk, Rebeck, & Moussa, 2011). Cleavage of amyloid precursor protein (APP) produces A $\beta$  and APP intracellular domain (AICD). TDP-43 interacts with AICD, up-regulating p53 mRNA and inducing apoptosis *in vitro* (J. Wang et al., 2014). Moreover, depletion of neuronal TDP-43 in AD mouse models exacerbates the disease, although diminishes the presence of A $\beta$  aggregates (LaClair et al., 2016).

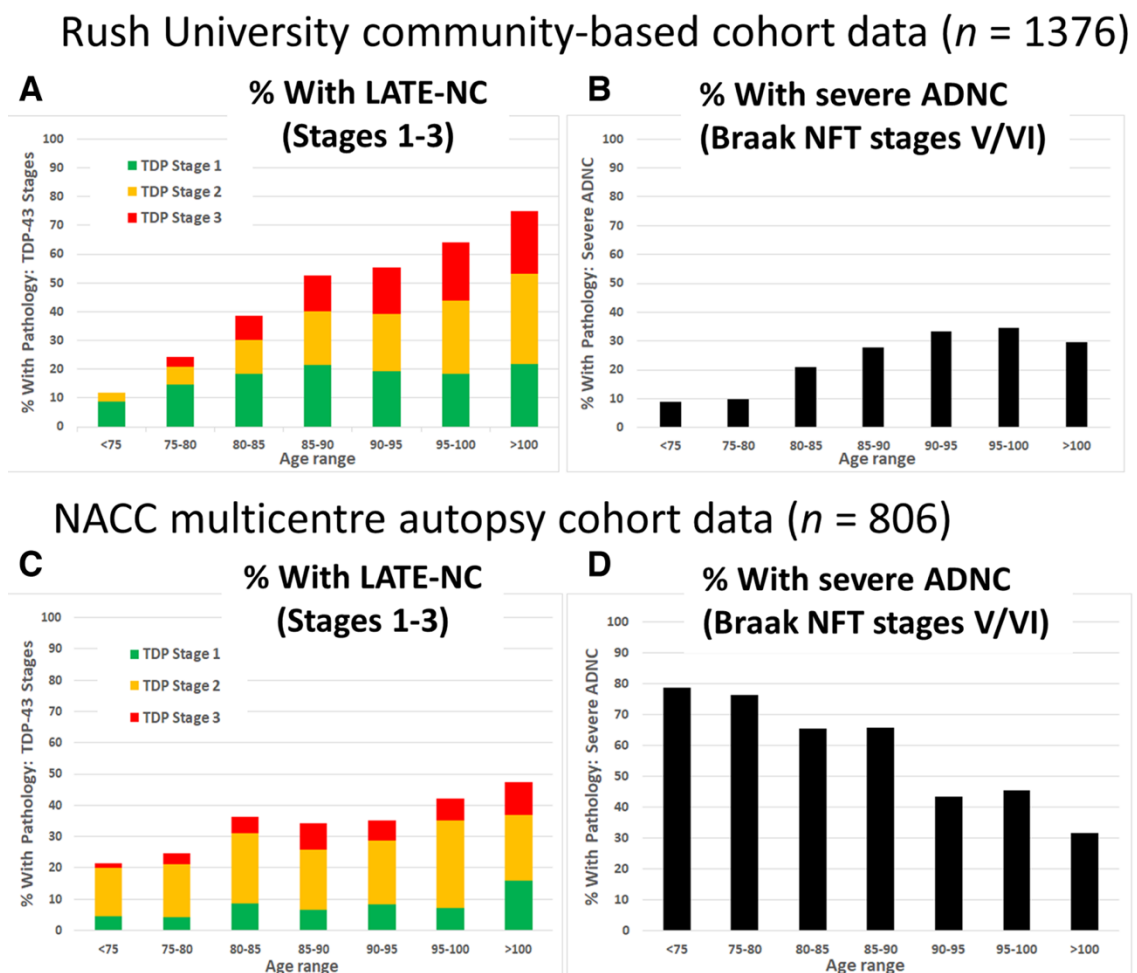


**Figure 17. LATE-NC and ADNC estimated prevalence.** LATE-NC and severe ADNC prevalence increase in advanced old ages in a community-based cohort, including people with and without dementia (A and B). LATE-NC prevalence is relatively stable between different age ranges in a cohort of people with AD(C). The prevalence of severe ADNC in AD patients diminishes in advanced old ages (D) (Nelson PT et al 2019).

## *Introduction*

Genetics of LATE are partially overlapped with FTD-TDP (other dementia linked to TDP-43 pathology), sharing *GRN* and *TMEM106B* mutations; and AD, sharing *APOE*  $\epsilon$ 4 allele. *ABCC9* and *KCNMB2* variants are also linked to LATE. However, genetic studies on LATE have been performed with varied inclusion/exclusion criteria, compromising the results (Nelson et al., 2019). A better definition and the finding of robust LATE biomarkers are necessary for clinical trial stratification, consistent genetic analyses and risk factor assessment (Nelson et al., 2019). Whether LATE is associated to changes in cryptic exon is not well characterized. A recent publication points to an increase in cryptic exon splicing in some advanced forms of Alzheimer (Sun et al., 2017). However, quantification of the relative impact in spliced transcripts and protein levels were not performed. This information can be useful for a better stratification of the disease and the selection criteria for drug candidates.

TDP-43 is a multifunctional protein linked to several neurodegenerative diseases, making it an excellent candidate for therapeutic targeting. Deciphering pathological consequences of TDP-43 would lead to possible treatments for ALS, LATE and FTD-TDP. However, there is a lack of TDP-43 peripheral biomarkers and specific drugs targeting TDP-43 pathology and its consequences.









## **1.6 ALS biomarkers**

### **1.6.1 General concepts**

A biomarker can be defined as a “characteristic that is objectively measured and evaluated as an indicator of normal biological or pathologic processes, or biological responses to a therapeutic intervention” (Strimbu & Tavel, 2010). Biomarkers can be classified by their purpose: diagnostic, prognostic, predictive, or pharmacodynamic. A diagnostic biomarker is related to the presence or absence of a characteristic in a specific disease. This type of biomarkers is useful for an early and robust diagnostic. Shortening diagnostic delay and start the treatment in early stages improve the disease outcome. Prognostic biomarkers inform about the natural history of the disease. ALS stratification into a homogenous prognostic group could be useful to design better RCTs. A candidate treatment could be useful in a subgroup of ALS, as it is the case with Edaravone (Abe et al., 2017). Predictive biomarkers are characteristics that allow the classification of the individuals according to their response to therapy. They are employed to choose the best therapy for every patient. Pharmacodynamic biomarkers inform about the magnitude of the effects of a drug. They are critical for dosage and monitoring (Califf, 2018).



## *Introduction*

The quality of the biomarkers can be measured by statistic tools such as the sensitivity and the specificity. Sensitivity (true positive rate) is the proportion of actual positives correctly identified. Specificity (true negative rate) is the proportion of actual negatives correctly identified. These statistical analysis can be employed to determine the quality of a given biomarker in Receiver Operating Characteristic (ROC) curve (Hajian-Tilaki, 2013). ROC curve is created by plotting different thresholds of sensitivity (Y-axis) and 1-specificity (X-axis) of the biomarker. Within ROC analyses we can choose the best threshold to classify a dichotomic variable for a given purpose. For example, in a population screening of an infectious disease, a high value (close to 1) of sensitivity is the best option, although the specificity could be lower. Identifying all the infected people with a higher false positive rate is more effective to stop the spreading than a lower true positive rate. However, when the purpose is a definitive diagnostic, a higher specificity threshold should be set up. Another important parameter of ROC analysis is the Area Under the Curve (AUC). This value (ranging from 0 to 1) summarizes the goodness of a given threshold, balancing both sensitivity and specificity. When the prevalence of the condition in a case-control study is considered in the proportion of true positive and true negative rates, we obtain the positive and negative predictive values (PPV and NPV) of the biomarker, being 1 (100%) a perfect test. The complement of PPV is the False Discovery Rate (FDR) (1-PPV) and is often used in statistical analyses of biomarkers.

As discussed above, ALS biomarkers have been proposed, comprising any measurable characteristic, including concentration of given molecules, electrophysiological records, muscular strength, respiratory capacity, and composite measures, such as the score in a functional test (ALSFRS-R) (Taga & Maragakis, 2018). Fluid-based biomarkers can come from cerebrospinal fluid (CSF), blood, urine, saliva, or similar. Due to the direct contact of this biofluid with the CNS, CSF is probably the most reliable source of them. However, extracting CSF is an invasive procedure (lumbar puncture), prone to side-effect and inadvisable to obtain repeatedly in longitudinal analyses. Blood, plasma/serum and urine could be more suitable sources of biomarkers. Nevertheless, it is not easy to assert whether a molecule found in these biofluids is a reflection of neurodegeneration.

### **1.6.2 Targeted strategies**

Currently, the most employed fluid-based biomarkers for ALS are the concentration of phosphorylated Neurofilament Heavy (pNfH) and Neurofilament Light (NfL) chains in CSF and blood (Poesen & Van Damme, 2019). Neurofilaments (NF) are specific components of the neuronal cytoskeleton. When a neuron dies, NFs are released to the CSF and subsequently to the blood. They are detected through Enzyme-Linked Immunosorbent Assay (ELISA) and electro-chemiluminescent immunoassay. NfL PPV in blood or CSF is around 95% and NPV 55% approximately (Poesen & Van Damme, 2019). These values for pNfH are 95% of PPV and 67% of NPV. In conclusion, neurofilament determination can predict almost all ALS patients, although are

## *Introduction*

not so efficient to discriminate ALS mimics. Moreover, these values are variable across studies. Neurofilaments are also a good prognostic biomarker and are correlated with ALSFRS-R score decline and survival. A longitudinal study highlights an important increase in early stage and a stabilization in later stages, suggesting limited use of NFs for monitoring the progression (McCombe et al., 2015). However, the prognosis of different ALS subtypes or genetic forms is not always reflected in neurofilament levels (Poesen & Van Damme, 2019). Although several studies indicate that NFs are good biomarkers, some experts think that further larger and longitudinal studies elucidating some properties of these proteins, such as blood and CSF half-life, are needed to establish their clinical use (Taga & Maragakis, 2018).

Another frequently used biomarker in ALS is the concentration of plasma creatinine (Van Eijk et al., 2018). This protein is related to muscle mass, which is progressively lost during the disease. Plasma creatinine kinase is detected with an enzyme-linked colorimetric assay, which is inexpensive and easy to perform. These concentrations strongly correlate with ALSFRS-R, muscle strength and overall survival in a longitudinal study (Van Eijk et al., 2018). Moreover, it has been successfully used for monitoring disease progression in an RCT (Bozik et al., 2014).

Major disease proteins (TDP-43, SOD1 and C9ORF72) have also been postulated as biomarker candidates of ALS. SOD1 protein levels in CSF is a pharmacodynamic biomarker of ASO response in SOD1 fALS (Winer et al., 2013). Additionally, the detection of specific peptides derived from pathological aggregates have been proposed as pharmacodynamic biomarkers for recent SOD1 anti-aggregation RCTs (Benatar et al., 2018; Gertsman et al., 2019). Regarding C9ORF72 biomarkers, there is only one study demonstrating an increase in poly-GP DPR in CSF from C9ORF72 HRE carriers (Lehmer et al., 2017). However, the levels are the same for asymptomatic and symptomatic carriers. This biomarker is excellent to detect the carriers but lacks prognostic and diagnostic value. A similar pharmacodynamic biomarker of SOD1 would be useful for the ongoing phase I RCT C9ORF72 ASO (ClinicalTrials.gov Identifier: NCT03626012).

TDP-43-related biomarkers are potentially useful because the prevalence of its pathology in ALS is 97% of the cases. The measurement of specific TDP-43 pathological signature in biofluid is challenging because this protein is ubiquitously expressed. The first attempt to find a TDP-43 biomarker was just two years after the discovery of TDP-43 as the principal component of protein aggregates in ALS. In this study, TDP-43 CSF levels were higher in ALS than healthy controls, although with a great dispersion between subjects and without a diagnostic value. However, the authors did not find differences in pathological phosphorylated TDP-43 neither cleaved forms, suggesting a limited reflection of the disease (Steinacker et al., 2008). Other studies analyzed changes in TDP-43 expression and localization in Peripheral Blood Mononuclear Cells (PBMCs). TDP-43 is mislocalized to the cytoplasm in PBMCs from ALS patients (De Marco et al., 2011).

## *Introduction*

Another study found an increase of TDP-43 expression in ALS PBMCs but not in the plasmatic soluble fraction. Additionally, a ROC analysis was performed in this study. TDP-43 levels in combination with other RNA-related protein levels resulted in high AUC value discriminating ALS from other neurological diseases (AUC= 0.75). Nevertheless, authors did not report the data of PPV, NPV nor FDR (Luotti et al., 2020). TDP-43 alterations should not be extrapolated to other cell types (Codron et al., 2018). Further studies from independent groups are necessary to elucidate the reproducibility of TDP-43-based biomarkers. In this sense it is not known whether biomarkers of TDP-43 focused at their functions (i.e. splicing control) could be useful in ALS management. For that reason, we wonder whether cryptic exons are higher expressed in peripheral blood mononuclear cells (PBMCs) from ALS patients. Moreover, we also wanted to investigate a broader TDP-43 mislocalization that could take place in anucleate cells (platelets) and if it could be employed as a biomarker.

### **1.6.3 Non-targeted approaches**

The emergence of omic profiling (genomic, transcriptomic, proteomic, metabolomic and lipidomic) has revolutionized the biomarker field (**Figure 20**). Non-targeted approaches are based on the detection of global changes of known and unknown molecules. This strategy is useful when we do not know the origin of the possible alterations and we want to cover the maximum range of potential biomarkers. Non-targeted omic approaches usually found multiple significant hits. Multivariate analyses are useful tools to obtain a better picture of the changes between groups (Worley & Powers, 2013). In this sense, powerful multivariate analyses might be employed as the Principal Component Analysis (PCA) and Partial Least Squares Discriminant Analysis (PLS-DA). PCA is an unsupervised analysis, which means the sample is not matched in its experimental group before the analysis. PCA clusters several variables to reduce the dimensionality of the sample and plot the results in two or three dimensions or components. PLS-DA is similar to PCA by plotting the results. The main difference is that PLS-DA is a supervised analysis and the group identity is matched to the sample before the analysis. Sometimes this supervised analysis can be overoptimistic by overfitting the results (Rodríguez-Pérez, Fernández, & Marco, 2018) so it requires adequate FDR correction.

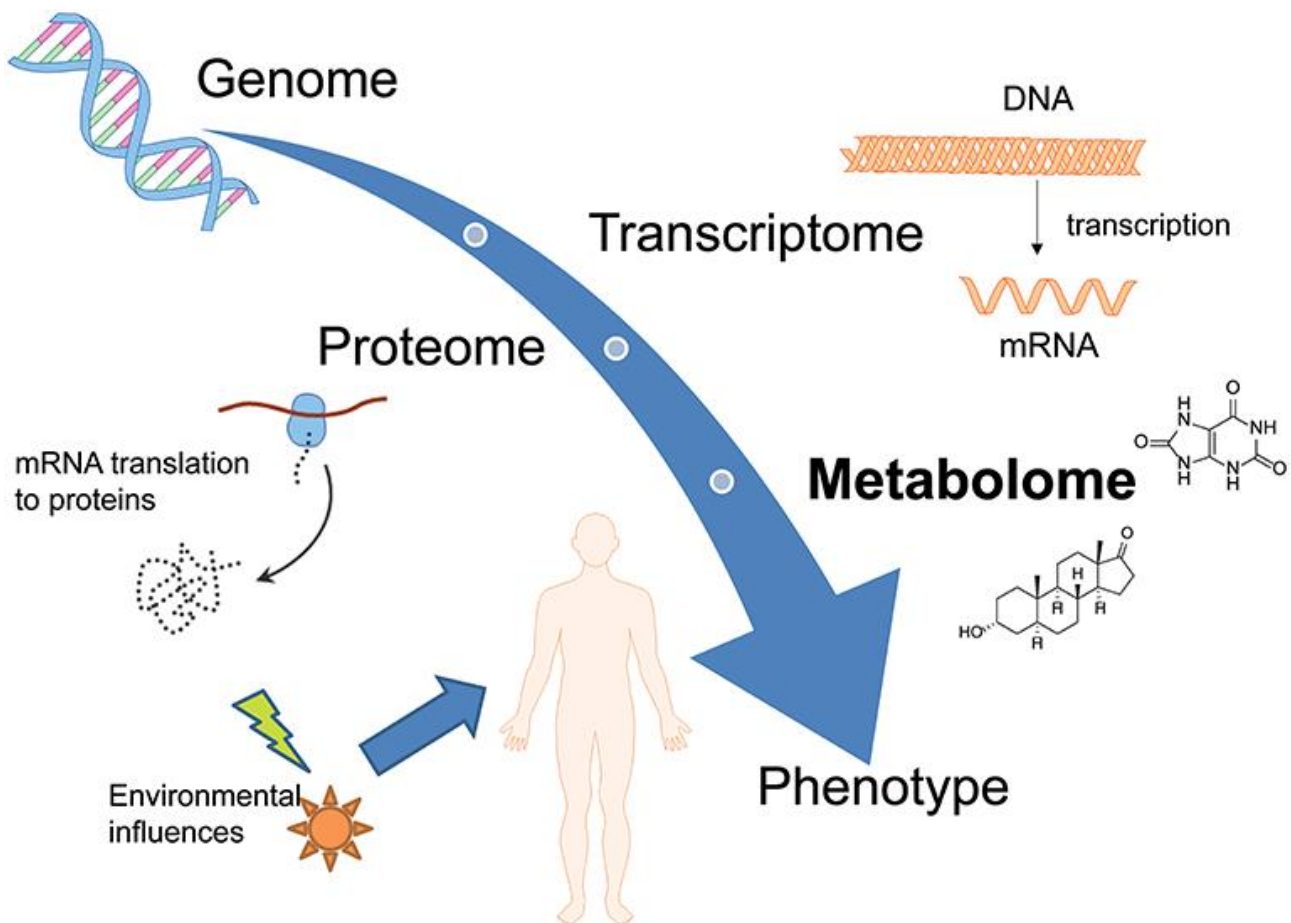


**Figure 20. Omics sciences overview.** The metabolome/lipidome is the downstream output of the genome and is a reflection of all the changes in the transcriptome and the proteome. It is also influenced by the environment (Steuer AE et al 2019).

Genomic analyses have been used to find new genes associated with ALS. Ongoing genomic studies, like the MinE Project, are providing very valuable information about the genomic architecture of this disease (Van Rheenen, Pulit, et al., 2018). One of the advantages of this omic approach is the high stability of the genome in time and good characterization of the targets since the Human Genome Project in 2001. However, as already mentioned, SV elements are still poorly understood. The next level of complexity is the transcriptome, defined as the complete set of RNA transcripts under specific circumstances (**Figure 20**).

Blood (or other fluid or tissues) transcriptomic analysis can be assessed to find biomarkers. In ALS, a ROC analysis of whole-blood transcriptome resulted in an AUC= 0.9 discriminating ALS from controls but an AUC= 0.68 in ALS vs mimics (Van Rheenen, Diekstra, et al., 2018). However, this transcriptomic profiling was not as useful as a prognostic biomarker. Interestingly, RNA binding (several mutations linked to ALS belong to this category) was the molecular function with the highest number of differently expressed genes in ALS (Van Rheenen, Diekstra, et al., 2018). A recent study of blood transcriptomic profile identified the upregulation of neutrophil gene expression and downregulation of hypoxia-related genes. Moreover, they obtained an accuracy of 87% comparing

## *Introduction*

ALS vs control and ALS vs mimic using machine learning. This value is significantly higher than NFs accuracy (49-53%). This approach also resulted in a new way of patient stratification according to a higher expression of myeloid lineage-specific genes or lymphoid-specific genes (Swindell, Kruse, List, Berryman, & Kopchick, 2019).

The proteome is the product of the transcriptome translation. CSF proteome analysis revealed significant differences in several proteins in ALS. ROC analysis using four of these proteins for ALS diagnosis resulted in an AUC= 0.94. However, this was, in fact, a preliminary study with some limitations. Authors mixed in the same ALS group (n= 15) sALS and fALS patients; and the group "NON" (n= 7) was formed by healthy controls mixed with other neurodegenerative diseases (Collins, An, Hood, Conrads, & Bowser, 2015). Plasma and PBMC proteomic can be useful for disease stratification. Curiously, senescence-related proteins are upregulated in ALS fast progressors (Zubiri et al., 2018). Several proteomic studies have been performed in ALS for biomarker research. The use of different technology, samples, experimental design, statistical analysis resulted in different conclusions and candidates (Hedl et al., 2019).

Metabolomic, lipidomic or metabolipidomic approaches are based on the global search for metabolites (**Figure 20**). A metabolite is any small molecule (i.e. lower than 3 kDa) produced by the ongoing biological reactions in a determined system (cell, tissue, biofluid) and at a specific timepoint. Depending on the solubility, metabolites can be included in the metabolome (those soluble in inorganic phases like water/methanol) or the lipidome (those soluble in organic phases like chloroform). However, some metabolites can be found in both phases. The combination of metabolomics and lipidomics can be defined as metabolipidomics (Veyrat-Durebex et al., 2019). One of the characteristics of these approaches is the extremely high dynamic behavior of the metabolipidome. This offers a high chance to find significant differences between metabolites, but reproducibility is sometimes challenging. Metabolomic profiling of CSF in ALS patients can be a source of diagnostic biomarkers according to independent groups. However, even using a similar methodology (<sup>1</sup>H-NMR), they found distinctly altered metabolites (Hélène Blasco et al., 2010; Gray et al., 2015). Moreover, metabolomics has also a prognostic value for RCTs and can be used to design therapies (pharmacometabolomics) (Hélène Blasco et al., 2018). CSF lipidomics is also useful for diagnostic and prognostic. Several phospholipids, specially Phosphatidylcholine PC(36:4) are differentially expressed in ALS (H. Blasco et al., 2017). Moreover, CSF lipidomics can also predict the ALSFR-R decline with an accuracy of 71% (H. Blasco et al., 2017). Plasma samples can also be used for metabolipidomic profiling in ALS. Plasma metabolomic analysis was used as a diagnostic biomarker (ALS vs mimics) with 65% sensitivity and 81% specificity (AUC of 0.76) (Lawton et al., 2014).

## *Introduction*

Non-targeted approaches usually report a huge amount of data that is not reproduced in other laboratories. Moreover, the interpretation is often challenging. In the case of metabolipidomics, external inputs (like diet, lifestyle conditions, physical activity, to name a few) can be a source of confounding factors. Additionally, the identification of metabolites is not always achieved, and the databases are constantly being improved.

In this sense the specific changes in lipids found in platelets from ALS patients are not known. These blood particles contain a high content of mitochondria, an affected organelle in ALS (Vandoorne, De Bock, & Van Den Bosch, 2018). Platelet metabolomic has been used to analyze mitochondrial bioenergetic function (Chacko et al., 2019). In this thesis we analyzed the lipid composition of platelets and correlated with clinical parameters.

## **2 HYPOTHESIS**

## *Hypothesis*

As commented in the introductory section, ALS is a devastating motor neuron disease that does neither have effective treatments, nor proficient biomarkers. Several pathways are implicated in the pathophysiology, such as impaired proteostasis, neuroinflammation and cryptic exon pathology.

One of the processes that can link these pathological mechanisms is aging and senescence. Aging is associated with an increase in senescent cells in many tissues. These cells switch their phenotype to a pro-inflammatory type, secreting several cytokines and chemokines. The elimination of these cells has reported benefits in neurodegenerative animal models of AD and PD. Moreover, aging is also strongly associated with TDP-43 mislocalization and aggregation. More than 70% of people over 100 years old display LATE-NC. After TDP-43 mislocalization, cryptic exons are spliced in several genes, inducing mRNA instability and promoting its degradation. One of the cryptic exons repressed by TDP-43 is in *ATG4B*, an important autophagy gene, essential to maintain the proteostasis.

On the other hand, little is known about TDP-43 pathology in platelets and PBMCs and its consequences in metabolomic changes. Whether the findings observed in the central nervous system could be reflected in these cells and its potential use as biomarkers remains elusive.

Based on previous evidence, we hypothesize that cryptic exons are increased in affected CNS regions in ALS and LATE patients, influenced by disease status. Moreover, these cryptic exons are degraded in the cytoplasm. This leads to lower protein expression, thus affecting several functions, like autophagy. Concomitantly, neuroinflammation associated with ALS can be explained by premature aging and cell stress. This process leads to an increase in senescent cells and SASP in the spinal cord. The elimination of senescent cells with senolytic administration (Navitoclax) or pro-resolving treatment (DHA enriched diet) could alleviate neuroinflammation and disease progression. The abovementioned changes are partially reflected in platelets and PBMCs, inducing metabolipidomic changes that can be used as biomarkers candidates.



## **3 OBJECTIVES**

## *Objectives*

In order to validate the hypothesis, we propose the following objectives:

**Objective 1:** To determine the quantitative impact of the cryptic exon splicing from ALS and LATE-AD samples.

- Objective 1.1: To set up a quantitative method based on SYBR Green RT-qPCR to determine the splicing rate of ATG4B, GPSM2 and PFKP cryptic exons.
- Objective 1.2: To quantify the abovementioned cryptic exons in spinal cord, frontal cortex, brainstem, occipital cortex and PBMCs from ALS and control samples.
- Objective 1.3: To quantify the abovementioned cryptic exons in hippocampus from AD and LATE samples.
- Objective 1.4: To analyze the correlation with cryptic exon parameters with clinical parameters.
- Objective 1.5: To determine the NMD effect on mRNA and protein levels of cryptic exon-containing genes.
- Objective 1.6: To generate a TDP-43 loss of function cell model for quantifying cryptic exon splicing and its consequences in autophagy.
- Objective 1.7: To set up a fluorescence-based method to study ATG4B cryptic splicing.
- 

**Objective 2:** To study the cellular senescence, neuroinflammation and senolytic and pro-resolving therapies in G93A-hSOD1 ALS mouse model.

- Objective 2.1: To quantify the expression of senescence related genes (p16 and p21) and SASP (Il-1a, Il-6, Ifn-a, Ifn-b) in spinal cord of G93A-hSOD1 mouse at different disease stages by RT-qPCR.
- Objective 2.2: To analyze p16 and p21 histological expression pattern by IHQ and IF.
- Objective 2.3: To treat hSOD1-G93A mice with senolytic drug Navitoclax and determine disease progression, survival and senescence-related markers (p16 and p21) in spinal cord.
- Objective 2.4: To perform a dietary intervention with pro-resolving DHA enriched diet and analyze its effect on disease progression, survival, neuroinflammation, spinal cord fatty acid content and oxidative stress.

**Objective 3:** To analyze TDP-43-based biomarkers and metabolomic changes in platelets and PBMCs from ALS patients.

- Objective 3.1: To determine TDP-43 levels in platelets from ALS patients.

## *Objectives*

- Objective 3.2: To quantify abovementioned cryptic exons in PBMCs from ALS patients.
- Objective 3.3: To analyze metabolomic changes in platelets from ALS patients.
- Objective 3.4: To determine the biomarker potential for diagnosis and prognosis of abovementioned parameters studied in Objective 3.

## **4 MATERIALS AND METHODS**

### **Isolation of Peripheral Blood Mononuclear Cells and platelets**

Peripheral Blood Mononuclear Cells (PBMCs) and platelets were isolated from peripheral blood using Histopaque-1077 (10771, SIGMA). Briefly, 3 ml of Ficoll were added to the bottom of a centrifuge tube. Carefully, 3 ml of blood were layer onto Ficoll without mixing the phases. The tubes were centrifuge at 400g for 30 minutes at RT with the lowest acceleration and brake program. The upper phase was removed, and the opaque interphase was collected into a new tube. The interphase was the washed with PBS and centrifuged at 300g. The supernatant contained platelet fraction and the pellet PBMCs. PBMCs were washed with PBS and centrifuged at 300g. Platelets were centrifuged at 360g and the pellet were discarded. Supernatant was collected and centrifuge at 800g. The resulting pellet was washed with PBS and centrifuged at 800g to obtain the platelets. Both fractions were observed with an optical microscope to ensure that were enriched in PBMCs or platelets.

### **Fatty Acid Compositional Analyses**

Samples were homogenized in an ice-chilled buffer containing 180 mM KCl, 5 mM MOPS, 2 mM EDTA, 1 mM diethylenetriaminepentaacetic acid, and 1  $\mu$ M of freshly prepared butylated hydroxyl toluene (BHT) at pH 7.3. Lipids were extracted with chloroform/methanol (2:1, v/v) 0.01% BHT for 2 times as described in (Pamplona, Dalfó, et al., 2005). The chloroform phase was then evaporated under N<sub>2</sub> steam. After the evaporation, FAs were transesterified with in 2 ml of 5% methanolic HCL at 75 °C for 90 min, resulting in the formation of FA methyl esters (FAMES). FAME extraction was performed by adding n-pentane and saturated NaCl solution (2:1 v/v). After a centrifugation, n-pentane phase was separated and evaporated under N<sub>2</sub> steam. Finally, 80  $\mu$ l of CS<sub>2</sub> were employed to dissolve the FAMES for GC-FID analysis.

Separation was performed in a DBWAX capillary column (30 m  $\times$  0.25 mm  $\times$  0.20 $\mu$ m) in an Agilent GC System 7890A with a Series Injector 7683B and a flame ionization detector (Agilent Technologies, Santa Clara, CA). The injection port was maintained at 220 °C and the detector at 250 °C. The temperature program was as follows: 2 min at 100 °C, then an increase of 10 °C/min to 200 °C, then 5 °C/min to 240 °C, and finally maintained at 240 °C for 10 min. For fatty acid methyl ester integration, we compared the peaks with the retention time of authentic standards (Larodan Fine Chemicals, Malmö, Sweden) injected according to the same method. Results were expressed as mol%. The fatty acid-derived indexes were calculated with the following formulas: Saturated fatty acids (SFA) =  $\Sigma$ % of saturated fatty acids; unsaturated fatty acids (UFA) =  $\Sigma$ % unsaturated fatty acids; monounsaturated fatty acids (MUFA) =  $\Sigma$ % of monoenoic fatty acids; polyunsaturated fatty acids series n-3 (PUFAn-3) =  $\Sigma$ % of polyunsaturated fatty acids n-3 series; polyunsaturated fatty

## Materials and Methods

acids series n-6 (PUFA n-6) =  $\Sigma\%$  of polyunsaturated fatty acids n-6 series; average chain length (ACL) =  $[(\Sigma\% \text{ total } 14 \times 14) + \dots + (\Sigma\% \text{ total } n \times n)]/100$  (n= carbon atom number); peroxidability index (PI) =  $[(\Sigma \text{mol}\% \text{ monoenoic} \times 0.025) + (\Sigma \text{mol}\% \text{ dienoic} \times 1) + (\Sigma \text{mol}\% \text{ trienoic} \times 2) + (\Sigma \text{mol}\% \text{ tetraenoic} \times 4) + (\Sigma \text{mol}\% \text{ pentaenoic} \times 6) + (\Sigma \text{mol}\% \text{ hexaenoic} \times 8)]$ ; double-bond index (DBI) =  $[(\Sigma \text{mol}\% \text{ monoenoic}) + (2 \times \Sigma \text{mol}\% \text{ dienoic}) + (3 \times \Sigma \text{mol}\% \text{ trienoic}) + (4 \times \Sigma \text{mol}\% \text{ tetraenoic}) + (5 \times \Sigma \text{mol}\% \text{ pentaenoic}) + (6 \times \Sigma \text{mol}\% \text{ hexaenoic})]$ ; anti-inflammatory index (AI) =  $(20:3n-6) + (20:5n-3) + (22:5n-3) + (22:6n-3)/(20:4n-6)$ , according previously published methods (Pamplona, Dalfó, et al., 2005).

## Western blot analysis

Protein from cells and platelets was extracted adding 100  $\mu\text{L}$  of radioimmunoprecipitation (RIPA) buffer with Protease Inhibitor Cocktail (1X) to the pellet. Protein from tissue was extracted homogenizing the sample in a buffer containing 180 mM KCl, 5 mM MOPS, 2 mM EDTA, 1 mM diethylenetriaminepentaacetic acid, and 1  $\mu\text{M}$  of freshly prepared butylated hydroxyl toluene (BHT) at pH 7. After sonication, protein quantification was performed with Bradford assay (5000006, Bio-Rad). Fifteen  $\mu\text{g}$  of protein were loaded onto a 12% acrylamide SDS-PAGE gel. Membranes were blocked with I-Block (T2015, Thermo Fisher Scientific) for 1 hour and incubated overnight with primary incubated in TBS-T 0.05% (**Table 2**). After primary antibody incubation, membranes were washed 3 times with TBS-T 0.05% and incubated with secondary antibody for 1h. Immobilon™ Western Chemiluminiscent HRP Substrate (WBKLS0500, Merck Millipore) was used for immunodetection. Membranes were stained with Coomassie Brilliant Blue G (27815, Sigma) for normalization. Specific bands were quantified with ImageLab v5.2.1 (Bio-Rad).

Table 2. Antibody dilutions.

Target	Western Blot dilution	IF/IHQ dilution	Manufacturer	Catalogue number
TDP-43	1:1000	-	Proteintech	10782–2-AP
ATG4B	1:500	-	Sigma	A2981
GPSM2	1:500	-	Abcam	ab84571
PFKP	1:500	-	Atlas Antibodies	HPA018257
Syntaxin 3	1:1000	-	Abcam	ab4113
8-oxo-dG	-	1:200	Abcam	ab62623
γH2Ax	-	1:200	Abcam	ab2893
SMI-32	-	1:200	Covance	SMI-32
p16	-	IF 1:200	Abcam	ab54210
p16	-	IHQ 1:100	ROCHE	clone E6H4
p21WAF1/Cip1	-	IHQ 1:100	Agilent Technologies-DAKO	clone SX118
Beta III Tubulin	-	1:200	Abcam	ab18207
GFAP	-	1:200	Abcam	ab7260
Iba1	-	1:200	Abcam	ab5076

### RNA extraction, cDNA synthesis, and quantitative RT-PCR (RT-qPCR)

RNA was extracted from PBMCs using TRI Reagent (Thermo Fisher Scientific, AM9738) following the manufacturer’s instructions. RNA concentrations were measured using a NanoDrop ND-1000 (Thermo Fisher Scientific). One microgram of RNA was used for retrotranscription employing TaqMan Reverse Transcription Reagent using random hexamers (Thermo Fisher Scientific, N8080234).

Cryptic exons were quantified as previously described (Torres et al., 2020, 2018). Briefly, RT-qPCR experiments were performed using a CFX96 instrument (Bio-Rad, Hercules, California, USA) with SYBR Select Master mix for CFX (Thermo Fisher Scientific, 4472937). Each 20 μL of reaction contained 4μL cDNA, 10 μL SYBR Select Master Mix, 0.2 nM of forward primer and 0.2 nM of reverse primer solutions and 4 μL PCR grade water. RT-qPCR run protocol was as follows: 50 °C for 2 minutes and 95 °C for 2 minutes, with the 95 °C for 15 seconds and 60 °C for 1 minute steps repeated for 40 cycles; and a melting curve test from 65°C to 95 °C at a 0.1 °C/s measuring rate. Primers employed in these experiments are listed in (**Table 3**). Cryptic exon inclusion or Percentage Spliced-In (PSI) was estimated using the following formula:  $100 \times 2^{(-\text{Conserved exon } C_q - \text{Cryptic exon } C_q)}$ .

**Table 3. Sequence of RT-qPCR oligos.**

<b>Gene</b>	<b>Forward primer 5'-3'</b>	<b>Reverse primer 5'-3'</b>
<i>ATG4B</i> cryptic	CTGAGTGTGCATGGATGAGTG	TTGCTGGCACCAATCATTGAA
<i>ATG4B</i> Total	AACGCATTCATCGACAGGAAG	TTTGCGCTATCTGGTGAATGG
<i>GPSM2</i> cryptic	GTGTGTATGAGAGAGAGAGCGA	AGAAGCTTCCATTCTGTTCATCA
<i>GPSM2</i> Total	GGACGTGCCTTTGGAAATCTT	TTTGCAATAAGGAGACGCTGC
<i>PFKP</i> cryptic	ACGTTTGCAAACATCAGGAG	GCCTTCAACTCTCCGTTAC
<i>PFKP</i> Total	GACCTTCGTTCTGGAGGTGAT	CACGGTTCTCCGAGAGTTTG
<i>RFP</i> cryptic	GAGAGCGTGTGTCTGGATGT	CGGAAC TTCACCATGGCTCA
<i>RFP</i> Total	TCTACAAGGTGAAGTTCCGCG	TCTTCTTCTGCATTACGGGGC
<i>TARDBP</i>	CTGCGGGAGTTCTTCTCTCA	CGCAATCTGATCATCTGCAA
<i>GAPDH</i>	CCCTTCATTGACCTCAACTACATG	TGGGATTTCCATTGATGACAAG
<i>Adipor2</i> cryptic	AGAAGTGGAGTTACAATTGTG	AAACAAACTCTTCCATTTCGTT
<i>Adipor2</i> Total	TGTTTGTAAGGTGTGGGAAGG	GTTGCCCGTCTCTGTGTGTAT
<i>Cdkn2a</i> (p16)	CCCAACGCCCCGAACT	GCAGAAGAGCTGCTACGTGAA
<i>Cdkn1a</i> (p21)	TTGCCAGCAGAATAAAAGGTG	TTTGCTCCTGTGCGGAAC
<i>Il1a</i>	AGCGCTCAAGGAGAAGACC	CCAGAAGAAAATGAGGTCGG
<i>Il6</i>	ACCAGAGGAAATTTTCAATAGGC	TGATGCACTTGCAGAAAACA
<i>Ifna</i>	ATGGCTAGGCTCAGCACTTTC	CTCACTCAGACTTGCCAGCA
<i>Ifnb</i>	AGCTCCAAGAAAGGACGAACA	GCCCTGTAGGTGAGGTTGAT
<i>Actb</i>	GTGACGTTGACATCCGTAAAGA	GCCGGACTCATCGTACTCC

### Animal Experiments

For the fifth paper, a colony of the strain B6.Cg-Tg(SOD1\*G93A)1Gur/J JAX catalogue stock number 004435 was purchased at The Jackson Laboratories (Bar Harbor, MN, USA). Mice were maintained



## *Materials and Methods*

in C57BL/6J background and maintained in B6SJL backgrounds by male founder crossing with B6SJLF1/J for fourth paper. After genotyping and weaning, animals were placed at 12:12 hours dark / light cycle, at 22±2°C temperature, 50%±10 relative humidity, in individual cages (at 21 days). Navitoclax (T2101, Targemol) was diluted in 60% Phosal 50 PG (Lipoid), 30% PEG400 (Sigma, 91893) 10% EtOH. Navitoclax was administered by oral gavage at a dose of 50 mg kg<sup>-1</sup> body during five consecutive days followed by 16 days of rest. Treatment cycles were repeated until clinical endpoint (righting reflex >20 s). Spinal cords were rapidly excised, frozen in liquid N<sub>2</sub> and stored at -80 °C. This study was approved by the Animal Research and Ethics Committee at the University of Lleida. Animals were weighed weekly. All diets were stored at 4 °C for its better preservation. All experimental diets were isocaloric and without nutritional deficits. After 9 days under control diet, mice were randomized to follow on the same control diet (#PMI5015, PMI International LabDiet, St. Louis, MO), a low-n-3 diet (TD 00522, Harlan Teklad, Madison, WI), or the same low n-3 supplemented with 0.6% (w/w) DHA (Martek Bioscience, Columbia, MD), as previously described (Calon et al., 2004). For food intake calculation, pellets were weighed and removed weekly. The intake of n-3 fatty acids was calculated by accounting individual food intake and the amount of linolenic acid plus DHA specified in the diet. Blood was obtained by tail vein puncture. For animal sacrifice, mice were anesthetized with 2.5% isoflurane.

Spinal cords were rapidly excised, snap-frozen in liquid N<sub>2</sub>, and stored at – 80 °C. All experimental procedures were approved by the Institutional Animal Care Committee of the University of Lleida, according to local laws and to the Directive 2010/63/EU of the European Parliament. The minimal number of animals was calculated according to the deviation of fatty acid profiles in previous experiments (Cacabelos et al., 2014).

### **Genotyping**

Both DNA extraction and PCR-based genotyping have been previously described (RE Neuromol Med o similar). Briefly, tail DNA was extracted using the XNAT Kit (# 2740, Sigma-Aldrich, Sant Louis, MO). Primers employed for hSOD1 transgene genotyping were:

II2F (IMR042) 5'-CTAGGCCACAGAATTGAAAGATCT-3'

IIR2 (IMR043) 5'-GTAGGTGGAAATTCTAGCATCATCC-3'

hSOD1F (IMR113) 5'-CATCAGCCCTAATCCATCTGA-3'

hSOD1R (IMR114) 5'-CGCGACTAACAAATCAAAGTGA-3'

IL2 genotyping was assessed as a technical positive control.

## *Materials and Methods*

Thermal Cycler v2.08 (Applied Biosystems, Carlsbad, CA) was used to perform the following PCR protocol: Pre-denaturation for 5 min at 95 °C, denaturation for 1 min at 94 °C, annealing for 45 sec at 50 °C, elongation for 4 min at 72 °C and finally, after 35 cycles, elongation for another 7 min at 72 °C. The amplification products were resolved in 1% agarose stained with SYBR safe (S33102, Thermo Fisher Scientific, Waltham, MA) following manufacture protocol and electrophoresed for 30 min under constant 100 V. Images were taken under 365nm UV light lamp from (Alpha Innotech, Santa Clara, CA) with the software acquisition Digidoc RT2 (Alpha Innotech).

### **Stride Length Analysis**

Phenotypical analyses for motor neuron loss have been previously described (Cacabelos et al., 2014). Briefly, mice were trained flat narrow corridor (5 cm wide, 70 cm long) three times per week for 1 month. After this training, animal hind limbs were stained with a non-toxic colorant and put on a paper which served to track the walking behaviour along the corridor. A minimum of 5-7 continuous strides was recorded to calculate the mean value of the animal 3 days per week. The firsts footprints were discarded as the mice tend to walk faster when are released to the corridor. Stride and stance length were measured manually and blinded manner. Corridors were periodically ventilated to avoid cross contamination of volatile compounds present in mice.

### **Protein Oxidative Modifications**

The concentration of protein oxidative modifications glutamic semialdehyde (GSA), amino adipic semialdehyde (AASA), glycoxidative modification carboxyethyllysine (CEL), mixed lipoxidative glycoxidative modification (CML) and lipoxidative modification malondialdehyde lysine (MDAL) was analyzed by Gas Chromatography–mass spectrometry (GC/MS) in lumbar spinal cord homogenates as indicated (Pamplona, Dalfó, et al., 2005). Briefly, 0.5 mg of proteins from lysate were reduced with an overnight incubation in 500 mM NaBH<sub>4</sub> (final concentration) in 0.2 M borate buffer, containing 1 drop of hexanol as an anti-foam reagent. Reduced proteins were then re-precipitated with 20% of 10% trichloroacetic acid (final concentration). Internal standards used for relative quantification were the following: [2H<sub>8</sub>]lysine (d<sub>8</sub>-Lys; CDN Isotopes); [2H<sub>4</sub>]CML (d<sub>4</sub>-CML), [2H<sub>4</sub>]CEL (d<sub>4</sub>-CEL), [2H<sub>8</sub>]MDAL (d<sub>8</sub>-MDAL), [2H<sub>5</sub>]5-hydroxy-2-aminovaleric acid (for GSA quantitation) and [2H<sub>4</sub>]6-hydroxy-2-aminocaproic acid (for AASA quantitation). Proteins were hydrolyzed by incubation at 155°C for 30 min in 1 ml of 6 N HCl. Samples were dried using SpeedVac (SPD131DDA, Thermo Fisher Scientific, Waltham, MA ).For preparation of the methyl esters, the hydrolysates were dissolved in 1.5 ml of freshly prepared 1 N methanolic HCl and heated for 30 min at 65°C. Solvent was evaporated at room temperature under a stream of N<sub>2</sub>, then 1.5 ml trifluoroacetic anhydride was added, and the mixture was incubated at room temperature for 1h. The resulting N,O-trifluoroacetyl

## *Materials and Methods*

methyl ester derivatives were analyzed in Agilent model 6890 gas chromatograph equipped with a 30-m HP-5MS capillary column (30 m × 0.25 mm × 0.25 μm) coupled to a Agilent model 5973A mass selective detector (Agilent, Barcelona, Spain) under the condition previously described (Pamplona, Dalfó, et al., 2005).

### **Analysis of Cytokines in Plasma**

After blood obtention, it was centrifuged at 8000 rpm for 6 min to retrieve plasma. Plasma was stored at  $\leq -20$  °C until cytokine analysis. Cytokine levels from plasma were measured using the BD Biosciences Cytometric Bead Array Mouse Inflammation Kit (BD, Franklin Lakes, NJ, USA).

### **Immunofluorescence**

Animals were anesthetized by an intraperitoneal injection of pentobarbital and ketamine, 20 mg/kg and 60 mg/kg respectively in PBS. Mice were then perfused with saline solution followed by ice cold 4% paraformaldehyde (Sigma-Aldrich, Sant Louis, MO, USA) solution (freshly prepared with pH 7.4 phosphate buffer). Spinal cords were extracted, and fixation was continued by incubation in 4% paraformaldehyde made in pH 7.4 phosphate buffer overnight at 4°C. The next day, samples were cryopreserved in 30% sucrose, (made in pH 7.4 phosphate buffer) 48 hours. After this time, tissue was encased in a cubic recipient (Peel-A-Way Disposable Embedding Molds- S-22, Polysciences Inc., Warrington, PA), and embedded in tissue freezing medium (Triangle Biomedical Sciences Inc., Newcastle, UK) and frozen (-80°C). The lumbar spinal cord was then cut at a 16 μm section depth and resulting seeded on a gelatin-coated slide. Samples were permeabilized with 0.4% Triton X-100 PBS for 30 min and blocked with 5% normal horse serum in 0.4% Triton X-100 PBS (blocking solution) for 2h at room temperature. Primary antibody was performed in blocking solution overnight at 4°C. Then, the slices were washed with PBS three times for 10 min at room temperature, followed by the secondary antibody (diluted 1:800 in PBS), goat anti-mouse Alexa Fluor 555 (A21422, Thermo Fisher Scientific, Waltham, MA) and goat anti-rabbit Alexa Fluor 488 (A11008, Thermo Fisher Scientific, Waltham, MA) incubation for 1h at room temperature in darkness. Sections were finally counterstained with 1 μg/ml 4,6-diamidino-2-phenylindole dihydrochloride (DAPI) in PBS for 10 min at RT and mounted on slides with Fluoromount-G® (Southern Biotech, 0100). Samples were imaged using a laser scanning confocal microscope with FV500 (Olympus) for immunofluorescence imaging. Immunoreactivity quantification was analyzed with the Image J software (Rasband, W.S., ImageJ, U. S. National Institutes of Health, Bethesda, Maryland, USA, <https://imagej.nih.gov/ij/>, 1997-2018).

## **Immunohistochemistry**

One control and one transgenic paraformaldehyde fixed paraffin embedded tissue slides were dried for 1h at 65° before pre-treatment procedure of deparaffinization, rehydration and epitope retrieval in the Pre-Treatment Module (Agilent Technologies-DAKO, PT-LINK) at 95°C for 20 min in 50x Tris/EDTA buffer, pH 9. For p21 immunohistochemical staining, p21WAF1/Cip1 antibody (Agilent Technologies-DAKO, clone SX118) 1:100 dilution was used. After incubation, the reaction was visualized with the EnVision™ FLEX Detection Kit (Agilent Technologies-DAKO) using diaminobenzidine chromogen as a substrate. For p16 immunohistochemical staining, p16 INK4a antibody was used using CINtec® Histology Kit (ROCHE, clone E6H4) following manufacturer's instructions. Sections were counterstained with hematoxylin.

## **Senescence-associated $\beta$ -galactosidase activity**

Briefly, paraformaldehyde-fixed frozen sections were incubated with X-gal solution (20 mg/ml X-Gal (SIGMA), 5 mM K<sub>3</sub>Fe(CN)<sub>6</sub>, 5 mM K<sub>4</sub>Fe(CN)<sub>6</sub> and 2 mM MgCl<sub>2</sub>) in PBS at pH 6.0 overnight at 37 °C. To allow comparison between specimens, all samples were assayed simultaneously. Then, neurons were stained with Green Fluorescent Nissl Stain (Thermo Fisher Scientific, N21480) diluted 1:150 in PBS and incubated 20 minutes at room temperature. The slices were then washed 3x with PBS for 10 minutes at room temperature and 1x with PBS for 2 hours at room temperature. Nuclei were stained with DAPI (SIGMA, 32670). Images of the stained sections were taken using inverted microscope (Olympus, IX71S8F-2). Eight randomly selected areas of each mouse (N=2-3 per group) of the ventral horn of lumbar spinal cord sections were photographed at 20x magnification for visual analysis. The whole section of SA- $\beta$ -Gal stained slices was photographed at 4x magnification.

## **Cell culture**

HeLa and 3T3 cells were maintained in Dulbecco's Modified Eagle's Medium (11965, Thermo Fisher Scientific), 10% FBS (10270, Thermo Fisher Scientific), 100 U/ml Penicillin-Streptomycin (15140-122, Thermo Fisher Scientific) at 37°C and 5% CO<sub>2</sub>. NSC-34 cells were maintained in MEM-Advanced Medium (12492013, Thermo Fisher Scientific) and MTT assay (M5655, SIGMA) was employed to estimate cell viability. TDP-43 knockdown HeLa cells were obtained transducing cells with a TDP-43 shRNA (TDP-43 KD) or scrambled (SCR) lentivirus. 50000 cells were seeded in 6-well plate and transduced with lentivirus the same day. Cell media was changed the next day. Cells were harvested 96-hour post-transduction. Human neural tissue cells were obtained from Axol (Axol Biosciences, ax0018). iPSC-Derived Neural Stem Cells derived from integration-free, induced

## *Materials and Methods*

pluripotent stem cells under fully defined neural induction condition were expanded and differentiated following System A of the manufacturer's protocol (version 5.0). For siRNA and ASO treatment, 20 nM (final concentration) of TARDBP siRNA (EHU109221, SIGMA) for human and *mmsiTDP-43s*: 5'-AGGAAUCAGCGUGCAUAUA-3' *mmsiTDP-43as*: 5'-UAUAUGCACGCUGAUUCCU-3' for mouse or scrambled siRNA was mixed with ASO at 5, 10, 20, 40 or 100 nM (final concentration in well) in 100 µl Opti-MEM (31985062, Thermo Fisher Scientific) mix. 2 µl/well of RNAiMAX (13778100, Thermo Fisher Scientific) were mixed with ASOs (**Table 4**) and siRNA mix for 20 minutes at room temperature on the bottom of the well. 2 ml of DMEM (11965092, Thermo Fisher Scientific) supplemented with 10% FBS containing 100.000 HeLa or 3T3 cells/well were seeded onto mixed transfection. After 24 hours, transfection media was removed and changed to DMEM 10% FBS media. 48 hours post-transfection, cells were collected for posterior analyses.

## **Organotypic Spinal Cord Culture**

Lumbar spinal cord slices from P8 rat pups were obtained as described (J. D. Rothstein, Jin, Dykes-Hoberg, & Kuncl, 1993). Slices were maintained in 50% minimal essential medium,

## *Materials and Methods*

25 mM HEPES, 25% Hank's balanced salt solution with D-glucose 25.6 mg/l, 25% heat-inactivated horse serum, and 2 mM L-glutamine (Invitrogen, Carlsbad, CA, USA). Five complete slices from the lumbar region were transferred to 30-mm-diameter Millipore Millicell-CM (0.22  $\mu$ m; Millipore Corporation, Bedford, MA, USA) membrane inserts. The inserts were placed in 6-well culture trays (35-mm-diameter Falcon; BD), with 1-ml culture medium: 50% (vol/vol) minimal essential medium (MEM) with 25 mM HEPES (Invitrogen), 25% (vol/vol) heat-inactivated horse serum, and 25% (vol/vol) Hank's balanced salt solution (HBSS) supplemented with D-glucose (25.6 mg/ml; SIGMA), 2 mM L-glutamine, 100 U/ml penicillin, and 100  $\mu$ g/ml streptomycin (Invitrogen). Organotypic cultures were incubated at 37 °C in a 5% CO<sub>2</sub>–95% O<sub>2</sub> humidified incubator, and the culture medium was changed 4 h after harvesting and then twice a week. Cultures were let to stabilize for 10 days; after this point, the motoneuron population reaches a steady number and remains stable from 1 to 4 weeks. Thus, the treatments, inducing chronic excitotoxicity with threohydroxyaspartate (THA) at 100  $\mu$ M, with DHA and/or  $\alpha$ -tocopherol, 500  $\mu$ M each, started 10 days after the explant procedure. After 15 days of treatment, cultures were harvested and fixed in 4% paraformaldehyde in 0.1 M phosphate buffer, pH 7.4, overnight at 4°C and processed for immunohistochemistry.

### **Fluorescent TDP-43 cryptic splicing function reporter**

pRint was a gift from Mariano Garcia-Blanco (Addgene plasmid #24218; <http://n2t.net/addgene:24218>; RRID: Addgene\_24218). This plasmid was modified by Agentide to introduce ATG4B cryptic exon in the Multiple Cloning Site between the two exons of RFP. HeLa cells were transfected using 1  $\mu$ g of plasmid and 1  $\mu$ l of Lipofectamine 2000 (11668-027, Thermo Fisher Scientific) mixed in Opti-MEM (31985-047, Thermo Fisher Scientific) 72 hours post-transduction. After 24 hours cells were visualized and harvested.

### **Metabolites extraction**

100  $\mu$ L of PBS and 300  $\mu$ L of ice-cold acetone were added to platelet pellet. Samples were vortex-mixed for 10 seconds and incubated 30 minutes at 4 °C. Samples were then centrifuge at 4 °C for 10 minutes at 1000 xg. Supernatant was separated into a clean glass tube and evaporated in Speed Vac. 250  $\mu$ L of methanol and 500  $\mu$ L of chloroform were added together with standard mix. Samples were vortex-mixed for 10 seconds, 200  $\mu$ l de KCl 0,7% were added, vortex-mixed for 10 seconds and centrifuge at 4 °C for 10 minutes at 1000 xg. Upper and bottom phases were separated. Bottom

## *Materials and Methods*

phase contained chloroform soluble metabolites (lipids) and upper phase contained methanol soluble metabolites (employed for the metabolomic analysis).

### **Metabolomic analysis**

For the metabolomic study, an Agilent 1290 liquid chromatography system coupled to an ESI-Q-TOF MS/MS 6520 instrument (Agilent Technologies, Santa Clara, CA, US) was used. In all cases, 2  $\mu$ L of extracted sample was applied onto a reversed-phase column (Zorbax SB-Aq 1.8  $\mu$ m 2.1  $\times$  50 mm; Agilent Technologies) equipped with a precolumn (Zorbax-SB-C8 Rapid Resolution Cartridge 2.1  $\times$  30 mm 3.5  $\mu$ m; Agilent Technologies) with a column temperature of 60 °C. The flow rate was 0.6 mL/min. Solvent A was composed of water containing 0.2% acetic acid and solvent B was composed of methanol 0.2% acetic acid. The gradient started at 2% B and increased to 98% B in 13 min and held at 98% B for 6 min. Post-time was established in 5 min.

Data were collected in positive electrospray mode time of flight operated in full-scan mode at 100–3000 m/z in an extended dynamic range (2 GHz), using N<sub>2</sub> as the nebulizer gas (5 L/min, 350 °C). The capillary voltage was 3500 V with a scan rate of 1 scan/s. The ESI source used a separate nebulizer for the continuous, low-level (10 L/min) introduction of reference mass compounds: 121.050873, 922.009798 (positive ion mode) and 119.036320, 966.000725 (negative ion mode), which were used for continuous, online mass calibration. MassHunter Data Analysis Software (Agilent Technologies) was used to collect the results, and MassHunter Qualitative Analysis Software (Agilent Technologies) to obtain the molecular features of the samples, representing different, co-migrating ionic species of a given molecular entity using the Molecular Feature Extractor algorithm (Agilent Technologies), as described (Jove et al., 2015).

### **Statistical analyses**

Metaboanalyst software ([www.metaboanalyst.ca](http://www.metaboanalyst.ca)) and GraphPad Prism (GraphPad Software, San Diego, CA, USA) were used for the analyses. Unpaired t-test was used to estimate significant differences between ALS vs CTL and Fast Progressors vs Slow Progressors in metabolipidomic, FA profile, Western Blot and RT-qPCR analyses. Spearman's rank correlation analysis was employed to estimate the association between two variables. Statistical significance was considered when  $p < 0.05$ .

# **5 ARTICLES**



## **5.1 Article 1**

**Title:** Cryptic exon splicing function of TARDBP interacts with autophagy in nervous tissue.

**Authors:** Pascual Torres, Omar Ramírez-Núñez, Ricardo Romero-Guevara, Gisel Barés, Ana B. Granado-Serrado, Victòria Ayala, Jordi Boada, Laia Fontdevila, Mònica Povedano, Daniel Sanchís, Reinald Pamplona, Isidre Ferrer and Manuel Portero-Otín.

**Journal:** Autophagy

**Published:** 28/07/2018

**DOI:** 10.1080/15548627.2018.1474311




## Cryptic exon splicing function of TARDBP interacts with autophagy in nervous tissue

Pascual Torres, Omar Ramírez-Núñez, Ricardo Romero-Guevara, Gisel Barés, Ana B. Granado-Serrano, Victòria Ayala, Jordi Boada, Laia Fontdevila, Monica Povedano, Daniel Sanchís, Reinald Pamplona, Isidro Ferrer & Manuel Portero-Otín


To cite this article: Pascual Torres, Omar Ramírez-Núñez, Ricardo Romero-Guevara, Gisel Barés, Ana B. Granado-Serrano, Victòria Ayala, Jordi Boada, Laia Fontdevila, Monica Povedano, Daniel Sanchís, Reinald Pamplona, Isidro Ferrer & Manuel Portero-Otín (2018) Cryptic exon splicing function of TARDBP interacts with autophagy in nervous tissue, *Autophagy*, 14:8, 1398-1403, DOI: [10.1080/15548627.2018.1474311](https://doi.org/10.1080/15548627.2018.1474311)


To link to this article: <https://doi.org/10.1080/15548627.2018.1474311>

 View supplementary material [↗](#)

 Published online: 28 Jul 2018.

 Submit your article to this journal [↗](#)








 Article views: 784

 View related articles [↗](#)

 View Crossmark data [↗](#)

 Citing articles: 13 View citing articles [↗](#)

## Cryptic exon splicing function of TARDBP interacts with autophagy in nervous tissue

Pascual Torres<sup>a</sup>, Omar Ramírez-Núñez<sup>a</sup>, Ricardo Romero-Guevara<sup>a</sup>, Gisel Barés<sup>b</sup>, Ana B. Granado-Serrano <sup>a</sup>, Victòria Ayala <sup>a</sup>, Jordi Boada <sup>a</sup>, Laia Fontdevila<sup>a</sup>, Monica Povedano<sup>c</sup>, Daniel Sanchis <sup>b</sup>, Reinald Pamplona <sup>a</sup>, Isidro Ferrer <sup>d</sup>, and Manuel Portero-Otín <sup>a</sup>

<sup>a</sup>Metabolic Pathophysiology Research Group, Department of Experimental Medicine, University of Lleida-IRBLleida, Lleida, Spain; <sup>b</sup>Cell Signalling and Apoptosis Group, Department of Basic Medical Sciences, University of Lleida-IRBLleida, Lleida, Spain; <sup>c</sup>Neurology Service, Bellvitge University Hospital, L'Hospitalet de Llobregat, Barcelona, Spain; <sup>d</sup>Department of Pathology and Experimental Therapeutics, University of Barcelona-CIBERNED, L'Hospitalet de Llobregat, Barcelona, Spain

### ABSTRACT

TARDBP (TAR DNA binding protein) is one of the components of neuronal aggregates in sporadic amyotrophic lateral sclerosis (ALS) and frontotemporal lobar degeneration. We have developed a simple quantitative method to evaluate TARDBP splicing function that was applied to spinal cord, brainstem, motor cortex, and occipital cortex in ALS ( $n = 8$ ) cases compared to age- and gender-matched control ( $n = 17$ ). Then, we quantified the abundance of a TARDBP-spliced cryptic exon present in *ATG4B* (autophagy related 4B cysteine peptidase) mRNA. Results of these analyses demonstrated that the loss of this *TARDBP* function in spinal cord, brainstem, motor cortex, and occipital cortex differentiated ALS from controls (area under the curve of receiver operating characteristic: 0.85). Significant correlations were also observed between cryptic exon levels, age, disease duration, and aberrant mRNA levels. To test if *TARDBP* function in splicing is relevant in *ATG4B* major function (autophagy) we downregulated *TARDBP* expression in human neural tissue and in HeLa cells, demonstrating that TARDBP is required for maintaining the expression of *ATG4B*. Further, *ATG4B* overexpression alone is sufficient to completely prevent the increase of SQSTM1 induced by *TARDBP* downregulation in human neural tissue cells and in cell lines. In conclusion, the present findings demonstrate abnormal alternative splicing of *ATG4B* transcripts in ALS neural tissue in agreement with *TARDBP* loss of function, leading to impaired autophagy.

**Abbreviations:** ALS: amyotrophic lateral sclerosis; *ATG4B*: autophagy related 4B cysteine peptidase; AUC: area under the curve; FTL: frontotemporal lobar degeneration; iPSC: induced pluripotent stem cells; ROC: receiver operating characteristic; *TARDBP*: TAR DNA binding protein; RT-qPCR: quantitative RT-PCR

### ARTICLE HISTORY

Received 1 February 2017  
Revised 21 April 2018  
Accepted 2 May 2018

### KEYWORDS

Amyotrophic lateral sclerosis; autophagy related 4B cysteine peptidase; biomarker; splicing variant

## Introduction

TARDBP (TAR DNA binding protein) is one of the components of neuronal aggregates in sporadic amyotrophic lateral sclerosis (ALS) and frontotemporal lobar degeneration (FTLD). Whether these aggregates are associated with *TARDBP* loss of function is not known. TARDBP is involved in the splicing of cryptic exons of selected mRNAs, such as of *ATG4B* (autophagy related 4B cysteine peptidase). Cryptic exons are considered splicing variants that may introduce frameshifts or stop codons, among other changes in the resulting mRNA. These aberrant mRNA have been demonstrated in motor cortex and middle temporal gyrus of ALS and FTLD patients [1]. However, it was undetermined whether ALS target locations also presented cryptic exons. Further, whether these mRNA anomalies have any impact in translation of the corresponding proteins was unknown. In this brief report, we have developed a simple quantitative method to evaluate this TARDBP splicing function that was applied to samples of various central nervous system regions from ALS cases compared to age- and gender-matched control

individuals. Further, we have characterized the effects of TARDBP loss in autophagy role of *ATG4B*.

## Results and discussion

RNA was extracted from 50–100 mg homogenized nervous tissue. We quantified the abundance of TARDBP-spliced cryptic exons present in *ATG4B* mRNAs with RT-qPCR. RT-qPCR results agree with the loss of TARDBP function in spinal cord, brainstem, motor cortex, and occipital cortex differentiating ALS from controls (area under the curve of ROC: 0.85, Figure 1(a)). Next, we observed that the abundance of cryptic exons in the *ATGB* transcript was mainly influenced by ALS status ( $p < 0.005$  for ALS status,  $p = 0.69$  for brain region and  $p = 0.1$  for interaction in 2-way ANOVA) (Figure 1(b)). Significant correlations were also observed between bulbar levels of cryptic exons and age (Figure 1(c)). Indeed, a more severe phenotype of the disease (i.e., shorter duration of disease after diagnosis) was associated with higher level of aberrant mRNAs (Figure 1(d)).

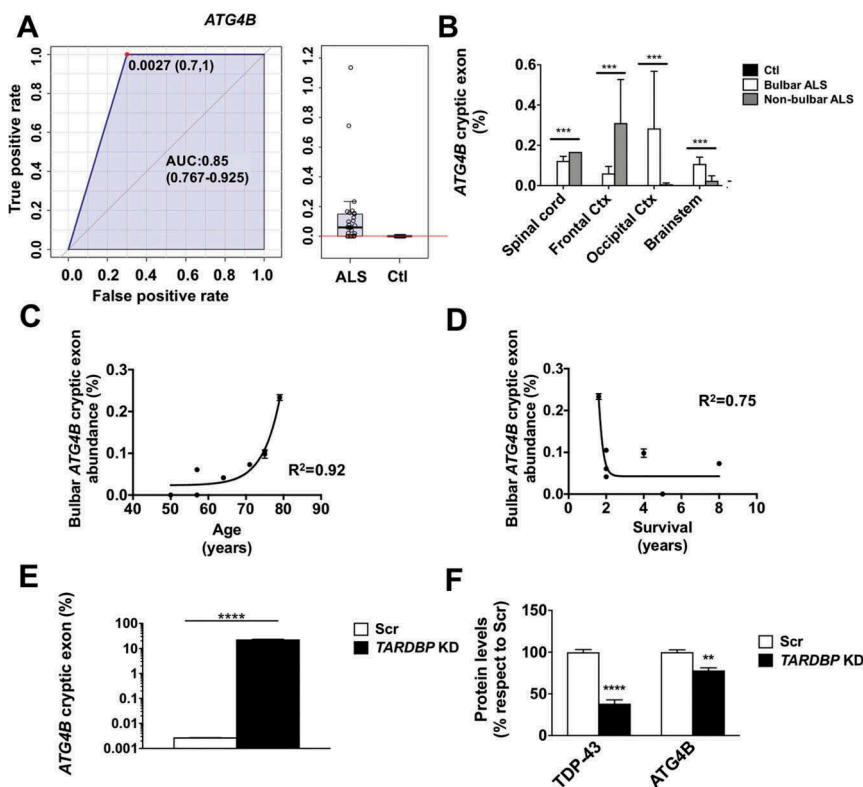


**Figure 1.** The abundance of TARDBP regulated cryptic exons in *ATG4B* mRNA is an ALS tissue biomarker and *TARDBP* knockdown leads to down regulation of *ATG4B*. (a) Values of *ATG4B* mRNA analyses ( $\pm$  standard error) indicate that *ATG4B* cryptic exon levels are higher in samples from ALS when compared with controls. (b) RT-qPCR of *ATG4B* cryptic exons show different expression levels in spinal cord, frontal cortex, occipital cortex, and brain stem; *ATG4B* aberrant mRNA levels depend on ALS type (bulbar vs non-bulbar cases). (c) *ATG4B* cryptic exon levels in brainstem of ALS patients have a positive correlation with age and (d) a negative correlation with disease duration. Further, *TARDBP* knockdown (KD) in human neural tissue cells differentiated from iPSC induced significant increase of the amount of *ATG4B* cryptic exon levels, as quantified by RT-qPCR (e), with a downregulation of *ATG4B* protein (f) evaluated by western blot and quantified by densitometry. Bars indicate mean values with standard error. For (g) \*\*\*  $p < 0.001$  for disease type in a 2-way ANOVA accounting for disease type and region. In (e) and (f) \*\*\*\*  $p < 0.0001$  and \*\*  $p < 0.001$  after Student's t test (e) or post hoc Bonferroni analyses (f). AUC, area under the curve.

To demonstrate if TARDBP function is relevant in maintenance of *ATG4B* mRNA we downregulated *TARDBP* in human nervous tissue cells. The results demonstrate that *TARDBP* downregulation increased the amount of cryptic exons to up 20% of *ATG4B* mRNA (Figure 1(e)) and causes a loss of 30% of *ATG4B* protein (Figure 1(f)). Nonsense-mediated decay of aberrant *ATG4B* mRNA may explain the hereby observed loss of *ATG4B* in human cells. The fact that this mRNA anomaly would target mainly motor neurons – a quantitatively minor cell population in these tissues – could account for the low percentage of mRNA affected and the apparent lack of quantitative differences of *ATG4B* protein in nervous tissue samples observed (data not shown). Of note, sequence analyses suggest that loss of function of TARDBP on *ATG4B* cryptic exon introduces a premature stop codon leading to loss of residues 317–393 in the resulting protein. Because these residues contain 2 phosphorylation sites required for *ATG4B* protein activity [2], their loss induced by cryptic exon inclusion may result in defective autophagy.

To test if TARDBP function in splicing is relevant in *ATG4B* major cellular function (macroautophagy/autophagy) we downregulated *TARDBP* expression in HeLa cells. Results showed that *TARDBP* is required for maintaining the expression of *ATG4B*, as loss of *TARDBP* leads to an approximately 50% loss of *ATG4B* mRNA (Figure 2(a)) and protein (Figure 2(b)) in HeLa cells, in association with the presence of cryptic

exons in 38% of *ATG4B* mRNA (Figure 2(a)). *TARDBP* is required to orchestrate a physiological autophagy response, as reinforced by the failure of *TARDBP*-deficient cells to increase *ATG4B* mRNA in cases of autophagy induction (Figure 2(a)); *TARDBP*-deficient HeLa cells also exhibited increased baseline levels of SQSTM1 (Figure 2(c)), a hallmark of autophagy disturbance [3].

*TARDBP* deficiency might affect autophagy by other mechanisms, besides *ATG4B* downregulation, as it modifies the expression of transcripts of approximately 41 genes. However, *ATG4B* overexpression alone is sufficient to completely prevent the increase of SQSTM1 induced by *TARDBP* downregulation in HeLa and human neural tissue cells (Figure 2(d)). Noteworthy, *ATG4B* loss was not compensated by increased expression of other *ATG4B* homologs (Figure S6, ESM). Previous data have shown that SQSTM1 interacts with TARDBP aggregates in ALS [4]. Together, the present data point to a novel mechanism implicating autophagy as a relevant factor in the pathogenesis of sporadic ALS, in addition to the involvement of autophagy pathway components in familial ALS including *ALS2*, *OPTN*, and *SIGMAR1* [5].

Besides *ATG4B* mRNA, other genes, such as *GPSM2* (*G protein signaling modulator 2*) are also influenced by TARDBP dysfunction [1]. We also designed a RT-qPCR method for analysis of cryptic exon inclusion in its mRNA. The results confirm that abundance of cryptic exons in *GPSM2* mRNA

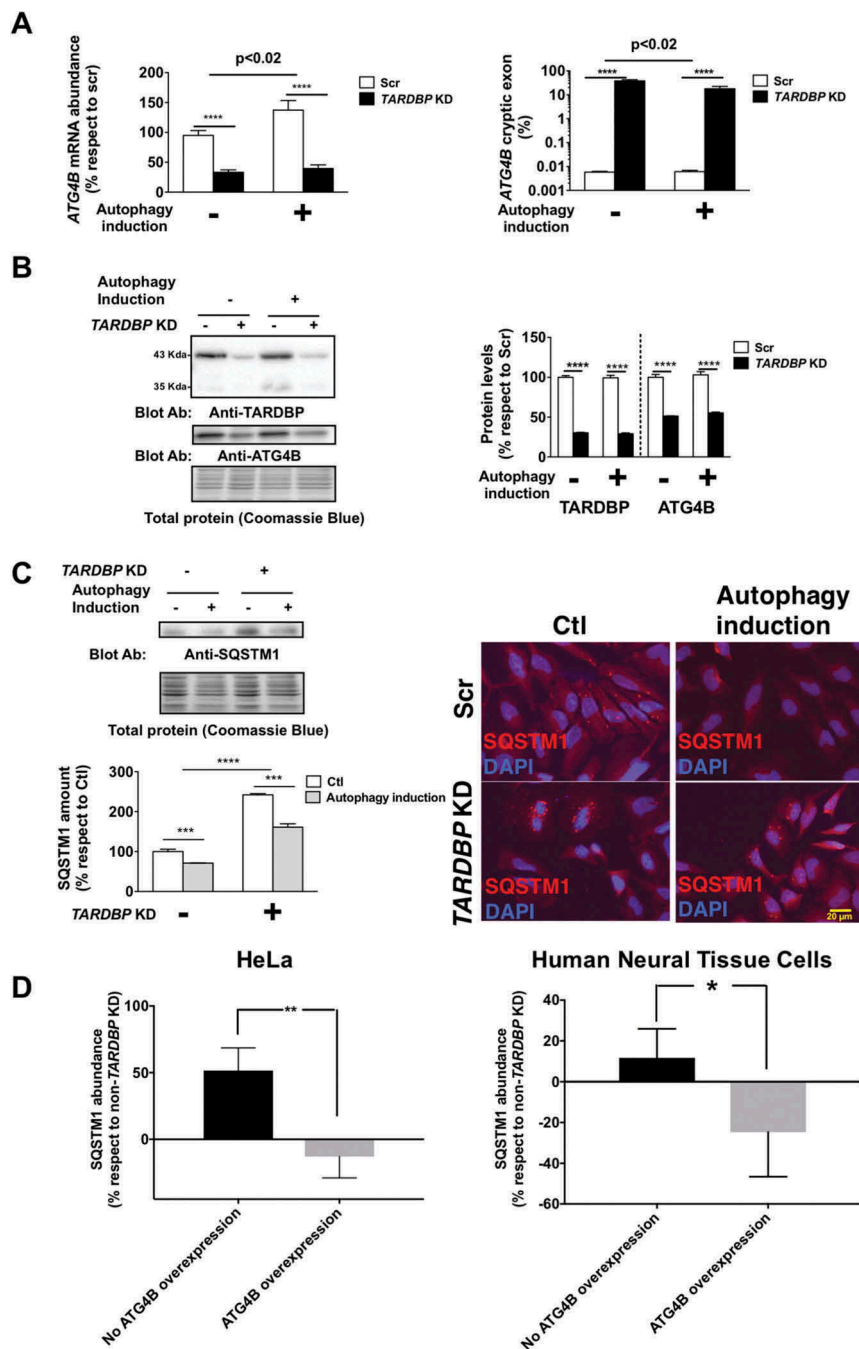


**Figure 2.** *TARDBP* is required for a homeostatic autophagy response. (a) *TARDBP* knockdown (KD) in HeLa cells leads to decreased *ATG4B* mRNA levels (left panel) linked to increased amounts of *ATG4B* mRNA with cryptic exons (right panel); this is associated with a failure to enhance *ATG4B* mRNA expression as a response to autophagy stimulation by nutrient deprivation. (b) *TARDBP* protein loss is associated with *ATG4B* decrease as shown by western blot (left panel) and densitometry (right panel). (c) Functional analyses reveal that loss of *TARDBP* in HeLa cells induces increased levels of SQSTM1 as shown by western blot (left panel) and immunofluorescence (right panel), suggesting a functional loss of autophagy flux. (d) The increase in SQSTM1 induced by *TARDBP* knockdown is rescued by *ATG4B* overexpression, as shown by densitometry analyses, either in HeLa cells (left panel) or in Human Neural Tissue primary cells (right panel). Blots are representative of different experiments ( $n = 3-5$ ). Bars indicate mean values ( $\pm$  standard error). For (a), (b) and (c) \*\*\*\* $p < 0.0001$ , \*\*\* $p < 0.001$  after 2-way ANOVA. For (d) \* $p < 0.05$  and \*\* $p < 0.01$  in Student's *t* test.

could also be useful for ALS diagnosis (area under the curve of ROC for *GPSM2* aberrant mRNA: 0.89, Figure 3(a)). Levels of *GPSM2* aberrant mRNA are significantly influenced both by brain region and ALS type (bulbar ALS vs non-bulbar ALS; 2-way ANOVA:  $p < 0.001$  for interaction,  $p < 0.0001$  for disease status and  $p = 0.0061$  for brain region, Figure 3(b)). Bulbar cases show higher levels of these mRNA in brain stem and occipital cortex, in comparison to spinal cord and frontal

cortex, being opposite for non-bulbar cases. These results might be explained by spreading of the disease pathological traits (i.e., loss of *TARDBP* function) between adjacent anatomical locations, as indicated previously by neuroimaging techniques [6]. Furthermore, levels of cryptic exons in *GPSM2* in frontal cortex correlate with those in spinal cord (Figure 3(c)). Interestingly, and supporting the involvement of the loss of this *TARDBP* function as a common mechanism

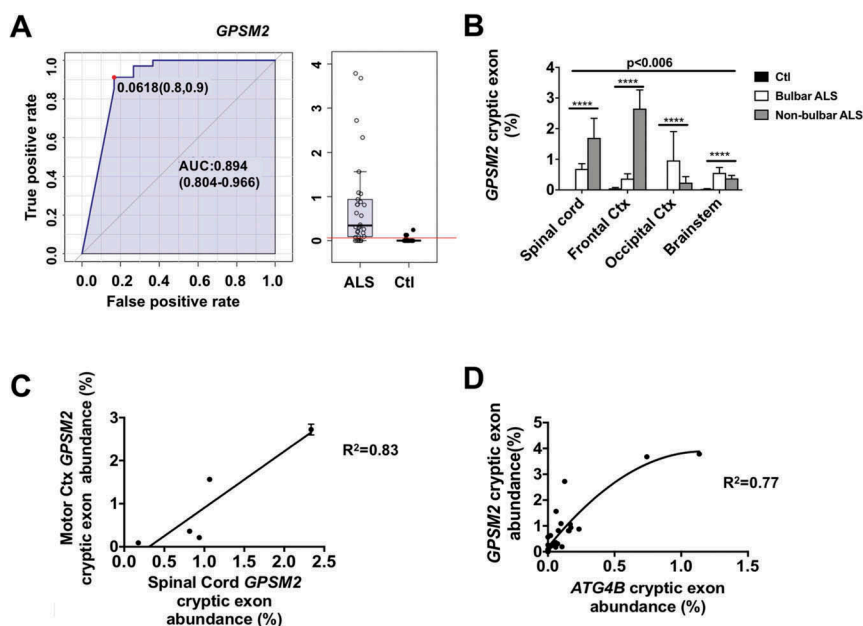


**Figure 3.** *GPSM2* cryptic exon abundance depends on disease type and region. Values of *GPSM2* mRNA analyses ( $\pm$  standard error) indicate that (a) *GPSM2* cryptic exon levels are higher in samples from ALS when compared with controls. (b) RT-qPCR of *GPSM2* cryptic exons shows different expression levels in spinal cord, frontal cortex, occipital cortex, and brain stem. (c) Linear regression between the amount of cryptic exons in *GPSM2* in lumbar spinal cord and motor cortex (Ctx). (d) Tissue concentrations of cryptic exons in *ATG4B* and *GPSM2* correlate positively in a non-linear fashion. For (b), \*\*\*  $p < 0.001$  and \*\*\*\*  $p < 0.0001$  for disease type in a 2-way ANOVA accounting for disease type and anatomic region. AUC, area under the curve.

for appearance of both cryptic exons, levels of aberrant mRNA in *GPSM2* correlate with those in *ATG4B* mRNAs in every tissue evaluated (Figure 3(d)).

In conclusion, we show the usefulness of tissue RT-qPCR in searching for cryptic exons as a rapid method to analyze TARDBP function, with potential implications in ALS diagnosis. We recognize that the usefulness for ALS diagnoses, based on this preliminary study, should be further substantiated by employing a larger number of individuals. This is evidenced by the shape of the ROC curve indicated above, showing the impact of a relative low number of specimens analyzed. Nonetheless, the present findings demonstrate abnormal alternative splicing of *ATG4B* transcripts in ALS neural tissue in agreement with *TARDBP* loss of function, leading to impaired autophagy.

## Materials and methods

### Neuronal tissues

All samples were obtained from the Institute of Neuropathology and the University of Barcelona Brain Bank following the guidelines of the local ethics committees. Extensive pathological studies were done for ALS diagnosis as previously described [7]. Samples from different anatomical locations were from 5 males and 3 females aged between 50 and 79 years affected with typical neurological and neuropathological characteristics of sporadic ALS. The post-mortem delay between death and tissue processing was between 3 and 16 h. Age- and gender-matched controls with no clinical evidence of neurological disease and with a normal neuropathological study were processed in parallel (see Table S1, Electronic Supplemental Material (ESM)).

### Cell culture and treatments

HeLa cells were maintained in Dulbecco's Modified Eagle's Medium (Thermo Fisher Scientific, 11965), 10% FBS (Thermo Fisher Scientific, 10270), 100 U/ml penicillin-streptomycin (Thermo Fisher Scientific, 15140-122) at 37°C and 5% CO<sub>2</sub>. Human neural tissue cells were obtained from Axol (Axol Biosciences, ax0018). Briefly, iPSC-Derived Neural Stem Cells derived from integration-free, induced pluripotent stem cells under fully defined neural induction condition were expanded and differentiated following System A of the manufacturer's protocol (version 5.0).

*TARDBP* knockdown cells were obtained by transducing cells with a *TARDBP* shRNA lentivirus (see below for further details). Cell media were changed the day after the transduction and the cells were cultured for further 96 h to allow *TARDBP* silencing.

For inducing autophagy by nutrient deprivation, cells were infected with scrambled or *TARDBP* shRNA as indicated above, and for the last 16 h after transduction the medium was replaced with complete fresh medium, as control, or HBSS (Thermo Fisher Scientific, 14025), for nutrient starvation.

### ShRNA design

Primer was designed against the sequence 5'-GACGATGGTGTGACTGCAAAC-3' for human *TARDBP* and cloned in the pSUPER (Oligoengine, pSUPER). Then, an EcoRI-ClaI fragment containing the H1 promoter for RNA polymerase III and the shRNA sequence was cut from pSUPER and subcloned into the pLVTHM plasmid, a gift from Didier Trono (Addgene, 12247) [8]. shRNA vector, the

plasmids psPAX2 (Addgene, 12260) and pMD2.G (Addgene, 12259) (both a gift from Dr. Trono) were transfected together using the polyethylenimine transfection method (Sigma-Aldrich, 408727) into HEK293T cells. The HEK293T medium was collected after 48 h of transfection and centrifuged at  $50,000 \times g$  for 3 h. The final viral pellet was diluted in sterile phosphate-buffered saline (Thermo Fisher Scientific, 10010015) plus 2% bovine serum albumin (Sigma-Aldrich, A4503). The efficacy of the shRNA was demonstrated by western blot.

### RNA extraction, cDNA synthesis, conventional PCR and quantitative RT-PCR (RT-qPCR)

RNA was extracted from cells and tissue samples using TRI Reagent (Thermo Fisher Scientific, AM9738) following the manufacturer's instructions. RNA concentrations were measured using a NanoDrop ND-1000 (Thermo Fisher Scientific). One microgram of RNA was used for retrotranscription employing TaqMan Reverse Transcription Reagent using random hexamers (Thermo Fisher Scientific, N8080234).

Primers used to perform conventional PCR reaction were those previously described [1], purchased from Roche Oligo synthesis service (Roche Diagnostics, Barcelona, Spain). For *ATG4B* forward: 5'-TGTGTCTGGATGTGAGCGTG-3', reverse 5'-TCTAGGGACAGGTTTCAGGACG-3'; for *GPSM2* forward: 5'-AGTGGACATGTGGTGGTAAGAA-3', reverse: 5'-GCTTCAAAGAATGACACGCCA-3'; for *GAPDH* (PCR control) forward: 5'-ATCCCATCACCATCTTCCAG-3', reverse: 5'-CCATCACGCCACAGTTTCC-3'. PCR conditions were as follows: initial denaturation at 98°C for 30 sec, followed by 40 cycles of 98°C for 30 sec, 63°C for 12 sec and 72°C for 30 sec. Gel analyses demonstrated the presence of potential *ATG4B* and *GPSM2* cryptic exons in samples from ALS patients (Figure S1, ESM), whose identity was ensured by Sanger sequencing (> 99% sequence homology, E value ranging between 1 and  $3e-40$ ) as shown in Figure S2 and Figure S3 (ESM).

In order to quantify the level of cryptic exons we developed a RT-qPCR method. Briefly, RT-qPCR experiments were performed using a CFX96 instrument (Bio-Rad) with SYBR Select Master Mix (Thermo Fisher Scientific, 4472908). Each 20  $\mu$ L of reaction contained 4  $\mu$ L cDNA, 10  $\mu$ L SYBR Select Master Mix, 0.2 nM of forward primer and 0.2 nM of reverse primer solutions and 4  $\mu$ L PCR grade water. Primers developed for mRNAs quantification by RT-qPCR are listed in Table S2 (ESM). Oligonucleotides for human *GPSM2* and human *ATG4B* were designed with Primer3 [9] (<http://primer3.ut.ee>). *GAPDH* oligo and *ATG4B* homologs have been previously described [10,11]. All oligonucleotides were purchased from Sigma-Aldrich. Three technical replicates for all RT-qPCR reactions were conducted. For all RT-qPCR primers, quality control was performed for their specificity, sensitivity, melting curves and standard curves as shown in Figure S4 and Figure S5 (ESM). The RT-qPCR run protocol was as follows: 50°C for 2 min and 95°C for 2 min, with the 95°C for 15 sec and 60°C for 1 min steps repeated for 40 cycles; and a melting curve test from 65°C to 95°C at a 0.1°C/

sec measuring rate. Cryptic exon abundances were normalized by total mRNA for each gene with the following formula [12]:

$$\Delta Cq = Cq (\text{total mRNA}) - Cq (\text{cryptic mRNA})$$

$$\text{Cryptic exon abundance} = 2^{-\Delta Cq}$$

For total *ATG4b* mRNA relative expression, we used the formula as follows:

$$\Delta Cq = Cq (\text{total ATG4B}) - Cq (\text{GAPDH})$$

$$\Delta \Delta Cq = \Delta Cq (\text{target}) - \Delta Cq (\text{control})$$

$$\text{ATG4B mRNA fold change} = 2^{-\Delta \Delta Cq}$$

### Western blot analysis

Protein from cells was extracted using radioimmunoprecipitation buffer with 1X Halt Protease Inhibitor Cocktail (Thermo Fisher Scientific, 1861278). After sonication, protein quantification was performed with the Bradford assay [13] using a commercial reagent (Bio-Rad, 5000006). Fifteen micrograms of protein were loaded onto a 12% acrylamide SDS-PAGE gel. Membranes were blocked with I-Block (Thermo Fisher Scientific, T2015) for 1 h and incubated overnight with the antibodies and conditions listed in Table 1.

After primary antibody incubation, membranes were washed 3 times with TBS-T 0.05% (20 mM Tris, 125 mM NaCl, 0.05% TWEEN 20 [Sigma-Aldrich, P7949], pH 7.6) and incubated with secondary antibody for 1 h. Immobilon™ Western Chemiluminiscent HRP Substrate (Merck Millipore, WBKLS0500) was used for immunodetection. Membranes were stained with Coomassie Brilliant Blue G (Sigma-Aldrich, 27815) for normalization. Specific bands were quantified with ImageLab v5.2.1 (Bio-Rad).

### ATG4B overexpression

HeLa or human neural tissue primary cells derived from iPSC were transfected after 72 h of transduction with shRNA or scrambled with Lipofectamine 2000 (Thermo Fisher, 11668) according to the manufacturer's protocol. Briefly, 0.5  $\mu$ L of Lipofectamine were used per 0.5  $\mu$ g of *ATG4B* overexpression plasmid (Sino Biological Inc., HG20407-UT). Complexes were formed in 500  $\mu$ L of Opti-MEM (Thermo Fisher, 31985070). The mixture was added to the cells grown in complete medium and collected after 24 h post-transfection.

**Table 1.** Antibodies and conditions employed.

Target	Dilution	Source
TARDBP	1:1000 in TBS-T 0.05%	Proteintech, 10782-2-AP
ATG4B	1:250 in TBS-T 0.05%	Sigma-Aldrich, A2981
SQSTM1	1:1000 in TBS-T 0.05% (Western blot); 1:100 in PBS (immunocytofluorescence)	Cell Signalling Technology, 5114
Secondary anti-rabbit, HRP conjugate	1:50000 in TBS-T 0.05%	Thermo Fisher Scientific, 31460
Secondary anti-rabbit, Alexa Fluor® 546 conjugate	1:800 in PBS	Thermo Fisher Scientific, A11010

## Immunofluorescence

HeLa cells (10,000) were seeded in a 24-well plate onto glass coverslips. After 3 h of seeding, cells were transduced and treated as described above. Cells were washed twice with sterile PBS pH 7.4 (Thermo Fisher Scientific, 10010015) and fixed with 4% formaldehyde (Sigma-Aldrich, 252549) solution in PBS for 10 min at room temperature. After fixation, cells were washed twice with PBS, permeabilized and blocked with PBS containing 0.5% Triton X-100 (Sigma-Aldrich, X100) 10% normal goat serum (Abcam, ab7481) for 15 min followed by primary antibody incubation overnight at 4°C. Cells thereafter were washed 2 times with PBS and incubated with secondary antibody and DAPI (Sigma-Aldrich, D9542) at 1 µg/ml for 1 h at room temperature and mounted with Fluoromount-G (Southern Biotech, 0100-01). Immunofluorescence controls, performed by omitting the primary antibodies, resulted in the abolition of the immunostaining in all cases.

## Statistical analysis

All statistics and figures were performed with GraphPad Prism (GraphPad Software), unless indicated otherwise. For receiver operating characteristic (ROC) analyses, we employed the Metaboanalyst platform [14]. Student's *t* or 2-way ANOVA tests were used to analyze the differences between groups. Associations between variables were studied with non-linear and linear regression analyses. The 0.05 level was selected as the point of minimal statistical significance in every comparison.

## Disclosure statement

No potential conflict of interest was reported by the authors.

## Funding

This work was supported by the Instituto de Salud Carlos III, FEDER Funds [Grant numbers: PI14-001115, PI14-0757 and PI17-00134] "A way to make Europe"; by the Ministerio de Educación, Cultura y Deporte [FPU16/01446]; by the Generalitat de Catalunya, DIUE [Grant number: FI2017-2020]; by the Fundació Miquel Valls [Grant number: Jack Van den Hoek donation]; by FUNDELA; by the RedELA [Grant number: Plataforma Investigación] and by the European Union FP7-PEOPLE-2013-COFUND [Grant number: IRBLLEIDA-IPP].

## ORCID

Ana B. Granado-Serrano  <http://orcid.org/0000-0002-5328-513X>  
 Victòria Ayala  <http://orcid.org/0000-0002-1496-966X>  
 Jordi Boada  <http://orcid.org/0000-0001-5109-4244>  
 Daniel Sanchis  <http://orcid.org/0000-0003-0047-8533>  
 Reinald Pamplona  <http://orcid.org/0000-0003-4337-6107>  
 Isidro Ferrer  <http://orcid.org/0000-0001-9888-8754>  
 Manuel Portero-Otín  <http://orcid.org/0000-0002-1823-0299>

## References

- [1] Ling JP, Pletnikova O, Troncoso JC, et al. TDP-43 repression of nonconserved cryptic exons is compromised in ALS-FTD. *Science*. 2015;80(349):650–655.
- [2] Yang Z, Wilkie-Grantham RP, Yanagi T, et al. ATG4B (Autophagin-1) phosphorylation modulates autophagy. *J Biol Chem*. 2015;290:26549–26561.
- [3] Bjørkøy G, Lamark T, Pankiv S, et al. Monitoring autophagic degradation of p62/SQSTM1. *Methods Enzymol*. 2009;452:191–197.
- [4] Teyssou E, Takeda T, Lebon V, et al. Mutations in SQSTM1 encoding p62 in amyotrophic lateral sclerosis: genetics and neuropathology. *Acta Neuropathol*. 2013;125(4):511–522.
- [5] Menzies FM, Fleming A, Rubinsztein DC. Compromised autophagy and neurodegenerative diseases. *Nat Rev Neurosci*. 2015;16:345–357.
- [6] Van Weehaeghe D, Ceccarini J, Willekens SM, et al. Is there a glucose metabolic signature of spreading TDP-43 pathology in Amyotrophic Lateral Sclerosis? *Q J Nucl Med Mol Imaging*. 2017. DOI:10.23736/S1824-4785.17.03009-6
- [7] Ilieva EV, Ayala V, Jové M, et al. Oxidative and endoplasmic reticulum stress interplay in sporadic amyotrophic lateral sclerosis. *Brain*. 2007;130(Pt 12):3111–3123.
- [8] Wiznerowicz M, Trono D. Conditional suppression of cellular genes: lentivirus vector-mediated drug-inducible RNA interference. *J Virol*. 2003;77(16):8957–8961.
- [9] Untergasser A, Cutcutache I, Koressaar T, et al. Primer3 - new capabilities and interfaces. *Nucleic Acids Res*. 2012;40(15):e115.
- [10] Romani C, Calza S, Todeschini P, et al. Identification of optimal reference genes for gene expression normalization in a wide cohort of endometrioid endometrial carcinoma tissues. *PLoS ONE*. 2014;9(12):e113781.
- [11] Pan B, Chen Y, Song H, et al. Mir-24-3p downregulation contributes to VP16-DDP resistance in small-cell lung cancer by targeting ATG4A. *Oncotarget*. 2015;6(1):317–331.
- [12] Pfaffl MW. A new mathematical model for relative quantification in real-time RT-PCR. *Nucleic Acids Res*. 2001;29(9):e45.
- [13] Bradford MM. A rapid and sensitive method for the quantitation of microgram quantities of protein utilizing the principle of protein-dye binding. *Anal Biochem*. 1976;72:248–254.
- [14] Xia J, Wishart DS. Using metaboanalyst 3.0 for comprehensive metabolomics data analysis. *Curr Protoc Bioinform*. 2016;55:14.10.1–14.10.91.



## **5.2 Article 2**

**Title:** Selected cryptic exons accumulate in hippocampal cell nuclei in Alzheimer's disease with and without associated TDP-43 proteinopathy.

**Authors:** Pascual Torres, Pol Andrés-Benito, Anna Fernández-Bernal, Marta Ricart, Victòria Ayala, Reinald Pamplona, Isidre Ferrer and Manuel Portero-Otín.

**Journal:** Brain: a journal of neurology

**Published:** 04/02/2020

**DOI:** 10.1093/brain/awaa013

## LETTER TO THE EDITOR

### Selected cryptic exons accumulate in hippocampal cell nuclei in Alzheimer's disease with and without associated TDP-43 proteinopathy

Pascual Torres,<sup>1</sup> Pol Andrés-Benito,<sup>2,3,4</sup> Anna Fernàndez-Bernal,<sup>1</sup> Marta Ricart,<sup>1</sup> Victòria Ayala,<sup>1</sup> Reinald Pamplona,<sup>1</sup> Isidro Ferrer<sup>2,3,4,5,6</sup> and  Manuel Portero-Otin<sup>1</sup>

1 Department of Experimental Medicine, IRBLleida, University of Lleida, Lleida, Spain

2 Department of Pathology and Experimental Therapeutics, University of Barcelona, Barcelona, Spain

3 CIBERNED (Network Centre of Biomedical Research of Neurodegenerative Diseases), Institute of Health Carlos III, Ministry of Economy and Competitiveness, Barcelona, Spain

4 Bellvitge Biomedical Research Institute (IDIBELL), Hospitalet de Llobregat, Barcelona, Spain

5 Senior Consultant, Bellvitge University Hospital, Barcelona, Spain

6 Institute of Neurosciences, University of Barcelona, Barcelona, Spain

Correspondence to: Manuel Portero-Otin

Department of Experimental Medicine, IRBLleida, University of Lleida, Lleida, Spain

E-mail: manuel.portero@mex.udl.cat

Sir,

Nelson *et al.* (2019) recently reported in a consensus working paper that the presence of TDP-43 pathology restricted to the limbic system, alters the disease phenotype in old aged individuals, most of them suffering from Alzheimer's disease-related pathology; so they named this alteration limbic-predominant age-related TDP-43 encephalopathy (LATE). As TDP-43 proteinopathy was already described in Alzheimer's disease, other opinions casted doubt on whether this is a novel entity or not (Josephs *et al.*, 2019). Other researchers propose to include LATE in the differential diagnosis of frontotemporal dementia in elderly patients (Larner and Griffiths, 2019). Beyond nomenclature, the precise classification of Alzheimer's disease subtypes and co-morbidities, and the identification of TDP-43 targets may serve to improve drug discovery and better clinical trial designs. TDP-43 is a complex protein with multiple physiological and pathological functions in RNA biology (Prasad *et al.*, 2019). Among them, TDP-43 splicing repression has been postulated as a key pathological feature in amyotrophic lateral sclerosis (ALS), and frontotemporal lobar degeneration-TDP (FTLD) (Donde *et al.*, 2019b). Interestingly, TDP-43 is frequently associated with non-conserved UG repeats in pre-mRNA in the vicinity of splicing sites (Ling *et al.*, 2015) of selected

mRNAs, including autophagy-related 4B cysteine peptidase (*ATG4B*), G protein signalling modulator 2 (*GPSM2*), platelet-phosphofructokinase (*PFKP*). As a consequence of the nuclear depletion of TDP-43, there is an increase in non-conserved (cryptic) exon splicing which introduces random sequences in these mRNAs (Humphrey *et al.*, 2017). This phenomenon occurs in ALS-FTLD-TDP (Ling *et al.*, 2015), and Alzheimer's disease (Sun *et al.*, 2017). We previously demonstrated that TDP-43 can regulate autophagy by repressing cryptic exon incorporation in *ATG4B* mRNA, thus preventing function decay (Torres *et al.*, 2018). Quantification analyses in ALS nervous tissue suggested low inclusion of cryptic exons (0.1% for *ATG4B* and 1% for *GPSM2*) but with robust diagnostic capacities. In this work we used the same methodology to ascertain whether Alzheimer's disease patients, compatible with LATE diagnosis, also had higher cryptic exon inclusion rates. Thus, we quantified the inclusion ratio of selected cryptic exons in *ATG4B*, *GPSM2* and *PFKP* mRNAs in the hippocampus total homogenates and in nuclear enriched fraction from cases with Alzheimer's disease-related pathology and TDP-43 pathology (AD + TDP-43 proteinopathy) and Alzheimer's disease-related pathology without TDP-43 proteinopathy, being compared to control individuals (Supplementary material).

Immunohistochemistry to TDP-43 discriminated between AD+TDP-43 proteinopathy ( $n = 6$  cases) and Alzheimer's disease without TDP-43 proteinopathy ( $n = 11$  cases). Alzheimer's disease stages varied from II to V neurofibrillar tangle degeneration in both groups. Five cases without neuropathological lesions were considered as controls. The hippocampus was affected in every case and alterations were characterized by decreased nuclear TDP-43 immunoreactivity (nuclear clearance), large numbers of fine TDP-43-immunoreactive threads and occasional neuronal intracytoplasmic granular or globular inclusions (Supplementary Fig. 1). Although TDP-43 pathology varied from one case to another, Cases 2 and 3 exhibited more TDP-43 alterations than the other four cases.

Reverse transcriptase quantitative PCR of hippocampal total homogenates showed that three AD+TDP-43 cases had *ATG4B* cryptic exons (Cases 1, 3 and 5). The same cases and one other (Case 6) had *GPSM2* cryptic exons. Two cases (Cases 2 and 4) had no *ATG4B* and *GPSM2* cryptic exons in total homogenates of the hippocampus (Table 1). Interestingly, not all the samples with AD+TDP-43 contain detectable levels of cryptic exons in *ATG4B* and *GPSM2* (four of six cases). In contrast, a low percentage of Alzheimer's disease cases without TDP-43

pathology express detectable levels of cryptic exons in *ATG4B* and *GPSM2* (2 of 11 cases). In the present series, the majority of cases did not present cognitive impairment and the neurofibrillary tangle (NFT) staging of Alzheimer's disease pathology was consistent with the neurological status. However, TDP-43 pathology was present in cases at stages II, III and V of NFT pathology, which was accompanied by increased cryptic exons; and cryptic exons were recognized in two Alzheimer's disease cases without Alzheimer's disease pathology and stages III and IV of Braak. In summary, our observations show abnormal responses of cryptic exons of selected genes mainly linked to, but not exclusive of, limbic TDP-43 proteinopathy in the context of LATE- neuropathological changes (LATE-NC) without hippocampal sclerosis and vascular disease. As TDP-43 pathology in the limbic system increases with age, it is presumably that cryptic exon pathology also increases with age in cases with LATE-NC (Sun *et al.*, 2017).

To estimate the degree of the cryptic exon mRNA decay, we correlated total homogenate and nuclear cryptic exon inclusion. After nuclear extraction protocol, we obtained round-shaped, DAPI-positive organelles consistent with cell nuclei (Fig. 1A). We quantified the levels of cryptic

**Table 1 Summary of cohort and results**

Case	Gender	Age	Diagnosis	PMD	Cryptic ATG4B		Cryptic GPSM2		Cryptic PFKP	
					% Total	% Nuclear	% Total	% Nuclear	% Total	% Nuclear
<b>AD + TDP-43</b>										
1	Male	80	AD III/0 + TDP	4 h 20 m	0.18	0.58	0.15	0.11	5.32	18.37
2	Male	76	AD II/A + TDP <sup>a</sup>	21 h 45 m	ND	ND	ND	ND	6.70	5.78
3	Male	77	AD V/C + TDP	16 h	1.15	5.96	4.26	8.90	20.60	38.36
4	Male	79	AD III/A + TDP <sup>a</sup>	4 h 30 m	ND	ND	ND	0.02	3.67	6.38
5	Male	76	AD II/A + TDP	20 h 25 m	0.10	0.31	0.14	0.17	-	-
6	Female	92	AD V/0 + TDP	7 h	ND	0.05	0.02	0.06	-	-
<b>Alzheimer's disease</b>										
7	Female	90	AD III/B	4 h	ND	ND	ND	ND	-	-
8	Male	72	AD III/0	3 h 30 m	ND	ND	ND	ND	1.44	5.98
9	Female	82	AD III/A	3 h 5 m	ND	ND	ND	ND	4.31	8.42
10	Male	79	AD IV/A	5 h	ND	ND	ND	ND	3.43	47.20
11	Male	79	AD IV/A	2 h 45 m	0.73	ND	ND	ND	102.15	7.42
12	Female	74	AD III/A	9 h 30 m	0.36	1.39	0.20	ND	9.57	246.27
13	Male	85	AD IV/B	14 h	ND	ND	ND	ND	-	-
14	Female	81	AD III/B	14 h	ND	ND	ND	ND	-	-
15	Female	74	AD III/0	5 h	ND	ND	ND	ND	-	-
16	Male	74	AD III/A	7 h 35 m	ND	ND	ND	ND	-	-
17	Female	83	AD III/A	5 h 40 m	ND	ND	ND	ND	-	-
<b>Control</b>										
18	Male	49	NL	7 h 35 m	ND	ND	ND	ND	103.91	34.30
19	Male	71	NL	12 h	ND	ND	ND	ND	2.25	9.91
20	Female	66	NL	8 h	ND	ND	ND	ND	3.10	3.70
21	Male	58	NL	4 h	ND	0.03	ND	ND	1.30	2.94
22	Female	79	NL	7 h	ND	ND	ND	ND	6.16	-

Subjects included Alzheimer's disease cases without TDP-43 proteinopathy (Alzheimer's disease), cases with AD+TDP-43, and healthy controls (Control). Gender, age, diagnosis (Braak staging of NFT degeneration, I-V, and amyloid- $\beta$  plaques, 0-C), post-mortem delay (PMD), and the percentage of inclusion of cryptic exons in the hippocampus total homogenate and nuclear fractions are presented. TDP pathology corresponded to stage 2. - = not assessed; AD = Alzheimer's disease; ND = no detectable; NL = no lesions. <sup>a</sup>Associated Lewy body pathology (Case 2, stage 5; and Case 4, stage 3).

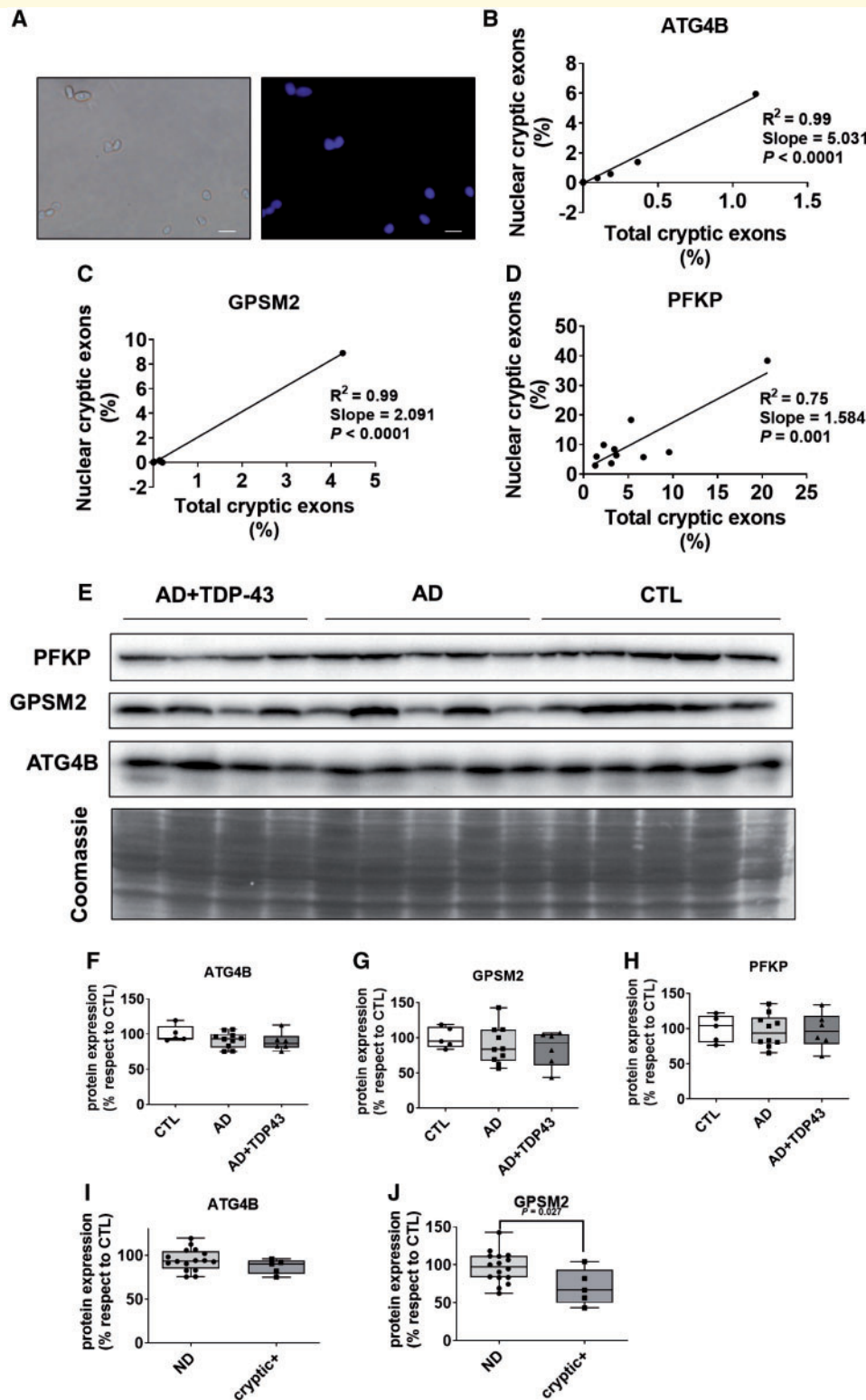


**Figure 1** Cryptic exons related to TDP-43 dysfunction are found in hippocampal samples from patients with Alzheimer's disease. **(A)** DAPI staining indicated the presence of cell nuclei in the enriched fraction isolated from frozen samples. Cryptic exons in mRNAs from *ATG4B* **(B)**, *GPSM2* **(C)** and *PFKP* **(D)** are higher in the nuclear enriched fraction than in total homogenate and they are positively correlated with total levels in hippocampus homogenate. **(E)** Western blot analysis of hippocampal samples quantified in **F** for *ATG4B*, in **G** for *GPSM2* and in **H** for *PFKP*, showing that protein levels are not significantly different in Alzheimer's disease, AD + TDP-43 and controls. **(I)** Panel shows that while *ATG4B* is not different between samples with cryptic exons non-detectable (ND) and samples showing cryptic exons (cryptic +), *GPSM2* protein levels are lower in the cryptic + group **(J)**. *P*-value in **J** by Student's *t*-test. Boxes display the interval between 25th and 75th percentiles (q1 and q3); lines inside boxes indicate median values; whiskers indicate the maximum and minimum values. Scale bar = 25  $\mu$ m. AD = Alzheimer's disease; CTL = control.

exon inclusion in *GPSM2*, *ATG4B* and *PFKP* mRNAs in both nuclear and total homogenates. Total and nuclear *GPSM2* cryptic exons were found in the same AD+TDP43 cases, whereas *ATG4B* was additionally observed in Case 6, in which *ATG4B* cryptic exons were not detected in total homogenates (Table 1). Curiously, no cryptic exon alterations were found in the two cases with Lewy body disease-associated pathology (Cases 2 and 4) (Table 1). Regarding Alzheimer's disease cases without TDP-43 proteinopathy, only one (Case 12) showed *ATG4B* and *GPSM2* cryptic exons in total hippocampus homogenates and in the nuclear fraction. Another (Case 11) showed *ATG4B* cryptic exons in total homogenates but not in nuclear fractions of the hippocampus (Table 1).

We determined a high correlation between total and nuclear fraction ( $R^2 = 0.99$ ) with a 5-fold increase of *ATG4B* cryptic exon inclusion in the nuclear fraction (Fig. 1B). Correlation for *GPSM2* was also high ( $R^2 = 0.99$ ) with 2.1-fold increase of cryptic exon incorporation in the nucleus (Fig. 1C). *PFKP* cryptic exon inclusion was 1.6-fold higher in the nucleus with a  $R^2 = 0.75$  of correlation with total homogenate (Fig. 1D). *ATG4B* and *GPSM2* cryptic exons were not detected in total homogenates of the hippocampus in control cases. Only cryptic *ATG4B* was detected in the nuclear fraction in one control (Case 21) (Table 1).

In contrast with these data, *PFKP* cryptic exon was detected in all the samples analysed (four of six AD+TDP-43 proteinopathy, 5 of 11 Alzheimer's disease without TDP-43 pathology, and four of five controls) independently of the group (Table 1). Some of them exceed 100% of inclusion, indicating a higher inclusion of cryptic exon than the conserved one (Table 1).

To quantify the impact of the mRNA decay in the resulting protein, we quantified *ATG4B*, *GPSM2* and *PFKP* expression by western blotting in total homogenates of the hippocampus. No differences in protein expression were identified among the three groups (Fig. 1E–J). Dividing the samples between those showing cryptic exons and those not, *ATG4B* proteins were not different (Fig. 1I), though *GPSM2* protein expression was lower in samples showing cryptic exon inclusion (Fig. 1J).

*ATG4B* cryptic exon-containing mRNA is the highest sensitive analysed gene to undergo degradation by non-sense-mediated decay as its nuclear expression is 5-fold higher than in total homogenate. This finding supports that *ATG4B* may be a preferential target for therapy, more specifically because of the importance of autophagy proteins in TDP-43-related diseases (Donde *et al.*, 2019a, b). Curiously, TDP-43 loss of splicing repression function does not impact on the total amount of the resulting *ATG4B* protein in the present series. However, these results must be interpreted with caution as the sensibility of western blotting might not be sufficient to detect subtle differences among samples; and the majority of cases are early stages of Alzheimer's disease.

It is worth stressing that altered expression of cryptic exons linked to TDP-43 or not, may occur in the

hippocampus at early stages of Alzheimer's disease pathology preceding neurological symptoms of cognitive impairment. As TDP-43 proteinopathy is not rare in cognitively normal older adults (Nascimento *et al.*, 2018), the present findings have added value regarding brain ageing.

Due to the lack of significant differences of *PFKP* cryptic exon inclusion between controls and AD+TDP-43 samples, we wanted to validate the specific TDP-43 regulation on *PFKP* cryptic exon splicing using a cellular model. TDP-43 knockdown HeLa cells showed inclusion of cryptic exon in 35% of *PFKP* transcripts (Supplementary Fig. 2) and decay of 80% of the mRNA and protein, similar to *ATG4B* and *GPSM2* (Supplementary Fig. 2). To shed further light on the cryptic exon splicing regulation, we performed *in vitro* experiments to ascertain if *in silico* predicted sites of cryptic exon splicing could be validated. The results suggest that RNA sequence is not the only factor for TDP-43 interaction (Supplementary Fig. 3). Thus, *ATG4B* cryptic exon contains weak splice acceptor site (AG/CA) and weak splice donor site (TG/GT). Weak splice variants depend on tissue-specific elements (epigenetic context, RNA-binding proteins), whereas strong variants are included efficiently in all tissues. This generates alternative splicing diversity so natural selection has the opportunity to preserve those that confer a useful function for the tissue (Jaganathan *et al.*, 2019). Nevertheless, this cryptic exon splicing is not influenced by TDP-43 and its inclusion may depend on other intronic splicing enhancers. These results suggest a reduced list of candidate genes that must be validated, and the need for experimental validation of bioinformatics. Globally, the presented data emphasize the complexity of TDP-43 proteinopathy, which almost certainly extends beyond one mechanistic factor—multiple toxic gains and losses of function being present for this protein in CNS diseases.

## Data availability

The data that support the findings of this study are openly available in the Figshare repository at <https://doi.org/10.6084/m9.figshare.10565960>

## Acknowledgements

We thank I. Sánchez, D. Argilés and M. Martí for their skillful assistance. We thank T. Yohannan for editorial help.

## Funding

Grants were received from the Instituto de Salud Carlos III (PI 17-000134) to M.P.O., from the Generalitat de Catalunya 2017SGR696 and from Spanish Ministry of Science, Innovation and Universities (Program RETOS ref. RTI2018-099200-B-I00) to R.P. P.T. is a predoctoral fellow from the Ministerio de Educacion (FPU16/01446). Support was also received in the form of a FUNDELA Grant, RedELA-Plataforma Investigación and the

Fundació Miquel Valls (Jack Van den Hoek donation). FEDER funds are acknowledged (“A way to make Europe”).

## Competing interests

The authors report no competing interests.

## Supplementary material

Supplementary material is available at *Brain* online.

## References

- Donde A, Sun M, Jeong YH, Wen X, Ling J, Lin S, et al. Upregulation of ATG7 attenuates motor neuron dysfunction associated with depletion of TARDBP/TDP-43. *Autophagy* 2019a; 1–11. doi:10.1080/15548627.2019.1635379.
- Donde A, Sun M, Ling JP, Braunstein KE, Pang B, Wen X, et al. Splicing repression is a major function of TDP-43 in motor neurons. *Acta Neuropathol* 2019b; 138: 813–26.
- Humphrey J, Emmett W, Fratta P, Isaacs AM, Plagnol V. Quantitative analysis of cryptic splicing associated with TDP-43 depletion. *BMC Med. Genomics* 2017; 10: 38. doi:10.1186/s12920-017-0274-1.
- Jaganathan K, Kyriazopoulou Panagiotopoulou S, McRae JF, Darbandi SF, Knowles D, Li YI, et al. Predicting splicing from primary sequence with deep learning. *Cell* 2019; 176: 535–48.e24.
- Josephs KA, Mackenzie I, Frosch MP, Bigio EH, Neumann M, Arai T, et al. LATE to the PART-y. *Brain* 2019; 142: e47. doi:10.1093/brain/awz224.
- Larner AJ, Griffiths TD. Limbic-predominant age-related TDP-43 encephalopathy (LATE). *Brain* 2019; 142: e42.
- Ling JP, Pletnikova O, Troncoso JC, Wong PC. TDP-43 repression of nonconserved cryptic exons is compromised in ALS-FTD. *Science* 2015; 349: 650–5.
- Nascimento C, Di Lorenzo Alho AT, Bazan Conceição Amaral C, Leite REP, Nitrini R, Jacob-Filho W, et al. Prevalence of transactive response DNA-binding protein 43 (TDP-43) proteinopathy in cognitively normal older adults: systematic review and meta-analysis. *Neuropathol Appl Neurobiol* 2018; 44: 286–97.
- Nelson PT, Dickson DW, Trojanowski JQ, Jack CR, Boyle PA, Arfanakis K, et al. Limbic-predominant age-related TDP-43 encephalopathy (LATE): consensus working group report. *Brain* 2019; 142: 1503–27.
- Prasad A, Bharathi V, Sivalingam V, Girdhar A, Patel BK. Molecular mechanisms of TDP-43 misfolding and pathology in amyotrophic lateral sclerosis. *Front Mol Neurosci* 2019; 12: 25.
- Sun M, Bell W, LaClair KD, Ling JP, Han H, Kageyama Y, et al. Cryptic exon incorporation occurs in Alzheimer’s brain lacking TDP-43 inclusion but exhibiting nuclear clearance of TDP-43. *Acta Neuropathol* 2017; 133: 923–31.
- Torres P, Ramírez-Núñez O, Romero-Guevara R, Barés G, Granado-Serrano AB, Ayala V, et al. Cryptic exon splicing function of TARDBP interacts with autophagy in nervous tissue. *Autophagy* 2018; 14: 1398–403.

## SUPPLEMENTAL DATA

### Methods

#### *Patients and brain samples*

Brain samples were obtained from the Institute of Neuropathology brain bank (now a branch of the HUB-ICO-IDIBELL biobank) following the guidelines of the Spanish legislation (Real Decreto 1716/2011) and the approval of the Institutional Ethics Committee of the Bellvitge University Hospital. Samples were available following the generous donation of persons dying of different conditions in a general hospital. Most of cases in these series did not have suffered from neurological symptoms, particularly cognitive impairment and dementia. The brain was obtained between 3h and 21 h after death and the corpse was preserved at 4°C during the post-mortem delay. The brain was removed from the skull as the first step of the autopsy, and one hemisphere and alternate sections of the brain stem and cerebellum were cut on coronal sections, from which small pieces of selected areas were dissected, put on separate labeled plastic bags, and immediately frozen and stored at 80°C. The other hemisphere and the rest of the brain were fixed in 4% buffered formalin for no less than four weeks. Selected regions were embedded in paraffin, and de-waxed paraffin sections processed for neuropathological studies as detailed elsewhere (Ferrer, 2014). Three groups were considered: a) cases with AD-related pathology (6 females and five males; age:  $80.3 \pm 5.3$ ); b) cases with AD-related pathology and TDP-43 proteinopathy at least in the amygdala and hippocampus (stage 2 of LATE-NC according to (Nelson *et al.*, 2019; Prasad *et al.*, 2019)) (one female and four males, age:  $79.3 \pm 5.2$ ); and c) middle-aged individuals with no neuropathological lesions (2 females and 3 males; age:  $64.6 \pm 10.3$ ).

AD cases were categorized following the nomenclature of Braak for neurofibrillary tangle degeneration (stages I-VI), and  $\beta$ -amyloid plaques (0-C). Eight cases with only AD-related pathology showed stages III/0-B, and three cases stages IV/A-B. Only 2 (cases 10 and 13) had suffered from mild cognitive impairment; none of them had dementia. Four cases with AD-related pathology and TDP-43 proteinopathy had stages II-III/0-B; and two AD stage V/0-C). The patients with AD stage V suffered from dementia; one patient with associated Lewy body disease (LBD: stage 5 of Braak; case 2 had also dementia); another with LBD (case 4) has not; and the rest of cases with low-stage AD-related pathology plus TDP-43 proteinopathy were cognitively normal. Therefore, pathological and clinical data correlate in our series as has been reported for old people (Braak *et al.*, 2011; Ferrer, 2012; Braak and Del Tredici, 2015). It can be interpreted that cases without  $\beta$ -amyloid pathology are PART (primary aging related tauopathy (Crary *et al.*, 2014; Prasad *et al.*, 2019); however, this is not the point in the present context as PART is also considered as part of AD (Crary *et al.*, 2014; Duyckaerts *et al.*, 2015; Prasad *et al.*, 2019)

#### *Immunohistochemistry*

De-waxed paraffin sections 4-micron-thick were boiled in citrate buffer (20 min) to retrieve protein antigenicity. Endogenous peroxidases were blocked by incubation in 10% methanol-1% H<sub>2</sub>O<sub>2</sub> solution

(15min) followed by 3% normal horse serum solution. Then the sections were incubated at 4°C overnight with the rabbit polyclonal anti-TDP-43 antibody (Abcam, Cambridge, UK) at a dilution of 1:200. Following incubation with the primary antibody, the sections were incubated with EnVision + system peroxidase (Dako, Agilent Technologies, Santa Clara, CA, USA) for 30 min at room temperature. The peroxidase reaction was visualized with diaminobenzidine and H<sub>2</sub>O<sub>2</sub>. The sections were lightly counterstained with haematoxylin. Control of the immunostaining included omission of the primary antibody; no signal was obtained following incubation with only the secondary antibody.

#### *Nuclear enrichment*

Nuclei were extracted from portions of the hippocampus according to a variation of the Blobber and Potter protocol (Blobel and Potter, 1966). We started from about 0.270 g of frozen tissue, which was allowed to thaw at 4°C. All subsequent steps, unless noted otherwise, were performed at this temperature. Once thawed, samples were cut into very small pieces with a scalpel and transferred to a 2mL eppendorff, where the tissue was homogenized in two volumes(w/v) of 0.25M sucrose in cold TKM (0.05M Tris, 0.025M KCl, MgCl<sub>2</sub> 0.005M) and commercial protease Inhibitor Cocktail, 1861278, Thermo Fisher Scientific). The homogenization was performed with a Dounce-type homogenizer with a glass tight plunger (20-40 strokes). At the end of this step, 100µL of the homogenate was transferred to a new tub for Western Blot Analysis and the rest (400µL) were mixed with 800µL of 2.3M sucrose in TKM by inversion. In an ultracentrifuge tube (Beckman Coulter, 344057), 500µL of 2.3M sucrose in TKM were added at the bottom of the tube. Carefully, the homogenate was added at the top of the tube, ensuring well defined phases of sucrose. The homogenates were centrifuged at 124,000 xg at 4°C for 30 minutes in Optima L-100XP ultracentrifuge (Beckman Coulter, SW 55 Ti rotor). The resulting pellet was re-suspended in 1ml of TRI Reagent (Thermo Fisher Scientific, AM9738). The presence of nuclei was confirmed by fluorescence microscopy after staining with DAPI at 1µg/mL.

#### *RNA extraction, cDNA synthesis and RT-qPCR*

One milliliter of TRI Reagent (AM9738, Thermo Fisher Scientific) was added to 50-100mg of frozen hippocampus or isolated nuclei or cells. The tissue was mechanically homogenized using T 10 basic ULTRA-TURRAX® (IKA). 200µL of chloroform was added to each sample and mixed by inversion. After 5 minutes of incubation at room temperature, the samples were centrifuged at 12,000 xg (15 minutes at 4°C) to separate the phases. The aqueous phase was separated into a new tube and mixed by vortexing with 500µL of isopropanol. After an incubation of 10 minutes at room temperature, RNA was precipitated through spun at 12,000 xg (10 minutes at 4°C). The resulting supernatant was removed and the pellet was washed with a 75% ethanol. After vortexing, the samples were centrifuged again at 12,000 xg (10 minutes at 4°C). The supernatant was discarded and the RNA pellet was allowed to air dry at room temperature (5-10 minutes). The RNA was re-suspended with 50µL of RNase-free water, quantified with Nanodrop



(Nanodrop technologies, ND-1000 UV/Vis Spectrophotometer), and stored at  $-80^{\circ}\text{C}$  until use. One microgram of RNA was used for retrotranscription employing TaqMan Reverse Transcription Reagent using random hexamers (N8080234, Thermo Fisher Scientific). RT-qPCR experiments were performed using a CFX96 instrument (Bio-Rad, Hercules, California, USA) with SYBR Select Master mix for CFX (4472937, Thermo Fisher Scientific). Each  $20\mu\text{L}$  of reaction contained  $4\mu\text{L}$  cDNA,  $10\mu\text{L}$  SYBR Select Master Mix,  $0.2\text{ nM}$  of forward primer and  $0.2\text{ nM}$  of reverse primer solutions and  $4\mu\text{L}$  PCR grade water. RT-qPCR run protocol was as follows:  $50^{\circ}\text{C}$  for 2 minutes and  $95^{\circ}\text{C}$  for 2 minutes, with the  $95^{\circ}\text{C}$  for 15 seconds and  $60^{\circ}\text{C}$  for 1 minute steps repeated for 40 cycles; and a melting curve test from  $65^{\circ}\text{C}$  to  $95^{\circ}\text{C}$  at a  $0.1^{\circ}\text{C/s}$  measuring rate. Primers employed in these experiments are listed in Supplemental Table 1. Cryptic exon inclusion was estimated using the following formula:  $100 \times 2^{(-\text{Conserved exon } Cq - \text{Cryptic exon } Cq)}$ . *PFKP* mRNA expression was normalized with *GAPDH* mRNA expression.

### *Western Blot Analyses*

Protein from tissue was extracted adding  $100\mu\text{L}$  of radioimmunoprecipitation buffer with Protease Inhibitor Cocktail (1X, Thermo Fisher Scientific) to the sample derived after the homogenization step of nuclei isolation protocol. HeLa cells were harvested with  $100\mu\text{L}$  of radioimmunoprecipitation buffer with Protease Inhibitor Cocktail (1X) for protein extraction. After sonication, protein quantification was performed with Bradford assay (5000006, Bio-Rad). Fifteen  $\mu\text{g}$  of protein were loaded onto a 12% acrylamide SDS-PAGE gel. Membranes were blocked with I-Block (T2015, Thermo Fisher Scientific) for 1 hour and incubated overnight with antibodies anti-ATG4B (A2981, Sigma), anti-GPSM2 (ab84571, Abcam) and anti-PFKP (HPA018257, Atlas Antibodies) diluted 1:500 in TBS-T 0.05%. After primary antibody incubation, membranes were washed 3 times with TBS-T 0.05% and incubated with secondary antibody for 1h. Immobilon™ Western Chemiluminiscent HRP Substrate (WBKLS0500, Merck Millipore) was used for immunodetection. Membranes were stained with Coomassie Brilliant Blue G (27815, Sigma) for normalization. Specific bands were quantified with ImageLab v5.2.1 (Bio-Rad).

### *Cell culture*

HeLa cells were maintained in Dulbecco's Modified Eagle's Medium (11965, Thermo Fisher Scientific), 10% FBS (10270, Thermo Fisher Scientific), 100U/ml Penicillin-Streptomycin (15140-122, Thermo Fisher Scientific) at  $37^{\circ}\text{C}$  and 5%  $\text{CO}_2$ . TDP-43 knockdown cells were obtained transducing cells with a *TDP-43* shRNA (TDP-43 KD) or scrambled (SCR) lentivirus. Cell media were changed the day after the transduction and the cells were cultured for further 96 hours to allow TDP-43 silencing (Torres *et al.*, 2018).

### *Fluorescent TDP-43 cryptic splicing function reporter*

pRint was a gift from Mariano Garcia-Blanco (Addgene plasmid #24218; [http://n2t.net/addgene:24218;RRID:Addgene\\_24218](http://n2t.net/addgene:24218;RRID:Addgene_24218)). This plasmid was modified by Agentide (Agentide Inc, NY, USA) to introduce *ATG4B* cryptic exon in the multiple cloning site between the two exons of *rfp* (Supplemental Table 2). HeLa cells were transfected using 1 µg of plasmid and 1 µl of Lipofectamine 2000 (11668-027, Thermo Fisher Scientific) mixed in Opti-MEM (31985-047, Thermo Fisher Scientific) 72 hours post-transduction. After 24 hours cells were visualized and harvested.

### *Statistical analysis*

All statistics and figures were performed with GraphPad Prism (GraphPad Software, San Diego, CA, USA), unless indicated otherwise. Student's T test or ANOVA test were used to analyze the differences between groups. Associations between variables were studied with lineal regression analyses. The 0.05 level was selected as the point of minimal statistical significance in every comparison.

Supplemental table 1. Primers employed for RT-qPCR analyses.

<b>Genes</b>	<b>Forward</b>	<b>Reverse</b>
Total <i>ATG4B</i>	5'-AACGCATTCATCGACAGGAAG-3'	5'-TTTGCCTATCTGGTGAATGG-3'
Cryptic <i>ATG4B</i>	5'-CTGAGTGTGCATGGATGAGTG-3'	5'-TTGCTGGCACCAATCATTGAA-3'
Total <i>GPSM2</i>	5'-GGACGTGCCTTTGGAAATCTT-3'	5'-TTTGAATAAGGAGACGCTGC-3'
Cryptic <i>GPSM2</i>	5'-GTGTGTATGAGAGAGAGAGCGA-3'	5'-AGAAGCTTCCATTCTGTTCATCA-3'
Total <i>PFKP</i>	5'-GACCTTCGTTCTGGAGGTGAT-3'	5'-CACGGTTCTCCGAGAGTTTG-3'
Cryptic <i>PFKP</i>	5'-ACGTTTGCAAAACATCAGGAG-3'	5'-GCCTTCAACTCTCCGTTTAC-3'
Total <i>rfp</i>	5'-TCTACAAGGTGAAGTTCCGCG-3'	5'-TCTTCTTCTGCATTACGGGGC-3'
Cryptic <i>rfp</i>	5'-GAGAGCGTGTGTCTGGATGT-3'	5'-CGGAACTTCACCATGGCTCA-3'
<i>GAPDH</i>	5'-CCCTTCATTGACCTCAACTACATG-3'	5'-TGGGATTTCCATTGATGACAAG-3'

Supplemental Table 2. Sequence of plasmid employed for evaluation of TDP-43 function.

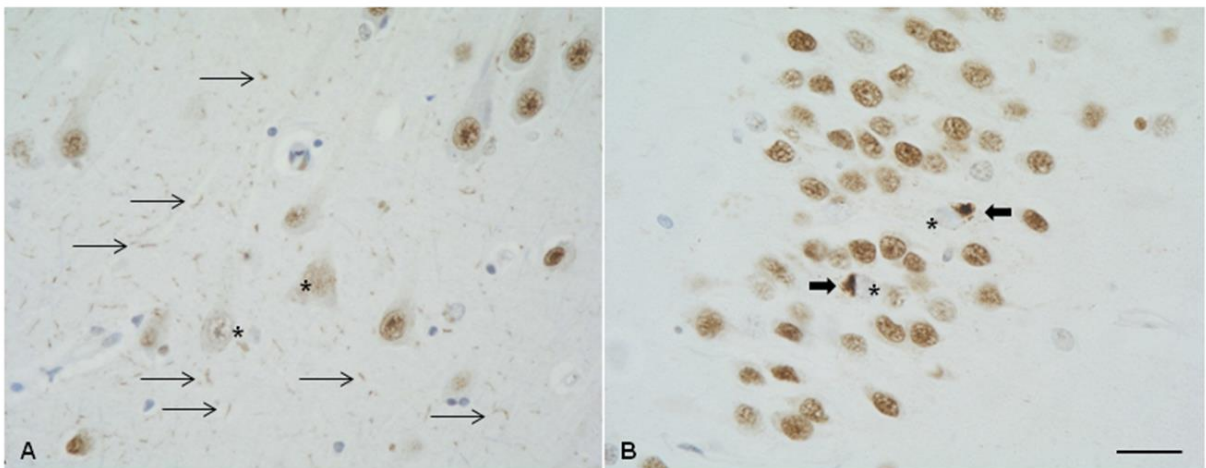
GACGGATCGGGAGATCTCCCGATCCCCTATGGTGCACCTCTCAGTACAATCTGCTCTGATGCCGCATAGTT  
AAGCCAGTATCTGCTCCCTGCTTGTGTGTTGGAGGTCGCTGAGTAGTGCGCGAGCAAAATTTAAGCTAC  
ACAAGGCAAGGCTTGACCGACAATTGCATGAAGAATCTGCTTAGGGTTAGGCGTTTTGCGCTGCTTCG  
CGATGTACGGGCCAGATATACGCGTTGACATTGATTATTGACTAGTTATTAATAGTAATCAATTACGGGG  
TCATTAGTTCATAGCCCATATATGGAGTTCGCGGTTACATAACTTACGGTAAATGGCCCCGCTGGCTGAC  
CGCCCAACGACCCCGCCATTGACGTCAATAATGACGTATGTTCCCATAGTAACGCCAATAGGGACTT  
TCCATTGACGTCAATGGGTGGAGTATTTACGGTAAACTGCCACTTGGCAGTACATCAAGTGTATCATAT  
GCCAAGTACGCCCCCTATTGACGTCAATGACGGTAAATGGCCCCGCTGGCATTATGCCCAGTACATGAC  
CTTATGGGACTTTCCTACTTGGCAGTACATCTACGTATTAGTCATCGCTATTACCATGGTGTATGCGGTTTT  
GGCAGTACATCAATGGGCGTGGATAGCGGTTTGACTCACGGGGATTTCCAAGTCTCCACCCCATTGACG  
TCAATGGGAGTTTGTGTTTGGCACCAAAATCAACGGGACTTTCCAAATGTTCGTAACAACCTCCGCCCATI  
GACGCAAATGGGCGGTAGGCGTGTACGGTGGGAGGTCTATATAAGCAGAGCTCTCTGGCTAACTAGAG  
AACCCACTGCTTACTGGCTTATCGAAATTAATACGACTCACTATAGGGAGACCCAAGCTGGCTAGCGTTI  
AACTTAAGCTTACCATGGTGGCCTCCTCCGAGGACGTCATCAAAGAGTTCATGCGCTTCAAGGTGCGC  
ATGGAGGGCTCCGTGAACGGCCACGAGTTCGAGATCGAGGGCGAGGGCGAGGGCCGCCCTACGAGGG  
CACCCAGACCGCCAAGCTGAAGGTGACCAAGGGCGGCCCCCTGCCCTTCGCTGGGACATCCTGTCCCC  
CCAGTTCAGTACGGCTCCAAGCGTACGTGAAGCACCCCGCCGACATCCCCGACTACAAGAAGCTGTC  
CTCCCCGAGGGCTTCAAGTGGGAGCGGTGATGAACTTCGAGGACGGCGGCGTGGTGACCGTGACCCA  
GGACTCCTCCCTGCAGGACGGCACGCTGATCTACAAGgtgagtatggatccctgttgggaatgacgaggaaaacttccgattttgctt  
tttttttcagCATGTTGGGATAAGTACTGTGTTACGTTGGTGGGAATCTGAAGGGTATAAGAGCCGGAAGTGT  
GTCCTTGACCCCTCACGTCCCTCCCCAGGCACCACCTCCTGTGCAGCCTTCATGGCCTTCGAGTGGCCC  
AGAGAGCGTGTGTCTGGATGTGAGCGTGTGGGCGCGTGTGAGTGTGCATGGATGAGTGTGAGCCAT  
GgtgagtgttccccctcacactacattaaacacacggcgggggcccttcccttttttctcagGTGAAGTTCGCGGCACCAACTTCCCC  
CCCGACGGCCCCGTAATGCAGAAGAAGACCATGGGCTGGGAGGCCTCCACCGAGCGCCTGTACCCCCG  
GACGGCGTGTGAAGGGCGAGATCCACCAGGCCCTGAAGCTGAAGGACGGCGGCCACTACCTGGTGGAA  
GTTCAAGACCATCTACATGGCCAAGAAGCCCGTGCAGCTGCCCGGCTACTACTACGTGGACACCAAGCT  
GGACATCACCTCCCAACGAGGACTACACCATCGTGGAACAGTACGAGCGCTCCGAGGGGCCGCCACC  
ACCTGTTCCCTGTAGACCGGTCATCATCACCATCACCATTGAGTTTAAACCCGCTGATCAGCCTCGACTGT  
GCCTTCTAGTTGCCAGCCATCTGTTGTTTGGCCCTCCCCCGTGCCTTCTTGACCCTGGAAGGTGCCACTC  
CCACTGTCCTTTCCTAATAAAAATGAGGAAATTGCATCGCATTGTCTGAGTAGGTGTCAATTCTATTCTGGG  
GGGTGGGGTGGGGCAGGACAGCAAGGGGGAGGATTGGGAAGACAATAGCAGGCATGCTGGGGATGCG  
GTGGGCTCTATGGCTTCTGAGGCGGAAAGAACCAGCTGGGGCTCTAGGGGGTATCCCCACGCGCCCTGT  
AGCGGCGCATTAAAGCGCGGCGGGTGTGGTGGTTACGCGCAGCGTGACCGCTACACTTGCCAGCGCCCTA  
GCGCCCGCTCCTTTCGTTTCTTCCCTTCTTCTCGCCACGTTTCGCCGGCTTTCGCCGTCAAGCTCTAAA  
TCGGGGGCTCCCTTAGGGTTCCGATTTAGTGCTTTACGGCACCTCGACCCCAAAAACTTGATTAGGGT  
GATGGTTCACGTAGTGGGCCATCGCCCTGATAGACGGTTTTTCGCCCTTTGACGTTGGAGTCCACGTTCT  
TTAATAGTGGACTCTTGTTCCAAACTGGAACAACACTCAACCCTATCTCGGTCTATTCTTTTGATTTATAA  
GGGATTTTGCCGATTTCCGGCCTATTGGTTAAAAAATGAGCTGATTTAACAATAATTTAACGCGAATTAAT  
TCTGTGGAATGTGTGTCAGTTAGGGTGTGGAAAGTCCCCAGGCTCCCCAGCAGGCAGAAGTATGCAAAG  
CATGCATCTCAATTAGTCAGCAACCAGGTGTGGAAAGTCCCCAGGCTCCCCAGCAGGCAGAAGTATGCA  
AAGCATGCATCTCAATTAGTCAGCAACCATAGTCCCGCCCTAACTCCGCCCATCCCGCCCTAACTCCG  
CCAGTTCGCCCATTCTCCGCCCATGGCTGACTAATTTTTTTTATTTATGCAGAGGCCGAGGCCGCCCTC  
TGCTTCTGAGCTATTCCAGAAGTAGTGAGGAGGCTTTTTTGGAGGCCTAGGCTTTTGCAAAAAGCTCCCG  
GGAGCTTGTATATCCATTTTCGGATCTGATCAGCACGTGTTGACAATTAATCATCGGCATAGTATATCGG  
CATAGTATAATACGACAAGGTGAGGAACTAAACCATGGCCAAGCCTTTGTCTCAAGAAGAATCCACCCT  
CATTGAAAGAGCAACGGCTACAATCAACAGCATCCCCATCTCTGAAGACTACAGCGTCGCCAGCGCAGC  
TCTCTTAGCGACGGCCGATCTTCACTGGTGTCAATGTATATCATTTTACTGGGGGACCTTGTGCAGAA  
CTCGTGGTGTGGGCACTGCTGCTGCTGCGGCAGCTGGCAACCTGACTTGTATCGTCGCGATCGGAAAT

GAGAACAGGGGCATCTTGAGCCCCTGCGGACGGTGCCGACAGGTGCTTCTCGATCTGCATCCTGGGATC  
AAAGCCATAGTGAAGGACAGTGATGGACAGCCGACGGCAGTTGGGATTCGTGAATTGCTGCCCTCTGGT  
TATGTGTGGGAGGGCTAAGCACTTCGTGGCCGAGGAGCAGGACTGACACGTGCTACGAGATTCGATTC  
CACCGCCGCTTCTATGAAAGGTTGGGCTTCGGAATCGTTTTCCGGGACGCCGGCTGGATGATCCTCCAG  
CGCGGGGATCTCATGCTGGAGTTCTTCGCCACCCCAACTTGTTTATTGCAGCTTATAATGGTTACAAAT  
AAAGCAATAGCATCACAAATTCACAAATAAAGCATTTTTTTTCACTGCATTCTAGTTGTGGTTTGTCCAA  
ACTCATCAATGTATCTTATCATGTCTGTATACCGTCGACCTCTAGCTAGAGCTTGGCGTAATCATGGTCA  
TAGCTGTTTTCTGTGTGAAATTGTTATCCGCTCACAATTCACACAACATACGAGCCGGAAGCATAAAGT  
GTAAAGCCTGGGGTGCCTAATGAGTGAGCTAACTCACATTAATTGCGTTGCGCTCACTGCCCGCTTCCA  
GTCGGGAAACCTGTCGTGCCAGCTGCATTAATGAATCGGCCAACGCGCGGGGAGAGGGCGGTTTGCAT  
TGGGCGCTCTCCGCTTCCCTCGCTCACTGACTCGCTCGCTCGGTCGTTCCGGCTGCGGGGAGCGGTATCA  
GCTCACTCAAAGGCGGTAATACGGTTATCCACAGAATCAGGGGATAACGCAGGAAAGAACATGTGAGC  
AAAAGGCCAGCAAAGGCCAGGAACCGTAAAAAGGCCGCGTTGCTGGCGTTTTTCCATAGGCTCCGCC  
CCCTGACGAGCATCACAAAATCGACGCTCAAGTCAGAGGTGGCGAAACCCGACAGGACTATAAAGAT  
ACCAGGCGTTTCCCCCTGGAAGCTCCCTCGTGCCTCTCCTGTTCCGACCCTGCCGTTACCGGATACCT  
GTCCGCTTTCTCCCTTCGGGAAGCGTGGCGCTTTCTCATAGCTCACGCTGTAGGTATCTCAGTTCGGTGT  
AGGTCGTTTCGCTCCAAGCTGGGCTGTGTGCACGAACCCCCGTTTCAGCCCGACCGCTGCGCCTTATCCGG  
TAACTATCGTCTTGAGTCCAACCCGGTAAGACACGACTTATCGCCACTGGCAGCAGCCACTGGTAACAG  
GATTAGCAGAGCGAGGTATGTAGGCGGTGCTACAGAGTCTTGAAGTGGTGGCCTAACTACGGCTACAC  
TAGAAGAACAGTATTTGGTATCTGCGCTCTGCTGAAGCCAGTTACCTTCGGAAAAAGAGTTGGTAGCTC  
TTGATCCGGCAAACAACCACCGCTGGTAGCGGTGGTTTTTTTTGTTTGCAAGCAGCAGATTACGCGCAG  
AAAAAAGGATCTCAAGAAGATCCTTTGATCTTTTCTACGGGGTCTGACGCTCAGTGGAACGAAAATC  
ACGTTAAGGGATTTTGGTCATGAGATTATCAAAAAGGATCTTCACCTAGATCCTTTTAAATTAATAATGA  
AGTTTTAAATCAATCTAAAGTATATATGAGTAAACTTGGTCTGACAGTTACCAATGCTTAATCAGTGAGG  
CACCTATCTCAGCGATCTGTCTATTTTCGTTTCATCCATAGTTGCCTGACTCCCCGTCGTGTAGATAACTACG  
ATACGGGAGGGCTTACCATCTGGCCCCAGTGCTGCAATGATACCGCGAGACCCACGCTCACCGGCTCCA  
GATTTATCAGCAATAAACCAGCCAGCCGGAAGGGCCGAGCGCAGAAGTGGTCCTGCAACTTTATCCGCC  
TCCATCCAGTCTATTAATTGTTGCCGGGAAGCTAGAGTAAGTAGTTCGCCAGTTAATAGTTTGCGCAACG  
TTGTTGCCATTGCTACAGGCATCGTGGTGTACGCTCGTCGTTTGGTATGGCTTCATTCAGCTCCGGTTCC  
CAACGATCAAGGCGAGTTACATGATCCCCCATGTTGTGCAAAAAGCGGTTAGCTCCTTCGGTCCCTCCG  
ATCGTTGTCAGAAGTAAGTTGGCCGCACTGTTATCACTCATGGTTATGGCAGCACTGCATAATTCTCTTA  
CTGTATGCCATCCGTAAGATGCTTTTCTGTGACTGGTGAGTACTCAACCAAGTCATTCTGAGAATAGTG  
TATGCGGCGACCGAGTTGCTCTTGCCCGGCGTCAATACGGGATAATACCGCGCCACATAGCAGAACTTT  
AAAAGTGCTCATCATTGGAAAACGTTCTTCGGGGCGAAAATCTCAAGGATCTTACCGCTGTTGAGATC  
CAGTTCGATGTAACCCACTCGTGCACCCAACTGATCTTCAGCATCTTTTACTTTACCAGCGTTTCTGGGT  
GAGCAAAAACAGGAAGGCAAAATGCCGCAAAAAGGGAATAAGGGCGACACGGAAATGTTGAATACT  
CATACTCTTCTTTTCAATATTATTGAAGCATTATCAGGGTTATTGTCTCATGAGCGGATACATATTTG  
AATGTATTTAGAAAAATAAACAATAGGGGTTCCGCGCACATTTCCCGAAAAGTGCCACCTGACGTC

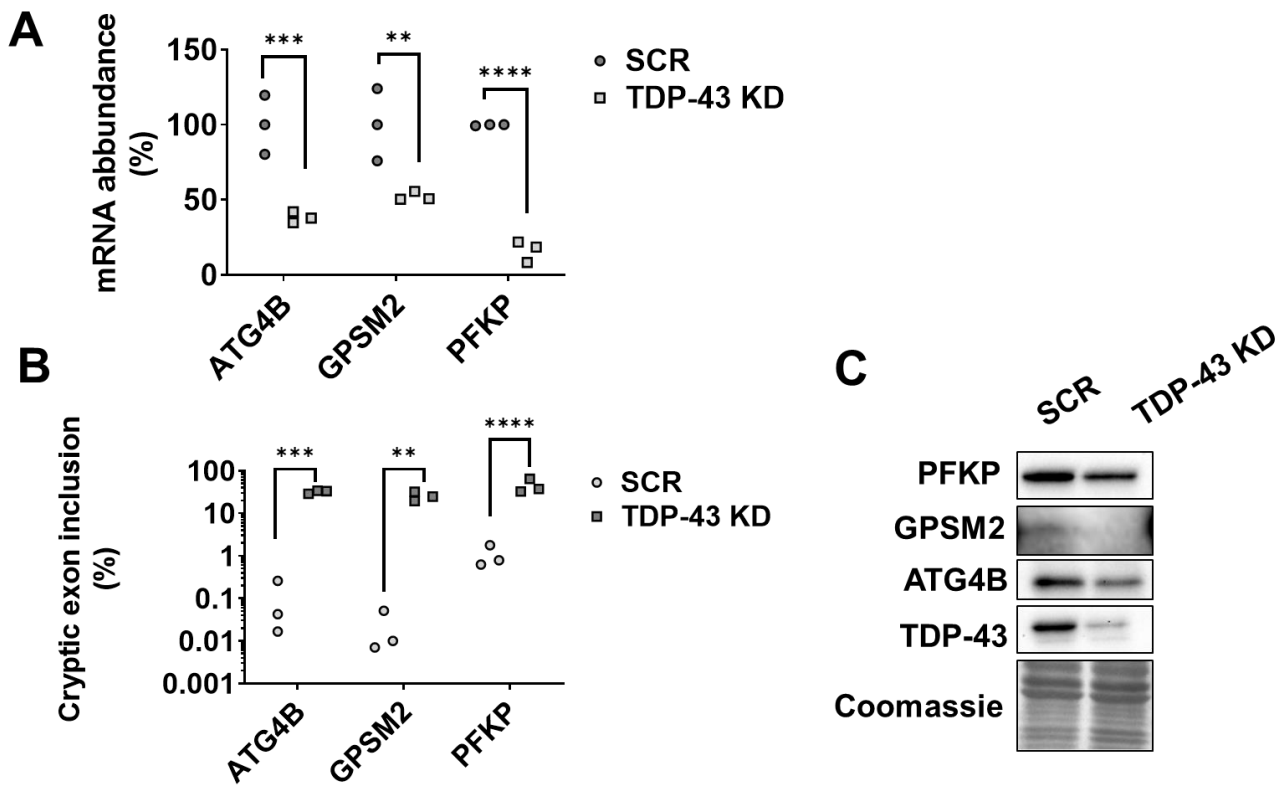
RFP ORF; Intron from original vector; Intron from ATG4B; ATG4B cryptic exon

Supplemental Figure 1. TDP-43 immunoreactivity in CA1 hippocampus (A) and dentate gyrus (B) in two AD cases with TDP-43 proteinopathy. Altered TDP-43 localization is characterized by decreased almost absent nuclear TDP-43 immunoreactivity (\*), and appearance of fine TDP-43 immunoreactive threads (thin arrows) in the neuropil (A) and TDP-43-positive cytoplasmic or nuclear inclusions (thick arrows) (B). Scale bar= 25  $\mu$ m.

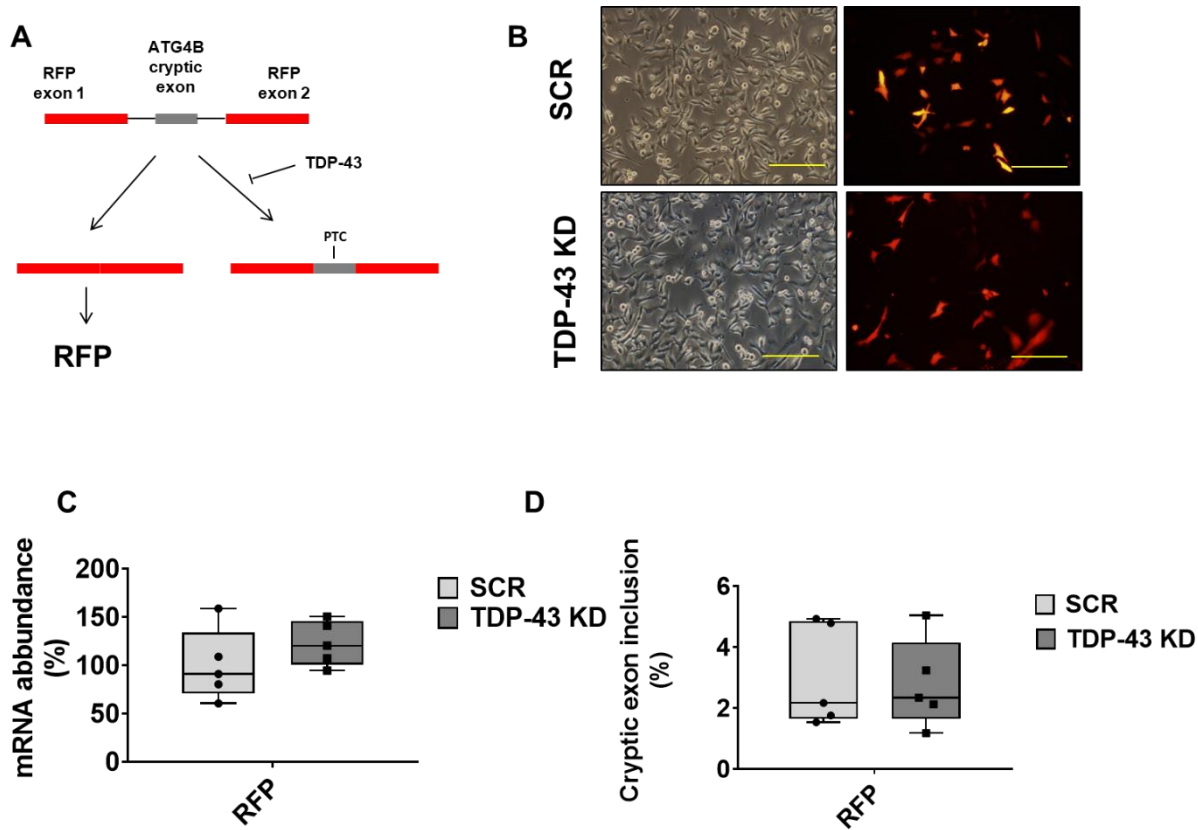
### Supplemental Figure 1



Supplemental Figure 2. TDP-43 regulation of *ATG4B*, *GPSM2* and *PFKP* in HeLa cells. *ATG4B*, *GPSM2* and *PFKP* cryptic exon splicing is induced in *TDP-43* knock-down (KD) HeLa cells in comparison to scrambled (SCR) (A). The reduction of TDP-43 leads to a mRNA (B) and protein decay (C). \*\*p < 0.01; \*\*\*p < 0.001. \*\*\*\*p < 0.0001 by Sidak's multiple comparison test after two-way ANOVA.

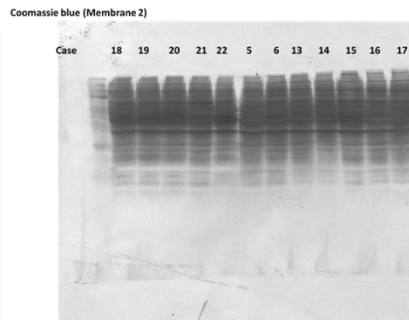
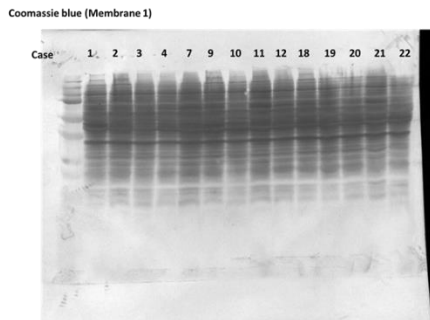
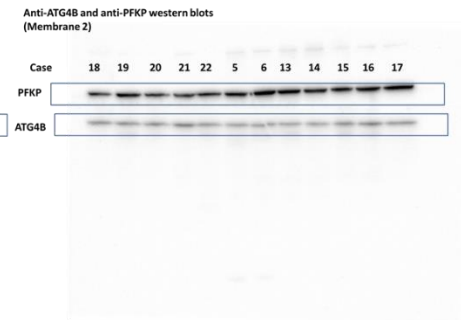
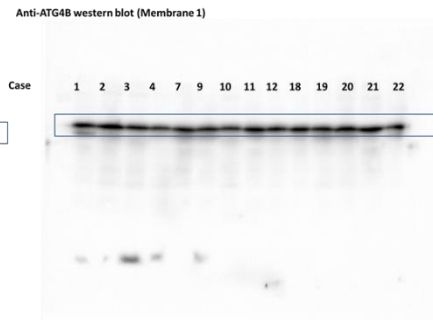
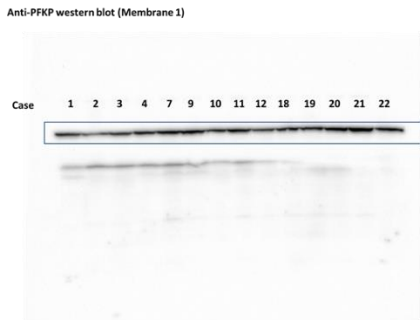
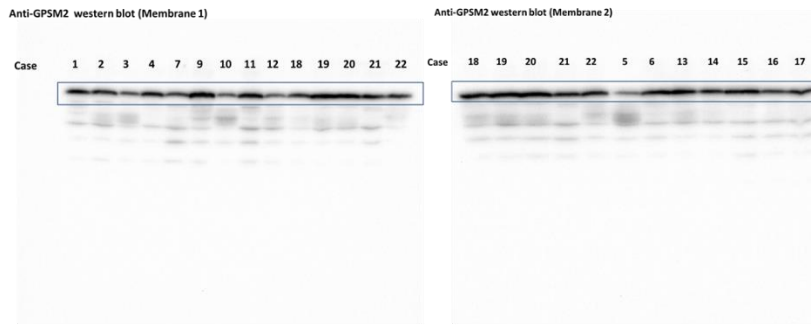


Supplemental Figure 3. Red fluorescent protein (RFP) cryptic splicing reporter. *ATG4B* cryptic exon was inserted between the two exons of *rfp* ORF (A). *rfp* cryptic splicing reporter plasmid emits fluorescence in scrambled (SCR) and *TDP-43* knock-down (KD) cells (B) *rfp* mRNA levels were similar in KD and SCR transduced cells (C). *ATG4B* cryptic exon in RFP remained repressed in SCR and *TDP-43* KD cells. (D). Premature Stop Codon (PTC). Boxes display the interval between 25th and 75th percentiles (q1 and q3); lines inside boxes indicate median values; whiskers indicate the maximum and minimum values. Scale bar represents 100  $\mu$ m.

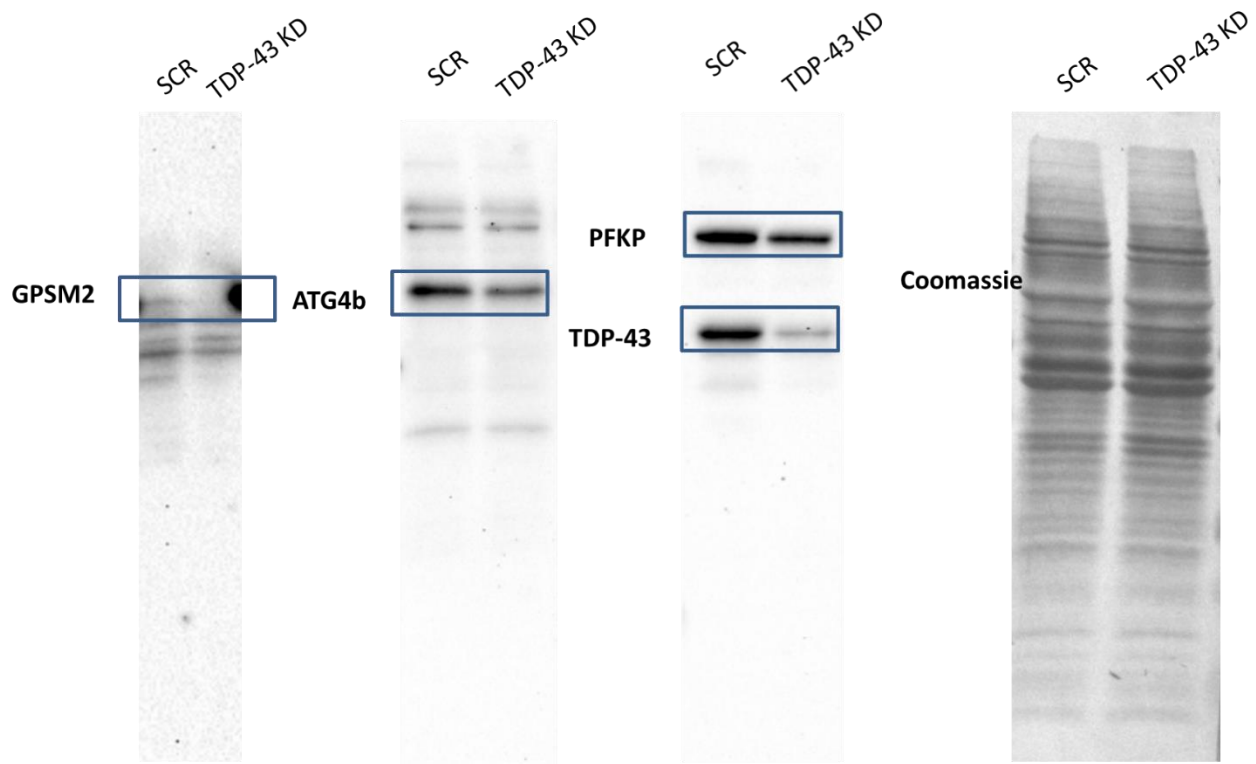




# Supplemental Figure 4. Uncropped western blots employed for figure 1E



Supplemental Figure 5. Uncropped western blots employed for Supplemental Figure 2



## Bibliography

Blobel G, Potter VR. Nuclei from rat liver: isolation method that combines purity with high yield. *Science* 1966; 154: 1662–1665.

Crary JF, Trojanowski JQ, Schneider JA, Abisambra JF, Abner EL, Alafuzoff I, *et al.* Primary age-related tauopathy (PART): a common pathology associated with human aging. *Acta Neuropathol.* 2014; 128: 755–766.

Duyckaerts C, Braak H, Brion J-P, Buée L, Del Tredici K, Goedert M, *et al.* PART is part of Alzheimer disease. *Acta Neuropathol.* 2015; 129: 749–756.

Ferrer I. Brain Banking. In: Aminoff M.J. and Daroff R.B. (eds.) *Encyclopedia of the Neurological Sciences*, 2nd edition, 2014, vol. 1, pp. 467-473. Oxford: Academic Press.

Nelson PT, Dickson DW, Trojanowski JQ, Jack CR, Boyle PA, Arfanakis K, *et al.* Limbic-predominant age-related TDP-43 encephalopathy (LATE): consensus working group report. *Brain* 2019; 142: 1503–1527.

Prasad A, Bharathi V, Sivalingam V, Girdhar A, Patel BK. Molecular Mechanisms of TDP-43 Misfolding and Pathology in Amyotrophic Lateral Sclerosis. *Front. Mol. Neurosci.* 2019; 12: 25.

Torres P, Ramírez-Núñez O, Romero-Guevara R, Barés G, Granado-Serrano AB, Ayala V, *et al.* Cryptic exon splicing function of TARDBP interacts with autophagy in nervous tissue. *Autophagy* 2018; 14: 1398–1403.

## **5.3 Article 3**

**Title:** Exon skipping Antisense Oligonucleotides to correct ATG4B cryptic splicing

**Authors:** Pascual Torres, Miguel Angel Varel, Mathew J A Wood, Reinald Pamplona and Manuel Portero-Otin

**Not Published**































## *Figures and Tables*







## 5.4 Article 4

**Title:** Gender-Specific Beneficial Effects of Docosahexaenoic Acid Dietary Supplementation in G93A-SOD1 Amyotrophic Lateral Sclerosis Mice.

**Authors:** Pascual Torres, Daniel Cacabelos, Jèssica Pairada, Kylynda C. Bauer, Jordi Boada, Laia Fontdevila, Chiara Rossi, Mònica Povedano, Isidre Ferrer, Reinald Pamplona, B. Brett Finlay, Manuel Portero-Otín and Victòria Ayala.

**Journal:** Neurotherapeutics

**Published:** 21/11/2019

**DOI:** 10.1007/s13311-019-00808-2



# Gender-Specific Beneficial Effects of Docosahexaenoic Acid Dietary Supplementation in G93A-SOD1 Amyotrophic Lateral Sclerosis Mice

Pascual Torres<sup>1</sup> · Daniel Cacabelos<sup>1</sup> · Jèssica Pairada<sup>1</sup> · Kylynda C Bauer<sup>2,3</sup> · Jordi Boada<sup>1</sup> · Laia Fontdevila<sup>1</sup> · Chiara Rossi<sup>1</sup> · Monica Povedano<sup>4</sup> · Isidre Ferrer<sup>5,6</sup> · Reinald Pamplona<sup>1</sup> · B. Brett Finlay<sup>2,3,7</sup> · Manuel Portero-Otín<sup>1</sup> · Victòria Ayala<sup>1</sup>

Published online: 21 November 2019  
© The American Society for Experimental NeuroTherapeutics, Inc. 2019

## Abstract

Docosahexaenoic acid (DHA) is an essential fatty acid modulating key nervous system functions, including neuroinflammation, and regulation of pre- and postsynaptic membrane formation. DHA concentration decreases in the lumbar spinal cord (LSC) of amyotrophic lateral sclerosis (ALS) patients and murine preclinical models. Using a dietary supplementation, we increased DHA levels (2% mean increase,  $p < 0.01$ ) in the LSC of the familial ALS murine model B6SJL-Tg(SOD1\*G93A)1Gur/J. This DHA-enriched diet significantly increases male mouse survival by 7% (average 10 days over 130 days of life expectancy), and delays motor dysfunction (based on stride length) and transgene-associated weight loss ( $p < 0.01$ ). DHA supplementation led to an increased anti-inflammatory fatty acid profile (ca 30%,  $p < 0.01$ ) and a lower concentration of circulating proinflammatory cytokine TNF- $\alpha$  ( $p < 0.001$  in males). Furthermore, although DHA-treated mice did not exhibit generally decreased protein oxidative markers (glutamic and amino adipic semialdehydes, carboxyethyllysine, carboxymethyllysine, and malondialdehydelysine), dietary intake of DHA reduced immunoreactivity towards DNA oxidative damage markers (8-oxo-dG) in the LSC. *In vitro* we demonstrate that DHA and  $\alpha$ -tocopherol addition to a model of motor neuron demise (neonatal rat organotypic spinal cord model under chronic excitotoxicity) also preserves motor neuron number, in comparison with untreated spinal cords. Also, beneficial effects on cell viability were evidenced for the motor neuron cell line NSC-34 in front of H<sub>2</sub>O<sub>2</sub> insult ( $p < 0.001$ ). Globally we show a sex-specific benefit of dietary DHA supplementation in the G93A ALS mouse model, compared with mice fed an isocaloric control or a n-3-depleted diet. These changes were associated with an increased DHA concentration in the LSC and were compatible with *in vitro* results showing DHA neuroprotective properties. These results suggest the need for further study on the interaction of gender-influenced biological parameters and DHA in ALS pathogenesis.

**Key Words** Polyunsaturated fatty acids · protein oxidative modification · neuroinflammation · estrogens · n-3 fatty acids

Pascual Torres and Daniel Cacabelos are considered first-authors.

✉ Manuel Portero-Otín  
manuel.portero@mex.udl.cat

✉ Victòria Ayala  
Victoria.Ayala@mex.udl.cat

<sup>1</sup> Departament de Medicina Experimental, Institut de Recerca Biomèdica de Lleida-Universitat de Lleida, Av. Rovira Roure 80, 25198 Lleida, Spain

<sup>2</sup> Department of Microbiology and Immunology, University of British Columbia, Vancouver, BC, Canada

<sup>3</sup> Michael Smith Laboratories, University of British Columbia, Vancouver, BC, Canada

<sup>4</sup> Functional Unit of Amyotrophic Lateral Sclerosis (UFELA), Service of Neurology, Bellvitge University Hospital, Hospitalet de Llobregat, Spain

<sup>5</sup> Department of Pathology and Experimental Therapeutics, University of Barcelona, Hospitalet de Llobregat, Spain

<sup>6</sup> Biomedical Network Research Center on Neurodegenerative Diseases (CIBERNED), Institute Carlos III, Hospitalet de Llobregat, Spain

<sup>7</sup> Department of Biochemistry and Molecular Biology, University of British Columbia, Vancouver, BC, Canada

## Introduction

Characterized by a progressive loss of upper and/or lower motor neurons, amyotrophic lateral sclerosis (ALS) is the motor neuron disease with the highest incidence amongst adult humans. Neuronal loss leads to muscular atrophy, paralysis, and death after a median disease duration of 3 years. Although 90% of the cases are not associated to heritable mutations (sporadic ALS or sALS), the remaining 10% are related to mutations and inherited directly (familial ALS or fALS) [1]. One of the earliest genes whose mutations were associated with fALS was Cu,Zn-superoxide dismutase [2]. Genetic findings led to the development of the G93A-hSOD1 transgenic mouse as an animal model of motor neuron disease [3]. Moreover, sex differences are observed in ALS, with higher incidence and prevalence in men than in women, and distinct clinical phenotypes (men exhibit faster progression) [4]. These findings are also present in experimental ALS models [5].

Docosahexaenoic acid (DHA) [22:6(n-3)] is an n-3 polyunsaturated fatty acid (n-3 PUFA). In humans, DHA precursors are essential fatty acids. DHA precursors must be ingested from dietary sources, as essential fatty acids cannot be synthesized *de novo* in human cells. DHA is usually localized in cell membranes as a phospholipid component. The central nervous system (CNS) is especially rich in DHA [6]. Here, DHA regulates inflammatory processes [7], regulates formation of pre- and postsynaptic membrane components and cerebral hemodynamics [8, 9], and also promotes developmental processes [10] and memory [11].

Although underlying causes of motor neuron degeneration in ALS remain largely unknown [4], DHA is depleted in spinal cord postmortem samples of ALS patients, suggesting a contribution of changes in fatty acid metabolism in the pathogenesis of ALS [12]. However, the contribution of DHA depletion to the disease remains largely uncharacterized. Alternatively, previous work on DHA metabolism and neurodegeneration demonstrates a positive role of this lipid in Parkinson's disease [13], neuroinflammation [14], cognitive impairment [15], Alzheimer's disease [16], and neuropathic pain [17]. Previously, we showed that a general change in polyunsaturated fatty acid content in diets could influence disease evolution in the B6SJL-Tg (SOD1-G93A)1Gur/J transgenic mice [18]. However, whether this was due to direct changes in DHA was unknown.

In this study, we evaluated the neuroprotective effect of dietary DHA supplementation in a preclinical model of motor neuron demise, the B6SJL-Tg (SOD1-G93A)1Gur/J transgenic mice [3]. We investigated whether DHA nutritional interventions modulated n-3 amounts in the spinal cord in the disease evolution, influencing survival, weight loss, motor function-related variables, and fatty acid profiles at 3 different ages (presymptomatic stage, disease onset, and endpoint).

## Methods

### Animals and Diets

A colony of the strain B6SJL-Tg (SOD1-G93A)1Gur/J (JAX catalog stock number 002726; from now on G93A) was purchased at The Jackson Laboratories (Bar Harbor, MN, USA). Mice were maintained in B6SJL backgrounds by male founder crossing with B6SJL F1/J. Genotyping was performed following the manufacturer's instructions. A total of 10 to 12 animals were used to assess survival analyses and 5 to 9 mice for analytical measurements. After genotyping and weaning (21 days), animals were placed at a 12:12-h dark/light cycle, at  $22 \pm 2$  °C temperature, and at  $50\% \pm 10$  relative humidity, in individual cages. Animals were weighed weekly. All diets were stored at 4 °C for its better preservation. All experimental diets were isocaloric and without nutritional deficits. After 9 days under control diet, mice were randomized to follow on the same control diet (#PMI5015, PMI International LabDiet, St. Louis, MO), a low-n-3 diet (TD 00522, Harlan Teklad, Madison, WI), or the same low n-3 supplemented with 0.6% (w/w) DHA (Martek Bioscience, Columbia, MD), as previously described [19, 20]. For food intake calculation, pellets were weighed and removed weekly. The intake of n-3 fatty acids was calculated by accounting individual food intake and the amount of linolenic acid plus DHA specified in the diet. Blood was obtained by tail vein puncture. For animal sacrifice, mice were anesthetized with 2.5% isoflurane. Spinal cords were rapidly excised, snap-frozen in liquid N<sub>2</sub>, and stored at  $-80$  °C. All experimental procedures were approved by the Institutional Animal Care Committee of the University of Lleida, according to local laws and to the Directive 2010/63/EU of the European Parliament. The minimal number of animals was calculated according to the deviation of fatty acid profiles in previous experiments [18].

### Genotyping

Both DNA extraction and PCR-based genotyping have been previously described [18]. Briefly, tail DNA was extracted using the XNAT Kit (# 2740, Sigma-Aldrich, St. Louis, MO). Primers employed for hSOD1 transgene genotyping were as follows: *I12F* (IMR042) 5'-CTAGGCCACAGAAT TGAAAGATCT-3', *I1R2* (IMR043) 5'-GTAG GTGGAAATTCTAGCATCATCC-3', *hSOD1F* (IMR113) 5'-CATCAGCCCTAATCCATCTGA-3', *hSOD1R* (IMR114) 5'-CGCGACTAACAATCAAAGTGA-3'. Murine *IL2* genotyping was assessed as a technical positive control, as indicated by providers (JAX catalog stock number 002726). Thermal Cycler v2.08 (Applied Biosystems, Carlsbad, CA) was used to perform the following PCR protocol: predenaturation for 5 min at 95 °C, denaturation for 1 min at 94 °C, annealing for 45 s at 50 °C, elongation for 4 min at



72 °C, and finally, after 35 cycles, elongation for another 7 min at 72 °C. The amplification products were resolved in 1% agarose stained with SYBR safe (S33102, Thermo Fisher Scientific, Waltham, MA) following the manufacturer protocol and electrophoresed for 30 min under constant 100 V. Images were taken under a 365-nm UV light lamp from Alpha Innotech (Santa Clara, CA) with the software acquisition Digidoc RT2 (Alpha Innotech, Santa Clara, CA).

### Stride Length Analysis

Phenotypic analyses for motor neuron loss have been previously described [18]. Briefly, mice were trained at a flat narrow corridor (5 cm wide, 70 cm long) 3 times per week for 1 month. After this training, animal hind limbs were stained with a nontoxic colorant and put on a paper which served to track the walking behavior along the corridor. A minimum of 5 to 7 continuous strides was recorded to calculate the mean value of stride measurements for each animal 3 days per week. The first footprints were discarded as the mice tend to walk faster when they are released to the corridor. Stride and stance lengths were measured manually and in a blinded manner. Corridors were periodically ventilated to avoid cross-contamination of volatile compounds present in mice.

### Fatty Acid Compositional Analyses

After controlled thawing, samples were kept at 4 °C on ice during the homogenization. A buffer containing 180 mM KCl, 5 mM MOPS, 2 mM EDTA, 1 mM diethylenetriaminepentaacetic acid, and 1 μM of freshly prepared butylated hydroxyl toluene (BHT) at pH 7.3 was used, employing a 1:20 (sample weight:homogenization buffer volume ratio). A homogenizer device (T10 basic UltraTurraX, IKA, Staufen, Germany) was employed for mechanical homogenization (15 s at 15,000 rpm). Protein concentrations were measured by the Bradford method [21].

After the homogenization, lipids from the sample were extracted with chloroform/methanol (2:1, v/v) 0.01% BHT for 3 times as described in [22]. The chloroform phase was evaporated under N<sub>2</sub>. Then, the fatty acids were transesterified by incubation of lipids in freshly prepared 5% methanolic HCl for 90 min at 75 °C. The extraction of the resulting fatty acid methyl esters was performed by adding n-pentane and saturated NaCl solution (2:1 v/v). The n-pentane phase was removed under nitrogen. The remaining product was dissolved in 80 μl of CS<sub>2</sub> for gas chromatography. Separation was assessed by a DBWAX capillary column (30 m × 0.25 mm × 0.20 μm) in an Agilent GC System 7890A with a Series Injector 7683B and a flame ionization detector (Agilent Technologies, Santa Clara, CA). The injection port was maintained at 220 °C and the detector at 250 °C. The temperature program was as follows: 2 min at 100 °C, then an increase of 10 °C/min to 200 °C, then

5 °C/min to 240 °C, and finally maintained at 240 °C for 10 min. For fatty acid methyl ester integration, we compared the peaks with the retention time of authentic standards (Larodan Fine Chemicals, Malmö, Sweden) injected according to the same method. Results were expressed as mol%.

The fatty acid-derived indexes [22] were calculated with the following formulas: Saturated fatty acids (SFA) = Σ % of saturated fatty acids; unsaturated fatty acids (UFA) = Σ % unsaturated fatty acids; monounsaturated fatty acids (MUFA) = Σ % of monoenoic fatty acids; polyunsaturated fatty acids series n-3 (PUFA-n-3) = Σ % of polyunsaturated fatty acids n-3 series; polyunsaturated fatty acids series n-6 (PUFA-n-6) = Σ % of polyunsaturated fatty acids n-6 series; average chain length (ACL) = [(Σ % total 14 × 14) + ... + (Σ % total n × n)]/100 (n = carbon atom number); peroxidizability index (PI) = [(Σ mol% monoenoic × 0.025) + (Σ mol% dienoic × 1) + (Σ mol% trienoic × 2) + (Σ mol% tetraenoic × 4) + (Σ mol% pentaenoic × 6) + (Σ mol% hexaenoic × 8)]; double-bond index (DBI) = [(Σ mol% monoenoic) + (2 × Σ mol% dienoic) + (3 × Σ mol% trienoic) + (4 × Σ % mol tetraenoic) + (5 × Σ mol% pentaenoic) + (6 × Σ mol% hexaenoic)]; anti-inflammatory index (AI) = (20:3n-6) + (20:5n-3) + (22:5n-3) + (22:6n-3)/(20:4n-6). This index accounts for potential changes in cell membrane phospholipids (altering the substrate of cyclooxygenases from arachidonic acid to EPA/DHA), providing eicosanoids and other derivatives that have lower inflammatory potential, as specific prostaglandins (PGE<sub>3</sub>) and other products [23].

### Protein Oxidative Modifications

The concentration of protein oxidative modifications glutamic semialdehyde (GSA), amino adipic semialdehyde (AASA), glycoxidative modification carboxyethyllysine (CEL), mixed lipooxidative glycoxidative modification carboxymethyllysine (CML), and lipooxidative modification malondialdehyde lysine (MDAL) was analyzed by gas chromatography–mass spectrometry (GC/MS) in lumbar spinal cord homogenates as indicated [22]. Briefly, 0.5 mg of proteins from lysate was reduced with an overnight incubation in 500 mM NaBH<sub>4</sub> (final concentration) in 0.2 M borate buffer, containing a 1 drop of hexanol as an antifoam reagent. Reduced proteins were then re-precipitated with 20% trichloroacetic acid (final concentration). Internal standards used for relative quantification were the following: [<sup>2</sup>H<sub>8</sub>] lysine (*d*<sub>8</sub>-Lys; CDN isotopes); [<sup>2</sup>H<sub>4</sub>] CML (*d*<sub>4</sub>-CML), [<sup>2</sup>H<sub>4</sub>] CEL (*d*<sub>4</sub>-CEL), [<sup>2</sup>H<sub>8</sub>] MDAL (*d*<sub>8</sub>-MDAL), [<sup>2</sup>H<sub>5</sub>] 5-hydroxy-2-aminovaleric acid (for GSA quantitation), and [<sup>2</sup>H<sub>4</sub>] 6-hydroxy-2-aminocaproic acid (for AASA quantitation). Proteins were hydrolyzed by incubation at 155 °C for 30 min in 1 ml of 6 N HCl. Samples were dried using a Speed-Vac centrifugal evaporator (SPD131DDA; Thermo

Fisher Scientific, Waltham, MA). For the preparation of the methyl esters, the hydrolysates were dissolved in 1.5 ml of freshly prepared 1 N methanolic HCl and heated for 30 min at 65 °C. The solvent was evaporated at room temperature under a stream of N<sub>2</sub>; then, 1.5 ml trifluoroacetic anhydride was added, and the mixture was incubated at room temperature for 1 h. The resulting N, O-trifluoroacetyl methyl ester derivatives were analyzed in Agilent model 6890 gas chromatograph equipped with a 30-m HP-5MS capillary column (30 m × 0.25 mm × 0.25 μm) coupled to an Agilent model 5973A mass selective detector (Agilent, Barcelona, Spain) under the conditions previously described [18].

### Analysis of Cytokines in Plasma

After blood obtention, it was centrifuged at 8000 rpm for 6 min to retrieve plasma. Plasma was stored at ≤ -20 °C until cytokine analysis. Cytokine levels from plasma were measured using the BD Biosciences Cytometric Bead Array Mouse Inflammation Kit (BD, Franklin Lakes, NJ, USA).

### Organotypic Spinal Cord Culture

Lumbar spinal cord slices from P8 rat pups were obtained as described [24]. Slices were maintained in 50% minimal essential medium, 25 mM HEPES, 25% Hank's balanced salt solution with D-glucose 25.6 mg/l, 25% heat-inactivated horse serum, and 2 mM L-glutamine (Invitrogen, Carlsbad, CA, USA). Five complete slices from the lumbar region were transferred to 30-mm-diameter Millipore Millicell-CM (0.22 μm; Millipore Corporation, Bedford, MA, USA) membrane inserts. The inserts were placed in 6-well culture trays (35-mm-diameter Falcon; BD), with 1-ml culture medium: 50% (vol/vol) minimal essential medium (MEM) with 25 mM HEPES (Invitrogen), 25% (vol/vol) heat-inactivated horse serum, and 25% (vol/vol) Hank's balanced salt solution (HBSS) supplemented with D-glucose (25.6 mg/ml; Sigma, St. Louis, MO, USA), 2 mM L-glutamine, 100 U/ml penicillin, and 100 μg/ml streptomycin (Invitrogen). Organotypic cultures were incubated at 37 °C in a 5% CO<sub>2</sub>-95% O<sub>2</sub> humidified incubator, and the culture medium was changed 4 h after harvesting and then twice a week. Cultures were let to stabilize for 10 days; after this point, the motoneuron population reaches a steady number and remains stable from 1 to 4 weeks [24]. Thus, the treatments, inducing chronic excitotoxicity with threo-hydroxyaspartate (THA) at 100 μM, with DHA and/or α-tocopherol, 500 μM each, started 10 days after the explant procedure. After 15 days of treatment, cultures were harvested and fixed in 4% paraformaldehyde in 0.1 M phosphate buffer, pH 7.4, overnight at 4 °C and processed for immunohistochemistry.

### NSC-34 Cell Culture and Viability

NSC-34 (kindly given by Prof. JE Esquerda, University of Lleida, Spain) were grown in MEM-Advanced medium (Invitrogen) supplemented with 10% heat-inactivated fetal bovine serum (Invitrogen), 2 mM L-glutamine (Invitrogen), and 20 U/ml penicillin and 20 μg/ml streptomycin (Invitrogen) as antibiotics. Cells were kept at 37 °C in humidified atmosphere with 5% of CO<sub>2</sub> [24]. Cell viability in cell cultures was determined by using the MTT-based Cell Toxicity Colorimetric Assay Kit (Sigma) according to the manufacturer's instructions. The results were expressed as the percentage of viability *versus* untreated cells.

### Immunohistochemistry

Animals were anesthetized by an intraperitoneal injection of pentobarbital and ketamine, 20 mg/kg and 60 mg/kg respectively in PBS. Mice were then perfused with saline solution followed by ice-cold 4% paraformaldehyde (Sigma-Aldrich, St. Louis, MO, USA) solution (freshly prepared with pH 7.4 phosphate buffer). Spinal cords were extracted and fixation was continued by incubation in 4% paraformaldehyde made in pH 7.4 phosphate buffer overnight at 4 °C. The next day, samples were cryopreserved in 30% sucrose (made in pH 7.4 phosphate buffer) for 48 h. After this time, tissue was encased in a cubic recipient (Peel-A-Way Disposable Embedding Molds-S-22, Polysciences Inc., Warrington, PA), and embedded in tissue-freezing medium (Triangle Biomedical Sciences Inc., Newcastle, UK) and frozen (-80 °C). The lumbar spinal cord was then cut at a 16-μm section depth and resulting seeded on a gelatin-coated slide. In the case of organotypic slices, these were directly seeded onto the slides. Samples were permeabilized with 0.4% Triton X-100 PBS for 30 min and blocked with 5% normal horse serum in 0.4% Triton X-100 PBS (blocking solution) for 2 h at room temperature. Primary antibody (diluted according to manufacturer's instructions) incubation, anti-8-oxo-dG (ab62623, Abcam, Cambridge, UK), anti-γH2Ax (ab2893, Abcam), anti-GFAP (ab7260, Abcam) anti-Iba1 (ab5076, Abcam), and anti-SMI-32 (Covance, Princeton, NJ), was performed in blocking solution overnight at 4 °C. Then, the slices were washed with PBS 3× for 10 min at room temperature, followed by the secondary antibody (diluted 1:800 in PBS), goat anti-mouse Alexa Fluor 555 (A21422, Thermo Fisher Scientific, Waltham, MA) and/or goat anti-rabbit Alexa Fluor 488 (A11008, Thermo Fisher Scientific, Waltham, MA), incubation for 1 h at room temperature in darkness. Sections were finally counterstained with 4,6-diamidino-2-phenylindole dihydrochloride (DAPI, 1 μg/ml) in PBS for 5 min at RT and mounted on slides with Vectashield (Vector Laboratories, Burlingame, CA). In selected sections, the

primary antibody was omitted to assure labeling specificity. Confocal microscopy was performed with a Fluoview 1000 microscope (Olympus Corporation, Tokyo, Japan) for immunofluorescence imaging. Immunoreactivity quantification and motor neuron count (in the case of organotypic culture) were analyzed with the ImageJ software [25], by selecting motor region from anterior horns in the spinal cord. Motor neurons were putatively identified by soma size, low DAPI fluorescence, and anterior location. All measurements and analyses were done in a double-blinded fashion.

## Statistical Analyses

All data are plotted on graphs as mean  $\pm$  S.E.M. All statistics were performed using the SPSS software (SPSS Inc., Chicago, IL) or the Prism software (GraphPad Software, San Diego, CA). Differences between groups were analyzed by the Kaplan–Meyer analyses, Student's *t* tests, or ANOVA with post hoc analyses, after normality assessment by the Kolmogorov–Smirnov test. Correlations between variables were evaluated by Pearson's statistic. The 0.05 level was selected as the point of minimal statistical significance in every comparison.

## Results

### Dietary DHA Supplementation Extends G93A Mouse Survival, Prevents Weight Loss, and Improves Motor Function in a Sex-Specific Manner

In order to determine the potential benefits of DHA supplementation, we analyzed the survival of ALS mice by sex and diet. The Kaplan–Meyer analysis revealed a longer survival of G93A male mice survival under DHA-supplemented diet (Fig. 1a). The low-n-3 diet did not induce a significant loss in survival (Fig. 1a). Female G93A mice survival did not exhibit any differences between the 3 diet groups analyzed (Fig. 1a). Moreover, weight loss, indicating motor neuron impairment in this model, was significantly influenced by diet in G93A male mice (Fig. 1b), but not in females (Fig. 1b). Regarding the motor function, we also assessed gait strides to determine the impact of diet on motility. Results indicate a slower decrement on stride length and stance length in G93A male mice under DHA-supplemented diet compared with those under control and low-n-3 diets (Fig. 1c and d) and a lower effect of diet and motor function interaction in female G93A mice (Fig. 1c and d). Noteworthy, food intake, revealing motor function, also showed gender-influenced differences to diets (Fig. 1e).

### DHA Dietary Supplementation Increases DHA Contents and Decreases AA Concentrations in the LSC of G93A Mice

To confirm DHA bioavailability in the LSC and the feasibility to modify fatty acid content using dietary intervention, we measured LSC fatty acid profile. A significant correlation was present between the n-3 intake (DHA + linolenic) and LSC DHA content, irrespective of gender (Fig. 2a) before disease onset (age < 90 days). We then compared LSC fatty acid composition in the presymptomatic stage (60 days), at disease onset (90 days) and endpoint. Fatty acid profile analysis of LSC revealed that DHA content in LSC decreases according to disease advancement. In contrast, DHA supplementation induces a significant increase of DHA concentration in LSC at 60 days and 90 days and a decrease of this fatty acid under the low-n-3 diet (Fig. 2b). Moreover, in males, DHA supplementation increased DHA content in LSC at all times, an effect not exhibited in females (Fig. 2b). In contrast with the increase of DHA, arachidonic acid (AA) content showed a statistically significant decrease in the group with the DHA-supplemented diet either at a presymptomatic stage, at disease onset, and at endpoint both in males and in females (Fig. 2c).

### Diet Influences Protein Oxidative Damage

Previous data show that oxidative modifications are sensitive to changes in dietary fatty acid profile [18]. In order to evaluate protein oxidative modifications of LSC, we quantified by GC-MS the concentrations of GSA, AASA, CML, CEL, and MDAL, representative markers of protein modifications. GSA was higher in 60-day-old mice, but reduced at 90 days and endpoint in LSC from G93A mice under DHA diet mice, compared with low-n-3 diet both in males and females (Fig. 3a). AASA is decreased at 60-day-old mice in the DHA diet group in males and females (Fig. 3b). AASA showed an increase at 90 days and endpoint in the DHA diet group compared with a presymptomatic stage in transgenic males and females, but AASA decrease at endpoint was only observed in female DHA-treated mice. CML quantification (Fig. 3c) in G93A mice fed with DHA diet resulted in reduced levels at 60 days old, respective to the male mice fed a control diet group in male or female mice on the low-n-3 diet. At 90 days old, G93A male mice fed with DHA diet showed reduced levels of CML compared with those fed with low-n-3 diet. G93A females exhibited a reduction compared with the control diet group but were not different in the low-n-3 group. At endpoint, diet did not influence in CML content of transgenic male mice. In contrast, CML levels in transgenic female mice were lower in the DHA diet group. Interestingly, age was not a significant factor influencing CML content. A decrease in CEL levels was only observed in female mice at the 60-day

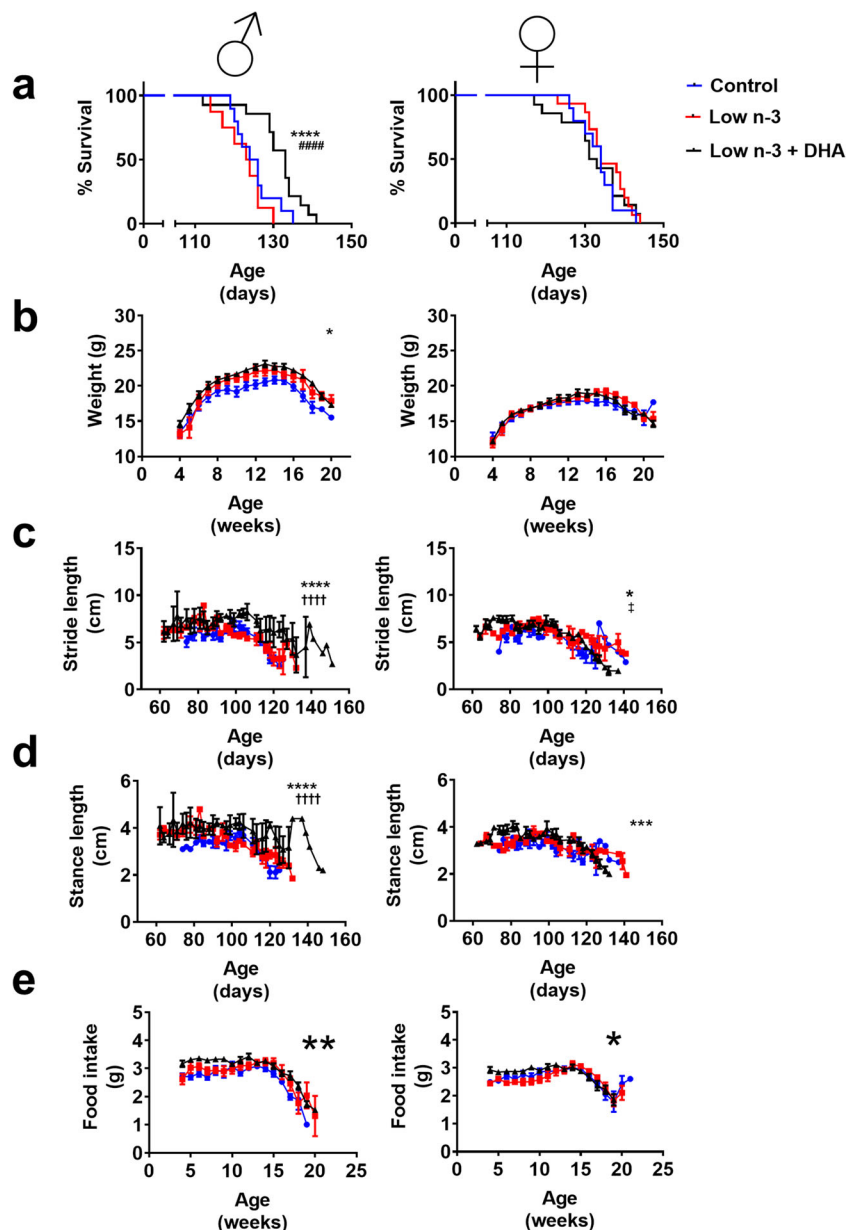


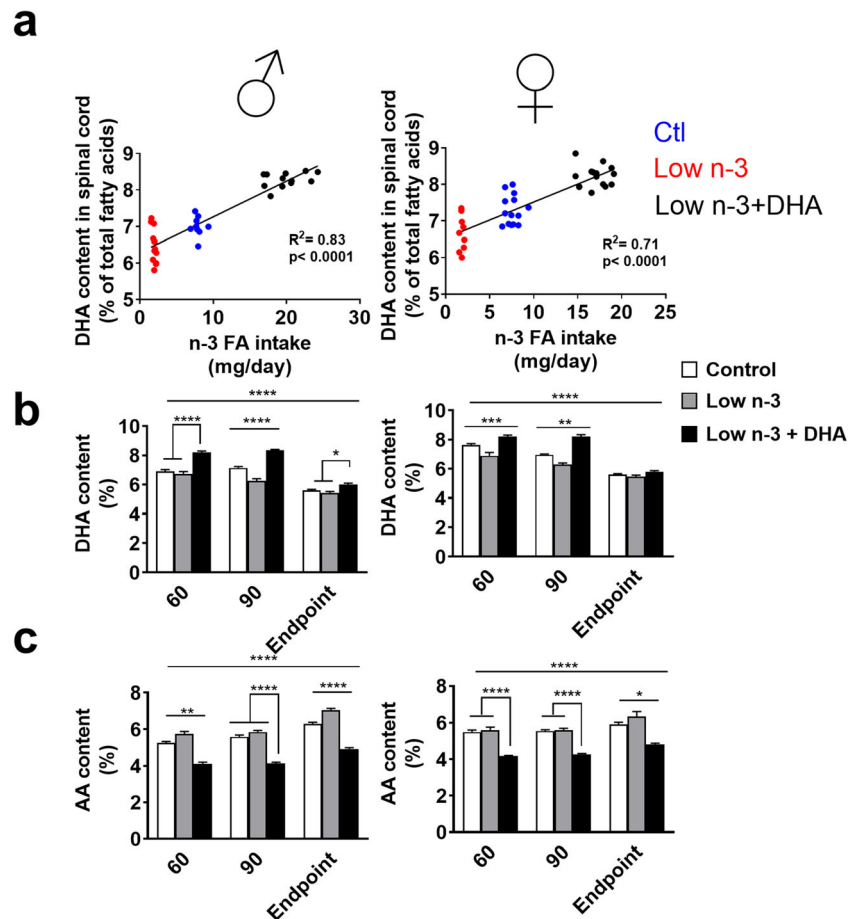
**Fig. 1** DHA dietary supplementation increases the survival of G93A male mice. DHA supplementation increases percent survival in males (**a**) but not in females. Growth curves also show diet-induced differences in males (**b**), though age at the maximum weight is not altered. Disease evolution, as measured by loss of stride (**c**) and stance (**d**) lengths, and daily food intake (**e**), also indicates the protective effect of dietary DHA supplementation in males, but not in females. Percent survival in (**a**) was estimated by Kaplan–Meyer analyses. Two-way ANOVA with repeated measures was employed for (**b**), (**c**), (**d**), and (**e**). In the case of (**b**), in males, this analyses showed a  $p = 0.0119$  for diet effect and  $p < 0.0001$  for age effect, and diet and age interaction is not significant; for females,  $p = 0.6278$  for diet effect,  $p < 0.0001$  for age effect; but in this case, age and diet interaction being significant,  $p = 0.0046$ . For (**c**), in males, diet effect showed a  $p = 0.031$ , age effect  $p = 0.0007$ , and age and diet interaction

was not significant; for females, diet effect showed a  $p = 0.22$ , with age effect  $p < 0.0001$ , and age and diet interaction with  $p = 0.037$ . For (**d**), in males, age effect was  $p = 0.01$  with diet  $p = 0.13$  and interaction between age and diet  $p = 0.21$ ; for females, age effect was  $p = 0.0011$ , diet factor  $p = 0.15$ , and interaction between age and diet  $p = 0.027$ . For (**e**), in males, this analyses showed a  $p = 0.0011$  for diet effect,  $p < 0.0001$  for age effect, and  $p = 0.048$  for diet and age interaction; for females, a  $p = 0.1395$  for diet effect,  $p < 0.0001$  for age effect, and age and diet interaction being significant,  $p < 0.0001$ . In all cases, matching between individuals was effective ( $p < 0.0001$ ). Error bars represent  $\pm$  S.E.M. \*\*\*\* $p < 0.0001$ , \*\*\* $p < 0.001$ , and \* $p < 0.05$  in control versus low-n-3 + DHA diet comparisons, whereas †††† $p < 0.0001$  in low-n-3 versus low-n-3 + DHA diet comparisons and † $p < 0.05$  in control versus low-n-3 diet groups in post hoc multiple comparisons

time point (Fig. 3d). At 90 days, both males and females of the DHA group exhibited lower CEL levels than low-n-3 diet

group, with CEL levels comparable between the control and DHA-supplemented mice. At endpoint, males under DHA

**Fig. 2** Dietary DHA supplementation increases DHA contents and lowers AA concentrations in the lumbar spinal cords of G93A mice. (a) DHA content of the lumbar spinal cords correlates significantly (see inside the graph for Pearson correlation coefficients) with dietary intake of n-3 fatty acids in 90-day-old males (linear regression:  $p < 0.001$ ;  $r^2 = 0.58$ ) and females (linear regression:  $p < 0.001$ ;  $r^2 = 0.24$ ). Consequently, across different ages, males supplemented with DHA have higher DHA levels in LSC with similar results in females, with the exception of endpoint period (b). Similarly, AA is reduced in LSC in male mice under the DHA diet, as well as in females (c). Bars indicate mean values, whereas error bars represent S.E.M. Significant differences between dietary groups ( $*p < 0.05$ ,  $**p < 0.01$ ,  $***p < 0.001$ ) were evaluated by a Bonferroni post hoc analysis after 2-way ANOVA, accounting age and diet



supplementation did not show significant differences in CEL content compared with the other diet groups. Nevertheless, females fed with DHA diet exhibited lower levels of CEL compared with those fed with the low-n-3 diet, but not the control diet group. In this case, age was a relevant factor for CEL levels in LSC of males and females. Finally, G93A male mice fed with DHA diet exhibited reduced levels of MDAL (Fig. 3e) at the presymptomatic stage compared with those fed with control and low-n-3 diets; this reduction was not present in females. At 90 days old, diet did not induce any changes in MDAL content in males. However, females under the DHA diet exhibited lower levels of this marker than those fed with the control diet. At endpoint, there were no significant differences of MDAL levels for males in all experimental groups. DHA supplementation diminished MDAL levels in female mice at all time points. These results suggest that MDAL modulates ALS disease progression in G93A female, but not in male, mice.

### DHA-Enriched Diet Influences Inflammatory Constraints in LSC and Plasma

To explore other mechanisms explaining DHA beneficial effects, we evaluated the potential inflammatory modulation

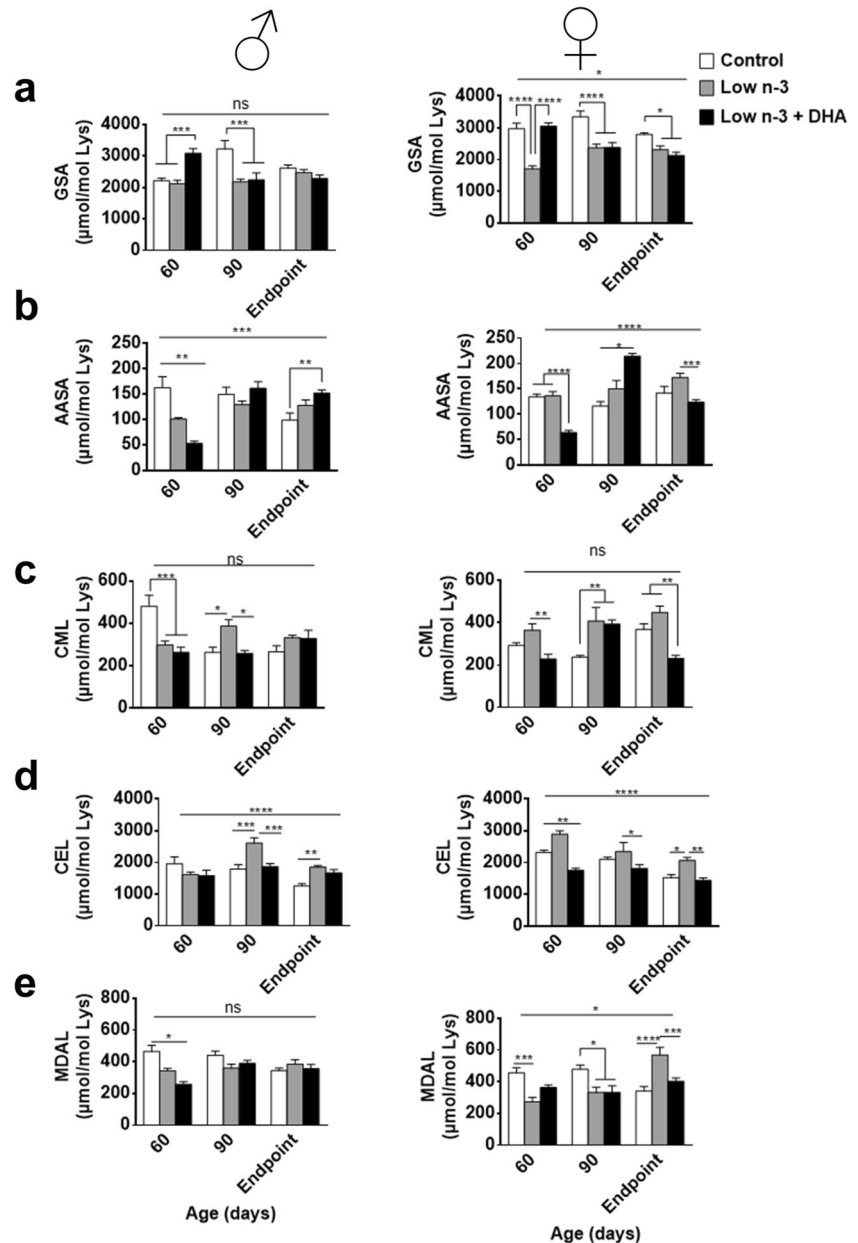
properties of DHA intake. Thus, anti-inflammatory index of LSC fatty acid profiles was increased on the DHA-enriched diet groups (Fig. 4a). Interestingly, this index was decreased at the endpoint stage in all groups. Of note, and reinforcing the complexity of gender–diet interaction, anti-inflammatory index did not show gender differences; it was equally increased in males and females.

To focus on the potential mechanisms leading to DHA survival effects, further experiments were performed in male mice. In order to confirm the role of DHA intake as an inflammation modulator, we quantified plasma concentrations of IL-12, TNF- $\alpha$ , IFN- $\gamma$ , MCP-1, IL-10, and IL-6 at 90 days. These analyses showed a statistically significant influence of DHA dietary enrichment in plasma TNF- $\alpha$  concentrations (Fig. 4b).

### Effect of Dietary DHA Could Involve Several Mechanisms

DHA exerts pleiotropic functions, including interaction with synaptic components [26]. To evaluate this potential function, we evaluated syntaxin 3 levels in male G93A mice. DHA supplementation enhanced syntaxin 3 concentrations in LSC at early stages of motor neuron dysfunction (Fig. 5a). The concentration of other neuron-specific components, such as

**Fig. 3** Heterogenic effects of DHA dietary supplementation over protein oxidative modifications in the proteins of LSC of G93A mice. Oxidative damage as measured by GSA (a) and AASA (b) contents in LSC proteins shows gender- and age-sensitive profiles. In contrast, CML, a marker of mixed lipoxidative and glycoxidative modifications (c), and CEL, a marker of methylglyoxal-derived modifications (d), generally exhibit decreased levels at 90-day and endpoint stages, irrespective of gender. Noteworthy, MDAL, a marker of lipoxidative modifications, shows a significant decrease in males only at earlier stages (e). Bars indicate mean values, whereas error bars represent  $\pm$  S.E.M. Significant differences between dietary groups (\* $p < 0.05$ , \*\* $p < 0.01$ , \*\*\* $p < 0.001$ , \*\*\*\* $p < 0.0001$ ) were evaluated by a Bonferroni post hoc analysis after 2-way ANOVA, accounting age and diet

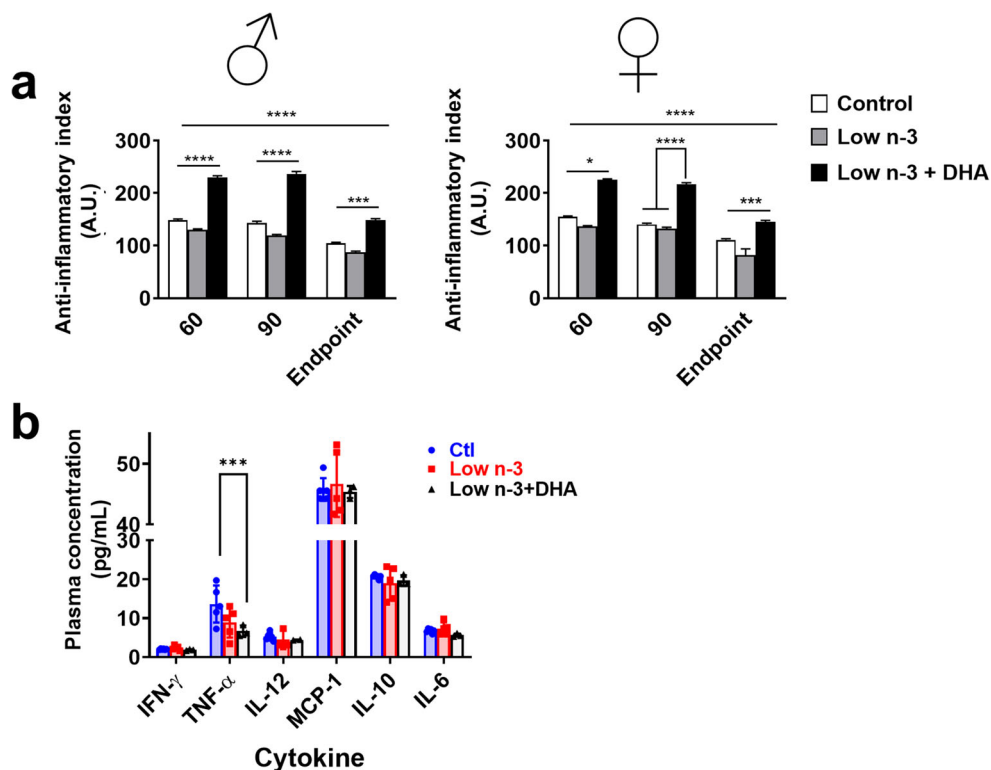


neurofilaments (reacting to SMI-32 antibody), was also enhanced by DHA treatment, as shown by confocal microscopy imaging (Fig. 5b). This was associated with increased ubiquitin immunoreactivity, suggesting enhanced protein repair (Fig. 5b). Indeed even DNA show increased oxidative damage in G93A mice [27]. We evaluated the presence of 8-oxo-7,8-dihydro-2'-deoxyguanosine (8-oxo-dG), a direct marker of oxidative modification of DNA in LSC, focused to 90-day male group comparing control diet and DHA-supplemented diet. 8-Oxo-dG immunoreactivity was significantly lower in spinal cord slices from animals fed with DHA diet compared with those fed with the control diet (Fig. 5c). The DNA damage response is a mechanism to combat threats posed by DNA

damage, induced in ALS [28]. To evaluate whether this mechanism was affected by dietary DHA intake, we utilized confocal microscopy to assess the amount of  $\gamma\text{H2Ax}$  foci, a surrogate for DNA damage response.  $\gamma\text{H2Ax}$  immunoreactivity in LSC of 90-day male ALS mice was lower in 90-day-old G93A male mice fed with the DHA diet when compared with those mice fed with the control diet (Fig. 5c).

In order to evaluate further mechanisms of DHA effects, we evaluated GFAP immunostaining, an indication of astrogliosis, related to disease activity [29]. The results show that, at 90 days, DHA supplementation did not induce a significant change in the levels of glial proliferation (Fig. 5d). Similarly, we evaluated the percentage of anti-Iba1-positive

**Fig. 4** DHA diet influences inflammatory constraints in G93A mice. Anti-inflammatory indexes of fatty acid profiles from LSC of G93A mice are significantly enhanced by DHA supplementation, irrespective of age and gender (a). In line with this, plasmatic TNF- $\alpha$  concentration is also decreased in 90-day-old G93A male mice (b). Bars indicate mean values, whereas error bars represent  $\pm$  S.E.M. In (a), significant differences between dietary groups ( $*p < 0.05$ ,  $***p < 0.001$ ,  $****p < 0.0001$ ) were evaluated by a Bonferroni post hoc analysis after 2-way ANOVA, accounting age and diet. In (b), differences between dietary groups were evaluated by an ANOVA analysis followed by a Bonferroni post hoc analysis, being  $***p < 0.001$



cells, as a marker for microglia infiltration [30]. These analyses show that low n-3 intake, with or without DHA addition, diminishes the percentage of anti-Iba1-positive cells (Fig. 5e).

### Neuroprotective DHA Effects Are Extended to Other Motor Neuron Disease Models

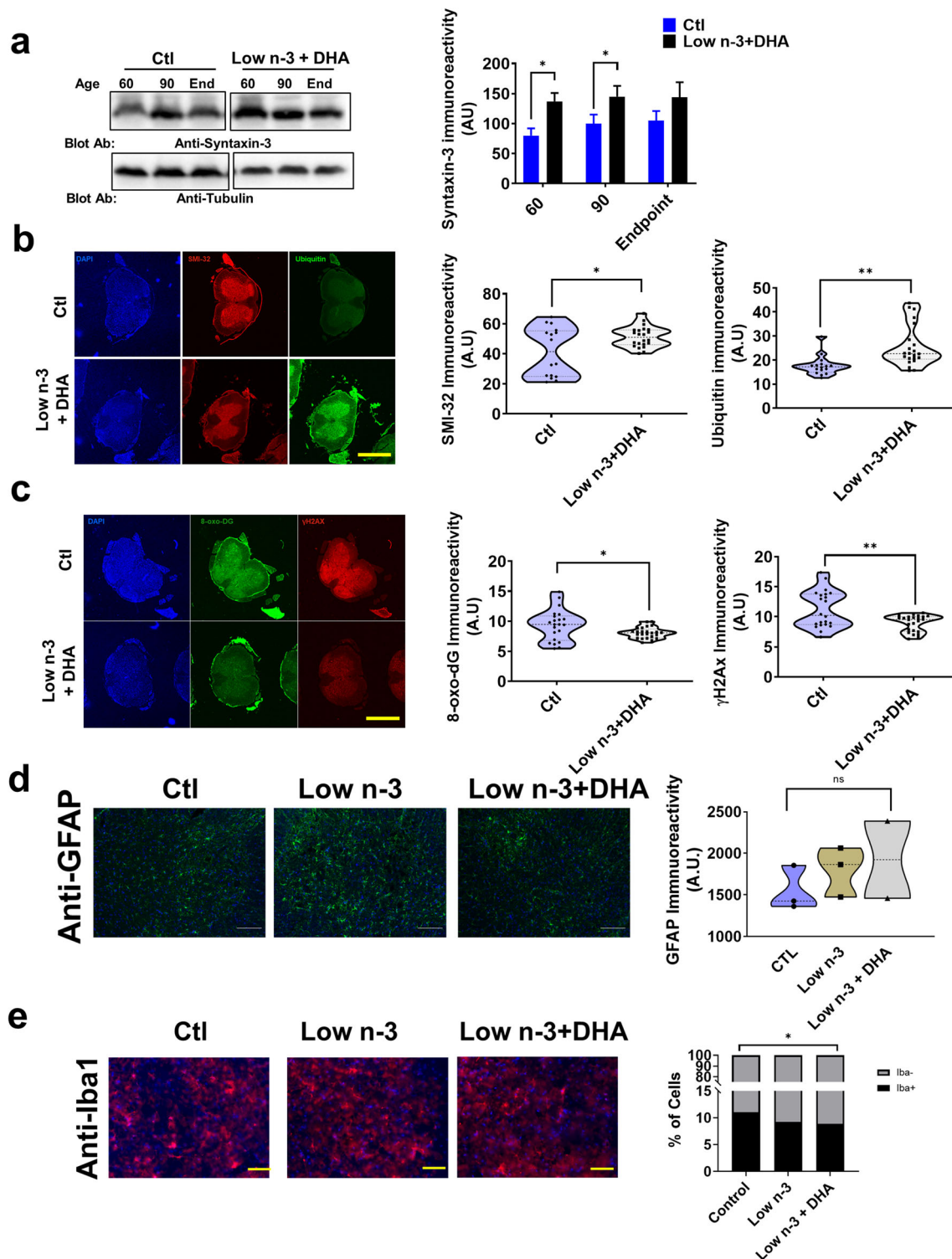
In order to evaluate if DHA protective effects could be extended to other models of motor neuron demise, we evaluated the effect of DHA supplementation in 2 different cellular models of motor neuron death: in chronic excitotoxicity *in vitro* and in the motor neuron-like cell line NSC-34. The results show that, in organotypic cultures under chronic excitotoxicity impinged by THA treatment, DHA alone was not able to reverse motor neuron loss, but in the presence of  $\alpha$ -tocopherol (Fig. 6a). However, DHA alone was able to prevent the toxicity of H<sub>2</sub>O<sub>2</sub> in NSC-34 in a significant manner (Fig. 6b).

## Discussion

We show a gender-diet interaction in the G93A-hSOD1 mouse model of ALS. Dietary DHA supplementation has beneficial effects in male survival, slowing ALS progression and improving motor function.

Previous data suggests the influence of gender in dietary PUFA changes in ALS progression, reinforcing the importance of the diet-gender interaction in ALS [18]. Further, there

are marked differences in neuroinflammatory constraints between genders in mice [31]. Thus, estrogen-sensitive differences in microglia and lymphocyte biology may explain differences in neurodegeneration. Studies also indicate estrogen-dependent pathways enhancing DHA production in females *versus* males [32]. In light of these previous evidence, our data suggest that in G93A mice, dietary DHA is able to modulate sex-associated neuroinflammation constraints. Globally, DHA supplementation improves some neurodegenerative disorders [19], providing an effective therapeutic treatment in a model of spinal cord injury [33]. We also observed that DHA supplementation mitigates oxidative stress markers in the ALS spinal cord. Although the evidence of beneficial effects of DHA in the CNS exists, diets increased in eicosapentaenoic acid (EPA)- a precursor of DHA- decreased survival in G93A mice [34]. Therefore, the present study highlights the relevance of specific effects of the different n-3 fatty acids in diet regarding central nervous system metabolism. In contrast to DHA supplementation, EPA exposure is not able to decrease arachidonic acid content in the spinal cord [34]. Nevertheless, AA is required for proinflammatory signaling and significantly decreasing LSC AA levels could potentially prevent an exacerbation of cyclooxygenase-mediated inflammation [35]. Moreover, earlier findings report that DHA-enriched diet induces beneficial changes on mitochondrial metabolism that EPA diet cannot reproduce [36]. Our experiments prove the feasibility of increasing DHA content in LSC of G93A mice within a dietary supplementation. In contrast to other



neurodegenerative processes [19], low n-3 levels (without n-3 deficiency) did not lead to relevant changes in survival in comparison with standard linolenic intake, suggesting a crucial and specific role for DHA, compared with other linolenic-derived molecules on ALS pathophysiology. Adding complexity to this fact, anti-inflammatory indexes were equally

affected in males and females, thereby indicating that males, in addition to changes in fatty acid profiles, are benefited by yet unknown mechanisms dependent on dietary DHA content.

Protein oxidative damage modifications have been previously linked to Alzheimer's disease [22]. Nevertheless, in the G93A mouse model, protein oxidative damage does not



◀ **Fig. 5** Dietary DHA supplementation leads to changes in synaptic components as well as in DNA and protein repair mechanisms in G93 male mice, without changes in astrogliosis or microglial infiltration. **(a)** Representative Western blot analyses evaluating levels of syntaxin 3 in LSC. In the right panel, the quantitative analyses of Western blot signals, adjusted to tubulin content. **(b)** Representative confocal images (left) and quantitative analyses (right) of neurofilament (SMI-32) and ubiquitin immunoreactivities in whole LSC sections of 90-day-old G93A male mice. **(c)** Representative confocal images (left) and quantitative analyses (right) of DNA repair mechanisms ( $\gamma$ H2Ax) and DHA-related decreases in DNA oxidative damage (8-oxo-dG) in whole LSC sections of 90-day-old G93A male mice, measured in immunohistochemistry. **(d)** Representative confocal images showing a lack of DHA-related changes in GFAP immunostaining in whole SC sections of 90-day-old G93A male mice, quantified in right panels. **(e)** Representative confocal images showing low-n-3 and low-n-3 + DHA-related decreases in the proportion of Iba1 immunoreactive cells in whole SC sections of 90-day-old G93A male mice, quantified in right panels. In **(a)**, bars indicate mean values, whereas error bars represent  $\pm$  S.E.M ( $n = 4$  experiments). Points in **(b)**, **(c)**, and **(d)** indicate different sections, belonging to at least 3 different animals for each dietary treatment. Differences between dietary groups were evaluated by Student's  $t$  test analyses (or  $\chi^2$  test for **(e)**), being  $*p < 0.05$  and  $**p < 0.01$ . Scale bars in **(b)** and **(c)** are 1000  $\mu$ m long and in **(d)** and **(e)** are 100  $\mu$ m and 50  $\mu$ m long, respectively

follow a clear tendency during disease progression. Moreover, although dietary n-3 fatty acid intake and aging influences protein oxidative damage, we observed no clear correlation regarding diet or age and protein oxidative stress. These markers are not correlated with a better outcome, and the biological processes associated with diet and age should be further studied to elucidate their impact in ALS pathology.

Neuroinflammation is involved in the progression of neurodegeneration in ALS through microglia activation [37]. In this sense, our data suggest that dietary fatty acids play an important role in modulating inflammation. Most of the nonsteroid anti-inflammatory drugs, like aspirin, are cyclooxygenase inhibitors and have been largely studied. Cyclooxygenase activity, using AA as a precursor, promotes inflammation and subsequent tissue damage. Prostaglandins, lipid AA derivatives, are increased in the serum of ALS patients [38]. Furthermore, inhibiting prostaglandin synthesis with anti-inflammatory reduces pathological features, such as loss of motor neurons in the spinal cord, and prolongs survival in G93A mice [35]. DHA has been postulated as an inflammatory-resolution promoter mainly through the action of resolvins, metabolic products of DHA enzymatic oxidation. These molecules are PPAR agonists, a transcription

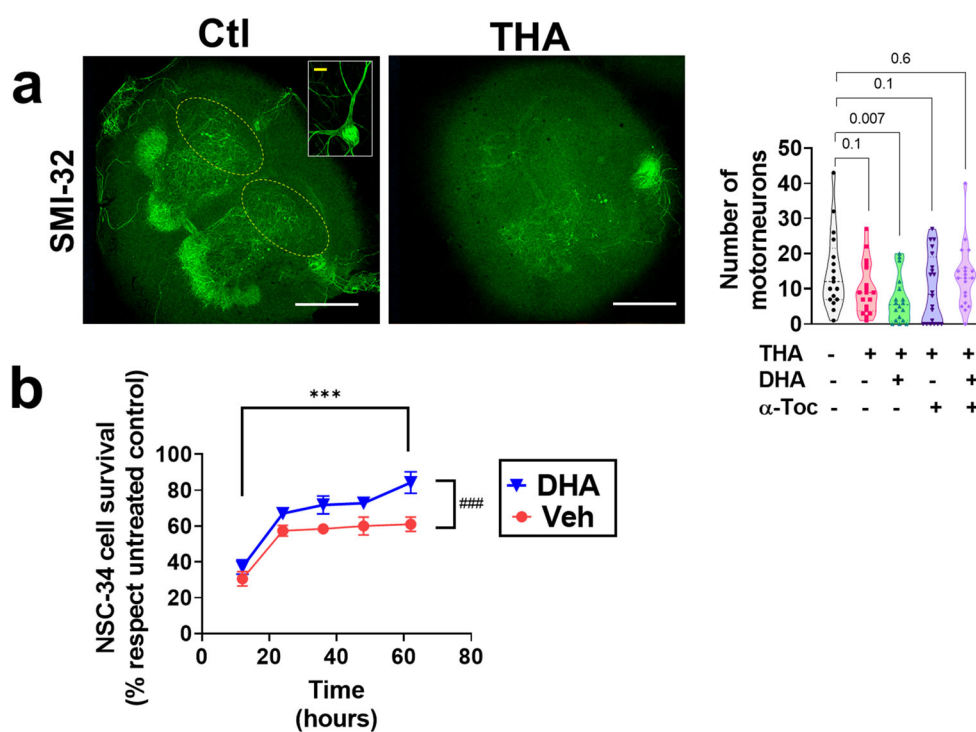


**Fig. 6** DHA is neuroprotective in experimental paradigms of motor neuron death. **(a)** Motor neuron loss induced by THA treatment involves an  $\alpha$ -tocopherol and DHA-sensitive mechanism. Representative confocal images showing the effect of excitotoxicity in the number of SMI-32-positive cells, compatible with motor neurons (inset showing a magnification) in ventral horns (identified by a yellow ellipse) of rat spinal cord organotypic cultures. Right panel shows the quantitative analyses of these micrographs evidencing diminished motor neuron cell number induced by THA, and this effect being prevented by

DHA and  $\alpha$ -tocopherol. In **(b)**, DHA (100  $\mu$ M) is able to prevent loss of viability of the motor neuron cell line NSC-34 induced by  $H_2O_2$  (0.1 mM). Graphs represent the means  $\pm$  S.E.M. ( $n = 4$  experiments). In **(a)**, points indicate the number of motor neurons of different slices, belonging to at least 4 different experiments. Numbers in **(a)** indicate the  $p$  value after post hoc analyses in 1-way ANOVA. In **(b)**,  $***p < 0.0001$  with reference to time effect and  $####p < 0.0001$  with reference to DHA effects by 2-way ANOVA. Scale bars in **(a)** are 100  $\mu$ m long (white bar) and 10  $\mu$ m long (yellow bar, inset)

factor which downregulates NF- $\kappa$ B, preventing inflammation and apoptosis [39]. Another anti-inflammatory mechanism of DHA is the competition of cellular incorporation with AA [40], therefore preventing the production of prostaglandins. Our data demonstrate the capacity of dietary DHA to significantly influence cytokine levels in plasma, supporting the potential modulatory effect of dietary DHA in neuroinflammation in this model. Of note, despite we observed a low-n-3-induced decrease in Iba1 positivity in the spinal cord, in common with previous data with EPA supplementation [34], this effect was not specific of DHA, as we observed in both low-n-3 diets. Contrasting also with the EPA supplementation experiment, our samples did not show any change of astrogliosis. All in all, these data highlight the complexity of the effects of DHA and other n-3 fatty acids in this ALS model.

We acknowledge, as limitations of the present work, that we did not offer an accurate count of motor neurons in spinal cords from the G93A mice. However, the fact that in 2 separate tissular and cellular models of motor neuron demise, DHA (either alone or in combination with  $\alpha$ -tocopherol) was able to prevent motor neuron loss, could allow us to hypothesize a similar effect *in vivo*. We also acknowledge some caveats, such as the increased ubiquitin immunostaining induced by DHA treatments. Usually, ubiquitin is considered a marker of defective proteostasis, but in our case, this might be viewed as a compensatory response.

Concerning potential translation of these results to the human disease context, nutrition for ALS management may be relevant for several reasons. Reports indicate that diet, specifically n-3 fatty acid consumption, plays an important role in ALS progress and may delay the onset of ALS [41]. These data support nutritional intervention as an interesting field to improve the quality of life of ALS patients, but specific issues (such as the interaction with gender) remain open to exploring further venues of dietary personalization in ALS care.

In conclusion, DHA exerts neuroprotective effects in male, but not in female, hSOD1-G93A mouse model of ALS. Further investigations are needed to elucidate this gender-diet interaction. Our data suggest that specific dietary fatty acid composition might be considered in the management of ALS patients.

**Acknowledgments** We thank D. Argilés and M. Martí for their skillful assistance. Grants were received from the Instituto de Salud Carlos III (PI 17-000134) to MPO and from the Generalitat de Catalunya 2017SGR696 to RP. PT is a predoctoral fellow from the Ministerio de Educacion (FPU16/01446). Support was also received in the form of a FUNDELA Grant, RedELA-Plataforma Investigación and the Fundació Miquel Valls (Jack Van den Hoek donation). FEDER funds are acknowledged (“A way to make Europe”).

**Compliance with Ethical Standards** All experimental procedures were approved by the Institutional Animal Care Committee of the University of Lleida, according to local laws and to the Directive 2010/63/EU of the European Parliament

## References

1. Bruijn LI, Miller TM, Cleveland DW. Unraveling the mechanisms involved in motor neuron degeneration in ALS. *Annu. Rev. Neurosci.* 2004;27:723–749.
2. Rosen DR, Siddique T, Patterson D, Figlewicz DA, Sapp P, Hentati A, et al. Mutations in Cu/Zn superoxide dismutase gene are associated with familial amyotrophic lateral sclerosis. *Nature.* 1993;362:59–62.
3. Gurney ME, Pu H, Chiu AY, Dal Canto MC, Polchow CY, Alexander DD, et al. Motor neuron degeneration in mice that express a human Cu,Zn superoxide dismutase mutation. *Science.* 1994;264:1772–1775.
4. Blasco H, Guennoc AM, Veyrat-Durebex C. Amyotrophic lateral sclerosis: a hormonal condition? *Amyotrophic Lateral Sclerosis* 2012;13:585–588.
5. Ajroud-Driss S, Siddique T. Sporadic and hereditary amyotrophic lateral sclerosis (ALS). *Biochim. Biophys. Acta.* 2015;1852:679–684.
6. Singh M. Essential fatty acids, DHA and human brain. *Indian J Pediatr.* 2005;72:239–242.
7. Serhan CN, Chiang N, Van Dyke TE. Resolving inflammation: dual anti-inflammatory and pro-resolution lipid mediators. *Nat. Rev. Immunol.* 2008;8:349–361.
8. Jackson PA, Reay JL, Scholey AB, Kennedy DO. DHA-rich oil modulates the cerebral haemodynamic response to cognitive tasks in healthy young adults: a near IR spectroscopy pilot study. *Br. J. Nutr.* 2012;107:1093–1098.
9. Chytrava G, Ying Z, Gomez-Pinilla F. Exercise contributes to the effects of DHA dietary supplementation by acting on membrane-related synaptic systems. *Brain Res.* 2010;1341:32–40.
10. Guesnet P, Alessandri J-M. Docosahexaenoic acid (DHA) and the developing central nervous system (CNS) - Implications for dietary recommendations. *Biochimie.* 2011;93:7–12.
11. Lee LK, Shahar S, Chin A-V, Yusoff NAM. Docosahexaenoic acid-concentrated fish oil supplementation in subjects with mild cognitive impairment (MCI): a 12-month randomised, double-blind, placebo-controlled trial. *Psychopharmacology.* 2013;225:605–612.
12. Ilijeva EV, Ayala V, Jové M, Dalfo E, Cacabelos D, Povedano M, et al. Oxidative and endoplasmic reticulum stress interplay in sporadic amyotrophic lateral sclerosis. *Brain.* 2007;130:3111–3123.
13. Hernando S, Requejo C, Herran E, Ruiz-Ortega JA, Morera-Herreras T, Lafuente JV, et al. Beneficial effects of n-3 polyunsaturated fatty acids administration in a partial lesion model of Parkinson’s disease: The role of glia and NRf2 regulation. *Neurobiol. Dis.* 2019;121:252–262.
14. Srikanth M, Chandrasaharan K, Zhao X, Chayaburakul K, Ong W-Y, Herr DR. Metabolism of Docosahexaenoic Acid (DHA) Induces Pyroptosis in BV-2 Microglial Cells. *Neuromolecul. Med.* 2018;20:504–514.
15. Zhou M-M, Ding L, Wen M, Che H-X, Huang J-Q, Zhang T-T, et al. Mechanisms of DHA-enriched phospholipids in improving cognitive deficits in aged SAMP8 mice with high-fat diet. *J. Nutr. Biochem.* 2018;59:64–75.
16. Ajith TA. A Recent Update on the Effects of Omega-3 Fatty Acids in Alzheimer’s Disease. *Curr Clin Pharmacol.* 2018;13:252–260.
17. Silva RV, Oliveira JT, Santos BLR, Dias FC, Martinez AMB, Lima CKF, et al. Long-Chain Omega-3 Fatty Acids Supplementation Accelerates Nerve Regeneration and Prevents Neuropathic Pain Behavior in Mice. *Front. Pharmacol.* 2017;8:723.
18. Cacabelos D, Ayala V, Ramirez-Nunez O, Granada-Serrano AB, Boada J, Serrano JCE, et al. Dietary lipid unsaturation influences survival and oxidative modifications of an amyotrophic lateral sclerosis model in a gender-specific manner. *Neuromolecul. Med.* 2014;16:669–685.

19. Calon F, Lim GP, Yang F, Morihara T, Teter B, Ubeda O, et al. Docosahexaenoic acid protects from dendritic pathology in an Alzheimer's disease mouse model. *Neuron*. 2004;43:633–645.
20. Muntané G, Janué A, Fernandez N, Odena MA, Oliveira E, Boluda S, et al. Modification of brain lipids but not phenotype in alpha-synucleinopathy transgenic mice by long-term dietary n-3 fatty acids. *Neurochem. Int.* 2010;56:318–328.
21. Bradford MM. A rapid and sensitive method for the quantitation of microgram quantities of protein utilizing the principle of protein-dye binding. *Anal. Biochem.* 1976;72:248–254.
22. Pamplona R, Dalfó E, Ayala V, Bellmunt MJ, Prat J, Ferrer I, et al. Proteins in human brain cortex are modified by oxidation, glycoxidation, and lipoxidation. Effects of Alzheimer disease and identification of lipoxidation targets. *J. Biol. Chem.* 2005;280:21522–21530.
23. Calder PC. n-3 polyunsaturated fatty acids, inflammation, and inflammatory diseases. *Am. J. Clin. Nutr.* 2006;83:1505S–1519S.
24. Rothstein JD, Jin L, Dykes-Hoberg M, Kuncl RW. Chronic inhibition of glutamate uptake produces a model of slow neurotoxicity. *Proc. Natl. Acad. Sci. USA.* 1993;90:6591–6595.
25. Rasband WS. US National Institutes of Health, Bethesda, Maryland, USA. <http://imagej.nih.gov/ij/>. 2011;
26. Dyall SC. Long-chain omega-3 fatty acids and the brain: a review of the independent and shared effects of EPA, DPA and DHA. *Front. Aging Neurosci.* 2015;7:52.
27. Aguirre N, Beal MF, Matson WR, Bogdanov MB. Increased oxidative damage to DNA in an animal model of amyotrophic lateral sclerosis. *Free Radic. Res.* 2005;39:383–388.
28. Farg MA, Konopka A, Soo KY, Ito D, Atkin JD. The DNA damage response (DDR) is induced by the C9orf72 repeat expansion in amyotrophic lateral sclerosis. *Hum. Mol. Genet.* 2017;26:2882–2896.
29. Keller AF, Gravel M, Kriz J. Live imaging of amyotrophic lateral sclerosis pathogenesis: disease onset is characterized by marked induction of GFAP in Schwann cells. *Glia.* 2009;57:1130–1142.
30. Ito D, Imai Y, Ohsawa K, Nakajima K, Fukuuchi Y, Kohsaka S. Microglia-specific localisation of a novel calcium binding protein, Iba1. *Brain Res. Mol. Brain Res.* 1998;57:1–9.
31. Sorge RE, Mapplebeck JCS, Rosen S, Beggs S, Taves S, Alexander JK, et al. Different immune cells mediate mechanical pain hypersensitivity in male and female mice. *Nat. Neurosci.* 2015;18:1081–1083.
32. Kitson AP, Stroud CK, Stark KD. Elevated production of docosahexaenoic acid in females: potential molecular mechanisms. *Lipids.* 2010;45:209–224.
33. Paterniti I, Impellizzeri D, Di Paola R, Esposito E, Gladman S, Yip P, et al. Docosahexaenoic acid attenuates the early inflammatory response following spinal cord injury in mice: in-vivo and in-vitro studies. *J. Neuroinflammation.* 2014;11:6.
34. Yip PK, Pizzasegola C, Gladman S, Biggio ML, Marino M, Jayasinghe M, et al. The omega-3 fatty acid eicosapentaenoic acid accelerates disease progression in a model of amyotrophic lateral sclerosis. *PLoS One.* 2013;8:e61626.
35. de Lima IV A, Bastos LFS, Limborço-Filho M, Fiebich BL, de Oliveira ACP. Role of prostaglandins in neuroinflammatory and neurodegenerative diseases. *Mediators Inflamm.* 2012;2012:946813.
36. Khairallah RJ, Sparagna GC, Khanna N, O'Shea KM, Hecker PA, Kristian T, et al. Dietary supplementation with docosahexaenoic acid, but not eicosapentaenoic acid, dramatically alters cardiac mitochondrial phospholipid fatty acid composition and prevents permeability transition. *Biochim. Biophys. Acta.* 2010;1797:1555–1562.
37. Frakes AE, Ferraiuolo L, Haidet-Phillips AM, Schmelzer L, Braun L, Miranda CJ, et al. Microglia induce motor neuron death via the classical NF- $\kappa$ B pathway in amyotrophic lateral sclerosis. *Neuron.* 2014;81:1009–1023.
38. Hzeckla J. Prostaglandin E2 is increased in amyotrophic lateral sclerosis patients. *Acta Neurol. Scand.* 2003;108:125–129.
39. Serhan CN, Krishnamoorthy S, Recchiuti A, Chiang N. Novel anti-inflammatory-pro-resolving mediators and their receptors. *Curr. Top. Med. Chem.* 2011;11:629–647.
40. Jaudszus A, Gruen M, Watzl B, Ness C, Roth A, Lochner A, et al. Evaluation of suppressive and pro-resolving effects of EPA and DHA in human primary monocytes and T-helper cells. *J. Lipid Res.* 2013;54:923–935.
41. Fitzgerald KC, O'Reilly ÉJ, Falcone GJ, McCullough ML, Park Y, Kolonel LN, et al. Dietary  $\omega$ -3 polyunsaturated fatty acid intake and risk for amyotrophic lateral sclerosis. *JAMA Neurol.* 2014;71:1102–1110.

**Publisher's Note** Springer Nature remains neutral with regard to jurisdictional claims in published maps and institutional affiliations.

## **5.5 Article 5**

**Title:** A non-canonical profile of senescence biomarkers in the spinal cord of the motor neuron disease mouse model hSOD1-G93A.

**Authors:** Pascual Torres, Carlos Anerillas, Mario Encinas, Mònica Povedano, Pol Andrés-Benito, Isidre Ferrer, Victòria Ayala, Reinald Pamplona, Manuel Portero-Otín.

**Not Published**

and neuroinflammation (D'Ambrosi et al. 2014). Thus, we hypothesized that cytoplasmic p16 could have a similar role in ALS. Like p16 cytoplasmic functions, p21 inhibits the ROCK/LIMK/Cofilin Pathway through MAPK signaling, inducing cytoskeleton remodeling (Tanaka et al. 2002)

We also analyzed another senescence canonical biomarker: SA- $\beta$ -gal activity. The main cellular populations expressing SA- $\beta$ -gal in ventral LSC are the motor neuron cells (Nissl+ cells in the ventral horn, with a motor-neuron compatible cellular size). Neurons of other LSC locations and the vast majority of Nissl- do not show SA- $\beta$ -gal activity (Fig. 1D and S1). Interestingly, SA- $\beta$ -gal activity was reduced during disease progression in motor neurons and in a small fraction of Nissl- cells (compatible with glia). Our findings agree with previously shown data demonstrating that SA- $\beta$ -gal activity in neurons is not associated with senescence, although it is increased in aging mouse brain (Piechota et al. 2016). Our results suggest that motor neurons contain more lysosomes in cell body than other cells, and that their biogenesis is compromised in this ALS mouse model. In this line, lysosomal mass deficit has already been described in this model, highlighting a role of hSOD1 aggregates disturbing lysosomal biogenesis (Xie et al. 2015) and potentially explaining our results from the SA- $\beta$ -gal activity assay.

Another marker commonly employed in senescence description is the increase in cytokines linked to SASP. In this case, we quantified the expression of typical SASP markers *Il1a* and *Il6*. We analyzed as well the expression of *Ifna* and *Ifnb* (corresponding to type-I IFN response) as they are postulated as late-senescence markers and could be helpful in determining senescence progression in the LSC of this model. The expression of *Ifna* was not detected in any of the analyzed samples (data not shown). We observed a different pattern of expression between *Il1a* (Fig. 3A) and *Il6* (Fig. 3B). *Il1a* is increased in the pre-symptomatic stage and is known to be the upstream regulator of IL-6 in SASP (Orjalo et al. 2009). IL-6 is increased in cerebrospinal fluid in ALS, AD, and Parkinson's disease (Chen et al. 2018). In contrast, *Ifnb* expression (Fig. 3C) is not altered, which could indicate that senescence in this model does not evolve a late phase. Overall, this might reflect a complex interaction between senescence, SASP, and changes in reactive glial cells and neurodegeneration.

Regarding TDP-43 splicing function, cryptic exon inclusion in *Adipor2* mRNA was higher in lumbar spinal cord in end-stage mice (Fig. 3D) and positively correlated with *p16* expression (Fig. 3E). The present data are the first to show specific alteration regarding

splicing function in this ALS model. Notably, this process is associated with an increase in the senescence marker *p16*, and the two processes are likely to be linked in the same pathway.

We wanted to explore the potential benefits of senolytic treatment due to the higher expression of senescence related genes in this mouse model. We performed Navitoclax treatment following the protocol described for Alzheimer Disease mouse model (Bussian et al., 2018). The treatment was initiated at 90 days old and finished at end point (Figure 4A). We estimated the disease progression by weight loss. Navitoclax treatment did not prevent weight loss, neither prolonged survival (Figure 4B and 4C). Finally, we quantified senescence and SASP genes in lumbar spinal cord. None of the analyzed genes showed statistically significant differences (Figure 4D). These results suggest differences in molecular effectors between AD and ALS. Navitoclax is an inhibitor of antiapoptotic protein Bcl2 (Zhu et al., 2016). Senescent cells are highly dependent of different antiapoptotic members. Senolysis is achieved when this antiapoptotic protein is inhibited, promoting cell death (Zhu et al., 2015). In the case of ALS, we speculate that Navitoclax treatment is not efficient because Bcl2 is not overactivated in our G93A mouse model (Vukosavic, Dubois-Dauphin, Romero, & Przedborski, 1999). However, Bcl-XL, a Bcl-2 family member, is overactive in astrocytes and provides pro-survival input and may mediate the activation of toxic astroglia (Lee, Kannagi, Ferrante, Kowall, & Ryu, 2009). It suggests that an specific inhibition Bcl-XL could have greater effects on disease progression.

In conclusion, the LSC from the hSOD1-G93A mouse, a model of familial ALS, exhibits a non-canonical profile of senescence biomarkers. It is characterized by an early increase in *p16* and a late increase in *p21*, with both displaying a mainly cytoplasmic pattern in glial cells without an increase in SA- $\beta$ -gal activity. In the case of SASP, it also has a dynamic profile with increasing levels of *Il1a* from the pre-symptomatic stage onward and an acute peak of expression in end-stage transgenic mice. Regarding AS, this tissue shows a dysfunctional splicing activity of TDP-43 in end-stage ALS mice. This is the first time that senescence markers, SASP, and TDP-43-associated splicing dysfunction have been described in this ALS mouse model. Navitoclax treatment (Figure 5A) is not enough to slow the disease progression (Figure 5B) and does not extend the survival. This treatment does not prevent the increase of senescence and SASP markers (Figure 5D). It suggests that senescence phenotype is not driven by Bcl2 expression of stressed or aged cells in this model (Zhu et al., 2015). Further studies are warranted to determine whether

senescence-linked phenomena are mechanistically involved in this fatal disease, clearing the pathway for therapeutic development.

## Experimental procedures

### *Animal Experiments*

A colony of the strain B6.Cg-Tg(SOD1\*G93A)1Gur/J JAX catalogue stock number 004435; from now on hSOD1G93A or G93A) was purchased at The Jackson Laboratories (Bar Harbor, MN, USA). Mice were maintained in C57BL/6J background. Genotyping was performed following manufacturer's instructions. After genotyping and weaning, animals were placed at 12:12 hours dark / light cycle, at 22±2°C temperature, 50%±10 relative humidity, in individual cages (at 21 days). Navitoclax (T2101, Targemol) was diluted in 60% Phosal 50 PG (Lipoid), 30% PEG400 (Sigma, 91893) 10% EtOH. Navitoclax was administered by oral gavage at a dose of 50 mg kg<sup>-1</sup> body during five consecutive days followed by 16 days of rest (N= 5 per group). Treatment cycles were repeated until clinical endpoint (righting reflex >20 s). Spinal cords were rapidly excised, frozen in liquid N<sub>2</sub> and stored at -80 °C. This study was approved by the Animal Research and Ethics Committee at the University of Lleida.

### *Cell culture*

3T3 cells were maintained in Dulbecco's Modified Eagle's Medium (11965, Thermo Fisher Scientific), 10% FBS (10270, Thermo Fisher Scientific), 100 U/ml Penicillin-Streptomycin (15140-122, Thermo Fisher Scientific) at 37°C and 5% CO<sub>2</sub>. For silencing, 20 nM (final concentration) of *TARDBP* siRNA mmsiTDP-43s: 5'-AGGAAUCAGCGUGCAUAUA-3' mmsiTDP-43as: 5'-UAUAUGCACGCUGAUUCCU-3' (siTDP) or scrambled siRNA (siCTL) was mixed in 100 µl Opti-MEM (31985062, Thermo Fisher Scientific) with 2 µl of RNAiMAX (13778100, Thermo Fisher Scientific) on the bottom of the well and incubated for 20 minutes at room temperature. 2 ml of DMEM (11965092, Thermo Fisher Scientific) supplemented with 10% FBS containing 100000 HeLa or 3T3 cells/well were seeded onto transfection mix. After 24 hours, transfection media was removed and changed to DMEM 10% FBS media. 48 hours post-transfection, cells were collected for posterior analyses.

### *Western Blot*

Protein from platelets was extracted adding 100  $\mu$ L of radioimmunoprecipitation (RIPA) buffer with Protease Inhibitor Cocktail (1X) to the pellet. After sonication, protein quantification was performed with Bradford assay (5000006, Bio-Rad). Fifteen  $\mu$ g of protein were loaded onto a 12% acrylamide SDS-PAGE gel. Membranes were blocked with I-Block (T2015, Thermo Fisher Scientific) for 1 hour and incubated overnight with primary incubated anti-TDP-43 (10782–2-AP, Proteintech) 1:1000 in TBS-T 0.05%. After primary antibody incubation, membranes were washed 3 times with TBS-T 0.05% and incubated with secondary antibody for 1h. Immobilon™ Western Chemiluminiscent HRP Substrate (WBKLS0500, Merck Millipore) was used for immunodetection. Membranes were stained with Coomassie Brilliant Blue G (27815, Sigma) for normalization. Specific bands were quantified with ImageLab v5.2.1 (Bio-Rad).

### *RNA extraction, cDNA synthesis and RT-qPCR*

1 ml of TRIzol reagent (Thermo Fisher Scientific, AM9738) was added to 50-100 mg of tissue. The tissue was then mechanically homogenized using T 10 basic ULTRA-TURRAX® (IKA). 200  $\mu$ l of chloroform was added to each sample and mixed. After 5 minutes of incubation at room temperature, the samples were centrifuged at 12,000 xg (15 mins, 4°C) to separate the phases. The aqueous phase was separated into a new tub and mixed by vortexing with 500  $\mu$ l of isopropanol. After an incubation of 10 minutes at room temperature, RNA was precipitated through spun at 12,000 xg (10 mins, 4°C). The resulting supernatant was removed, and the pellet was washed with a 75% ethanol. After vortexing, the samples were centrifuged again at 12,000 xg (10 mins, 4°C). The supernatant was discarded, and the RNA pellet was allowed to air dry at room temperature. The RNA was resuspended with 50  $\mu$ l of RNase-free water, quantified with Nanodrop (Nanodrop technologies, ND-1000 UV/Vis Spectofotometer) and stored at -80°C until further use. One microgram of RNA was used for retrotranscription employing TaqMan Reverse Transcription Reagent using random hexamers (Thermo Scientific, N8080234). RT-qPCR experimets were performed using a CFX96 instrument (Bio-Rad, Hercules, California, USA) with SYBR select Master mix (Thermo Fisher Scientific,



4472908). Each 20  $\mu$ L of reaction contained 4 $\mu$ L cDNA, 10  $\mu$ L SYBR Select Master Mix, 0.2 nM of forward primer and 0.2 nM of reverse primer solutions and 4  $\mu$ L PCR grade water. RT-qPCR run protocol was as follows: 50 °C for 2 minutes and 95 °C for 2 minutes, with the 95 °C for 15 seconds and 60 °C for 1 minute steps repeated for 40 cycles; and a melting curve test from 65°C to 95 °C at a 0.1 °C/s measuring rate. N=3-10 mice per group were used for RT-PCR experiments. Primers employed in these experiments are listed in Supplementary Table S1. *Actb* expression was used as housekeeping to normalize the other genes. Specific *Adipor2 cryptic* mRNA (primers annealed with cryptic exon) was normalized with *Adipor2* normal transcript (the primers annealed with conserved exons).

#### *Senescence-associated $\beta$ -galactosidase activity*

Briefly, paraformaldehyde-fixed frozen sections were incubated with X-gal solution (20 mg/ml X-Gal (SIGMA), 5 mM  $K_3Fe(CN)_6$ , 5 mM  $K_4Fe(CN)_6$  and 2 mM  $MgCl_2$ ) in PBS at pH 6.0 overnight at 37 °C. To allow comparison between specimens, all samples were assayed simultaneously. Then, neurons were stained with Green Fluorescent Nissl Stain (Thermo Fisher Scientific, N21480) diluted 1:150 in PBS and incubated 20 minutes at room temperature. The slices were then washed 3x with PBS for 10 minutes at room temperature and 1x with PBS for 2 hours at room temperature. Nuclei were stained with DAPI (SIGMA, 32670). Images of the stained sections were taken using inverted microscope (Olympus, IX71S8F-2). Eight randomly selected areas of each mouse (N=2-3 per group) of the ventral horn of lumbar spinal cord sections were photographed at 20x magnification for visual analysis. The whole section of SA- $\beta$ -Gal stained slices was photographed at 4x magnification.

#### *Immunofluorescence*

One control and one transgenic lumbar spinal cord were fixed in 4% paraformaldehyde made in PBS overnight at 4°C and cryopreserved in 30% sucrose in PBS 48 hours. The lumbar spinal cord was then cut at a 16  $\mu$ m section depth and resulting seeded on a gelatin-coated slide. Samples were permeabilized with 0.3% Triton X-100 PBS for 30 min and blocked with 5% BSA in PBS for 1h at room temperature. The primary antibody 1:100 anti-p16 (abcam, ab54210) and 1:200 anti-GFAP (abcam, ab7260) were diluted in 0.3%

Triton X-100 PBS and incubated overnight at 4°C. The slices were washed with PBS three times for 5 min at room temperature, followed by the secondary antibody (diluted 1:800 in PBS), goat anti-mouse Alexa Fluor 555 (Thermo Fisher Scientific, A21422) and goat anti-rabbit Alexa Fluor 488 (Thermo Fisher Scientific, A11008) incubation for 1h at room temperature in darkness. Sections were finally counterstained with 1 µg/ml 4,6-diamidino-2-phenylindole dihydrochloride (DAPI) in PBS for 10 min at RT and mounted on slides with Fluoromount-G® (Southern Biotech, 0100). Samples were imaged using a laser scanning confocal microscope Olympus FluoView FV10.

### *Immunohistochemistry*

One control and one transgenic paraformaldehyd fixed paraffin embedded tissue slides were dried for 1h at 65° before pre-treatment procedure of deparaffinization, rehydration and epitope retrieval in the Pre-Treatment Module (Agilent Technologies-DAKO, PT-LINK) at 95°C for 20 min in 50x Tris/EDTA buffer, pH 9. For p21 immunohistochemical staining, p21WAF1/Cip1 antibody (Agilent Technologies-DAKO, clone SX118) 1:100 dilution was used. After incubation, the reaction was visualized with the EnVision™ FLEX Detection Kit (Agilent Technologies-DAKO) using diaminobenzidine chromogen as a substrate. For p16 immunohistochemical staining, p16 INK4a antibody was used using CINtec® Histology Kit (ROCHE, clone E6H4) following manufacturer's instructions. Sections were counterstained with hematoxylin.

### *Statistical Analysis*

All statistical tests and graphs were performed using GraphPad Prism 6 (GraphPad Software). Normalized mRNA expression was analyzed with ordinary Two-way ANOVA test of the variables time and genotype. For multiple comparisons between genotypes, Bonferroni's multiple comparisons test was used. In SA-beta-gal activity experiments, p-value was determined by Chi-square's test. To evaluate relationship between *p16* and *Adipor2* cryptic mRNA levels a linear regression was tested.

## Acknowledgments

This study was supported by the Scientific and Technical Service of Immunohistochemistry, Lleida Institute for Biomedical Research, Dr. Pifarré Foundation, IRBLleida. Grants were received from the Instituto de Salud Carlos III (PI 17-000134) to MPO, from the Generalitat de Catalunya 2017SGR696 to RP, and from the Ministerio de Ciencia, Innovación y Universidades (BFU2017-83646-P, AEI, FEDER, UE) to ME. PT is a predoctoral fellow from the Spanish Ministry of Education [FPU16/01446]. Support was also received in the form of a FUNDELA Grant, RedELA-Plataforma Investigación and the Fundació Miquel Valls (Jack Van den Hoek donation). FEDER funds are acknowledged (“A way to make Europe”). We thank T. Yohannan for editorial assistance.

## References

- Chen X, Hu Y, Cao Z, Liu Q & Cheng Y (2018) Cerebrospinal Fluid Inflammatory Cytokine Aberrations in Alzheimer’s Disease, Parkinson’s Disease and Amyotrophic Lateral Sclerosis: A Systematic Review and Meta-Analysis. *Front. Immunol.* 9, 2122.
- Chen Y-W, Chu H-C, Ze-Shiang Lin, Shiah W-J, Chou C-P, Klimstra DS & Lewis BC (2013) p16 Stimulates CDC42-dependent migration of hepatocellular carcinoma cells. *PLoS One* 8, e69389.
- Coppé J-P, Desprez P-Y, Krtolica A & Campisi J (2010) The senescence-associated secretory phenotype: the dark side of tumor suppression. *Annu. Rev. Pathol.* 5, 99–118.
- D’Ambrosi N, Rossi S, Gerbino V & Cozzolino M (2014) Rac1 at the crossroad of actin dynamics and neuroinflammation in Amyotrophic Lateral Sclerosis. *Front. Cell Neurosci.* 8, 279.
- Hall BM, Balan V, Gleiberman AS, Strom E, Krasnov P, Virtuoso LP, Rydkina E, Vujcic S, Balan K, Gitlin II, Leonova KI, Consiglio CR, Gollnick SO, Chernova OB & Gudkov AV (2017) p16(Ink4a) and senescence-associated  $\beta$ -galactosidase can be induced in macrophages as part of a reversible response to physiological stimuli. *Aging (Albany, NY)* 9, 1867–1884.
- Hayflick L & Moorhead PS (1961) The serial cultivation of human diploid cell strains. *Exp. Cell Res.* 25, 585–621.

- Kurz DJ, Decary S, Hong Y & Erusalimsky JD (2000) Senescence-associated (beta)-galactosidase reflects an increase in lysosomal mass during replicative ageing of human endothelial cells. *J. Cell Sci.* 113 ( Pt 20), 3613–3622.
- Ling JP, Pletnikova O, Troncoso JC & Wong PC (2015) TDP-43 repression of nonconserved cryptic exons is compromised in ALS-FTD. *Science* 349, 650–655.
- McAleese KE, Walker L, Erskine D, Thomas AJ, McKeith IG & Attems J (2017) TDP-43 pathology in Alzheimer's disease, dementia with Lewy bodies and ageing. *Brain Pathol.* 27, 472–479.
- Niccoli T, Partridge L & Isaacs AM (2017) Ageing as a risk factor for ALS/FTD. *Hum. Mol. Genet.* 26, R105–R113.
- Orjalo AV, Bhaumik D, Gengler BK, Scott GK & Campisi J (2009) Cell surface-bound IL-1alpha is an upstream regulator of the senescence-associated IL-6/IL-8 cytokine network. *Proc. Natl. Acad. Sci. USA* 106, 17031–17036.
- Piechota M, Sunderland P, Wysocka A, Nalberczak M, Sliwinska MA, Radwanska K & Sikora E (2016) Is senescence-associated  $\beta$ -galactosidase a marker of neuronal senescence? *Oncotarget* 7, 81099–81109.
- Serrano M, Lin AW, McCurrach ME, Beach D & Lowe SW (1997) Oncogenic ras provokes premature cell senescence associated with accumulation of p53 and p16INK4a. *Cell* 88, 593–602.
- Sharpless NE & Sherr CJ (2015) Forging a signature of in vivo senescence. *Nat. Rev. Cancer* 15, 397–408.
- Stojiljkovic MR, Ain Q, Bondeva T, Heller R, Schmeer C & Witte OW (2019) Phenotypic and functional differences between senescent and aged murine microglia. *Neurobiol. Aging* 74, 56–69.
- Tanaka H, Yamashita T, Asada M, Mizutani S, Yoshikawa H & Tohyama M (2002) Cytoplasmic p21(Cip1/WAF1) regulates neurite remodeling by inhibiting Rho-kinase activity. *J. Cell Biol.* 158, 321–329.
- Tollervey JR, Curk T, Rogelj B, Briese M, Cereda M, Kayikci M, König J, Hortobágyi T, Nishimura AL, Zupunski V, Patani R, Chandran S, Rot G, Zupan B, Shaw CE & Ule J (2011) Characterizing the RNA targets and position-dependent splicing regulation by TDP-43. *Nat. Neurosci.* 14, 452–458.
- Torres P, Ramírez-Núñez O, Romero-Guevara R, Barés G, Granado-Serrano AB, Ayala V, Boada J, Fontdevila L, Povedano M, Sanchís D, Pamplona R, Ferrer I & Portero-Otín M (2018) Cryptic exon splicing function of TARDBP interacts with autophagy in nervous tissue. *Autophagy* 14, 1398–1403.

Trias E, Beilby PR, Kovacs M, Ibarburu S, Varela V, Barreto-Núñez R, Bradford SC, Beckman JS & Barbeito L (2019) Emergence of microglia bearing senescence markers during paralysis progression in a rat model of inherited ALS. *Front. Aging Neurosci.* 11, 42.

Xie Y, Zhou B, Lin M-Y & Sheng Z-H (2015) Progressive endolysosomal deficits impair autophagic clearance beginning at early asymptomatic stages in fALS mice. *Autophagy* 11, 1934–1936.

## Figure Legends

**Figure 1.** Increase in senescence markers in spinal cord during ALS progression. *p16* expression was progressively higher at 120 days and 150 days (a), whereas *p21* were only found to be increased at end stage (b). Both *p16* and *p21* exhibited cytoplasmic staining (c). Nissl+ cells of the ventral horn of the spinal cord (compatible with motor neurons) are the main contributor to SA-beta-gal activity in lumbar spinal cord and are almost depleted in this activity in hSOD1-G93A mice at 150 days, similarly to Nissl- (glia) cells (d). *p16* and *p21* expression are expressed as mean  $\pm$ SEM. Ns indicates  $p > 0.05$ ; \*\* $p < 0.01$ ; \*\*\* $p < 0.001$ ; \*\*\*\* $p < 0.0001$  for Student's t test or ANOVA, when appropriate. Red arrows indicate *p16* and *p21* positive cells. Green scale bar represents 100  $\mu$ m, yellow scale bar represents 500  $\mu$ m, and red scale bar represents 2500  $\mu$ m.

**Figure 2.** Cytoplasmic *p16*+ microglia (a) and astrocytes (b) are present in lumbar spinal cord of transgenic mice and absent in controls. Scale bar represents 500  $\mu$ m.

**Figure 3.** SASP markers and TDP-43 dysfunction are increased in LSC from transgenic hSOD-G93A mice. *Il1a* mRNA was higher from pre-symptomatic stage onward in transgenic mice and increased in later stages (a). *Il6* expression was more greatly induced in end-stage hSOD1-G93A mice (b). Cryptic exon in *Adipor2* mRNA was more incorporated in 150-day-old transgenic mice (d). *Il1a*, *Il6*, *Irfn*, and cryptic *Adipor2* expression are expressed as mean  $\pm$ SEM. The inclusion ratio of *Adipor2* cryptic exon

positively correlated with *p16* expression (e). ns  $p > 0.05$ ; \* $p < 0.05$ ; \*\*\* $p < 0.001$ ; \*\*\*\* $p < 0.0001$ .

**Figure 4.** *Adipor2* cryptic exon splicing is increased in *Tardbp* silenced cells. RT-qPCR of *Adipor2* cryptic exon showed a high increase (a) and Western Blot analyses of TDP-43 confirmed the reduction of this protein in silenced 3T3 cells (b). \* $p < 0.05$ .

**Figure 5.** Senolytic treatment using Navitoclax does not slow the disease progression. A chronic treatment was established with five consecutive doses followed by two weeks of resting (a). Weight loss was not different between Navitoclax and vehicle experimental groups (b). Survival time was also unaltered between groups (c), as senescence and SASP genes (d).

**Figure S1.** SA-beta-gal activity was decreased in 90- and 120-day-old hSOD1-G93A mice. Nissl+ cells are the main contributors of this activity, which is lower in ALS mice. In contrast, Nissl- cells exhibited a slight decrease in transgenic mice. \*\*\* $p < 0.001$ ; \*\*\*\* $p < 0.0001$ . Yellow scale bar represents 500  $\mu\text{m}$  and red scale bar represents 2500  $\mu\text{m}$ .

**Table 1.** SYBR Green probes used in RT-qPCR analysis.

Figure S1

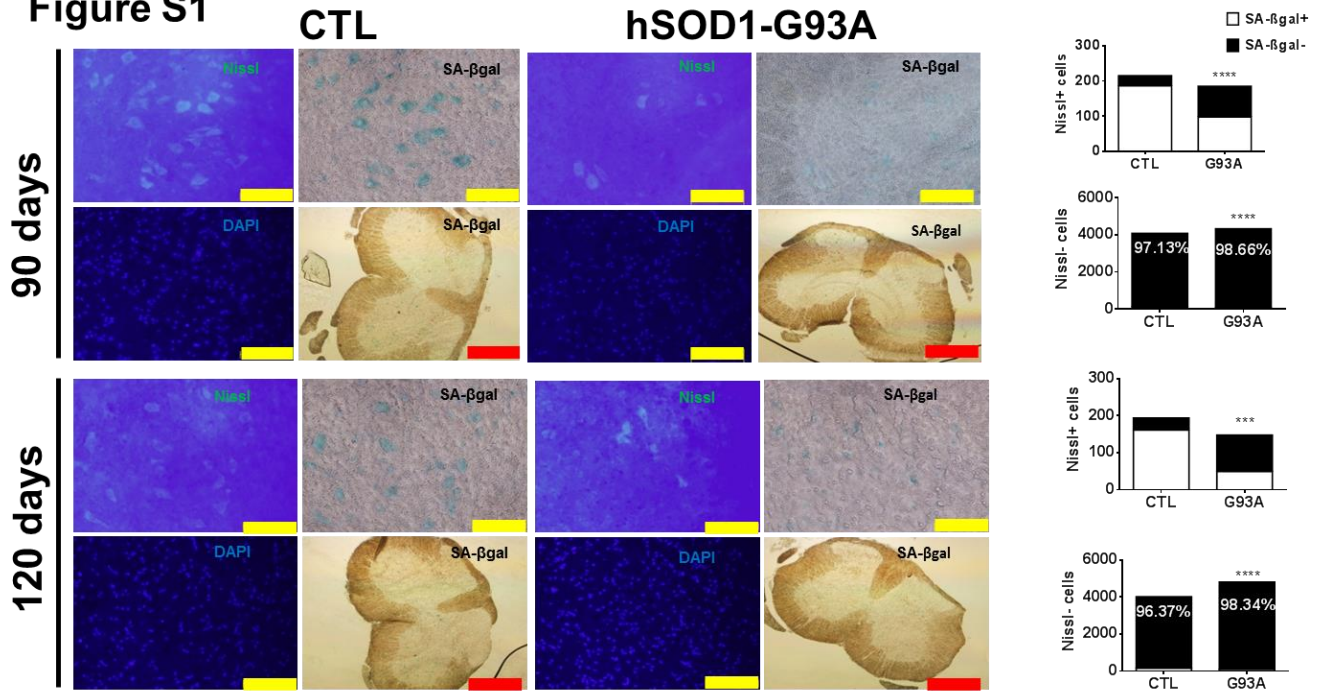


**Table 1.**

<b>Gene</b>	<b>Sequence</b>
<i>Actb</i> Fwd	GTGACGTTGACATCCGTAAAGA
<i>Actb</i> Rev	GCCGGACTCATCGTACTCC
<i>p16</i> Fwd	CCCAACGCCCCGA ACT
<i>p16</i> Rev	GCAGAAGAGCTGCTACGTGAA
<i>Il1a</i> Fwd	AGCGCTCAAGGAGAAGACC
<i>Il1a</i> Rev	CCAGAAGAAAATGAGGTCGG
<i>Il6</i> Fwd	ACCAGAGGAAATTTCAATAGGC
<i>Il6</i> Rev	TGATGCACTTGCAGAAAACA
<i>Ifna</i> Fwd	ATGGCTAGGCTCAGCACTTTC
<i>Ifna</i> Rev	CTCACTCAGACTTGCCAGCA
<i>Ifnb</i> Fwd	AGCTCCAAGAAAGGACGAACA
<i>Ifnb</i> Rev	GCCCTGTAGGTGAGGTTGAT
<i>Adipor2</i> Fwd	TGTTTGTAAGGTGTGGGAAGG
<i>Adipor2</i> Rev	GTTGCCCGTCTCTGTGTGTAT
<i>Adipor2</i> cryptic Fwd	AGAAGTGGAGTTACAATTGTG
<i>Adipor2</i> cryptic Rev	AAACAAACTCTTCCATTCGTT
<i>p21</i> Fwd	TTGCCAGCAGAATAAAAGGTG
<i>p21</i> Rev	TTTGCTCCTGTGCGGAAC





## **5.6 Article 6**

**Title:** TDP-43 and metabolipidomic biomarkers in circulating cells for ALS diagnosis and prognosis: a preliminary study.

**Authors:** Pascual Torres, Irene Pradas, Mònica Povedano, Raúl Domínguez, Mariona Jové, Victòria Ayala, Isidre Ferrer, Reinald Pamplona, Manuel Portero-Otin.

**Not Published**

# **TDP-43 and metabolomic biomarkers in circulating cells for ALS diagnosis and prognosis: a preliminary study.**

Pascual Torres <sup>a, 1</sup>, Irene Pradas <sup>a</sup>, Mònica Povedano <sup>b</sup>, Raul Dominguez <sup>b</sup>, Mariona Jové <sup>a</sup>, Victòria Ayala <sup>a</sup>, Isidre Ferrer <sup>c,d</sup>, Reinald Pamplona <sup>a</sup>, Manuel Portero-Otin <sup>a,1</sup>

<sup>a</sup> Department of Experimental Medicine, IRBLleida-UdL, Lleida, Spain.

<sup>b</sup> Functional Unit of Amyotrophic Lateral Sclerosis (UFELA), Service of Neurology, Bellvitge University Hospital, Hospitalet de Llobregat, Spain

<sup>c</sup> Department of Pathology and Experimental Therapeutics, University of Barcelona, Hospitalet de Llobregat, Spain

<sup>d</sup> Biomedical Network Research Center on Neurodegenerative Diseases (CIBERNED), Institute Carlos III, Hospitalet de Llobregat, Spain

<sup>1</sup> To whom correspondence should be addressed at Metabolic Pathophysiology Research Group, IRBLleida-UdL, Avda Rovira Roure 80 25196 Lleida, Spain at [pascual.torres@udl.cat](mailto:pascual.torres@udl.cat) or [manuel.portero@udl.cat](mailto:manuel.portero@udl.cat)

## **ABSTRACT**

Amyotrophic lateral sclerosis is a progressive neurodegenerative disease with a fatal outcome. Further, ALS prognosis is variable between individuals, suggesting distinct pathological mechanisms in different groups of progression. In this study, we study the potential use of platelet metabolomics for ALS prognosis, also with an examination of TDP-43 dependent phenomena. We separated platelets from 15 ALS patients recently diagnosed and 21 from healthy individuals. Western blot analysis was performed to quantify TDP-43 expression in platelets. We also analyzed the occurrence of TDP-43 controlled cryptic exon levels in selected mRNAs in corresponding peripheral blood mononuclear cells (PBMCs) by RT-qPCR. Mass-spectrometry coupled to liquid chromatography was employed for metabolomic analyses in platelets. The results demonstrate that cryptic exons, normally present in central nervous tissue of ALS patients, do not appear in platelets or PBMCs of this group. TDP-43 expression was not altered in platelet fraction from ALS patients. Regarding metabolomic analyses, the concentration of several phospholipids differentiated platelets from ALS patients. Greater differences were present when examining prognosis, with several metabolites differentiating ALS patients with variate prognosis, based on ALSFR-R changes. All in all, these results support the potential existence of metabolomic prognostic biomarkers in platelets.

## INTRODUCTION

Amyotrophic Lateral Sclerosis (ALS) is the most common adult-onset motor neuron disease. This devastating disorder has a survival time of 2-3 years after the diagnosis. Clinical manifestation of the disease is heterogeneous, and the diagnosis can take a year to be definite. ALS diagnostic is based on the presence of progressive upper and lower motor neuron symptoms by clinical examination and the absence of other diseases by electrophysiology and neuroimaging evidence that could explain the symptoms (Brooks, Miller, Swash, & Munsat, 2000). Depending on the degree of clinical evidence we can classify the patients into three groups: clinically possible, clinically probable and clinically definite. An accurate diagnosis might take one year after the first symptom. Diagnostic delay is an important predictor of survival time (Ganesalingam et al., 2009). Moreover, only clinically definite ALS patients in the early stages are candidates for Edaravone treatment (Abe et al., 2017).

One of the features of ALS is the heterogeneity in disease progression. The ALS Functional Rating Scale-Revised (ALSFERS-R) is a validated instrument for monitoring the disability of ALS patients. It takes into account the degree of disability in executing several functions and symptoms, including speech, salivation, swallowing, handwriting, patients with gastrostomy and >50% daily nutrition intake via G-tube (Yes/No), cutting food and handling utensils, dressing and hygiene, turning in bed and adjusting bedclothes, walking, climbing stairs, dyspnea, orthopnea and respiratory insufficiency. Normal ability to do these tasks are scored by 4 points, and 0 points if the person is unable to do it (Cedarbaum et al., 1999). Moreover, the decline in ALSFERS-R score (measured by ALSFERS-R slope) is useful to estimate the disease progression and the efficacy of a given treatment in Randomised Clinical Trials (RCT) (Castrillo-Viguera, Grasso, Simpson, Shefner, & Cudkowicz, 2010).

According to a mathematical model, the main contributors to disease prognosis are the clinical onset and the diagnostic delay (the time between the first symptoms and the diagnostic). Using these two variables, ALS patients can be divided into five clusters with non-overlapping survival duration. Curiously, 1200 of the 1467 patients of this study are grouped into two groups, suggesting a more homogenous disease than expected (Ganesalingam et al., 2009). Similar results were obtained in a recent study with a larger cohort and a larger number of clinical and biochemical variables (Kueffner et al., 2019). Differences in ALS progression between patients can reflect different

disease mechanisms. Patients stratification in homogenous progressing groups could improve clinical trial design (Lambrechts, Robberecht, & Carmeliet, 2007). Thus, research of reliable biomarkers for ALS is critical to increase for earlier diagnosis and to avoid clinical trial heterogeneity which can hinder drug discovery.

Metabolomics is an interesting tool for biomarker research since it can detect a wide range of metabolites. Metabolism is altered in nervous and peripheral tissues (Bouteloup et al., 2009; Vandoorne, De Bock, & Van Den Bosch, 2018), suggesting a wider impact of the disease and the possibility to determine changes in blood. Plasma is the most frequently used biofluid to assess metabolomic analyses. This approach reported several metabolites as candidates for ALS biomarkers. However, plasma is highly influenced by diet and other external inputs. It interferes with the reproducibility of the experiments. Moreover, technical variability of the studies also hinders reproducibility (H. Blasco et al., 2016).

In this study, we used platelets and PBMCs to search for metabolomic and TDP-43 related biomarkers. Previous studies demonstrated the potential use of metabolomics for ALS biomarkers research in plasma and in CSF. In addition, other studies have postulated TDP-43 PBMCs expression and mislocalization as ALS diagnostic biomarkers. However, little is known about those biomarkers in platelets, that are highly enriched in mitochondria (Zharikov & Shiva, 2013). Our results suggest a potential use of metabolomic and fatty acids profile for predicting ALS prognosis and a limited use for ALS diagnosis. Future experiments are necessary for biomarker validation.

## **RESULTS**

Metabolomic changes in platelets from ALS (Table 1) and age-matched CTL individuals were assessed by non-targeted methods LC-MS. 295 metabolites were included in the analyses. A total of 3 metabolites were statistically significant ( $p < 0.05$ ) between ALS and CTL (Table 2). The possible identities were assessed by hmdb database search, and by  $m/z$  and retention time compatibility with internal standards representative of lipid family

We performed non-supervised analyses to obtain a better picture of global differences between ALS and CTL platelet metabolomic changes. Hierarchical clustering was performed to demonstrate that ALS and CTL group were not separated (Figure 1A).

Moreover, another non-supervised analysis (Principal Component Analysis, PCA) was assessed. Similar to hierarchical clustering, PCA was not able to differentiate samples from ALS and CTL based in metabolomic profile (Figure 1B).

Although the lack of general differences in metabolomic profile, we performed ROC analysis. We obtained four metabolites with an AUC > 0.7 discriminating ALS and CTL (Table 3). We found PE(p-38:3) (Figure 2A), and unknown molecules (Figure 2B), PI(34:0)/PI(36:3) (Figure 2C) and LysoSM(d18:0) (Figure 2D) as top molecules using this strategy. All in all, these results show that the changes associated with ALS are rather low in magnitude in platelets, in contrast to data in plasma (Lawton et al., 2014).

We further explored other strategies for diagnostic biomarker research. We also quantified TDP-43 platelet expression by Western Blot analysis. The results showed no statistically significant differences between ALS and CTL group (Figure 3A and 3B). We quantify cryptic exon splicing in PBMCs from ALS and CTL as possible reporter of TDP-43 loss of function, based on findings on central nervous system (Torres et al., 2018). *ATG4B* and *GPSM2* cryptic exons were below the detection levels in PBMCs (data not shown), probably due to the low expression of these genes in these cells (based on Ct values from RT-qPCR assay). *PFKP* a gene expressed in PBMCs and also showing cryptic exons potentially regulated cryptic exon inclusion was not different between ALS and CTL PBMCs. To further confirm the specificity of TDP-43 regulated cryptic exons, we also quantified *PFKP* cryptic exon inclusion in frontal cortex and spinal cord from ALS patients. These results confirmed the specific effect of TDP-43 dysfunction, that induced an ALS-associated gain *ATG4B* and *GPSM2* (Torres et al., 2018) of cryptic exon splicing but not of *PFKP*. Of note, *PFKP* was induced in TDP-43 silenced HeLa cells. Thus, *PFKP* cryptic exon inclusion was different between analysed tissue (Figure 3A).

We also investigated the potential use of the abovementioned measurements for prognostic biomarkers identification. Therefore, we classified ALS patients into two groups, those with slow progression (<0,5 ALSFR slope, n=7) and those with fast progression (>0,5 ALSFR slope, n=8). Interestingly, the number of the statistically significant metabolites (15) was higher than ALS vs CTL comparison (Table 3). This was confirmed in non-supervised analyses, with high discrimination in PCA (Figure 4A) and hierarchical clustering (Figure 4B).

ROC analyses for metabolomic prognostic biomarkers were also better than case-control ones. 13 metabolites resulted in  $AUC > 0.8$ . The four most significant are plotted in (Figure 5). In order to find correlated metabolites with disease progression, we analysed the correlation by Spearman rank between their peak intensity and ALSFR slope. We detected 10 metabolites significantly correlated with ALSFR slope (Figure 7).

## DISCUSSION

Several metabolomic studies have been performed with ALS patients. Plasma is an excellent source for biomarker research because it is accessible and easy to extract. However, plasma metabolites are highly variable between individuals and potential pre-analytical factors, such as sample preparation, diet, and physical activity strongly influence its composition (Stevens, Hoover, Wang, & Zanetti, 2019). Additionally, a lack of external biomarker validation, together with the use of different technology and analysis hinder the progression of plasma metabolomic-based ALS biomarkers (H. Blasco et al., 2016; Lanznaster, de Assis, Corcia, Pradat, & Blasco, 2018). In order to avoid the variability in plasma metabolomics studies in ALS, platelets could be a suitable source of biomarkers (Chacko et al., 2019). The advantages are lower inter-individual variability and high mitochondrial content. They are also interesting for our study because of the lack of the nuclear compartment. TDP-43 presence should necessarily be derived from non-nuclear compartments.

Regarding platelet metabolomic biomarkers, our results suggest a limited use for diagnosis. TTESTs show 3 statistically significant metabolites. Two of them are identified as phospholipids. Platelet phospholipids are important for its activation (Koseoglu et al., 2015). Interestingly, previous results from an independent group observed several phospholipids differentially expressed in ALS in CSF and mito-ER fraction from fibroblast (Hélène Blasco et al., 2010; Veyrat-Durebex et al., 2019). On the other hand, any of the 5 statistically significant metabolites did not show an  $AUC > 0.8$  in ROC analysis. Unsupervised analyses reveal a partially hierarchical clustering between ALS and CTL groups, suggesting global differences in the metabolomic profile. Nevertheless, PCA analyses does not suggest that differences. Another candidate as diagnostic biomarkers are those related to TDP-43 expression and function. TDP-43 higher expression and cytoplasmic mislocalization have been found in PBMCs and platelets from ALS patients (De Marco et al., 2011; Hishizawa,

Yamashita, Akizuki, Urushitani, & Takahashi, 2019; Luotti et al., 2020). However, TDP-43 cryptic splicing function repression has not been assessed in PBMCs. Our results indicate a preserved TDP-43 splicing function in ALS PBMCs for the examined mRNAs, together with normal TDP-43 levels ALS platelets. We hypothesise that possible TDP-43 disturbances in PBMCs are not enough to alter its function (Luotti et al., 2020). We cannot discard the cell type-specific cryptic exons and maybe cryptic exons in other genes that we have not detected are present. Anyway, we confirm a different PFKP cryptic regulation between tissues, being PBMCs the most permissive for *PFKP* cryptic splicing, probably due to high abundance of *PFKP* mRNA concentration (based on Ct values from RT-qPCR assay). Notably, cryptic exon splicing has also a region-specific regulation in nervous tissue. Spinal cord is more permissive for *PFKP* cryptic splicing than motor cortex. It suggests a higher vulnerability of spinal cord to cryptic splicing. Similarly to previous results in Alzheimer's Disease (Torres et al., 2020), PFKP cryptic splicing is sensitive to TDP-43 silencing but it is not associated with disease status.

The use of platelet metabolomic biomarkers seems more promising. In this case, hierarchical clustering using top 25 metabolites separates almost perfectly fast progressors from slow progressors. Nevertheless, PCA separation is not as clear as hierarchical clustering. In addition, 13 metabolites display a high AUC value in ROC curves. The most significant correlated with ALSFR slope and with a higher AUC value are phospholipids, reinforcing the role of this class of lipids in the disease.

The main limitation of this study is the sample size and the fact that all the patients are from the same region, Catalonia. This could hinder the reproducibility of the study to other regions and could not be representative of this heterogeneous disease. However, within this preliminary data, we encourage its validation in larger cohorts

In conclusion, our results suggest metabolomic and fatty acid content analysis as a suitable source for ALS prognostic biomarkers, with limited value in case-control approaches. Several metabolites and FAs are potentially useful for predicting functional decline. Patient stratification can boost clinical research in well-defined ALS groups.



## **MATERIAL AND METHODS**

### *Human samples*

The study followed the guidelines of the relevant Spanish legislation (Real Decreto 1716/2011) and enjoyed the approval of the Institutional Ethics Committee of the Bellvitge University Hospital. CSF and blood (plasma) were obtained from 15 ALS cases in the Bellvitge University Hospital, Barcelona and Hospital Universitari Arnau de Vilanova de Lleida, Lleida between 2015 and 2016, and from 21 age-matched non-ALS individuals (controls). ALS cases were 9 women and 6 men (12 spinal, 2 bulbar and 1 respiratory) and age-matched controls (15 women and 6 men) (Table 1). Biological samples were obtained between 10 and 24 months after the beginning of symptoms, and ALS was diagnosed according to the El Escorial criteria for ALS. ALSFR was calculated and validated by two independent neurologists. Progression rate was calculated (at baseline or at last visit) as 48 minus the ALS Functional Rating Scale-Revised score, divided by the disease duration from onset of symptoms (Lu et al., 2015). We defined an ALSFR slope of 0.5 as the cutoff point for classifying progression rates as fast progressors (F) or slow progressors (S). Blood was obtained in the morning after overnight fasting.

### *Isolation of Peripheral Blood Mononuclear Cells and platelets*

Peripheral Blood Mononuclear Cells (PBMCs) and platelets were isolated from peripheral blood using Histopaque-1077 (10771, SIGMA). Briefly, 3 ml of Ficoll were added to the bottom of a centrifuge tube. Carefully, 3 ml of blood were layered onto Ficoll without mixing the phases. The tubes were centrifuged at 400g for 30 minutes at RT with the lowest acceleration and brake program. The upper phase was removed, and the opaque interphase was collected into a new tube. The interphase was washed with PBS and centrifuged at 300g. The supernatant contained the platelet fraction and the pellet PBMCs. PBMCs were washed with PBS and centrifuged at 300g. Platelets were centrifuged at 360g and the pellet was discarded. Supernatant was collected and centrifuged at 800g. The resulting pellet was washed with PBS and centrifuged at 800g to obtain the platelets. Both fractions were observed with an optical microscope to ensure that they were enriched in PBMCs or platelets.

### *Western blot analysis*

Protein from platelets was extracted adding 100  $\mu$ L of radioimmunoprecipitation (RIPA) buffer with Protease Inhibitor Cocktail (1X) to the pellet. After sonication, protein quantification was performed with Bradford assay (5000006, Bio-Rad). Fifteen  $\mu$ g of protein were loaded onto a 12% acrylamide SDS-PAGE gel. Membranes were blocked with I-Block (T2015, Thermo Fisher Scientific) for 1 hour and incubated overnight with anti-TDP-43 (Proteintech, 10782-2-AP) diluted 1:1000 in TBS-T 0.05%. After primary antibody incubation, membranes were washed 3 times with TBS-T 0.05% and incubated with secondary antibody for 1h. Immobilon™ Western Chemiluminiscent HRP Substrate (WBKLS0500, Merck Millipore) was used for immunodetection. Membranes were stained with Coomassie Brilliant Blue G (27815, Sigma) for normalization. Specific bands were quantified with ImageLab v5.2.1 (Bio-Rad).

#### *RNA extraction, cDNA synthesis, and quantitative RT-PCR (RT-qPCR)*

RNA was extracted from PBMCs using TRI Reagent (Thermo Fisher Scientific, AM9738) following the manufacturer's instructions. RNA concentrations were measured using a NanoDrop ND-1000 (Thermo Fisher Scientific). One microgram of RNA was used for retrotranscription employing TaqMan Reverse Transcription Reagent using random hexamers (Thermo Fisher Scientific, N8080234).

Cryptic exons were quantified as previously described (Torres et al., 2020, 2018). Briefly, RT-qPCR experiments were performed using a CFX96 instrument (Bio-Rad, Hercules, California, USA) with SYBR Select Master mix for CFX (Thermo Fisher Scientific, 4472937). Each 20  $\mu$ L of reaction contained 4 $\mu$ L cDNA, 10  $\mu$ L SYBR Select Master Mix, 0.2 nM of forward primer and 0.2 nM of reverse primer solutions and 4  $\mu$ L PCR grade water. RT-qPCR run protocol was as follows: 50 °C for 2 minutes and 95 °C for 2 minutes, with the 95 °C for 15 seconds and 60 °C for 1 minute steps repeated for 40 cycles; and a melting curve test from 65°C to 95 °C at a 0.1 °C/s measuring rate. Primers employed in these experiments are listed in Table 2. Cryptic exon inclusion or Percentage Spliced-In (PSI) was estimated using the following formula:  $100 \times 2^{-(\text{Conserved exon } Cq - \text{Cryptic exon } Cq)}$ .

#### *Metabolite extraction*

100  $\mu$ L of PBS and 300  $\mu$ L of ice-cold acetone were added to platelet pellet. Samples were vortex-mixed for 10 seconds and incubated 30 minutes at 4 °C. Samples were then centrifuge at 4 °C for 10 minutes at 1000 xg. Supernatant was separated into a

clean glass tube and evaporated in Speed Vac. 250  $\mu$ L of methanol and 500  $\mu$ L of chloroform were added together with standard mix. Samples were vortex-mixed for 10 seconds, 200  $\mu$ L of KCl 0.7% were added, vortex-mixed for 10 seconds and centrifuge at 4  $^{\circ}$ C for 10 minutes at 1000  $\times$ g. Upper and bottom phases were separated. Bottom phase contained chloroform soluble metabolites (lipids) and upper phase contained methanol soluble metabolites (employed for the metabolomic analysis).

### *Metabolomic analysis*

For the metabolomic study, an Agilent 1290 liquid chromatography system coupled to an ESI-Q-TOF MS/MS 6520 instrument (Agilent Technologies, Santa Clara, CA, US) was used. In all cases, 2  $\mu$ L of extracted sample was applied onto a reversed-phase column (Zorbax SB-Aq 1.8  $\mu$ m 2.1  $\times$  50 mm; Agilent Technologies) equipped with a precolumn (Zorbax-SB-C8 Rapid Resolution Cartridge 2.1  $\times$  30 mm 3.5  $\mu$ m; Agilent Technologies) with a column temperature of 60  $^{\circ}$ C. The flow rate was 0.6 mL/min. Solvent A was composed of water containing 0.2% acetic acid and solvent B was composed of methanol 0.2% acetic acid. The gradient started at 2% B and increased to 98% B in 13 min and held at 98% B for 6 min. Post-time was established in 5 min.

Data were collected in positive electrospray mode time of flight operated in full-scan mode at 100–3000 m/z in an extended dynamic range (2 GHz), using N<sub>2</sub> as the nebulizer gas (5 L/min, 350  $^{\circ}$ C). The capillary voltage was 3500 V with a scan rate of 1 scan/s. The ESI source used a separate nebulizer for the continuous, low-level (10 L/min) introduction of reference mass compounds: 121.050873, 922.009798 (positive ion mode) and 119.036320, 966.000725 (negative ion mode), which were used for continuous, online mass calibration. MassHunter Data Analysis Software (Agilent Technologies) was used to collect the results, and MassHunter Qualitative Analysis Software (Agilent Technologies) to obtain the molecular features of the samples, representing different, co-migrating ionic species of a given molecular entity using the Molecular Feature Extractor algorithm (Agilent Technologies), as described (Jove et al., 2015).

### *Data analysis*

All investigation was performed double-blinded. After decoding the data, molecular changes were extracted with MassHunter Qualitative Analysis (Agilent Technologies,

Barcelona, Spain), and the molecular profiles were obtained with MassHunter Profiler Professional (Agilent Technologies, Barcelona, Spain), as previously detailed (Servià et al., 2019). Molecules within a  $0.1\% \pm 0.25$  min retention time window and  $30\text{ppm} \pm 2\text{mDA}$  mass window were considered the same. Only common features (found in at least 50% of the samples of the same condition) were considered in order to minimize individual bias. Peak intensities were relativized by internal standard peak intensity. TTESTs (normalized by auto-scale option), Spearman correlations, multivariate analyses (principal component analyses (PCA) and hierarchical clustering) and ROC analyses were performed in Metaboanalyst.ca.

Molecules showing statistically significant expression (with p-value  $< 0.05$  in differential analyses) were annotated by comparing their exact mass and retention time, and isotopic distribution with the specific database (hmdb.ca) to obtain potential identities.

Western blot and RT-qPCR data were analyzed with GraphPad Prism. TTEST was employed for comparison.  $p < 0.05$  was used as the cutoff for significance.

## **ACKNOWLEDGEMENTS**

We acknowledge funding from the Spanish Ministry of Economy and Competitiveness, Institute of Health Carlos III (PI 17–00134) to MP-O; from the Spanish Ministry of Science, Innovation and Universities (RTI2018-099200-B-I00), and the Generalitat of Catalonia (Agency for Management of University and Research Grants (2017SGR696) and Department of Health (SLT002/16/00250)) to RP. PT is a predoctoral fellow from the Ministerio de Educacion (FPU16/01446). Support was also received in the form of a FUNDELA Grant, RedELA-Plataforma Investigación, and the Fundació Miquel Valls (Jack Van den Hoek donation). MJ is a professor under the Serra Hunter program (Generalitat de Catalunya). This study has been co-financed by FEDER funds from the European Union ("A way to build Europe"). IRBLleida is funded by a CERCA Programme/Generalitat of Catalonia.

## **REFERENCES**

Abe, K., Aoki, M., Tsuji, S., Itoyama, Y., Sobue, G., Togo, M., ... Yoshino, H. (2017). Safety and efficacy of edaravone in well defined patients with amyotrophic lateral

- sclerosis: a randomised, double-blind, placebo-controlled trial. *The Lancet Neurology*, 16(7), 505–512. [https://doi.org/10.1016/S1474-4422\(17\)30115-1](https://doi.org/10.1016/S1474-4422(17)30115-1)
- Blasco, H., Patin, F., Madji Hounoum, B., Gordon, P. H., Vourc'h, P., Andres, C. R., & Corcia, P. (2016, March 1). Metabolomics in amyotrophic lateral sclerosis: How far can it take us? *European Journal of Neurology*. Blackwell Publishing Ltd. <https://doi.org/10.1111/ene.12956>
- Blasco, H el ene, Corcia, P., Moreau, C., Veau, S., Fournier, C., Vourc'h, P., ... Andres, C. R. (2010). 1H-NMR-Based metabolomic profiling of CSF in early amyotrophic lateral sclerosis. *PLoS ONE*, 5(10). <https://doi.org/10.1371/journal.pone.0013223>
- Bouteloup, C., Desport, J. C., Clavelou, P., Guy, N., Derumeaux-Burel, H., Ferrier, A., & Couratier, P. (2009). Hypermetabolism in ALS patients: An early and persistent phenomenon. *Journal of Neurology*, 256(8), 1236–1242. <https://doi.org/10.1007/s00415-009-5100-z>
- Brooks, B. R., Miller, R. G., Swash, M., & Munsat, T. L. (2000). El Escorial revisited: Revised criteria for the diagnosis of amyotrophic lateral sclerosis. *Amyotrophic Lateral Sclerosis*, 1(5), 293–299. <https://doi.org/10.1080/146608200300079536>
- Castrillo-Viguera, C., Grasso, D. L., Simpson, E., Shefner, J., & Cudkowicz, M. E. (2010). Clinical significance in the change of decline in ALSFRS-R. *Amyotrophic Lateral Sclerosis*, 11(1–2), 178–180. <https://doi.org/10.3109/17482960903093710>
- Cedarbaum, J. M., Stambler, N., Malta, E., Fuller, C., Hilt, D., Thurmond, B., & Nakanishi, A. (1999). The ALSFRS-R: A revised ALS functional rating scale that incorporates assessments of respiratory function. *Journal of the Neurological Sciences*, 169(1–2), 13–21. [https://doi.org/10.1016/S0022-510X\(99\)00210-5](https://doi.org/10.1016/S0022-510X(99)00210-5)
- Chacko, B. K., Smith, M. R., Johnson, M. S., Benavides, G., Culp, M. L., Pilli, J., ... Darley-Usmar, V. M. (2019). Mitochondria in precision medicine; linking bioenergetics and metabolomics in platelets. *Redox Biology*, 22, 101165. <https://doi.org/10.1016/j.redox.2019.101165>
- De Marco, G., Lupino, E., Calvo, A., Moglia, C., Buccinn a, B., Grifoni, S., ... Chi d, A. (2011). Cytoplasmic accumulation of TDP-43 in circulating lymphomonocytes of ALS patients with and without TARDBP mutations. *Acta Neuropathologica*, 121(5), 611–622. <https://doi.org/10.1007/s00401-010-0786-7>
- Ganesalingam, J., Stahl, D., Wijesekera, L., Galtrey, C., Shaw, C. E., Leigh, P. N., & Al-Chalabi, A. (2009). Latent cluster analysis of ALS phenotypes identifies prognostically differing groups. *PLoS One*, 4(9), e7107. <https://doi.org/10.1371/journal.pone.0007107>
- Hishizawa, M., Yamashita, H., Akizuki, M., Urushitani, M., & Takahashi, R. (2019). TDP-43 levels are higher in platelets from patients with sporadic amyotrophic

- lateral sclerosis than in healthy controls. *Neurochemistry International*, 124, 41–45. <https://doi.org/10.1016/j.neuint.2018.12.009>
- Jove, M., Mauri-Capdevila, G., Suarez, I., Cambray, S., Sanahuja, J., Quilez, A., ... Purroy, F. (2015). Metabolomics predicts stroke recurrence after transient ischemic attack. *Neurology*, 84(1), 36–45. <https://doi.org/10.1212/WNL.0000000000001093>
- Koseoglu, S., Meyer, A. F., Kim, D., Meyer, B. M., Wang, Y., Dalluge, J. J., & Haynes, C. L. (2015). Analytical characterization of the role of phospholipids in platelet adhesion and secretion. *Analytical Chemistry*, 87(1), 413–421. <https://doi.org/10.1021/ac502293p>
- Kueffner, R., Zach, N., Bronfeld, M., Norel, R., Atassi, N., Balagurusamy, V., ... Stolovitzky, G. (2019). Stratification of amyotrophic lateral sclerosis patients: a crowdsourcing approach. *Scientific Reports*, 9(1), 690. <https://doi.org/10.1038/s41598-018-36873-4>
- Lambrechts, D., Robberecht, W., & Carmeliet, P. (2007, October). Heterogeneity in motoneuron disease. *Trends in Neurosciences*. <https://doi.org/10.1016/j.tins.2007.07.002>
- Lanznaster, D., de Assis, D. R., Corcia, P., Pradat, P. F., & Blasco, H. (2018). Metabolomics biomarkers: A strategy toward therapeutics improvement in ALS. *Frontiers in Neurology*. Frontiers Media S.A. <https://doi.org/10.3389/fneur.2018.01126>
- Lawton, K. A., Brown, M. V., Alexander, D., Li, Z., Wulff, J. E., Lawson, R., ... Berry, J. D. (2014). Plasma metabolomic biomarker panel to distinguish patients with amyotrophic lateral sclerosis from disease mimics. *Amyotrophic Lateral Sclerosis and Frontotemporal Degeneration*, 15(5–6), 362–370. <https://doi.org/10.3109/21678421.2014.908311>
- Lu, C. H., Macdonald-Wallis, C., Gray, E., Pearce, N., Petzold, A., Norgren, N., ... Malaspina, A. (2015). Neurofilament light chain: A prognostic biomarker in amyotrophic lateral sclerosis. *Neurology*, 84(22), 2247–2257. <https://doi.org/10.1212/WNL.0000000000001642>
- Luotti, S., Pasetto, L., Porcu, L., Torri, V., Elezgarai, S. R., Pantalone, S., ... Bonetto, V. (2020). Diagnostic and prognostic values of PBMC proteins in amyotrophic lateral sclerosis. *Neurobiology of Disease*, 139, 104815. <https://doi.org/10.1016/j.nbd.2020.104815>
- Servià, L., Jové, M., Sol, J., Pamplona, R., Badia, M., Montserrat, N., ... Trujillano, J. (2019, May 22). A prospective pilot study using metabolomics discloses specific fatty acid, catecholamine and tryptophan metabolic pathways as possible

- predictors for a negative outcome after severe trauma. *Scandinavian Journal of Trauma, Resuscitation and Emergency Medicine*. BioMed Central Ltd. <https://doi.org/10.1186/s13049-019-0631-5>
- Stevens, V. L., Hoover, E., Wang, Y., & Zanetti, K. A. (2019). Pre-analytical factors that affect metabolite stability in human urine, plasma, and serum: A review. *Metabolites*. MDPI AG. <https://doi.org/10.3390/metabo9080156>
- Torres, P., Andrés-Benito, P., Fernández-Bernal, A., Ricart, M., Ayala, V., Pamplona, R., ... Portero-Otin, M. (2020). Selected cryptic exons accumulate in hippocampal cell nuclei in Alzheimer's disease with and without associated TDP-43 proteinopathy. *Brain : A Journal of Neurology*, *143*(3), e20. <https://doi.org/10.1093/brain/awaa013>
- Torres, P., Ramírez-Núñez, O., Romero-Guevara, R., Barés, G., Granado-Serrano, A. B., Ayala, V., ... Portero-Otín, M. (2018). Cryptic exon splicing function of TARDBP interacts with autophagy in nervous tissue. *Autophagy*, *14*(8), 1398–1403. <https://doi.org/10.1080/15548627.2018.1474311>
- Vandoorne, T., De Bock, K., & Van Den Bosch, L. (2018, April 1). Energy metabolism in ALS: an underappreciated opportunity? *Acta Neuropathologica*. Springer Verlag. <https://doi.org/10.1007/s00401-018-1835-x>
- Veyrat-Durebex, C., Bris, C., Codron, P., Bocca, C., Chupin, S., Corcia, P., ... Blasco, H. (2019). Metabo-lipidomics of Fibroblasts and Mitochondrial-Endoplasmic Reticulum Extracts from ALS Patients Shows Alterations in Purine, Pyrimidine, Energetic, and Phospholipid Metabolisms. *Molecular Neurobiology*, *56*(8), 5780–5791. <https://doi.org/10.1007/s12035-019-1484-7>
- Zharikov, S., & Shiva, S. (2013). Platelet mitochondrial function: From regulation of thrombosis to biomarker of disease. In *Biochemical Society Transactions* (Vol. 41, pp. 118–123). Biochem Soc Trans. <https://doi.org/10.1042/BST20120327>

## FIGURE LEGENDS

**Figure 1.** Multivariate analyses of platelet metabolome for ALS and CTL comparison. PCA analysis show a limited effect of metabolomic data for disease status prediction (A), although hierarchal clustering analyses of 25 top differential metabolites highlights a partial discrimination (B).

**Figure 2.** ROC analyses of significant platelet metabolites for ALS diagnostic. Possible Identities of PI(34:0)/PI(36:3) for (A), lysoSM(d18:0)/Vitamin K 1,2,3-epoxide (B) and unknown for (C) and (D).

**Figure 3.** TDP-43 biomarkers in PBMCs and platelets. TDP-43 expression in platelets is not different between CTL and ALS (A and B). RT-qPCR of PFKP cryptic exon inclusion in PBMCs, spinal cord and motor cortex reveals differences between tissue but not between disease status. However, PFKP cryptic exon inclusion was induced in TARDBP silenced HeLa cells (C). \*\*\*\* $p < 0.0001$ , \*\* $p < 0.01$ .

**Figure 4.** Multivariate analyses for ALS prognostic. PCA analysis does not discriminate progressor groups (A), whereas hierarchal clustering analyses of 25 top differential metabolites grouped almost all sample according disease progression (B).

**Figure 5.** ROC analyses of top 4 statistically significant metabolites for fast and slow progressors discrimination. PC(38:3)/PE-NMe(40:3)/PC(O-38:5)/PE(P-38:4)/PA(42:0)/SM(d39:1) are the potential identities for (A), unknown (B) PE-NMe(42:7)/PC(40:7)/PA(46:7)/PS(38:3) for (C), DG(28:2)/LysoPC(20:2) for (D).

**Figure 6.** Spearman's rank correlation analyses of platelet metabolome and ALSFR slope. Potential identities DG(28:2)/PA(26:0)/LysoPC(20:2) for the most correlated, PC(38:3)/PE-NMe(40:3)/PE(38:4) for the second, PE-NMe(42:7)/PC(40:7)/PA(46:7)/PS(38:3) for the third, Sulforaphane-glutathione/Epicatechin 4'-glucuronide/Catechin 5-glucuronide/Catechin 4'-glucuronide for the fourth, Unknown for the fifth, TG(56:8) for the sixth, PC(38:3)/PE-NMe(40:1)/PE(38:4) for the seventh, TG(62:14) for the eighth, PE(42:0)/SM(42:1)/PC(38:2)/PE-NMe(40:1) for the ninth and Vitamin E for the tenth. \*\* $p < 0.01$ , \* $p < 0.05$ .

**Table 1.** Clinical characteristics of ALS cases.

**Table 2.** Metabolites differentially expressed in platelets in control (CTL) and amyotrophic lateral sclerosis (ALS) cases.

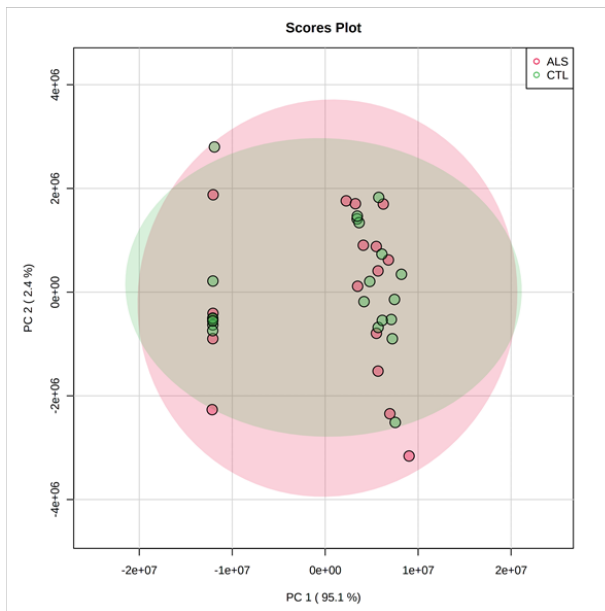
**Table 3.** Metabolites differentially expressed in platelets in Fast Progressors (F) and Slow Progressors (S).



# FIGURES AND TABLES

Figure 1.

**A**



**B**

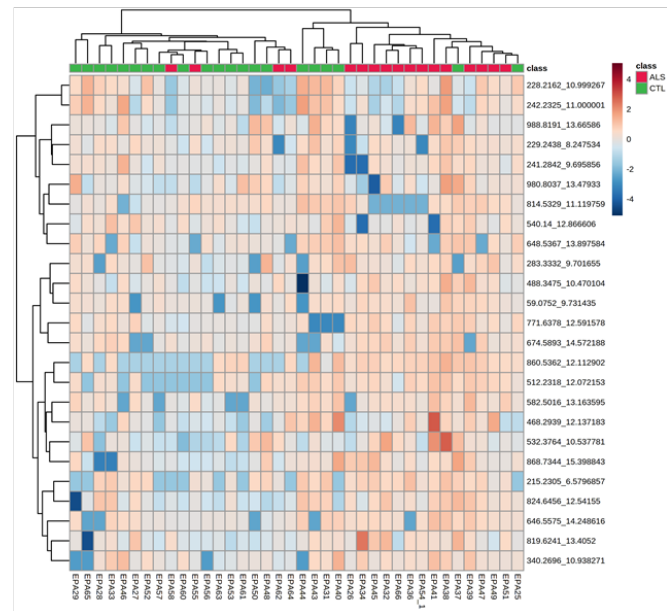


Figure 2.

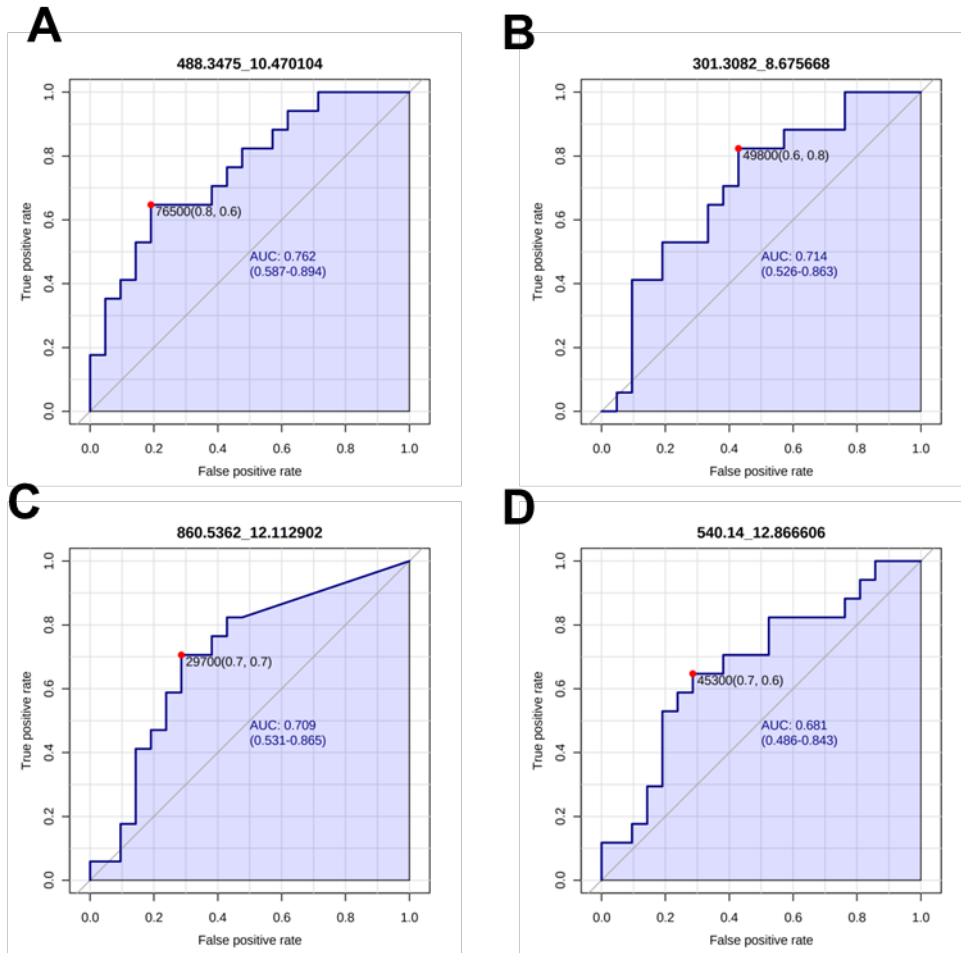


Figure 3.

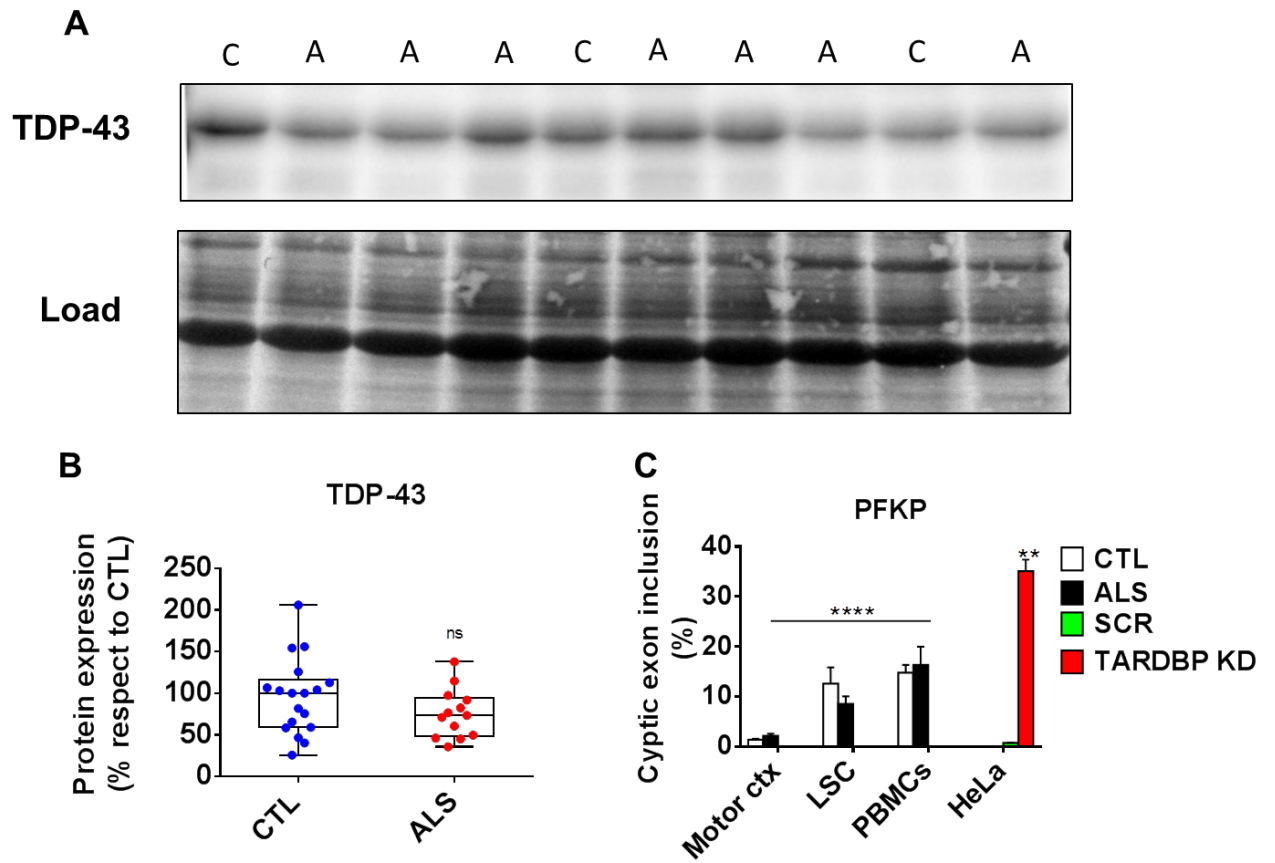




Figure 5.

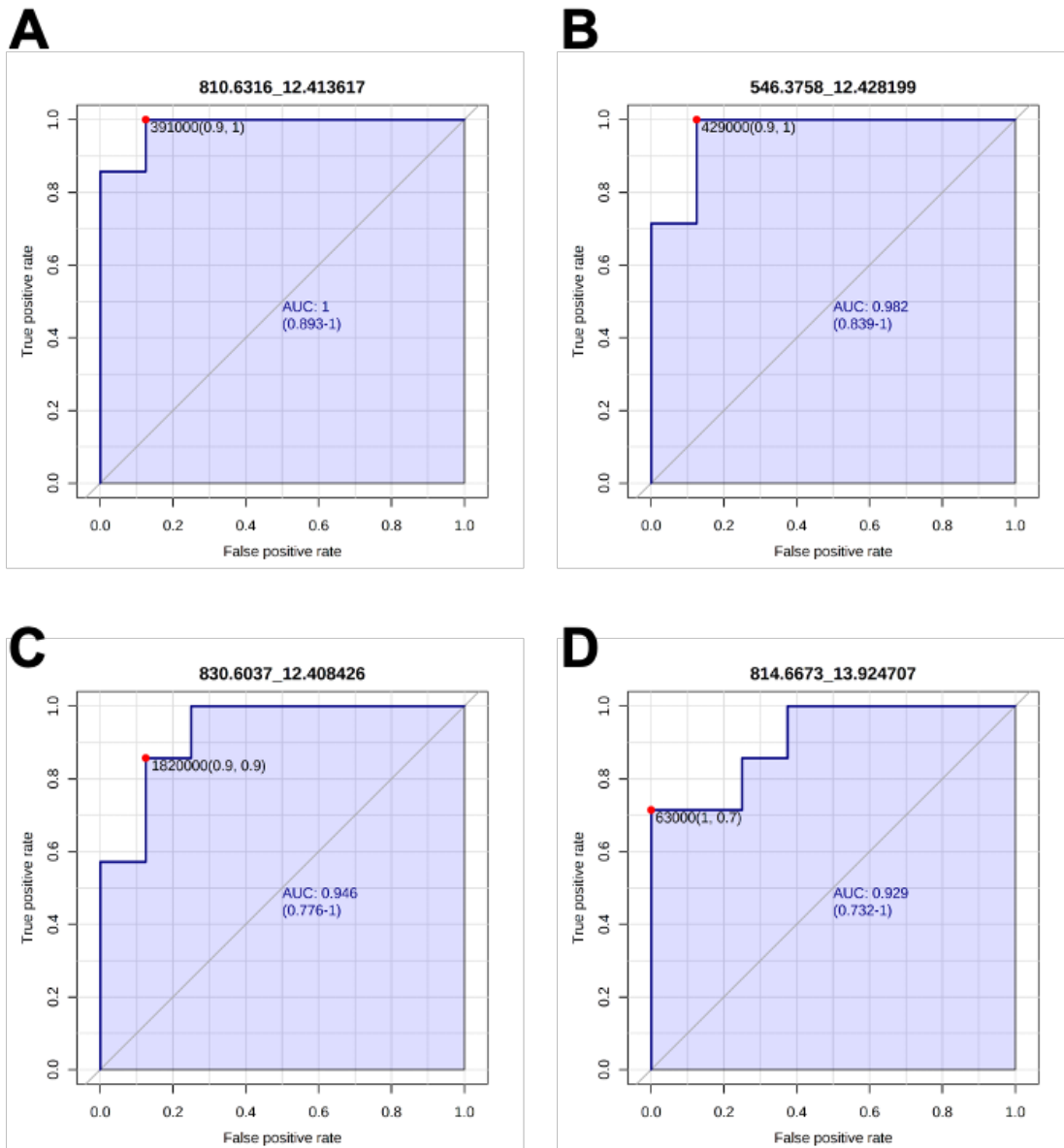
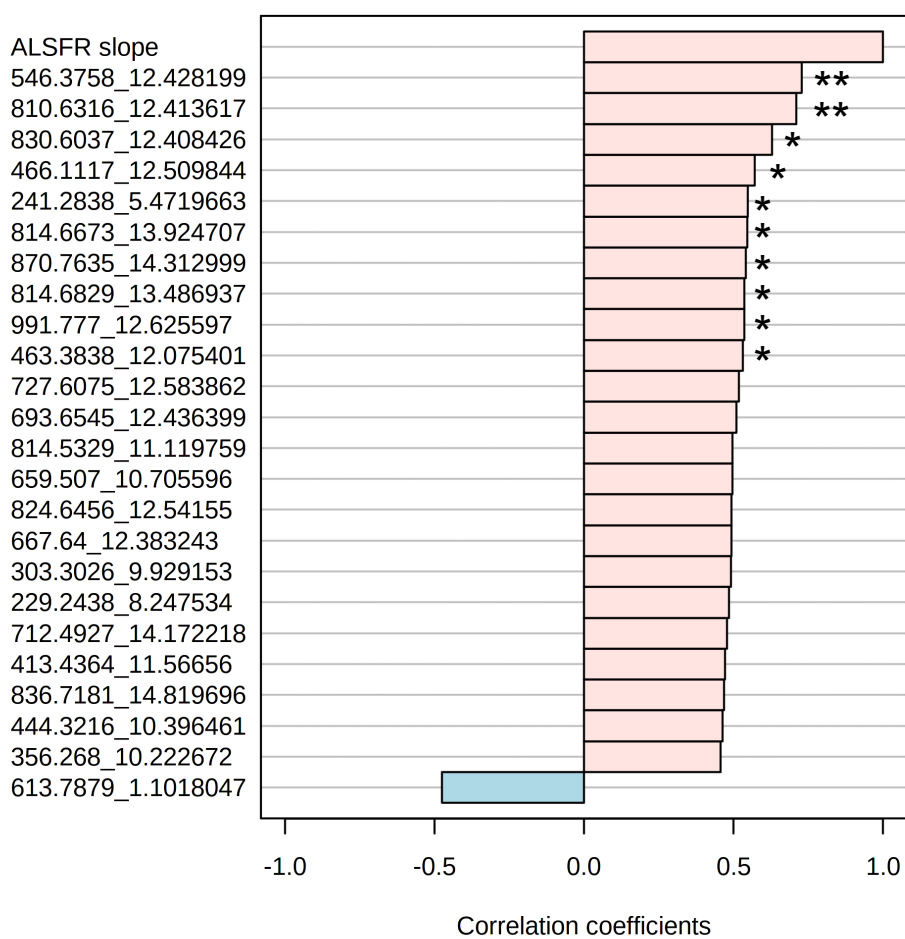


Figure 6.

Top 25 peaks(mz/rt) correlated with the ALSFR slope



**Table 1.**

Age at diagnosis (years)	60 ± 13
Gender	
Male	6
Female	9
Rate of progression (number of individuals)	
Fast progressors	8
Slow progressors	7
Onset type (number of individuals)	
Bulbar	2
Respiratory	1
Spinal	12

**Table 2.**

<b>ID 1</b>	<b>ID 2</b>	<b>ID 3</b>	<b>ALS vs CTL</b>	<b>p.value</b>	<b>-log10(p)</b>	<b>m/z@Retention Time</b>
PI(34:0)	PI(36:3)		up	0,026112	1,5832	860.5362@12.112902
PE-Nme(40:10)	PG(36:1)	PS(37:4)	up	0,042272	1,3739	814.5329@11.119759
Unknown			up	0,043974	1,3568	229.2438@8.247534



**Table 3.**

ID1	ID2	ID3	ID3	ID4	ID5	Fast vs Slow	p.value	-log10(p)	m/z@Retention Time
PC(38:3)	PE-NMe(40:3)	PC(O-38:5)	PE(P-38:4)	PA(42:0)	SM(d39:1)	up	0,003407	2,468	810.6316@1 2.413617
Unknown						up	8,92E-03	2,050	303.3026@9. 929153
Unknown						down	0,014973	1,825	613.7879@1. 1018047
Unknown						up	0,026437	1,578	571.4512@1 0.596755
Unknown						up	0,026554	1,576	991.777@12. 625597
Unknown						up	0,029159	1,535	622.5333@1 3.481535
Unknown						down	0,029457	1,531	1245.065@1 5.861232
Vitamin K1	trihydroxyvitamin D3					up	0,032839	1,484	449.3689@1 2.0759535
11beta-Hydroxytestosterone						down	0,033285	1,478	342.159@9.6 52441
DG(40:10)	PE-NMe2(29:0)	PE-NMe(30:0)	PE(31:0)	PC(28:0)	PA(33:1)	up	0,040465	1,393	659.507@10. 705596
PE-NMe(42:7)	PC(40:7)	PA(46:7)	PS(38:3)			up	0,041968	1,377	830.6037@1 2.408426
Unknown						up	0,04314	1,365	918.7538@1 5.182341
PS(DiMe(13,5)/MonoMe(9,5))	PE-NMe2(44:9)					up	0,04485	1,348	891.5647@1 0.987424
PC(20:0/P-18:0)	PC(O-18:1(9Z)/20:0)					up	0,048477	1,315	818.6945@1 4.304245
SM(d36:2)	Galactosylceramide (d36:1)	Ubiquinol 8	PC(O-34:1)	PC(16:0/P-18:0)		up	0,049474	1,306	727.6075@1 2.583862

## **6 DISCUSSION**

## Discussion

The works presented here attempt to fill the gap of two relevant issues in ALS research: new biomarkers and potential therapeutic approaches. ALS is a multifactorial disease, so we decided to analyze two important pathophysiological relevant processes: neuroinflammation and TDP-43 loss of function. We also tried to shed light on their association and with aging and age-related mechanisms. Moreover, we propose novel molecules and therapeutic approaches to target these pathological mechanisms. Finally, we have introduced a new metabolipidomic approach based on the analysis of platelets as a potential source of diagnostic and prognostic biomarkers.

Previous work in our lab was focused on the role of the nucleocytoplasmic equilibrium of TDP-43 in ALS and surrogate models. In the first year of this thesis, a relevant paper discovered a new set of splicing events of non-conserved (cryptic) exons that were not annotated as exons until then (J. P. Ling et al., 2015). These cryptic exons show UG rich sequences near 5' ss and/or 3' ss. These UG repeats were proposed as consensus for TDP-43 binding. Aimed by this exciting discovery, we tried to reproduce their results in other CNS locations to further explore the possible consequences of cryptic exon splicing on specific genes (*ATG4B* and *GPSM2*). In this report, the authors included one frontal cortex from an ALS donor, so we decided to analyze a larger ALS cohort, in a quantitative manner. Although their results comprising RT-PCR experiments, revealed a high number of unspecific amplified bands, we obtained a unique specific band using a different retrotranscription approach. These results demonstrated the presence of *ATG4B* and *GPSM2* cryptic exon in spinal cord and motor cortex only in ALS patients. We also observed a different expression between individuals, suggesting a different impact on the disease

In order to quantify the impact of this disease mechanism, we set up a quantitative RT-qPCR based on SYBR Green assay for measuring *ATG4B* and *GPSM2* cryptic exon splicing. We used specific primers annealing cryptic exon and constitutive exon to determine the percentage of splice-in (PSI) of cryptic exon inclusion in total *ATG4B* or *GPSM2* mRNA, thus improving a simple PCR as presented previously (J. P. Ling et al., 2015). Moreover, we also quantified cryptic exons in brainstem and occipital cortex and stratify the samples by clinical onset (bulbar or spinal ALS). Our results confirmed a correlation between the site of onset and the cryptic exon PSI. Bulbar ALS samples contained a higher PSI in brainstem, whereas spinal ALS had a higher PSI in spinal cord and frontal cortex. Interestingly, few samples displayed the highest cryptic exon PSI in occipital cortex, where TDP-43 pathology has not been detected. We hypothesize that TDP-43 loss of function is partially independent of aggregation and by using this method, we can detect early events in the disease before neuron loss. Another interesting result is the high AUC values in ROC analyses of *ATG4B* and *GPSM2* cryptic exon in CNS, suggesting the potential use of PSI as biomarkers. Furthermore, *ATG4B* cryptic exon PSI is correlated with disease duration and aging, suggesting a role in the progression. *ATG4B* cryptic exon PSI is ranged between 0-1% and 0-4% for *GPSM2* cryptic exon PSI. We associate these relatively low values with a) a very specific event in diseased motor neurons

## Discussion

and b) a high NMD elimination cryptic exons. The samples in the first paper are obtained post-mortem at the very end-stage of the disease. Therefore, few motor neurons are still in the tissue. TDP-43 is exported from the nucleus at the initial phase of neurodegeneration (Nana et al., 2019), suggesting a rise of cryptic exon during the disease. In line with this, *Adipor2* cryptic exon PSI just increase at the end-stage in the G93A mice, indicating that, at least in mice, TDP-43 dysfunction can be compensated by other mechanisms. Of note, TDP-43 loss of function in mice seems to affect non-autophagy targets, supporting the species specificity of TDP-43 function in central nervous system. For that reason, we also explored circulating cells from patients with ALS. Platelets are enriched in mitochondria and lack of nucleoplasm (Zharikov & Shiva, 2013), so TDP-43 in platelet is derived from nuclear export. This is the reason to use this fraction to analyze TDP-43 expression. *ATG4B* and *GPSM2* cryptic exons are not detected in PBMCs. *PFKP* cryptic exon PSI is higher in PBMCs than nervous tissue. However, no significant differences are detected in any tissue between ALS and control samples. This reflects a variability of cryptic splicing rate between tissue in humans. We did not observe differences in TDP-43 expression in platelets of ALS and control donors. Our results indicate a limited impact of TDP-43 pathology in blood cells in evaluated targets.

In order to understand the impact of cryptic exons in a controlled-manner, we performed TDP-43 gene silencing in HeLa cells. It results in a 30-50% of PSI and downregulation of the *ATG4B* protein by 50%. Moreover, autophagy was altered in TDP-43 knock-down HeLa and cortical primary neuron cells being rescued by *ATG4B* overexpression. Interestingly, *ATG4B* protein expression is highly associated with TDP-43 expression in several tissues. We concluded that TDP-43 regulates *ATG4B* expression, hence regulating autophagy (Kuang et al., 2012). Therefore, *ATG4B* expression is a candidate to restore autophagy function in ALS.

These results were amplified by evaluating the potential of cryptic exon splicing in another TDP-43 pathology (AD-LATE) and whether the G93A-SOD1 mice also display cryptic exon pathology. In 2019 a new classification of previously diagnosed AD patients was proposed (Nelson et al., 2019). They pinpointed to TDP-43 pathology as the pathological hallmark in the limbic system (especially in the hippocampus) for the staging of this new disease. We performed our cryptic exon RT-qPCRs in the hippocampus from AD disease with and without TDP-43 pathology. Moreover, we wanted to test the hypothesis of a strong NMD in cryptic exon. For this purpose, we purified the nuclear fraction from the tissue to compare it with the total homogenate. As NMD takes place in the cytosol we expected a high cryptic exon PSI in nuclei. We also introduced a new cryptic exon in the analysis, Platelet Phosphofructokinase (PFKP). This protein catalyzes an irreversible step of glycolysis. Energetic metabolism disturbances are frequently described in ALS (Vandoorne et al., 2018). Our results indicated that some of the AD patients without TDP-43 pathology exhibited cryptic exons. Moreover, those patients with cryptic exons coincide with advanced AD pathology (IV and V Braak Stage). These results support our hypothesis of TDP-43 loss of function could be dissociated from

## *Discussion*

aggregation, similarly to our finding in the occipital cortex from ALS samples. We also confirmed a high NMD effect, especially for *ATG4B* mRNA which nuclear fraction contained a 5-fold increase of cryptic exon PSI respect to the total homogenate. Curiously, even accounting the high sensitivity of *PFKP* cryptic exon PSI in TDP-43 knock-down HeLa cells, cryptic exon PSI was similar between control and AD samples. This result highlights the importance of experimental data in the validation of potential TDP-43 targets in the disease. In the same work, we found an association of cryptic exon expression with GPM2 protein decay, suggesting that different disease mechanisms may occur in those patients. Finally, we tried to set up a fluorescence-based method to study cryptic splicing activity. We engineered a Red Fluorescent Protein (RFP) containing mRNA divided into two exons and a cryptic exon in the middle of them. If the cryptic exon would be spliced, it could introduce a PTC avoiding the generation of red fluorescence. We failed in increasing cryptic exon PSI in a TDP-43 knock-down model. In this case, cryptic exon incorporated at the same rate (1-4%) in TDP-43 KD and control cells. We hypothesized that other sequences that we did not include in this plasmid (we just include TDP-43 UG binding elements of *ATG4B* cryptic exon) are necessary to enhance the splicing.



## *Discussion*

It is well accepted that age is a relevant risk factor for ALS (Al-Chalabi & Hardiman, 2013). Accounting the relationship between polyunsaturated fatty acids and ALS (Cacabelos et al., 2014), we continued the experiments of the DHA supplementation in G93A-SOD1 mice. DHA is the precursor of resolvins and was found depleted in the spinal cord from ALS donors (Ilieva et al., 2007). Moreover, DHA synthesis is regulated by cell stress. Previous results in our laboratory revealed that TDP-43 aggregation is associated with a downregulation of the DHA enzymatic pathway (Cacabelos, Ayala, et al., 2016). Both TDP-43 loss of function, and G93A-SOD1 overexpression (as shown below) can also trigger the transcription of inflammatory genes (L.-S. Wu et al., 2019). Dietary intervention can be a cost-effective therapy for ALS patients and G93A-SOD1 mouse can be used as a pre-clinical model. Other studies highlighted the importance of the diet and the maintenance of a BMI > 18.5 (Barone et al., 2019; Traxinger et al., 2013; Wills et al., 2014), avoiding hypermetabolism. DHA is an n-3 PUFA enriched in fish oil. DHA has been associated with multiple roles in CNS homeostasis and their products are critical for the resolution of the inflammatory process (Calder, 2015). For that reason, we fed G93A-SOD1 mice with three different isocaloric diets, a regular chow diet, a low n-3 PUFAs diet and a low n-3 PUFAs diet supplemented with DHA, following previously reports for modulation of AD in an experimental model (Calon et al., 2004). This experimental design allowed us to discriminate the specific effect of DHA. We introduced the diet at 30 days old. Our results indicate that we can increase the DHA content in the spinal within a dietary intervention. The incorporation of the DHA is negatively correlated with the ARA content, a n-6 PUFA with proinflammatory role. As a consequence, Anti-inflammatory Index (AI) in the spinal cord is increased in DHA supplemented mice. However, a relevant decrease in DHA spinal cord content is observed at the end-stage. We speculate with a lower dietary intake plus the consumption for fighting the inflammation, as observed in humans (Ilieva et al., 2007). We also quantified the protein oxidative damage in the spinal cord. Protein oxidation does not follow a pattern and we cannot conclude whether DHA prevents or enhances oxidation in this ALS mouse model.

Phenotypically, DHA supplementation enhances motor functions, delay weight loss and extend the survival time in male G93A-SOD1 mice but not in females. Sexual dimorphism is well known both in ALS patients and in animal models (Al-Chalabi & Hardiman, 2013). That may be one of the reasons why some studies are performed only with male mice to avoid variability in the experiment. Whatever the case, we are interested in sexual dimorphism since it has deep implications in FA metabolism (Cacabelos, Ramírez-Núñez, et al., 2016). Previous evidences demonstrated a general resilience of female mice to dietary restriction intervention (Kane, Sinclair, Mitchell, & Mitchell, 2018). Surprisingly, EPA (an n-3 PUFA with similar function of DHA) supplementation has the opposite effect in this mouse model (Yip et al., 2013), suggesting a critical role of specific n-3 PUFA in disease progression. Taken together, this work could suggest the basis to perform a clinical trial with DHA supplementation in ALS patients. Nevertheless, this work has some limitations that should be considered for its translation to the clinic. It is a mouse model of fALS and maybe the disease

## Discussion

mechanisms can be different. Moreover, the introduction of the diet is at pre-symptomatic stage and not at disease onset. It can be closer to diet habits (before the diagnostic) and can explain the protective role of fish intake observed in an epidemiologic study (Filippini et al., 2020). Further, an adequate profiling of ALS individuals could be useful, as we have shown that prognosis could be associated with relevant changes in FA contents in platelets,

In the same line of neuroinflammation and ageing, we wonder whether it can be related to cellular senescence and SASP, since recently published data support this theory in AD and PD mouse models (Chinta et al., 2018; Musi et al., 2018; P. Zhang et al., 2019). Senescence is a cell state that can be achieved through physiological aging (molecular damage accumulation in time) or after cell stress (oxidative, replicative, starvation, to name a few). In any case, as indicated in the Introduction, senescent cells switch to a secretory phenotype (SASP) and can alter the surrounding environment in a paracrine manner. It is also associated with chronic inflammation in most of the aged tissues, including CNS (Chinta et al., 2015). ALS pathology has similarities with AD. These similarities include inflammation, oxidative stress, neurodegeneration and protein aggregation. Notably, TDP-43 pathology incidence increases in oldest individuals up to 70% in those >100 years old age (Nelson et al., 2019). However, TDP-43 aggregation is not a prerequisite for TDP-43 loss of function as we detected in ALS and LATE-AD samples. TDP-43 can be regulated within post-translational modifications and allosteric effectors in cell stress situations (Dang et al., 2020; Duan et al., 2019). We hypothesize that cell stress in G93A-SOD1 mouse triggers senescence and SASP and is associated with TDP-43 loss of cryptic splicing repression, as shown by data of the fifth paper.

In this work, we analyzed the expression of senescence markers by RT-qPCR, immunofluorescence and immunohistochemistry of p16 and p21 in the spinal cord of G93A at disease onset, middle stage of disease and end-stage. SA-b-gal activity was also measured as one of the commonly used senescence markers. We also quantify the mRNA expression of several SASP components, *Il-1a*, *Il-6* and *Irfn-b*. TDP-43 loss of function was measured by the splicing rate of a mouse cryptic exon in *Adipor2* mRNA (Jeong et al., 2017). Both *p16* and *Il-1a* increase during the disease progression and *p21*, *Il-6* and *Adipor2* cryptic exon PSI just increase at the end-stage, suggesting that in earlier stages senescence does not operate or other mechanisms could compensate the noxious stimuli. *Irfn-b* expression remains unchanged. Our results demonstrate a dynamic behavior in senescence and SASP and a correlation with disease stage. Interestingly, *Adipor2* cryptic exon PSI is correlated with *p16* expression, suggesting common disease pathways to be further explored. SA-beta-gal activity in the spinal cord is mainly expressed in motor neurons. Contrary to our hypothesis, SA-beta-gal activity is progressively decreased in G93A-SOD1 mice in motor neurons. It might be explained by lysosomal biogenesis impairment and, consequently, autophagy defects (Y. Xie, Zhou, Lin, & Sheng, 2015). Senescence marker p16 in G93A-SOD1 is expressed in glial cells but not in neurons, as shown by confocal microscopy data. Glial senescence has been invoked previously in

## Discussion

neurodegeneration (Das & Svendsen, 2015; Ferrer, 2017; Vazquez- Villaseñor et al., 2019). Our data from fifth paper suggests that the overexpression of G93A-SOD1 transgene induces a transcriptional profile compatible with senescence and SASP. It triggers a cytotoxic phenotype of glia, thus promoting inflammation and neurodegeneration.

Aimed by the detection of senescence and SASP markers, we started a senolytic treatment with Navitoclax (ABT263), following the administration guideline described in (Bussian et al., 2018). We administered 50 mg/kg of Navitoclax by oral gavage five consecutive days followed by 16 days of rest. This treatment began at disease onset (90 days old mice) and finished at clinical endpoint. However, Navitoclax treatment does not prevent weight loss, neither extends lifespan. Senescence markers in treated mice remains unchanged. In contrast to pro-resolution molecules that are derived from PUFAs, senescence is highly variable between tissues. Senolytic drugs are not useful for all cell types (Zhu et al., 2016, 2015). Further experiments will elucidate the targetable molecular effectors of senescence and SASP in ALS. We hypothesize that a combination of pro-resolving drugs (DHA enriched diet or Resolvin D1), a proper senolytic and ASO targeting cryptic splicing of relevant genes can be a therapeutic strategy to inhibit several upstream harmful processes. Nevertheless, early diagnosis and proper patient stratification in RCTs can potentiate the effects of our proposal.

This stratification requires robust biomarkers. Thus, biomarker research can improve the diagnosis, prognosis and ALS RCT design. In this thesis, we focused the research on TDP-43-based and metabolomic biomarkers in platelets and PBMCs. The reasons for that were the previous data of TDP-43-based biomarkers in PBMCs (De Marco et al., 2011) and the possibility to analyze its splicing function. Regarding metabolomics, previous studies employed plasma samples. We thought that plasma can rapidly response to external factor, such as diet. Platelet composition are more stable in time and potentially it can be useful for longitudinal analyses and reproducibility in other laboratories.

Platelet metabolomics resulted in a similar profile between ALS and control samples. Only 3 were statistically significant and de AUC value of ROC analyses was lower than 0.8. However, hierarchal clustering analysis points to a partial discrimination of ALS and CTL. PCA analysis from metabolomic analysis does not separate the samples by its disease status. Regarding TDP-43 biomarkers, our results suggests that are not useful for ALS diagnostic. Neither platelet TDP-43 expression, nor cryptic splicing in PBMCs are suitable for this purpose. On the other hand, in this paper we highlight a differential cryptic exon inclusion between spinal cord, motor cortex and PBMCs. Motor cortex is the tissue with lower values of *PFKP* cryptic exon inclusion. Interestingly, we observed a better discrimination comparing fast and slow progressors. Thirteen metabolites were statically significant with an AUC higher than 0.8. Hierarchical cluster analysis showed a good separation into fast and



## *Discussion*

slow progressors. It reinforces the need of a better stratification of this heterogenous disease using prognostic biomarkers.

In this thesis we have some limitations. The most important one is the limitation of human samples in the first, second and sixth paper. A larger number of samples would have been more representative. This is specially a limiting factor for metabolipidomic analyses because is not a quantitative data and a large number of samples are often required for multivariate statistics. Sample stratification by clinical onset also lowers the statistics power in the sixth paper and the correlation with clinical and epidemiological parameters are suboptimal. However, the relatively low incidence of the disease, hinders the availability of the sample. Another important limitation is that we did not demonstrate that remaining motor neurons from ALS donors contain less quantity of ATG4B protein. Regarding fourth paper, resolvins (the effector of DHA metabolism) are not quantified. Moreover, a treatment with pure resolvins instead of DHA could enhance the pro-resolution effects (G. Liu et al., 2012). Since no effect was observed in Navitoclax treated mice, a specific biomarker detection would have been appreciated to verify the correct distribution of Navitoclax in the spinal cord.

In conclusion, in this thesis we have explored different ALS pathogenic mechanisms and how to target them. Cryptic exons are expressed in different regions of CNS in ALS, depending on disease onset site. They are also expressed in AD with and without TDP-43 pathology in the hippocampus and are enriched up to 5-fold in nuclear compartment. Their PSI is relatively low, but it can be associated with a massive death of motor neurons that are no longer expressing cryptic exons. ATG4B cryptic exon splicing can downregulate the protein levels, potentially impairing autophagy. DHA rich diet can ameliorate disease progression in G93A in a gender-specific manner. DHA probably exerts a pro-resolution effect in neuroinflammation of G93A-SOD1 mice. Also, senescence and SASP markers, linked to inflammation, are increased in G93A-SOD1 mice in spinal cord. Senescence marker p16 is correlated with Adipor2 cryptic exon derived from TDP-43 loss of function. However, senolytic treatment (Navitoclax) does not delay disease progression and death. Platelet metabolomics can be useful to predict disease progression and diagnosis.

# **7 CONCLUSIONS**

## Conclusions

First.- The function of TDP-43 cryptic exon splicing is compromised in nervous tissue specimens from ALS patients. This fact increases *ATG4B* and *GPSM2* mRNA cryptic exon inclusion rates between 0.1 and 3%. The inclusion of *ATG4B* cryptic exon associated with TDP-43 downregulation induces autophagy disturbances in cell models.

Second.- Inclusion rates of TDP-43 regulated *ATG4B* and *GPSM2* (but not *PFKP*) cryptic exons measurable by RT-qPCR are candidate biomarkers for ALS staging.

Third.- The loss of function of TDP-43 is also present in hippocampal samples of patients with advanced stages of Alzheimer's Disease with and without exhibiting TDP-43 pathology.

Fourth.- *ATG4B*, *GPSM2*, and *PFKP* mRNA containing cryptic exons are enriched up to 5-fold in nuclear compartments and degraded by non-sense mediated mRNA decay in the cytosol *in vivo*. In cell culture, cryptic exon splicing of *ATG4B* mRNA sequences requires distal elements in the pre-mRNA to be executed.

Fifth.- Confidential

Sixth.- A DHA enriched diet slows the disease progression and extends hSOD1-G93A male mice's survival. This diet increases DHA content in the lumbar spinal cord of mice. Its use prevents DNA oxidative damage and regulates plasmatic cytokine profile associated with hSOD1-G93A overexpression.

Seventh.- hSOD1-G93A mice exhibit a senescence and SASP transcriptional profile in the lumbar spinal cord. In the same model, Tdp-43 splicing function is altered at the end stage, and it is correlated with the expression of p16, a marker of cell senescence. Navitoclax, an inhibitor of cell senescence in other neurodegenerative models, does not prevent disease progression in hSOD1-G93A mice.

Eighth.- *ATG4B* and *GPSM2* cryptic exons are not detected in peripheral blood mononuclear cells. Neither *PFKP* cryptic exon in these cells nor the platelet concentration of TDP-43 does not exhibit potential use as ALS diagnostic biomarkers. In contrast, metabolomics analysis shows promise for further development of ALS prognosis and diagnosis biomarker development.

## **8 REFERENCES**

## References

- Abdul-Aziz, A. M., Sun, Y., Hellmich, C., Marlein, C. R., Mistry, J., Forde, E., ... Rushworth, S. A. (2019). Acute myeloid leukemia induces protumoral p16INK4a-driven senescence in the bone marrow microenvironment. *Blood*, *133*(5), 446–456. <https://doi.org/10.1182/blood-2018-04-845420>
- Abe, K., Aoki, M., Tsuji, S., Itoyama, Y., Sobue, G., Togo, M., ... Yoshino, H. (2017). Safety and efficacy of edaravone in well defined patients with amyotrophic lateral sclerosis: a randomised, double-blind, placebo-controlled trial. *The Lancet Neurology*, *16*(7), 505–512. [https://doi.org/10.1016/S1474-4422\(17\)30115-1](https://doi.org/10.1016/S1474-4422(17)30115-1)
- Abo-Rady, M., Kalmbach, N., Pal, A., Schludi, C., Janosch, A., Richter, T., ... Sternecker, J. L. (2020). Knocking out C9ORF72 Exacerbates Axonal Trafficking Defects Associated with Hexanucleotide Repeat Expansion and Reduces Levels of Heat Shock Proteins. *Stem Cell Reports*, *14*(3), 390–405. <https://doi.org/10.1016/j.stemcr.2020.01.010>
- Aguirre, N., Beal, M. F., Matson, W. R., & Bogdanov, M. B. (2005). Increased oxidative damage to DNA in an animal model of amyotrophic lateral sclerosis. *Free Radical Research*, *39*(4), 383–388. <https://doi.org/10.1080/10715760400027979>
- Aguzzi, A., Sigurdson, C., & Heikenwaelder, M. (2008). Molecular Mechanisms of Prion Pathogenesis. *Annual Review of Pathology: Mechanisms of Disease*, *3*(1), 11–40. <https://doi.org/10.1146/annurev.pathmechdis.3.121806.154326>
- Aizawa, H., Yamashita, T., Kato, H., Kimura, T., & Kwak, S. (2019). Impaired Nucleoporins Are Present in Sporadic Amyotrophic Lateral Sclerosis Motor Neurons that Exhibit Mislocalization of the 43-kDa TAR DNA-Binding Protein. *Journal of Clinical Neurology (Seoul, Korea)*, *15*(1), 62–67. <https://doi.org/10.3988/jcn.2019.15.1.62>
- Al-Chalabi, A., Calvo, A., Chio, A., Colville, S., Ellis, C. M., Hardiman, O., ... Pearce, N. (2014). Analysis of amyotrophic lateral sclerosis as a multistep process: A population-based modelling study. *The Lancet Neurology*, *13*(11), 1108–1113. [https://doi.org/10.1016/S1474-4422\(14\)70219-4](https://doi.org/10.1016/S1474-4422(14)70219-4)
- Al-Chalabi, A., Fang, F., Hanby, M. F., Leigh, P. N., Shaw, C. E., Ye, W., & Rijdsdijk, F. (2010). An estimate of amyotrophic lateral sclerosis heritability using twin data. *Journal of Neurology, Neurosurgery and Psychiatry*, *81*(12), 1324–1326. <https://doi.org/10.1136/jnnp.2010.207464>
- Al-Chalabi, A., & Hardiman, O. (2013). The epidemiology of ALS: a conspiracy of genes, environment and time. *Nature Reviews Neurology*, *9*(11), 617–628. <https://doi.org/10.1038/nrneurol.2013.203>
- Al Rashid, S. T., Dellaire, G., Cuddihy, A., Jalali, F., Vaid, M., Coackley, C., ... Bristow, R. G. (2005). Evidence for the direct binding of phosphorylated p53 to sites of DNA breaks in vivo. *Cancer Research*, *65*(23), 10810–10821. <https://doi.org/10.1158/0008-5472.CAN-05-0729>
- An, D., Fujiki, R., Iannitelli, D. E., Smerdon, J. W., Maity, S., Rose, M. F., ... Mazzoni, E. O. (2019). Stem cell-derived cranial and spinal motor neurons reveal proteostatic differences between ALS resistant and sensitive motor neurons. *ELife*, *8*. <https://doi.org/10.7554/eLife.44423>

## References

- Anding, A. L., & Baehrecke, E. H. (2017). Cleaning House: Selective Autophagy of Organelles. *Developmental Cell*, 41(1), 10–22. <https://doi.org/10.1016/j.devcel.2017.02.016>
- Aoki, Y., Manzano, R., Lee, Y., Dafinca, R., Aoki, M., Douglas, A. G. L., ... Wood, M. J. A. (n.d.). C9orf72 and RAB7L1 regulate vesicle trafficking in amyotrophic lateral sclerosis and frontotemporal dementia. <https://doi.org/10.1093/brain/awx024>
- Armon, C. (2009). Smoking may be considered an established risk factor for sporadic ALS. *Neurology*. Lippincott Williams and Wilkins. <https://doi.org/10.1212/WNL.0b013e3181c1df48>
- Arthur, K. C., Calvo, A., Price, T. R., Geiger, J. T., Chiò, A., & Traynor, B. J. (2016). Projected increase in amyotrophic lateral sclerosis from 2015 to 2040. *Nature Communications*, 7, 12408. <https://doi.org/10.1038/ncomms12408>
- Ayala, V., Granado-Serrano, A. B., Cacabelos, D., Naudí, A., Ilieva, E. V, Boada, J., ... Portero-Otin, M. (2011). Cell stress induces TDP-43 pathological changes associated with ERK1/2 dysfunction: implications in ALS. *Acta Neuropathologica*, 122(3), 259–270. <https://doi.org/10.1007/s00401-011-0850-y>
- Ayala, Y. M., Zago, P., D'Ambrogio, A., Xu, Y.-F., Petrucelli, L., Buratti, E., & Baralle, F. E. (2008). Structural determinants of the cellular localization and shuttling of TDP-43. *Journal of Cell Science*, 121(Pt 22), 3778–3785. <https://doi.org/10.1242/jcs.038950>
- Ayers, J. I., Fromholt, S., Koch, M., DeBosier, A., McMahon, B., Xu, G., & Borchelt, D. R. (2014). Experimental transmissibility of mutant SOD1 motor neuron disease. *Acta Neuropathologica*, 128(6), 791–803. <https://doi.org/10.1007/s00401-014-1342-7>
- Baker, D. J., Childs, B. G., Durik, M., Wijers, M. E., Sieben, C. J., Zhong, J., ... Van Deursen, J. M. (2016). Naturally occurring p16 Ink4a-positive cells shorten healthy lifespan. *Nature*, 530(7589), 184–189. <https://doi.org/10.1038/nature16932>
- Baker, D. J., Wijshake, T., Tchkonina, T., Lebrasseur, N. K., Childs, B. G., Van De Sluis, B., ... Van Deursen, J. M. (2011). Clearance of p16 Ink4a-positive senescent cells delays ageing-associated disorders. *Nature*, 479(7372), 232–236. <https://doi.org/10.1038/nature10600>
- Baker, S. J., Fearon, E. R., Nigro, J. M., Hamilton, S. R., Preisinger, A. C., Jessup, J. M., ... Vogelstein, B. (1989). Chromosome 17 deletions and p53 gene mutations in colorectal carcinomas. *Science*, 244(4901), 217–221. <https://doi.org/10.1126/science.2649981>
- Balderhaar, H. J. kleine, & Ungermann, C. (2013). CORVET and HOPS tethering complexes - coordinators of endosome and lysosome fusion. *Journal of Cell Science*, 126(Pt 6), 1307–1316. <https://doi.org/10.1242/jcs.107805>
- Barone, M., Viggiani, M. T., Introna, A., D'errico, E., Scarafino, A., Iannone, A., ... Simone, I. L. (2019). Nutritional prognostic factors for survival in amyotrophic lateral sclerosis patients undergone percutaneous endoscopic gastrostomy placement. *Amyotrophic Lateral Sclerosis and Frontotemporal Degeneration*, 20(7–8), 490–496. <https://doi.org/10.1080/21678421.2019.1643374>
- Baynes, J W, & Thorpe, S. R. (2000). Glycooxidation and lipoxidation in atherogenesis. *Free*

## References

- Radical Biology & Medicine*, 28(12), 1708–1716. [https://doi.org/10.1016/s0891-5849\(00\)00228-8](https://doi.org/10.1016/s0891-5849(00)00228-8)
- Baynes, John W. (2003). Chemical modification of proteins by lipids in diabetes. *Clinical Chemistry and Laboratory Medicine*, 41(9), 1159–1165. <https://doi.org/10.1515/CCLM.2003.179>
- Beard, J. D., & Kamel, F. (2015). Military service, deployments, and exposures in relation to amyotrophic lateral sclerosis etiology and survival. *Epidemiologic Reviews*, 37, 55–70. <https://doi.org/10.1093/epirev/mxu001>
- Benatar, M., Wu, J., Andersen, P. M., Atassi, N., David, W., Cudkovic, M., & Schoenfeld, D. (2018). Randomized, double-blind, placebo-controlled trial of arimoclomol in rapidly progressive SOD1 ALS. *Neurology*, 90(7), e565–e574. <https://doi.org/10.1212/WNL.0000000000004960>
- Bendotti, C., Tortarolo, M., Suchak, S. K., Calvaresi, N., Carvelli, L., Bastone, A., ... Mennini, T. (2001). Transgenic SOD1 G93A mice develop reduced GLT-1 in spinal cord without alterations in cerebrospinal fluid glutamate levels. *Journal of Neurochemistry*, 79(4), 737–746. <https://doi.org/10.1046/j.1471-4159.2001.00572.x>
- Benimetskaya, L., Loike, J. D., Khaled, Z., Loike, G., Silverstein, S. C., Cao, L., ... Stein, C. A. (1997). Mac-1 (CD11b/CD18) is an oligodeoxynucleotide-binding protein. *Nature Medicine*, 3(4), 414–420. <https://doi.org/10.1038/nm0497-414>
- Bennett, C. F., Baker, B. F., Pham, N., Swayze, E., & Geary, R. S. (2017). Pharmacology of Antisense Drugs. *Annual Review of Pharmacology and Toxicology*, 57(1), 81–105. <https://doi.org/10.1146/annurev-pharmtox-010716-104846>
- Bensimon, G., Lacomblez, L., & Meininger, V. (1994). A controlled trial of riluzole in amyotrophic lateral sclerosis. *New England Journal of Medicine*, 330(9), 585–591. <https://doi.org/10.1056/NEJM199403033300901>
- Berget, S. M., Moore, C., & Sharp, P. A. (1977). Spliced segments at the 5' terminus of adenovirus 2 late mRNA. *Proceedings of the National Academy of Sciences of the United States of America*, 74(8), 3171–3175. <https://doi.org/10.1073/pnas.74.8.3171>
- Bhat, R., Crowe, E. P., Bitto, A., Moh, M., Katsetos, C. D., Garcia, F. U., ... Torres, C. (2012). Astrocyte senescence as a component of Alzheimer's disease. *PloS One*, 7(9), e45069. <https://doi.org/10.1371/journal.pone.0045069>
- Bielski, B. H., Arudi, R. L., & Sutherland, M. W. (1983). A study of the reactivity of HO<sub>2</sub>/O<sub>2</sub><sup>-</sup> with unsaturated fatty acids. *J Biol Chem*, 258(8), 4759–4761. Retrieved from <http://www.ncbi.nlm.nih.gov/pubmed/6833274>
- Bjørkøy, G., Lamark, T., Pankiv, S., Øvervatn, A., Brech, A., & Johansen, T. (2009). Monitoring autophagic degradation of p62/SQSTM1. *Methods in Enzymology*, 452(C), 181–197. [https://doi.org/10.1016/S0076-6879\(08\)03612-4](https://doi.org/10.1016/S0076-6879(08)03612-4)
- Blasco, H., Veyrat-Durebex, C., Bocca, C., Patin, F., Vourc'H, P., Kouassi Nzoughet, J., ... Reynier, P. (2017). Lipidomics Reveals Cerebrospinal-Fluid Signatures of ALS. *Scientific*

## References

- Reports*, 7(1), 1–10. <https://doi.org/10.1038/s41598-017-17389-9>
- Blasco, H el ene, Corcia, P., Moreau, C., Veau, S., Fournier, C., Vourc'h, P., ... Andres, C. R. (2010). 1H-NMR-Based metabolomic profiling of CSF in early amyotrophic lateral sclerosis. *PLoS ONE*, 5(10). <https://doi.org/10.1371/journal.pone.0013223>
- Blasco, H el ene, Patin, F., Descat, A., Gar on, G., Corcia, P., Gel e, P., ... Pradat, P. F. (2018). A pharmaco-metabolomics approach in a clinical trial of ALS: Identification of predictive markers of progression. *PLoS ONE*, 13(6). <https://doi.org/10.1371/journal.pone.0198116>
- Bogdanov, M., Brown, R. H., Matson, W., Smart, R., Hayden, D., O'Donnell, H., ... Cudkovicz, M. (2000). Increased oxidative damage to DNA in ALS patients. *Free Radical Biology and Medicine*, 29(7), 652–658. [https://doi.org/10.1016/S0891-5849\(00\)00349-X](https://doi.org/10.1016/S0891-5849(00)00349-X)
- Bolognesi, B., Faure, A. J., Seuma, M., Schmiedel, J. M., Tartaglia, G. G., & Lehner, B. (2019). The mutational landscape of a prion-like domain. *Nature Communications*, 10(1), 4162. <https://doi.org/10.1038/s41467-019-12101-z>
- Bourassa, M. W., Brown, H. H., Borchelt, D. R., Vogt, S., & Miller, L. M. (2014). Metal-deficient aggregates and diminished copper found in cells expressing SOD1 mutations that cause ALS. *Frontiers in Aging Neuroscience*, 6(JUN), 110. <https://doi.org/10.3389/fnagi.2014.00110>
- Bouteloup, C., Desport, J. C., Clavelou, P., Guy, N., Derumeaux-Burel, H., Ferrier, A., & Couratier, P. (2009). Hypermetabolism in ALS patients: An early and persistent phenomenon. *Journal of Neurology*, 256(8), 1236–1242. <https://doi.org/10.1007/s00415-009-5100-z>
- Bozik, M. E., Mitsumoto, H., Brooks, B. R., Rudnicki, S. A., Moore, D. H., Zhang, B., ... Archibald, D. (2014). A post hoc analysis of subgroup outcomes and creatinine in the phase III clinical trial (EMPOWER) of dexpramipexole in ALS. *Amyotrophic Lateral Sclerosis and Frontotemporal Degeneration*, 15(5–6), 406–413. <https://doi.org/10.3109/21678421.2014.943672>
- Braak, H., & Braak, E. (1991, September). Neuropathological staging of Alzheimer-related changes. *Acta Neuropathologica*. Springer-Verlag. <https://doi.org/10.1007/BF00308809>
- Bradley, W G, Robison, S. H., & Tandan, R. (1987). Deficient repair of alkylation damage of DNA in Alzheimer's disease and amyotrophic lateral sclerosis cells. *Advances in Experimental Medicine and Biology*, 209, 3–6. [https://doi.org/10.1007/978-1-4684-5302-7\\_1](https://doi.org/10.1007/978-1-4684-5302-7_1)
- Bradley, Walter G., & Krasin, F. (1982). A New Hypothesis of the Etiology of Amyotrophic Lateral Sclerosis: The DNA Hypothesis. *Archives of Neurology*, 39(11), 677–680. <https://doi.org/10.1001/archneur.1982.00510230003001>
- Brady, O. A., Meng, P., Zheng, Y., Mao, Y., & Hu, F. (2011). Regulation of TDP-43 aggregation by phosphorylation and p62/SQSTM1. *Journal of Neurochemistry*, 116(2), 248–259. <https://doi.org/10.1111/j.1471-4159.2010.07098.x>
- Bravo-Hernandez, M., Tadokoro, T., Navarro, M. R., Platoshyn, O., Kobayashi, Y., Marsala, S., ... Marsala, M. (2020). Spinal subpial delivery of AAV9 enables widespread gene silencing and blocks motoneuron degeneration in ALS. *Nature Medicine*, 26(1), 118–130.



## References

- <https://doi.org/10.1038/s41591-019-0674-1>
- Brooks, B. R., Miller, R. G., Swash, M., & Munsat, T. L. (2000). El Escorial revisited: Revised criteria for the diagnosis of amyotrophic lateral sclerosis. *Amyotrophic Lateral Sclerosis*, *1*(5), 293–299. <https://doi.org/10.1080/146608200300079536>
- Buratti, E., & Baralle, F. E. (2008). Multiple roles of TDP-43 in gene expression, splicing regulation, and human disease. *Frontiers in Bioscience*. Front Biosci. <https://doi.org/10.2741/2727>
- Buratti, E., Dörk, T., Zuccato, E., Pagani, F., Romano, M., & Baralle, F. E. (2001). Nuclear factor TDP-43 and SR proteins promote in vitro and in vivo CFTR exon 9 skipping. *EMBO Journal*, *20*(7), 1774–1784. <https://doi.org/10.1093/emboj/20.7.1774>
- Burel, S. A., Hart, C. E., Cauntay, P., Hsiao, J., Machemer, T., Katz, M., ... Henry, S. P. (2016). Hepatotoxicity of high affinity gapmer antisense oligonucleotides is mediated by RNase H1 dependent promiscuous reduction of very long pre-mRNA transcripts. *Nucleic Acids Research*, *44*(5), 2093–2109. <https://doi.org/10.1093/nar/gkv1210>
- Bussian, T. J., Aziz, A., Meyer, C. F., Swenson, B. L., van Deursen, J. M., & Baker, D. J. (2018). Clearance of senescent glial cells prevents tau-dependent pathology and cognitive decline. *Nature*, *562*(7728), 578–582. <https://doi.org/10.1038/s41586-018-0543-y>
- Butti, Z., & Patten, S. A. (2019). RNA dysregulation in amyotrophic lateral sclerosis. *Frontiers in Genetics*. Frontiers Media S.A. <https://doi.org/10.3389/fgene.2018.00712>
- Cacabelos, D., Ayala, V., Granado-Serrano, A. B., Jové, M., Torres, P., Boada, J., ... Portero-Otín, M. (2016). Interplay between TDP-43 and docosahexaenoic acid-related processes in amyotrophic lateral sclerosis. *Neurobiology of Disease*, *88*, 148–160. <https://doi.org/10.1016/j.nbd.2016.01.007>
- Cacabelos, D., Ayala, V., Ramírez-Nunez, O., Granado-Serrano, A. B., Boada, J., Serrano, J. C. E., ... Portero-Otin, M. (2014). Dietary Lipid Unsaturation Influences Survival and Oxidative Modifications of an Amyotrophic Lateral Sclerosis Model in a Gender-Specific Manner. *NeuroMolecular Medicine*, *16*(4), 669–685. <https://doi.org/10.1007/s12017-014-8317-7>
- Cacabelos, D., Ramírez-Núñez, O., Granado-Serrano, A. B., Torres, P., Ayala, V., Moiseeva, V., ... Boada, J. (2016). Early and gender-specific differences in spinal cord mitochondrial function and oxidative stress markers in a mouse model of ALS. *Acta Neuropathologica Communications*, *4*(1), 3. <https://doi.org/10.1186/s40478-015-0271-6>
- Calder, P. C. (2015). Marine omega-3 fatty acids and inflammatory processes: Effects, mechanisms and clinical relevance. *Biochimica et Biophysica Acta - Molecular and Cell Biology of Lipids*. Elsevier. <https://doi.org/10.1016/j.bbalip.2014.08.010>
- Califf, R. M. (2018). Biomarker definitions and their applications. *Experimental Biology and Medicine*, *243*(3), 213–221. <https://doi.org/10.1177/1535370217750088>
- Calon, F., Lim, G. P., Yang, F., Morihara, T., Teter, B., Ubeda, O., ... Cole, G. M. (2004). Docosahexaenoic acid protects from dendritic pathology in an Alzheimer's disease mouse model. *Neuron*, *43*(5), 633–645. <https://doi.org/10.1016/j.neuron.2004.08.013>

## References

- Camacho, A., Esteban, J., & Paradas, C. (2018, January 1). Report by the Spanish Foundation for the Brain on the social impact of amyotrophic lateral sclerosis and other neuromuscular disorders. *Neurología*. Spanish Society of Neurology. <https://doi.org/10.1016/j.nrl.2015.02.003>
- Cartegni, L., Chew, S. L., & Krainer, A. R. (2002). Listening to silence and understanding nonsense: Exonic mutations that affect splicing. *Nature Reviews Genetics*. Nat Rev Genet. <https://doi.org/10.1038/nrg775>
- Castrillo-Viguera, C., Grasso, D. L., Simpson, E., Shefner, J., & Cudkovicz, M. E. (2010). Clinical significance in the change of decline in ALSFRS-R. *Amyotrophic Lateral Sclerosis*, 11(1–2), 178–180. <https://doi.org/10.3109/17482960903093710>
- Cautain, B., Hill, R., De Pedro, N., & Link, W. (2015). Components and regulation of nuclear transport processes. *FEBS Journal*. Blackwell Publishing Ltd. <https://doi.org/10.1111/febs.13163>
- Cedarbaum, J. M., Stambler, N., Malta, E., Fuller, C., Hilt, D., Thurmond, B., & Nakanishi, A. (1999). The ALSFRS-R: A revised ALS functional rating scale that incorporates assessments of respiratory function. *Journal of the Neurological Sciences*, 169(1–2), 13–21. [https://doi.org/10.1016/S0022-510X\(99\)00210-5](https://doi.org/10.1016/S0022-510X(99)00210-5)
- Celeste, A., Petersen, S., Romanienko, P. J., Fernandez-Capetillo, O., Chen, H. T., Sedelnikova, O. A., ... Nussenzweig, A. (2002). Genomic instability in mice lacking histone H2AX. *Science (New York, N. Y.)*, 296(5569), 922–927. <https://doi.org/10.1126/science.1069398>
- Chacko, B. K., Smith, M. R., Johnson, M. S., Benavides, G., Culp, M. L., Pilli, J., ... Darley-USmar, V. M. (2019). Mitochondria in precision medicine; linking bioenergetics and metabolomics in platelets. *Redox Biology*, 22, 101165. <https://doi.org/10.1016/j.redox.2019.101165>
- Chattopadhyay, M., Nwadiabia, E., Strong, C. D., Gralla, E. B., Valentine, J. S., & Whitelegge, J. P. (2015). The disulfide bond, but not zinc or dimerization, controls initiation and seeded growth in amyotrophic lateral sclerosis-linked Cu,Zn superoxide dismutase (SOD1) fibrillation. *Journal of Biological Chemistry*, 290(51), 30624–30636. <https://doi.org/10.1074/jbc.M115.666503>
- Che, M.-X., Jiang, Y.-J., Xie, Y.-Y., Jiang, L.-L., & Hu, H.-Y. (2011). Aggregation of the 35-kDa fragment of TDP-43 causes formation of cytoplasmic inclusions and alteration of RNA processing. *FASEB Journal : Official Publication of the Federation of American Societies for Experimental Biology*, 25(7), 2344–2353. <https://doi.org/10.1096/fj.10-174482>
- Chen, H.-J., Anagnostou, G., Chai, A., Withers, J., Morris, A., Adhikaree, J., ... de Bellerocche, J. S. (2010). Characterization of the properties of a novel mutation in VAPB in familial amyotrophic lateral sclerosis. *The Journal of Biological Chemistry*, 285(51), 40266–40281. <https://doi.org/10.1074/jbc.M110.161398>
- Chen, Q., Vazquez, E. J., Moghaddas, S., Hoppel, C. L., & Lesnefsky, E. J. (2003). Production of reactive oxygen species by mitochondria: Central role of complex III. *Journal of Biological Chemistry*, 278(38), 36027–36031. <https://doi.org/10.1074/jbc.M304854200>

## References

- Chen, Y.-Z., Bennett, C. L., Huynh, H. M., Blair, I. P., Puls, I., Irobi, J., ... Chance, P. F. (2004). DNA/RNA helicase gene mutations in a form of juvenile amyotrophic lateral sclerosis (ALS4). *American Journal of Human Genetics*, *74*(6), 1128–1135. <https://doi.org/10.1086/421054>
- Chia, R., Tattum, M. H., Jones, S., Collinge, J., Fisher, E. M. C., & Jackson, G. S. (2010). Superoxide dismutase 1 and tgSOD1 mouse spinal cord seed fibrils, suggesting a propagative cell death mechanism in amyotrophic lateral sclerosis. *PLoS One*, *5*(5), e10627. <https://doi.org/10.1371/journal.pone.0010627>
- Chiang, C., Scott, A. J., Davis, J. R., Tsang, E. K., Li, X., Kim, Y., ... Hall, I. M. (2017). The impact of structural variation on human gene expression. *Nature Genetics*, *49*(5), 692–699. <https://doi.org/10.1038/ng.3834>
- Chinta, S. J., Woods, G., Demaria, M., Rane, A., Zou, Y., McQuade, A., ... Andersen, J. K. (2018). Cellular Senescence Is Induced by the Environmental Neurotoxin Paraquat and Contributes to Neuropathology Linked to Parkinson's Disease. *Cell Reports*, *22*(4), 930–940. <https://doi.org/10.1016/j.celrep.2017.12.092>
- Chinta, S. J., Woods, G., Rane, A., Demaria, M., Campisi, J., & Andersen, J. K. (2015). Cellular senescence and the aging brain. *Experimental Gerontology*, *68*, 3–7. <https://doi.org/10.1016/j.exger.2014.09.018>
- Chou, C.-C., Zhang, Y., Umoh, M. E., Vaughan, S. W., Lorenzini, I., Liu, F., ... Rossoll, W. (2018). TDP-43 pathology disrupts nuclear pore complexes and nucleocytoplasmic transport in ALS/FTD. *Nature Neuroscience*, *21*(2), 228–239. <https://doi.org/10.1038/s41593-017-0047-3>
- Chow, C. Y., Landers, J. E., Bergren, S. K., Sapp, P. C., Grant, A. E., Jones, J. M., ... Meisler, M. H. (2009). Deleterious variants of FIG4, a phosphoinositide phosphatase, in patients with ALS. *American Journal of Human Genetics*, *84*(1), 85–88. <https://doi.org/10.1016/j.ajhg.2008.12.010>
- Chow, L. T., Gelinis, R. E., Broker, T. R., & Roberts, R. J. (1977). An amazing sequence arrangement at the 5' ends of adenovirus 2 messenger RNA. *Cell*, *12*(1), 1–8. [https://doi.org/10.1016/0092-8674\(77\)90180-5](https://doi.org/10.1016/0092-8674(77)90180-5)
- Cirulli, E. T., Lasseigne, B. N., Petrovski, S., Sapp, P. C., Dion, P. A., Leblond, C. S., ... Muñoz-Blanco, J. L. (2015). Exome sequencing in amyotrophic lateral sclerosis identifies risk genes and pathways. *Science*, *347*(6229), 1436–1441. <https://doi.org/10.1126/science.aaa3650>
- Codron, P., Cassereau, J., Vourc'h, P., Veyrat-Durebex, C., Blasco, H., Kane, S., ... Chevrollier, A. (2018). Primary fibroblasts derived from sporadic amyotrophic lateral sclerosis patients do not show ALS cytological lesions. *Amyotrophic Lateral Sclerosis & Frontotemporal Degeneration*, *19*(5–6), 446–456. <https://doi.org/10.1080/21678421.2018.1431787>
- Cohen, T. J., Lee, V. M. Y., & Trojanowski, J. Q. (2011). TDP-43 functions and pathogenic mechanisms implicated in TDP-43 proteinopathies. *Trends in Molecular Medicine*, *17*(11), 659–667. <https://doi.org/10.1016/j.molmed.2011.06.004>

## References

- Collins, M. A., An, J., Hood, B. L., Conrads, T. P., & Bowser, R. P. (2015). Label-free LC-MS/MS proteomic analysis of cerebrospinal fluid identifies protein/pathway alterations and candidate biomarkers for amyotrophic lateral sclerosis. *Journal of Proteome Research*, *14*(11), 4486–4501. <https://doi.org/10.1021/acs.jproteome.5b00804>
- Conicella, A. E., Dignon, G. L., Zerbe, G. H., Schmidt, H. B., D'Ordine, A. M., Kim, Y. C., ... Fawzi, N. L. (2020). TDP-43  $\alpha$ -helical structure tunes liquid–liquid phase separation and function. *Proceedings of the National Academy of Sciences of the United States of America*, *117*(11), 5883–5894. <https://doi.org/10.1073/pnas.1912055117>
- Cooper-Knock, J., Higginbottom, A., Stopford, M. J., Highley, J. R., Ince, P. G., Wharton, S. B., ... Shaw, P. J. (2015). Antisense RNA foci in the motor neurons of C9ORF72-ALS patients are associated with TDP-43 proteinopathy. *Acta Neuropathologica*, *130*(1), 63–75. <https://doi.org/10.1007/s00401-015-1429-9>
- Coppé, J.-P., Patil, C. K., Rodier, F., Sun, Y., Muñoz, D. P., Goldstein, J., ... Campisi, J. (2008). Senescence-Associated Secretory Phenotypes Reveal Cell-Nonautonomous Functions of Oncogenic RAS and the p53 Tumor Suppressor. *PLoS Biology*, *6*(12), e301. <https://doi.org/10.1371/journal.pbio.0060301>
- Coppedè, F., Mancuso, M., Lo Gerfo, A., Carlesi, C., Piazza, S., Rocchi, A., ... Siciliano, G. (2007). Association of the hOGG1 Ser326Cys polymorphism with sporadic amyotrophic lateral sclerosis. *Neuroscience Letters*, *420*(2), 163–168. <https://doi.org/10.1016/j.neulet.2007.04.067>
- Coppedè, F., & Migliore, L. (2015). DNA damage in neurodegenerative diseases. *Mutation Research*, *776*, 84–97. <https://doi.org/10.1016/j.mrfmmm.2014.11.010>
- Corey, D. R. (2017). Nusinersen, an antisense oligonucleotide drug for spinal muscular atrophy. *Nature Neuroscience*, *20*(4), 497–499. <https://doi.org/10.1038/nn.4508>
- Da Cruz, S., Bui, A., Saberi, S., Lee, S. K., Stauffer, J., McAlonis-Downes, M., ... Ravits, J. (2017). Misfolded SOD1 is not a primary component of sporadic ALS. *Acta Neuropathologica*, *134*(1), 97–111. <https://doi.org/10.1007/s00401-017-1688-8>
- Damme, M., Suntuio, T., Saftig, P., & Eskelinen, E.-L. (2015). Autophagy in neuronal cells: general principles and physiological and pathological functions. *Acta Neuropathologica*, *129*(3), 337–362. <https://doi.org/10.1007/s00401-014-1361-4>
- Dang, M., Kang, J., Lim, L., Li, Y., Wang, L., & Song, J. (2020). ATP is a cryptic binder of TDP-43 RRM domains to enhance stability and inhibit ALS/AD-associated fibrillation. *Biochemical and Biophysical Research Communications*, *522*(1), 247–253. <https://doi.org/10.1016/j.bbrc.2019.11.088>
- Dang, M., & Song, J. (2020). ALS-causing D169G mutation disrupts the ATP-binding capacity of TDP-43 RRM1 domain. *Biochemical and Biophysical Research Communications*, *524*(2), 459–464. <https://doi.org/10.1016/j.bbrc.2020.01.122>
- Das, M. M., & Svendsen, C. N. (2015). Astrocytes show reduced support of motor neurons with

## References

- aging that is accelerated in a rodent model of ALS. *Neurobiology of Aging*, 36(2), 1130–1139. <https://doi.org/10.1016/j.neurobiolaging.2014.09.020>
- Davis, S. A., Itaman, S., Khalid-Janney, C. M., Sherard, J. A., Dowell, J. A., Cairns, N. J., & Gitcho, M. A. (2018). TDP-43 interacts with mitochondrial proteins critical for mitophagy and mitochondrial dynamics. *Neuroscience Letters*, 678, 8–15. <https://doi.org/10.1016/j.neulet.2018.04.053>
- De Giorgio, F., Maduro, C., Fisher, E. M. C., & Acevedo-Aroza, A. (2019, January 1). Transgenic and physiological mouse models give insights into different aspects of amyotrophic lateral sclerosis. *DMM Disease Models and Mechanisms*. Company of Biologists Ltd. <https://doi.org/10.1242/dmm.037424>
- de la Ballina, L. R., Munson, M. J., & Simonsen, A. (2020). Lipids and Lipid-Binding Proteins in Selective Autophagy. *Journal of Molecular Biology*, 432(1), 135–159. <https://doi.org/10.1016/j.jmb.2019.05.051>
- De Marco, G., Lupino, E., Calvo, A., Moglia, C., Buccinnà, B., Grifoni, S., ... Chiò, A. (2011). Cytoplasmic accumulation of TDP-43 in circulating lymphomonocytes of ALS patients with and without TARDBP mutations. *Acta Neuropathologica*, 121(5), 611–622. <https://doi.org/10.1007/s00401-010-0786-7>
- DeJesus-Hernandez, M., Mackenzie, I. R., Boeve, B. F., Boxer, A. L., Baker, M., Rutherford, N. J., ... Rademakers, R. (2011). Expanded GGGGCC Hexanucleotide Repeat in Noncoding Region of C9ORF72 Causes Chromosome 9p-Linked FTD and ALS. *Neuron*, 72(2), 245–256. <https://doi.org/10.1016/j.neuron.2011.09.011>
- Demaria, M., Ohtani, N., Youssef, S. A., Rodier, F., Toussaint, W., Mitchell, J. R., ... Campisi, J. (2014). An essential role for senescent cells in optimal wound healing through secretion of PDGF-AA. *Developmental Cell*, 31(6), 722–733. <https://doi.org/10.1016/j.devcel.2014.11.012>
- Demple, B., & Harrison, L. (1994). Repair of Oxidative Damage to DNA: Enzymology and Biology. *Annual Review of Biochemistry*, 63(1), 915–948. <https://doi.org/10.1146/annurev.bi.63.070194.004411>
- Deter, R. L., & De Duve, C. (1967). Influence of glucagon, an inducer of cellular autophagy, on some physical properties of rat liver lysosomes. *The Journal of Cell Biology*, 33(2), 437–449. <https://doi.org/10.1083/jcb.33.2.437>
- Dianov, G., Bischoff, C., Piotrowski, J., Vilhelm, A., & Bohr. (1998). Repair pathways for processing of 8-oxoguanine in DNA by mammalian cell extracts. *Journal of Biological Chemistry*, 273(50), 33811–33816. <https://doi.org/10.1074/jbc.273.50.33811>
- Dias, N., & Stein, C. A. (2002, March). Antisense oligonucleotides: Basic concepts and mechanisms. *Molecular Cancer Therapeutics*.
- Díaz-Troya, S., Pérez-Pérez, M. E., Florencio, F. J., & Crespo, J. L. (2008, October 1). The role of TOR in autophagy regulation from yeast to plants and mammals. *Autophagy*. Taylor and Francis Inc. <https://doi.org/10.4161/auto.6555>

## References

- Dikic, I., & Elazar, Z. (2018). Mechanism and medical implications of mammalian autophagy. *Nature Reviews. Molecular Cell Biology*, 19(6), 349–364. <https://doi.org/10.1038/s41580-018-0003-4>
- Donnelly, C. J., Zhang, P. W., Pham, J. T., Heusler, A. R., Mistry, N. A., Vidensky, S., ... Rothstein, J. D. (2013). RNA Toxicity from the ALS/FTD C9ORF72 Expansion Is Mitigated by Antisense Intervention. *Neuron*, 80(2), 415–428. <https://doi.org/10.1016/j.neuron.2013.10.015>
- Dooley, H. C., Razi, M., Polson, H. E. J., Girardin, S. E., Wilson, M. I., & Tooze, S. A. (2014). WIPI2 links LC3 conjugation with PI3P, autophagosome formation, and pathogen clearance by recruiting Atg12-5-16L1. *Molecular Cell*, 55(2), 238–252. <https://doi.org/10.1016/j.molcel.2014.05.021>
- Duan, Y., Du, A., Gu, J., Duan, G., Wang, C., Gui, X., ... Fang, Y. (2019). PARylation regulates stress granule dynamics, phase separation, and neurotoxicity of disease-related RNA-binding proteins. *Cell Research*, 29(3), 233–247. <https://doi.org/10.1038/s41422-019-0141-z>
- Ekhtiari Bidhendi, E., Bergh, J., Zetterström, P., Forsberg, K., Pakkenberg, B., Andersen, P. M., ... Brännström, T. (2018). Mutant superoxide dismutase aggregates from human spinal cord transmit amyotrophic lateral sclerosis. *Acta Neuropathologica*, 136(6), 939–953. <https://doi.org/10.1007/s00401-018-1915-y>
- Elayadi, A. N., Braasch, D. A., & Corey, D. R. (2002). Implications of high-affinity hybridization by locked nucleic acid oligomers for inhibition of human telomerase. *Biochemistry*, 41(31), 9973–9981. <https://doi.org/10.1021/bi025907j>
- Ellegren, H. (2004, June). Microsatellites: Simple sequences with complex evolution. *Nature Reviews Genetics*. Nat Rev Genet. <https://doi.org/10.1038/nrg1348>
- Fang, T., Al Khleifat, A., Meurgey, J. H., Jones, A., Leigh, P. N., Bensimon, G., & Al-Chalabi, A. (2018). Stage at which riluzole treatment prolongs survival in patients with amyotrophic lateral sclerosis: a retrospective analysis of data from a dose-ranging study. *The Lancet Neurology*, 17(5), 416–422. [https://doi.org/10.1016/S1474-4422\(18\)30054-1](https://doi.org/10.1016/S1474-4422(18)30054-1)
- Faustino, N. A., & Cooper, T. A. (2003, February 15). Pre-mRNA splicing and human disease. *Genes and Development*. Genes Dev. <https://doi.org/10.1101/gad.1048803>
- Fecto, F., Yan, J., Vemula, S. P., Liu, E., Yang, Y., Chen, W., ... Siddique, T. (2011). SQSTM1 mutations in familial and sporadic amyotrophic lateral sclerosis. *Archives of Neurology*, 68(11), 1440–1446. <https://doi.org/10.1001/archneurol.2011.250>
- Ferrante, R. J., Browne, S. E., Shinobu, L. A., Bowling, A. C., Baik, M. J., MacGarvey, U., ... Beal, M. F. (2002). Evidence of Increased Oxidative Damage in Both Sporadic and Familial Amyotrophic Lateral Sclerosis. *Journal of Neurochemistry*, 69(5), 2064–2074. <https://doi.org/10.1046/j.1471-4159.1997.69052064.x>
- Ferrer, I. (2017). Diversity of astroglial responses across human neurodegenerative disorders and brain aging. *Brain Pathology*, 27(5), 645–674. <https://doi.org/10.1111/bpa.12538>
- Filippini, T., Fiore, M., Tesauro, M., Malagoli, C., Consonni, M., Violi, F., ... Vinceti, M. (2020).

## References

- Clinical and lifestyle factors and risk of amyotrophic lateral sclerosis: A population-based case-control study. *International Journal of Environmental Research and Public Health*, 17(3). <https://doi.org/10.3390/ijerph17030857>
- Forsberg, K., Graffmo, K., Pakkenberg, B., Weber, M., Nielsen, M., Marklund, S., ... Andersen, P. M. (2019). Misfolded SOD1 inclusions in patients with mutations in C9orf72 and other ALS/FTD-associated genes. *Journal of Neurology, Neurosurgery, and Psychiatry*, 90(8), 861–869. <https://doi.org/10.1136/jnnp-2018-319386>
- Forsberg, K., Jonsson, P. A., Andersen, P. M., Bergemalm, D., Graffmo, K. S., Hultdin, M., ... Brännström, T. (2010). Novel antibodies reveal inclusions containing non-native SOD1 in sporadic ALS patients. *PloS One*, 5(7), e11552. <https://doi.org/10.1371/journal.pone.0011552>
- Franceschi, C., & Campisi, J. (2014). Chronic inflammation (inflammaging) and its potential contribution to age-associated diseases. *The Journals of Gerontology. Series A, Biological Sciences and Medical Sciences*, 69 Suppl 1, S4-9. <https://doi.org/10.1093/gerona/glu057>
- Fratta, P., Mizielińska, S., Nicoll, A. J., Zloh, M., Fisher, E. M. C., Parkinson, G., & Isaacs, A. M. (2012). C9orf72 hexanucleotide repeat associated with amyotrophic lateral sclerosis and frontotemporal dementia forms RNA G-quadruplexes. *Scientific Reports*, 2, 1016. <https://doi.org/10.1038/srep01016>
- Frazier, K. S. (2015). Antisense Oligonucleotide Therapies: The Promise and the Challenges from a Toxicologic Pathologist's Perspective. *Toxicologic Pathology*, 43(1), 78–89. <https://doi.org/10.1177/0192623314551840>
- Freibaum, B. D., Lu, Y., Lopez-Gonzalez, R., Kim, N. C., Almeida, S., Lee, K. H., ... Taylor, J. P. (2015). GGGGCC repeat expansion in C9orf72 compromises nucleocytoplasmic transport. *Nature*, 525(7567), 129–133. <https://doi.org/10.1038/nature14974>
- Freibaum, B. D., & Taylor, J. P. (2017). The Role of Dipeptide Repeats in C9ORF72-Related ALS-FTD. *Frontiers in Molecular Neuroscience*, 10, 35. <https://doi.org/10.3389/fnmol.2017.00035>
- French, R. L., Grese, Z. R., Aligireddy, H., Dhavale, D. D., Reeb, A. N., Kedia, N., ... Ayala, Y. M. (2019). Detection of TAR DNA-binding protein 43 (TDP-43) oligomers as initial intermediate species during aggregate formation. *The Journal of Biological Chemistry*, 294(17), 6696–6709. <https://doi.org/10.1074/jbc.RA118.005889>
- Furukawa, Y., Kaneko, K., Watanabe, S., Yamanaka, K., & Nukina, N. (2011). A seeding reaction recapitulates intracellular formation of Sarkosyl-insoluble transactivation response element (TAR) DNA-binding protein-43 inclusions. *The Journal of Biological Chemistry*, 286(21), 18664–18672. <https://doi.org/10.1074/jbc.M111.231209>
- Gajdusek, D. C., Gibbs, C. J., & Alpers, M. (1966). Experimental transmission of a kuru-like syndrome to chimpanzees. *Nature*, 209(5025), 794–796. <https://doi.org/10.1038/209794a0>
- Gal, J., Ström, A.-L., Kwinter, D. M., Kilty, R., Zhang, J., Shi, P., ... Zhu, H. (2009). Sequestosome 1/p62 links familial ALS mutant SOD1 to LC3 via an ubiquitin-independent mechanism. *Journal of Neurochemistry*, 111(4), 1062–1073. <https://doi.org/10.1111/j.1471->

## References

4159.2009.06388.x

- Gal, J., Zhang, J., Kwinter, D. M., Zhai, J., Jia, H., Jia, J., & Zhu, H. (2011). Nuclear localization sequence of FUS and induction of stress granules by ALS mutants. *Neurobiology of Aging*, *32*(12), 2323.e27-40. <https://doi.org/10.1016/j.neurobiolaging.2010.06.010>
- Gami, P., Murray, C., Schottlaender, L., Bettencourt, C., De Pablo Fernandez, E., Mudanohwo, E., ... Lashley, T. (2015, October 26). A 30-unit hexanucleotide repeat expansion in C9orf72 induces pathological lesions with dipeptide-repeat proteins and RNA foci, but not TDP-43 inclusions and clinical disease. *Acta Neuropathologica*. Springer Verlag. <https://doi.org/10.1007/s00401-015-1473-5>
- Ganesalingam, J., Stahl, D., Wijesekera, L., Galtrey, C., Shaw, C. E., Leigh, P. N., & Al-Chalabi, A. (2009). Latent cluster analysis of ALS phenotypes identifies prognostically differing groups. *PloS One*, *4*(9), e7107. <https://doi.org/10.1371/journal.pone.0007107>
- Gargiulo, S., Anzilotti, S., Coda, A. R. D., Gramanzini, M., Greco, A., Panico, M., ... Pappatà, S. (2016). Imaging of brain TSPO expression in a mouse model of amyotrophic lateral sclerosis with 18F-DPA-714 and micro-PET/CT. *European Journal of Nuclear Medicine and Molecular Imaging*, *43*(7), 1348–1359. <https://doi.org/10.1007/s00259-016-3311-y>
- Gauthier, S., Feldman, H. H., Schneider, L. S., Wilcock, G. K., Frisoni, G. B., Hardlund, J. H., ... Wischik, C. M. (2016). Efficacy and safety of tau-aggregation inhibitor therapy in patients with mild or moderate Alzheimer's disease: a randomised, controlled, double-blind, parallel-arm, phase 3 trial. *Lancet (London, England)*, *388*(10062), 2873–2884. [https://doi.org/10.1016/S0140-6736\(16\)31275-2](https://doi.org/10.1016/S0140-6736(16)31275-2)
- Geary, R. S. (2009). Antisense oligonucleotide pharmacokinetics and metabolism. *Expert Opinion on Drug Metabolism & Toxicology*, *5*(4), 381–391. <https://doi.org/10.1517/17425250902877680>
- Gerbino, V., Kaunga, E., Ye, J., Canzio, D., O'Keeffe, S., Rudnick, N. D., ... Maniatis, T. (2020). The Loss of TBK1 Kinase Activity in Motor Neurons or in All Cell Types Differentially Impacts ALS Disease Progression in SOD1 Mice. *Neuron*. <https://doi.org/10.1016/j.neuron.2020.03.005>
- Gertsman, I., Wu, J., McAlonis-Downes, M., Ghassemian, M., Ling, K., Rigo, F., ... Da Cruz, S. (2019). An endogenous peptide marker differentiates SOD1 stability and facilitates pharmacodynamic monitoring in SOD1 amyotrophic lateral sclerosis. *JCI Insight*, *4*(10). <https://doi.org/10.1172/jci.insight.122768>
- Gibson, S. B., Downie, J. M., Tsetsou, S., Feusier, J. E., Figueroa, K. P., Bromberg, M. B., ... Pulst, S. M. (2017). The evolving genetic risk for sporadic ALS. *Neurology*, *89*(3), 226–233. <https://doi.org/10.1212/WNL.0000000000004109>
- Goberdhan, D. C. I., Wilson, C., & Harris, A. L. (2016). Amino Acid Sensing by mTORC1: Intracellular Transporters Mark the Spot. *Cell Metabolism*, *23*(4), 580–589. <https://doi.org/10.1016/j.cmet.2016.03.013>



## References

- Golde, T. E., & Miller, V. M. (2009). Proteinopathy-induced neuronal senescence: a hypothesis for brain failure in Alzheimer's and other neurodegenerative diseases. *Alzheimer's Research & Therapy*, 1(2), 5. <https://doi.org/10.1186/alzrt5>
- Grad, L. I., Yerbury, J. J., Turner, B. J., Guest, W. C., Pokrishevsky, E., O'Neill, M. A., ... Cashman, N. R. (2014). Intercellular propagated misfolding of wild-type Cu/Zn superoxide dismutase occurs via exosome-dependent and -independent mechanisms. *Proceedings of the National Academy of Sciences of the United States of America*, 111(9), 3620–3625. <https://doi.org/10.1073/pnas.1312245111>
- Gray, E., Larkin, J. R., Claridge, T. D. W., Talbot, K., Sibson, N. R., & Turner, M. R. (2015). The longitudinal cerebrospinal fluid metabolomic profile of amyotrophic lateral sclerosis. *Amyotrophic Lateral Sclerosis and Frontotemporal Degeneration*, 16(7–8), 456–463. <https://doi.org/10.3109/21678421.2015.1053490>
- Guillouf, C., Graña, X., Selvakumaran, M., De Luca, A., Giordano, A., Hoffman, B., & Liebermann, D. A. (1995). Dissection of the genetic programs of p53-mediated G1 growth arrest and apoptosis: blocking p53-induced apoptosis unmask G1 arrest. *Blood*, 85(10), 2691–2698. Retrieved from <http://www.ncbi.nlm.nih.gov/pubmed/7742528>
- Guo, H., Lai, L., Butchbach, M. E. R., Stockinger, M. P., Shan, X., Bishop, G. A., & Lin, C. G. (2003). Increased expression of the glial glutamate transporter EAAT2 modulates excitotoxicity and delays the onset but not the outcome of ALS in mice. *Human Molecular Genetics*, 12(19), 2519–2532. <https://doi.org/10.1093/hmg/ddg267>
- Guo, Q., Lehmer, C., Martínez-Sánchez, A., Rudack, T., Beck, F., Hartmann, H., ... Fernández-Busnadiego, R. (2018). In Situ Structure of Neuronal C9orf72 Poly-GA Aggregates Reveals Proteasome Recruitment. *Cell*, 172(4), 696-705.e12. <https://doi.org/10.1016/j.cell.2017.12.030>
- Gurney, M. E., Pu, H., Chiu, A. Y., Dal Canto, M. C., Polchow, C. Y., Alexander, D. D., ... Siddique, T. (1994). Motor neuron degeneration in mice that express a human Cu,Zn superoxide dismutase mutation. *Science*, 264(5166), 1772–1775. <https://doi.org/10.1126/science.8209258>
- Hadano, S., Hand, C. K., Osuga, H., Yanagisawa, Y., Otomo, A., Devon, R. S., ... Ikeda, J. E. (2001). A gene encoding a putative GTPase regulator is mutated in familial amyotrophic lateral sclerosis 2. *Nature Genetics*, 29(2), 166–173. <https://doi.org/10.1038/ng1001-166>
- Haidet-Phillips, A. M., Hester, M. E., Miranda, C. J., Meyer, K., Braun, L., Frakes, A., ... Kaspar, B. K. (2011). Astrocytes from familial and sporadic ALS patients are toxic to motor neurons. *Nature Biotechnology*, 29(9), 824–828. <https://doi.org/10.1038/nbt.1957>
- Hajian-Tilaki, K. (2013). Receiver operating characteristic (ROC) curve analysis for medical diagnostic test evaluation. *Caspian Journal of Internal Medicine*.
- Hamidou, B., Couratier, P., Besançon, C., Nicol, M., Preux, P. M., & Marin, B. (2014). Epidemiological evidence that physical activity is not a risk factor for ALS. *European Journal of Epidemiology*, 29(7), 459–475. <https://doi.org/10.1007/s10654-014-9923-2>

## References

- Hammond, S. M., Hazell, G., Shabanpoor, F., Saleh, A. F., Bowerman, M., Sleigh, J. N., ... Wood, M. J. A. (2016). Systemic peptide-mediated oligonucleotide therapy improves long-term survival in spinal muscular atrophy. *Proceedings of the National Academy of Sciences of the United States of America*, *113*(39), 10962–10967. <https://doi.org/10.1073/pnas.1605731113>
- Hardy, J., & Allsop, D. (1991). Amyloid deposition as the central event in the aetiology of Alzheimer's disease. *Trends in Pharmacological Sciences*. [https://doi.org/10.1016/0165-6147\(91\)90609-V](https://doi.org/10.1016/0165-6147(91)90609-V)
- HARMAN, D. (1956). Aging: a theory based on free radical and radiation chemistry. *Journal of Gerontology*, *11*(3), 298–300. <https://doi.org/10.1093/geronj/11.3.298>
- Hayashi, Y., Homma, K., & Ichijo, H. (2016, January 1). SOD1 in neurotoxicity and its controversial roles in SOD1 mutation-negative ALS. *Advances in Biological Regulation*. Elsevier Ltd. <https://doi.org/10.1016/j.jbior.2015.10.006>
- Hayflick, L. (1965). The limited in vitro lifetime of human diploid cell strains. *Experimental Cell Research*, *37*(3), 614–636. [https://doi.org/10.1016/0014-4827\(65\)90211-9](https://doi.org/10.1016/0014-4827(65)90211-9)
- Hayyan, M., Hashim, M. A., & Alnashef, I. M. (2016, March 9). Superoxide Ion: Generation and Chemical Implications. *Chemical Reviews*. American Chemical Society. <https://doi.org/10.1021/acs.chemrev.5b00407>
- He, S., & Sharpless, N. E. (2017, June 1). Senescence in Health and Disease. *Cell*. Cell Press. <https://doi.org/10.1016/j.cell.2017.05.015>
- Hebert, L. E., Weuve, J., Scherr, P. A., & Evans, D. A. (2013). Alzheimer disease in the United States (2010-2050) estimated using the 2010 census. *Neurology*, *80*(19), 1778–1783. <https://doi.org/10.1212/WNL.0b013e31828726f5>
- Hedl, T. J., Gil, R. S., Cheng, F., Rayner, S. L., Davidson, J. M., Luca, A. De, ... Lee, A. (2019). Proteomics approaches for biomarker and drug target discovery in als and ftd. *Frontiers in Neuroscience*. Frontiers Media S.A. <https://doi.org/10.3389/fnins.2019.00548>
- Hefferon, T. W., Groman, J. D., Yurk, C. E., & Cutting, G. R. (2004). A variable dinucleotide repeat in the CFTR gene contributes to phenotype diversity by forming RNA secondary structures that affect splicing. *Proceedings of the National Academy of Sciences of the United States of America*, *101*(10), 3504–3509. <https://doi.org/10.1073/pnas.0400182101>
- Henkel, J. S., Beers, D. R., Zhao, W., & Appel, S. H. (2009). Microglia in ALS: the good, the bad, and the resting. *Journal of Neuroimmune Pharmacology: The Official Journal of the Society on Neuroimmune Pharmacology*, *4*(4), 389–398. <https://doi.org/10.1007/s11481-009-9171-5>
- Hensley, K., Abdel-Moaty, H., Hunter, J., Mhatre, M., Mou, S., Nguyen, K., ... West, M. (2006). Primary glia expressing the G93A-SOD1 mutation present a neuroinflammatory phenotype and provide a cellular system for studies of glial inflammation. *Journal of Neuroinflammation*, *3*, 2. <https://doi.org/10.1186/1742-2094-3-2>
- Hergesheimer, R. C., Chami, A. A., de Assis, D. R., Vourc'h, P., Andres, C. R., Corcia, P., ... Blasco, H. (2019). The debated toxic role of aggregated TDP-43 in amyotrophic lateral

## References

- sclerosis: a resolution in sight? *Brain : A Journal of Neurology*, 142(5), 1176–1194.  
<https://doi.org/10.1093/brain/awz078>
- Herman, A. M., Khandelwal, P. J., Stanczyk, B. B., Rebeck, G. W., & Moussa, C. E. H. (2011).  $\beta$ -Amyloid triggers ALS-associated TDP-43 pathology in AD models. *Brain Research*, 1386, 191–199. <https://doi.org/10.1016/j.brainres.2011.02.052>
- Hernandez-Segura, A., Nehme, J., & Demaria, M. (2018, June 1). Hallmarks of Cellular Senescence. *Trends in Cell Biology*. Elsevier Ltd. <https://doi.org/10.1016/j.tcb.2018.02.001>
- Herrero, A., & Barja, G. (2000). Localization of the site of oxygen radical generation inside the complex I of heart and nonsynaptic brain mammalian mitochondria. *Journal of Bioenergetics and Biomembranes*, 32(6), 609–615. <https://doi.org/10.1023/A:1005626712319>
- Higelin, J., Catanese, A., Semelink-Sedlacek, L. L., Oeztuerk, S., Lutz, A.-K., Bausinger, J., ... Boeckers, T. M. (2018). NEK1 loss-of-function mutation induces DNA damage accumulation in ALS patient-derived motoneurons. *Stem Cell Research*, 30, 150–162.  
<https://doi.org/10.1016/j.scr.2018.06.005>
- Hillman, R. T., Green, R. E., & Brenner, S. E. (2004). An unappreciated role for RNA surveillance. *Genome Biology*, 5(2). <https://doi.org/10.1186/gb-2004-5-2-r8>
- Hirata, E., Ohya, Y., & Suzuki, K. (2017). Atg4 plays an important role in efficient expansion of autophagic isolation membranes by cleaving lipidated Atg8 in *Saccharomyces cerevisiae*. *PloS One*, 12(7), e0181047. <https://doi.org/10.1371/journal.pone.0181047>
- Hoelz, A., Debler, E. W., & Blobel, G. (2011). The Structure of the Nuclear Pore Complex. *Annual Review of Biochemistry*, 80(1), 613–643. <https://doi.org/10.1146/annurev-biochem-060109-151030>
- Hoelz, A., Glavy, J. S., & Beck, M. (2016). Toward the atomic structure of the nuclear pore complex: when top down meets bottom up. *Nature Structural & Molecular Biology*, 23(7), 624–630. <https://doi.org/10.1038/nsmb.3244>
- Högyes, E., Nyakas, C., Kiliaan, A., Farkas, T., Penke, B., & Luiten, P. G. M. (2003). Neuroprotective effect of developmental docosahexaenoic acid supplement against excitotoxic brain damage in infant rats. *Neuroscience*, 119(4), 999–1012.  
[https://doi.org/10.1016/S0306-4522\(03\)00198-2](https://doi.org/10.1016/S0306-4522(03)00198-2)
- Hong, S., Gronert, K., Devchand, P. R., Moussignac, R. L., & Serhan, C. N. (2003). Novel docosatrienes and 17S-resolvins generated from docosahexaenoic acid in murine brain, human blood, and glial cells: Autacoids in anti-inflammation. *Journal of Biological Chemistry*, 278(17), 14677–14687. <https://doi.org/10.1074/jbc.M300218200>
- Hua, Y., Vickers, T. A., Okunola, H. L., Bennett, C. F., & Krainer, A. R. (2008). Antisense Masking of an hnRNP A1/A2 Intronic Splicing Silencer Corrects SMN2 Splicing in Transgenic Mice. *American Journal of Human Genetics*, 82(4), 834–848.  
<https://doi.org/10.1016/j.ajhg.2008.01.014>
- Hudson, E. K., Hogue, B. A., Souza-Pinto, N. C., Croteau, D. L., Anson, R. M., Bohr, V. A., &

## References

- Hansford, R. G. (1998). Age-associated change in mitochondrial DNA damage. *Free Radical Research*, 29(6), 573–579. <https://doi.org/10.1080/10715769800300611>
- Huisman, M. H. B., Seelen, M., De Jong, S. W., Dorresteyn, K. R. I. S., Van Doormaal, P. T. C., Van Der Kooij, A. J., ... Veldink, J. H. (2013). Lifetime physical activity and the risk of amyotrophic lateral sclerosis. *Journal of Neurology, Neurosurgery and Psychiatry*, 84(9), 976–981. <https://doi.org/10.1136/jnnp-2012-304724>
- Humphrey, J., Emmett, W., Fratta, P., Isaacs, A. M., & Plagnol, V. (2017). Quantitative analysis of cryptic splicing associated with TDP-43 depletion. *BMC Medical Genomics*, 10(1), 38. <https://doi.org/10.1186/s12920-017-0274-1>
- Hyman, A. A., Weber, C. A., & Jülicher, F. (2014). Liquid-Liquid Phase Separation in Biology. *Annual Review of Cell and Developmental Biology*, 30(1), 39–58. <https://doi.org/10.1146/annurev-cellbio-100913-013325>
- Iguchi, Y., Katsuno, M., Niwa, J.-I., Takagi, S., Ishigaki, S., Ikenaka, K., ... Sobue, G. (n.d.). Loss of TDP-43 causes age-dependent progressive motor neuron degeneration. *A JOURNAL OF NEUROLOGY*. <https://doi.org/10.1093/brain/awt029>
- Ilieva, E. V., Ayala, V., Jove, M., Dalfo, E., Cacabelos, D., Povedano, M., ... Portero-Otin, M. (2007). Oxidative and endoplasmic reticulum stress interplay in sporadic amyotrophic lateral sclerosis. *Brain*, 130(12), 3111–3123. <https://doi.org/10.1093/brain/awm190>
- Ironside, J. W. (2012). Variant Creutzfeldt-Jakob disease: an update. *Folia Neuropathologica*, 50(1), 50–56. Retrieved from <http://www.ncbi.nlm.nih.gov/pubmed/22505363>
- Jaarsma, D., Haasdijk, E. D., Grashorn, J. A., Hawkins, R., van Duijn, W., Verspaget, H. W., ... Holstege, J. C. (2000). Human Cu/Zn superoxide dismutase (SOD1) overexpression in mice causes mitochondrial vacuolization, axonal degeneration, and premature motoneuron death and accelerates motoneuron disease in mice expressing a familial amyotrophic lateral sclerosis mutant SOD1. *Neurobiology of Disease*, 7(6 Pt B), 623–643. <https://doi.org/10.1006/nbdi.2000.0299>
- Jahreiss, L., Menzies, F. M., & Rubinsztein, D. C. (2008). The itinerary of autophagosomes: from peripheral formation to kiss-and-run fusion with lysosomes. *Traffic (Copenhagen, Denmark)*, 9(4), 574–587. <https://doi.org/10.1111/j.1600-0854.2008.00701.x>
- Jeon, G. S., Shim, Y.-M., Lee, D.-Y., Kim, J.-S., Kang, M., Ahn, S. H., ... Sung, J.-J. (2019). Pathological Modification of TDP-43 in Amyotrophic Lateral Sclerosis with SOD1 Mutations. *Molecular Neurobiology*, 56(3), 2007–2021. <https://doi.org/10.1007/s12035-018-1218-2>
- Jeon, O. H., Kim, C., Laberge, R.-M., Demaria, M., Rathod, S., Vasserot, A. P., ... Elisseeff, J. H. (2017). Local clearance of senescent cells attenuates the development of post-traumatic osteoarthritis and creates a pro-regenerative environment. *Nature Medicine*, 23(6), 775–781. <https://doi.org/10.1038/nm.4324>
- Jeong, Y. H., Ling, J. P., Lin, S. Z., Donde, A. N., Braunstein, K. E., Majounie, E., ... Wong, P. C. (2017). Tdp-43 cryptic exons are highly variable between cell types. *Molecular*

## References

- Neurodegeneration*, 12(1), 13. <https://doi.org/10.1186/s13024-016-0144-x>
- Jiang, J., Zhu, Q., Gendron, T. F., Saberi, S., McAlonis-Downes, M., Seelman, A., ... Lagier-Tourenne, C. (2016). Gain of Toxicity from ALS/FTD-Linked Repeat Expansions in C9ORF72 Is Alleviated by Antisense Oligonucleotides Targeting GGGGCC-Containing RNAs. *Neuron*, 90(3), 535–550. <https://doi.org/10.1016/j.neuron.2016.04.006>
- Jiang, L.-L., Xue, W., Hong, J.-Y., Zhang, J.-T., Li, M.-J., Yu, S.-N., ... Hu, H.-Y. (2017). The N-terminal dimerization is required for TDP-43 splicing activity. *Scientific Reports*, 7(1), 6196. <https://doi.org/10.1038/s41598-017-06263-3>
- Jiang, P., Nishimura, T., Sakamaki, Y., Itakura, E., Hatta, T., Natsume, T., & Mizushima, N. (2014). The HOPS complex mediates autophagosome-lysosome fusion through interaction with syntaxin 17. *Molecular Biology of the Cell*, 25(8), 1327–1337. <https://doi.org/10.1091/mbc.E13-08-0447>
- Jin, Y., Yang, Y., & Zhang, P. (2011). New insights into RNA secondary structure in the alternative splicing of pre-mRNAs. *RNA Biology*. Taylor and Francis Inc. <https://doi.org/10.4161/rna.8.3.15388>
- Jo, Y. K., Park, N. Y., Park, S. J., Kim, B.-G., Shin, J. H., Jo, D. S., ... Cho, D.-H. (2016). O-GlcNAcylation of ATG4B positively regulates autophagy by increasing its hydroxylase activity. *Oncotarget*, 7(35), 57186–57196. <https://doi.org/10.18632/oncotarget.11083>
- Johnson, B. S., Snead, D., Lee, J. J., McCaffery, J. M., Shorter, J., & Gitler, A. D. (2009). TDP-43 is intrinsically aggregation-prone, and amyotrophic lateral sclerosis-linked mutations accelerate aggregation and increase toxicity. *The Journal of Biological Chemistry*, 284(30), 20329–20339. <https://doi.org/10.1074/jbc.M109.010264>
- Johnson, J. M., Castle, J., Garrett-Engele, P., Kan, Z., Loerch, P. M., Armour, C. D., ... Shoemaker, D. D. (2003). Genome-Wide Survey of Human Alternative Pre-mRNA Splicing with Exon Junction Microarrays. *Science*, 302(5653), 2141–2144. <https://doi.org/10.1126/science.1090100>
- Johnson, J. O., Mandrioli, J., Benatar, M., Abramzon, Y., Van Deerlin, V. M., Trojanowski, J. Q., ... Traynor, B. J. (2010). Exome sequencing reveals VCP mutations as a cause of familial ALS. *Neuron*, 68(5), 857–864. <https://doi.org/10.1016/j.neuron.2010.11.036>
- Jonsson, P. A., Graffmo, K. S., Andersen, P. M., Brännström, T., Lindberg, M., Oliveberg, M., & Marklund, S. L. (2006). Disulphide-reduced superoxide dismutase-1 in CNS of transgenic amyotrophic lateral sclerosis models. *Brain: A Journal of Neurology*, 129(Pt 2), 451–464. <https://doi.org/10.1093/brain/awh704>
- Jove, M., Mauri-Capdevila, G., Suarez, I., Cambray, S., Sanahuja, J., Quilez, A., ... Purroy, F. (2015). Metabolomics predicts stroke recurrence after transient ischemic attack. *Neurology*, 84(1), 36–45. <https://doi.org/10.1212/WNL.0000000000001093>
- Joyce, P. I., MCGoldrick, P., Saccon, R. A., Weber, W., Fratta, P., West, S. J., ... Acevedo-Arozena, A. (2015). A novel SOD1-ALS mutation separates central and peripheral effects of

## References

- mutant SOD1 toxicity. *Human Molecular Genetics*, 24(7), 1883–1897.  
<https://doi.org/10.1093/hmg/ddu605>
- Kametaka, S., Matsuura, A., Wada, Y., & Ohsumi, Y. (1996). Structural and functional analyses of APG5, a gene involved in autophagy in yeast. *Gene*, 178(1–2), 139–143.  
[https://doi.org/10.1016/0378-1119\(96\)00354-X](https://doi.org/10.1016/0378-1119(96)00354-X)
- Kametani, F., & Hasegawa, M. (2018). Reconsideration of Amyloid Hypothesis and Tau Hypothesis in Alzheimer's Disease. *Frontiers in Neuroscience*, 12(JAN), 25.  
<https://doi.org/10.3389/fnins.2018.00025>
- Kane, A. E., Sinclair, D. A., Mitchell, J. R., & Mitchell, S. J. (2018, December 1). Sex differences in the response to dietary restriction in rodents. *Current Opinion in Physiology*. Elsevier Ltd.  
<https://doi.org/10.1016/j.cophys.2018.03.008>
- Kaneb, H. M., Folkmann, A. W., Belzil, V. V., Jao, L.-E., Leblond, C. S., Girard, S. L., ... Dion, P. A. (2015). Deleterious mutations in the essential mRNA metabolism factor, hGle1, in amyotrophic lateral sclerosis. *Human Molecular Genetics*, 24(5), 1363–1373.  
<https://doi.org/10.1093/hmg/ddu545>
- Kantarci, A., Aytan, N., Palaska, I., Stephens, D., Crabtree, L., Benincasa, C., ... Dedeoglu, A. (2018). Combined administration of resolvin E1 and lipoxin A4 resolves inflammation in a murine model of Alzheimer's disease. *Experimental Neurology*, 300, 111–120.  
<https://doi.org/10.1016/j.expneurol.2017.11.005>
- Kapustin, Y., Chan, E., Sarkar, R., Wong, F., Vorechovsky, I., Winston, R. M., ... Dibb, N. J. (n.d.). Cryptic splice sites and split genes. <https://doi.org/10.1093/nar/gkr203>
- Kato, M., Han, T. W., Xie, S., Shi, K., Du, X., Wu, L. C., ... McKnight, S. L. (2012). Cell-free formation of RNA granules: Low complexity sequence domains form dynamic fibers within hydrogels. *Cell*, 149(4), 753–767. <https://doi.org/10.1016/j.cell.2012.04.017>
- Kedersha, N., & Anderson, P. (2002). Stress granules: Sites of mRNA triage that regulate mRNA stability and translatability. In *Biochemical Society Transactions* (Vol. 30, pp. 963–969).  
<https://doi.org/10.1042/BST0300963>
- Khosravi, B., LaClair, K. D., Riemenschneider, H., Zhou, Q., Frottin, F., Mareljic, N., ... Edbauer, D. (2020). Cell-to-cell transmission of C9orf72 poly-(Gly-Ala) triggers key features of ALS/FTD. *The EMBO Journal*, e102811. <https://doi.org/10.15252/embj.2019102811>
- Kiernan, M. C., Vucic, S., Cheah, B. C., Turner, M. R., Eisen, A., Hardiman, O., ... Zoing, M. C. (2011). Amyotrophic lateral sclerosis. In *The Lancet* (Vol. 377, pp. 942–955).  
[https://doi.org/10.1016/S0140-6736\(10\)61156-7](https://doi.org/10.1016/S0140-6736(10)61156-7)
- Kikuchi, H., Furuta, A., Nishioka, K., Suzuki, S. O., Nakabeppu, Y., & Iwaki, T. (2002). Impairment of mitochondrial DNA repair enzymes against accumulation of 8-oxo-guanine in the spinal motor neurons of amyotrophic lateral sclerosis. *Acta Neuropathologica*, 103(4), 408–414.  
<https://doi.org/10.1007/s00401-001-0480-x>
- Kim, B. W., Jeong, Y. E., Wong, M., & Martin, L. J. (2020). DNA damage accumulates and

## References

- responses are engaged in human ALS brain and spinal motor neurons and DNA repair is activatable in iPSC-derived motor neurons with SOD1 mutations. *Acta Neuropathologica Communications*, 8(1). <https://doi.org/10.1186/s40478-019-0874-4>
- King, A. E., Woodhouse, A., Kirkcaldie, M. T. K., & Vickers, J. C. (2016). Excitotoxicity in ALS: Overstimulation, or overreaction? *Experimental Neurology*, 275 Pt 1, 162–171. <https://doi.org/10.1016/j.expneurol.2015.09.019>
- Kisby, G. E., Milne, J., & Sweatt, C. (1997). Evidence of reduced DNA repair in amyotrophic lateral sclerosis brain tissue. *NeuroReport*, 8(6), 1337–1340. <https://doi.org/10.1097/00001756-199704140-00004>
- Klionsky, D. J., Cregg, J. M., Dunn, W. A., Emr, S. D., Sakai, Y., Sandoval, I. V., ... Ohsumi, Y. (2003, October 1). A unified nomenclature for yeast autophagy-related genes. *Developmental Cell*. [https://doi.org/10.1016/S1534-5807\(03\)00296-X](https://doi.org/10.1016/S1534-5807(03)00296-X)
- Köhler, A., & Hurt, E. (2007, October). Exporting RNA from the nucleus to the cytoplasm. *Nature Reviews Molecular Cell Biology*. <https://doi.org/10.1038/nrm2255>
- Konopka, A., & Atkin, J. D. (2018). The Emerging Role of DNA Damage in the Pathogenesis of the C9orf72 Repeat Expansion in Amyotrophic Lateral Sclerosis. *International Journal of Molecular Sciences*, 19(10). <https://doi.org/10.3390/ijms19103137>
- Krashia, P., Cordella, A., Nobili, A., La Barbera, L., Federici, M., Leuti, A., ... Mercuri, N. B. (2019). Blunting neuroinflammation with resolvin D1 prevents early pathology in a rat model of Parkinson's disease. *Nature Communications*, 10(1). <https://doi.org/10.1038/s41467-019-11928-w>
- Kroemer, G., & Levine, B. (2008). Autophagic cell death: the story of a misnomer. *Nature Reviews Molecular Cell Biology*, 9(12), 1004–1010. <https://doi.org/10.1038/nrm2529>
- Kuang, E., Okumura, C. Y. M., Sheffy-Levin, S., Varsano, T., Shu, V. C.-W., Qi, J., ... Ronai, Z. A. (2012). Regulation of ATG4B stability by RNF5 limits basal levels of autophagy and influences susceptibility to bacterial infection. *PLoS Genetics*, 8(10), e1003007. <https://doi.org/10.1371/journal.pgen.1003007>
- Kueffner, R., Zach, N., Bronfeld, M., Norel, R., Atassi, N., Balagurusamy, V., ... Stolovitzky, G. (2019). Stratification of amyotrophic lateral sclerosis patients: a crowdsourcing approach. *Scientific Reports*, 9(1), 690. <https://doi.org/10.1038/s41598-018-36873-4>
- Kumar, V., Hasan, G. M., & Hassan, M. I. (2017, December 15). Unraveling the role of RNA mediated toxicity of C9orf72 repeats in C9-FTD/ALS. *Frontiers in Neuroscience*. Frontiers Media S.A. <https://doi.org/10.3389/fnins.2017.00711>
- Kuo, P. H., Doudeva, L. G., Wang, Y. T., Shen, C. K. J., & Yuan, H. S. (2009). Structural insights into TDP-43 in nucleic-acid binding and domain interactions. *Nucleic Acids Research*, 37(6), 1799–1808. <https://doi.org/10.1093/nar/gkp013>
- Kurz, D. J., Decary, S., Hong, Y., & Erusalimsky, J. D. (2000). Senescence-associated (beta)-galactosidase reflects an increase in lysosomal mass during replicative ageing of human

## References

- endothelial cells. *Journal of Cell Science*, 113(Pt 20), 3613–3622.
- Kuuluvainen, L., Kaivola, K., Mönkäre, S., Laaksovirta, H., Jokela, M., Udd, B., ... Myllykangas, L. (2019). Oligogenic basis of sporadic ALS: The example of SOD1 p.Ala90Val mutation. *Neurology. Genetics*, 5(3), e335. <https://doi.org/10.1212/NXG.0000000000000335>
- LaClair, K. D., Donde, A., Ling, J. P., Jeong, Y. H., Chhabra, R., Martin, L. J., & Wong, P. C. (2016). Depletion of TDP-43 decreases fibril and plaque  $\beta$ -amyloid and exacerbates neurodegeneration in an Alzheimer's mouse model. *Acta Neuropathologica*, 132(6), 859–873. <https://doi.org/10.1007/s00401-016-1637-y>
- Lagier-Tourenne, C., Baughn, M., Rigo, F., Sun, S., Liu, P., Li, H. R., ... Ravits, J. (2013). Targeted degradation of sense and antisense C9orf72 RNA foci as therapy for ALS and frontotemporal degeneration. *Proceedings of the National Academy of Sciences of the United States of America*, 110(47). <https://doi.org/10.1073/pnas.1318835110>
- Lander, E. S., Linton, L. M., Birren, B., Nusbaum, C., Zody, M. C., Baldwin, J., ... Morgan, M. J. (2001). Initial sequencing and analysis of the human genome. *Nature*, 409(6822), 860–921. <https://doi.org/10.1038/35057062>
- Lavin, M. F., & Gueven, N. (2006). The complexity of p53 stabilization and activation. *Cell Death and Differentiation*, 13(6), 941–950. <https://doi.org/10.1038/sj.cdd.4401925>
- Lawton, K. A., Brown, M. V., Alexander, D., Li, Z., Wulff, J. E., Lawson, R., ... Berry, J. D. (2014). Plasma metabolomic biomarker panel to distinguish patients with amyotrophic lateral sclerosis from disease mimics. *Amyotrophic Lateral Sclerosis and Frontotemporal Degeneration*, 15(5–6), 362–370. <https://doi.org/10.3109/21678421.2014.908311>
- Lee, J.-H., & Paull, T. T. (2007). Activation and regulation of ATM kinase activity in response to DNA double-strand breaks. *Oncogene*, 26(56), 7741–7748. <https://doi.org/10.1038/sj.onc.1210872>
- Lehmer, C., Oeckl, P., Weishaupt, J. H., Volk, A. E., Diehl-Schmid, J., Schroeter, M. L., ... Otto, M. (2017). Poly-GP in cerebrospinal fluid links C9orf72-associated dipeptide repeat expression to the asymptomatic phase of ALS/FTD. *EMBO Molecular Medicine*, 9(7), 859–868. <https://doi.org/10.15252/emmm.201607486>
- Li, M., Hou, Y., Wang, J., Chen, X., Shao, Z.-M., & Yin, X.-M. (2011). Kinetics comparisons of mammalian Atg4 homologues indicate selective preferences toward diverse Atg8 substrates. *The Journal of Biological Chemistry*, 286(9), 7327–7338. <https://doi.org/10.1074/jbc.M110.199059>
- Lin, W.-L., & Dickson, D. W. (2008). Ultrastructural localization of TDP-43 in filamentous neuronal inclusions in various neurodegenerative diseases. *Acta Neuropathologica*, 116(2), 205–213. <https://doi.org/10.1007/s00401-008-0408-9>
- Ling, J. P., Pletnikova, O., Troncoso, J. C., & Wong, P. C. (2015). TDP-43 repression of nonconserved cryptic exons is compromised in ALS-FTD. *Science*, 349(6248), 650–655. <https://doi.org/10.1126/science.aab0983>



## References

- Ling, Jonathan P., Chhabra, R., Merran, J. D., Schaughency, P. M., Wheelan, S. J., Corden, J. L., & Wong, P. C. (2016). PTBP1 and PTBP2 Repress Nonconserved Cryptic Exons. *Cell Reports*, 17(1), 104–113. <https://doi.org/10.1016/j.celrep.2016.08.071>
- Liu, E. Y., Russ, J., Wu, K., Neal, D., Suh, E., McNally, A. G., ... Lee, E. B. (2014). C9orf72 hypermethylation protects against repeat expansion-associated pathology in ALS/FTD. *Acta Neuropathologica*, 128(4), 525–541. <https://doi.org/10.1007/s00401-014-1286-y>
- Liu, G., Fiala, M., Mizwicki, M. T., Sayre, J., Magpantay, L., Siani, A., ... Wiedau-Pazos, M. (2012). Neuronal phagocytosis by inflammatory macrophages in ALS spinal cord: Inhibition of inflammation by resolvin D1. *American Journal of Neurodegenerative Diseases*, 1(1), 60–74.
- Liu, Q., Shu, S., Wang, R. R., Liu, F., Cui, B., Guo, X. N., ... Zhang, X. (2016). Whole-exome sequencing identifies a missense mutation in hnRNPA1 in a family with flail arm ALS. *Neurology*, 87(17), 1763–1769. <https://doi.org/10.1212/WNL.0000000000003256>
- Liu, Yansheng, González-Porta, M., Santos, S., Brazma, A., Marioni, J. C., Aebersold, R., ... Wickramasinghe, V. O. (2017). Impact of Alternative Splicing on the Human Proteome. *Cell Reports*, 20(5), 1229–1241. <https://doi.org/10.1016/j.celrep.2017.07.025>
- Liu, Yuanjing, Pattamatta, A., Zu, T., Reid, T., Bardhi, O., Borchelt, D. R., ... Ranum, L. P. W. (2016). C9orf72 BAC Mouse Model with Motor Deficits and Neurodegenerative Features of ALS/FTD. *Neuron*, 90(3), 521–534. <https://doi.org/10.1016/j.neuron.2016.04.005>
- Livingston, G., Huntley, J., Sommerlad, A., Ames, D., Ballard, C., Banerjee, S., ... Mukadam, N. (2020, August 8). Dementia prevention, intervention, and care: 2020 report of the Lancet Commission. *The Lancet*. Lancet Publishing Group. [https://doi.org/10.1016/S0140-6736\(20\)30367-6](https://doi.org/10.1016/S0140-6736(20)30367-6)
- Luchinat, E., Barbieri, L., Rubino, J. T., Kozyreva, T., Cantini, F., & Banci, L. (2014). In-cell NMR reveals potential precursor of toxic species from SOD1 fALS mutants. *Nature Communications*, 5, 5502. <https://doi.org/10.1038/ncomms6502>
- Luotti, S., Pasetto, L., Porcu, L., Torri, V., Elezgarai, S. R., Pantalone, S., ... Bonetto, V. (2020). Diagnostic and prognostic values of PBMC proteins in amyotrophic lateral sclerosis. *Neurobiology of Disease*, 139, 104815. <https://doi.org/10.1016/j.nbd.2020.104815>
- Ma, J., Liu, Z., Michelotti, N., Pitchiaya, S., Veerapaneni, R., Androsavich, J. R., ... Yang, W. (2013). High-resolution three-dimensional mapping of mRNA export through the nuclear pore. *Nature Communications*, 4, 2414. <https://doi.org/10.1038/ncomms3414>
- Mackenzie, I. R. A., Bigio, E. H., Ince, P. G., Geser, F., Neumann, M., Cairns, N. J., ... Trojanowski, J. Q. (2007). Pathological TDP-43 distinguishes sporadic amyotrophic lateral sclerosis from amyotrophic lateral sclerosis with SOD1 mutations. *Annals of Neurology*, 61(5), 427–434. <https://doi.org/10.1002/ana.21147>
- Mackenzie, I. R. A., Frick, P., Grässer, F. A., Gendron, T. F., Petrucelli, L., Cashman, N. R., ... Neumann, M. (2015). Quantitative analysis and clinico-pathological correlations of different dipeptide repeat protein pathologies in C9ORF72 mutation carriers. *Acta Neuropathologica*,

## References

- 130(6), 845–861. <https://doi.org/10.1007/s00401-015-1476-2>
- Majounie, E., Renton, A. E., Mok, K., Dopper, E. G. P., Waite, A., Rollinson, S., ... Logroscino, G. (2012). Frequency of the C9orf72 hexanucleotide repeat expansion in patients with amyotrophic lateral sclerosis and frontotemporal dementia: A cross-sectional study. *The Lancet Neurology*, 11(4), 323–330. [https://doi.org/10.1016/S1474-4422\(12\)70043-1](https://doi.org/10.1016/S1474-4422(12)70043-1)
- Malek, A. M., Barchowsky, A., Bowser, R., Youk, A., & Talbott, E. O. (2012). Pesticide exposure as a risk factor for amyotrophic lateral sclerosis: A meta-analysis of epidemiological studies. Pesticide exposure as a risk factor for ALS. *Environmental Research*, 117, 112–119. <https://doi.org/10.1016/j.envres.2012.06.007>
- Manabe, Y., Warita, H., Murakami, T., Shiote, M., Hayashi, T., Nagano, I., ... Abe, K. (2001). Early decrease of redox factor-1 in spinal motor neurons of presymptomatic transgenic mice with a mutant SOD1 gene. *Brain Research*, 915(1), 104–107. [https://doi.org/10.1016/S0006-8993\(01\)02870-0](https://doi.org/10.1016/S0006-8993(01)02870-0)
- Marchetto, M. C. N., Muotri, A. R., Mu, Y., Smith, A. M., Cezar, G. G., & Gage, F. H. (2008). Non-Cell-Autonomous Effect of Human SOD1G37R Astrocytes on Motor Neurons Derived from Human Embryonic Stem Cells. *Cell Stem Cell*, 3(6), 649–657. <https://doi.org/10.1016/j.stem.2008.10.001>
- Mariño, G., Fernández, A. F., Cabrera, S., Lundberg, Y. W., Cabanillas, R., Rodríguez, F., ... López-Otín, C. (2010). Autophagy is essential for mouse sense of balance. *Journal of Clinical Investigation*, 120(7), 2331–2344. <https://doi.org/10.1172/JCI42601>
- Martin, W., & Koonin, E. V. (2006). Introns and the origin of nucleus-cytosol compartmentalization. *Nature*, 440(7080), 41–45. <https://doi.org/10.1038/nature04531>
- Maruyama, H., Morino, H., Ito, H., Izumi, Y., Kato, H., Watanabe, Y., ... Kawakami, H. (2010). Mutations of optineurin in amyotrophic lateral sclerosis. *Nature*, 465(7295), 223–226. <https://doi.org/10.1038/nature08971>
- Masseret, E., Banack, S., Boumédiène, F., Abadie, E., Brient, L., Pernet, F., ... Preux, P. M. (2013). Dietary BMAA exposure in an amyotrophic lateral sclerosis cluster from southern France. *PLoS ONE*, 8(12), e83406. <https://doi.org/10.1371/journal.pone.0083406>
- Mathew, R., Karantza-Wadsworth, V., & White, E. (2007, December). Role of autophagy in cancer. *Nature Reviews Cancer*. <https://doi.org/10.1038/nrc2254>
- Matlin, A. J., Clark, F., & Smith, C. W. J. (2005, May). Understanding alternative splicing: Towards a cellular code. *Nature Reviews Molecular Cell Biology*. *Nat Rev Mol Cell Biol*. <https://doi.org/10.1038/nrm1645>
- McCampbell, A., Cole, T., Wegener, A. J., Tomassy, G. S., Setnicka, A., Farley, B. J., ... Miller, T. M. (2018). Antisense oligonucleotides extend survival and reverse decrement in muscle response in ALS models. *Journal of Clinical Investigation*, 128(8), 3558–3567. <https://doi.org/10.1172/JCI99081>
- McClory, S. P., Lynch, K. W., & Ling, J. P. (2018). HnRNP L represses cryptic exons. *RNA*, 24(6),

## References

- 761–768. <https://doi.org/10.1261/rna.065508.117>
- McCombe, P. A., Pfluger, C., Singh, P., Lim, C. Y. H., Airey, C., & Henderson, R. D. (2015). Serial measurements of phosphorylated neurofilament-heavy in the serum of subjects with amyotrophic lateral sclerosis. *Journal of the Neurological Sciences*, *353*(1–2), 122–129. <https://doi.org/10.1016/j.jns.2015.04.032>
- McCord, J. M., & Fridovich, I. (1969). Superoxide dismutase. An enzymic function for erythrocyte (hemocuprein). *Journal of Biological Chemistry*, *244*(22), 6049–6055.
- McDonald, K. K., Aulas, A., Destroismaisons, L., Pickles, S., Beleac, E., Camu, W., ... Vande Velde, C. (2011). TAR DNA-binding protein 43 (TDP-43) regulates stress granule dynamics via differential regulation of G3BP and TIA-1. *Human Molecular Genetics*, *20*(7), 1400–1410. <https://doi.org/10.1093/hmg/ddr021>
- McGlincy, N. J., & Smith, C. W. J. (2008, August). Alternative splicing resulting in nonsense-mediated mRNA decay: what is the meaning of nonsense? *Trends in Biochemical Sciences*. Trends Biochem Sci. <https://doi.org/10.1016/j.tibs.2008.06.001>
- McGoldrick, P., Zhang, M., van Blitterswijk, M., Sato, C., Moreno, D., Xiao, S., ... Rogaeva, E. (2018). Unaffected mosaic C9orf72 case: RNA foci, dipeptide proteins, but upregulated C9orf72 expression. *Neurology*, *90*(4), e323–e331. <https://doi.org/10.1212/WNL.0000000000004865>
- Mercado, P. A., Ayala, Y. M., Romano, M., Buratti, E., & Baralle, F. E. (2005). Depletion of TDP 43 overrides the need for exonic and intronic splicing enhancers in the human apoA-II gene. *Nucleic Acids Research*, *33*(18), 6000–6010. <https://doi.org/10.1093/nar/gki897>
- Miller, T. M., Pestronk, A., David, W., Rothstein, J., Simpson, E., Appel, S. H., ... Cudkovicz, M. E. (2013). An antisense oligonucleotide against SOD1 delivered intrathecally for patients with SOD1 familial amyotrophic lateral sclerosis: A phase 1, randomised, first-in-man study. *The Lancet Neurology*, *12*(5), 435–442. [https://doi.org/10.1016/S1474-4422\(13\)70061-9](https://doi.org/10.1016/S1474-4422(13)70061-9)
- Mindell, J. A. (2012). Lysosomal Acidification Mechanisms. *Annual Review of Physiology*, *74*(1), 69–86. <https://doi.org/10.1146/annurev-physiol-012110-142317>
- Mlgyera, H. D. (2005). New Maximum Likelihood Estimators for Eukaryotic Intron Evolution. *PLoS Computational Biology*, *1*(7), 0631–0638. <https://doi.org/10.1371/journal.pcbi.0010079>
- Mori, K., Weng, S.-M., Arzberger, T., May, S., Rentzsch, K., Kremmer, E., ... Edbauer, D. (2013). The C9orf72 GGGGCC repeat is translated into aggregating dipeptide-repeat proteins in FTL/ALS. *Science (New York, N.Y.)*, *339*(6125), 1335–1338. <https://doi.org/10.1126/science.1232927>
- Mowat, M., Cheng, A., Kimura, N., Bernstein, A., & Benchimol, S. (1985). Rearrangements of the cellular p53 gene in erythroleukaemic cells transformed by Friend virus. *Nature*, *314*(6012), 633–636. <https://doi.org/10.1038/314633a0>
- Münch, Christian, O'Brien, J., & Bertolotti, A. (2011). Prion-like propagation of mutant superoxide dismutase-1 misfolding in neuronal cells. *Proceedings of the National Academy of Sciences of*

## References

- the United States of America*, 108(9), 3548–3553. <https://doi.org/10.1073/pnas.1017275108>
- Münch, Christoph, Sedlmeier, R., Meyer, T., Homberg, V., Sperfeld, A. D., Kurt, A., ... Ludolph, A. C. (2004). Point mutations of the p150 subunit of dynactin (DCTN1) gene ALS. *Neurology*, 63(4), 724–726. <https://doi.org/10.1212/01.WNL.0000134608.83927.B1>
- Murakami, T., Nagai, M., Miyazaki, K., Morimoto, N., Ohta, Y., Kurata, T., ... Abe, K. (2007). Early decrease of mitochondrial DNA repair enzymes in spinal motor neurons of presymptomatic transgenic mice carrying a mutant SOD1 gene. *Brain Research*, 1150(1), 182–189. <https://doi.org/10.1016/j.brainres.2007.02.057>
- Murphy, N. A., Arthur, K. C., Tienari, P. J., Houlden, H., Chiò, A., & Traynor, B. J. (2017). Age-related penetrance of the C9orf72 repeat expansion. *Scientific Reports*, 7(1). <https://doi.org/10.1038/s41598-017-02364-1>
- Musi, N., Valentine, J. M., Sickora, K. R., Baeuerle, E., Thompson, C. S., Shen, Q., & Orr, M. E. (2018). Tau protein aggregation is associated with cellular senescence in the brain. *Aging Cell*, 17(6), e12840. <https://doi.org/10.1111/acer.12840>
- Nagai, M., Re, D. B., Nagata, T., Chalazonitis, A., Jessell, T. M., Wichterle, H., & Przedborski, S. (2007). Astrocytes expressing ALS-linked mutated SOD1 release factors selectively toxic to motor neurons. *Nature Neuroscience*, 10(5), 615–622. <https://doi.org/10.1038/nn1876>
- Nakatogawa, H., Ishii, J., Asai, E., & Ohsumi, Y. (2012). Atg4 recycles inappropriately lipidated Atg8 to promote autophagosome biogenesis. *Autophagy*, 8(2), 177–186. <https://doi.org/10.4161/auto.8.2.18373>
- Nakatogawa, H., Suzuki, K., Kamada, Y., & Ohsumi, Y. (2009). Dynamics and diversity in autophagy mechanisms: lessons from yeast. *Nature Reviews. Molecular Cell Biology*, 10(7), 458–467. <https://doi.org/10.1038/nrm2708>
- Nana, A. L., Sidhu, M., Gaus, S. E., Hwang, J.-H. L., Li, L., Park, Y., ... Seeley, W. W. (2019). Neurons selectively targeted in frontotemporal dementia reveal early stage TDP-43 pathobiology. *Acta Neuropathologica*, 137(1), 27–46. <https://doi.org/10.1007/s00401-018-1942-8>
- Nelson, P. T., Dickson, D. W., Trojanowski, J. Q., Jack, C. R., Boyle, P. A., Arfanakis, K., ... Schneider, J. A. (2019). Limbic-predominant age-related TDP-43 encephalopathy (LATE): consensus working group report. *Brain: A Journal of Neurology*, 142(6), 1503–1527. <https://doi.org/10.1093/brain/awz099>
- Neumann, M., Sampathu, D. M., Kwong, L. K., Truax, A. C., Micsenyi, M. C., Chou, T. T., ... Lee, V. M.-Y. (2006). Ubiquitinated TDP-43 in Frontotemporal Lobar Degeneration and Amyotrophic Lateral Sclerosis. *Science*, 314(5796), 130–133. <https://doi.org/10.1126/SCIENCE.1134108>
- Nguyen, D. K. H., Thombre, R., & Wang, J. (2019). Autophagy as a common pathway in amyotrophic lateral sclerosis. *Neuroscience Letters*, 697, 34–48. <https://doi.org/10.1016/j.neulet.2018.04.006>

## References

- Nonaka, T., Masuda-Suzukake, M., Arai, T., Hasegawa, Y., Akatsu, H., Obi, T., ... Hasegawa, M. (2013). Prion-like properties of pathological TDP-43 aggregates from diseased brains. *Cell Reports*, 4(1), 124–134. <https://doi.org/10.1016/j.celrep.2013.06.007>
- Nordin, A., Akimoto, C., Wuolikainen, A., Alstermark, H., Jonsson, P., Birve, A., ... Andersen, P. M. (2015). Extensive size variability of the GGGGCC expansion in C9orf72 in both neuronal and non-neuronal tissues in 18 patients with ALS or FTD. *Human Molecular Genetics*, 24(11), 3133–3142. <https://doi.org/10.1093/hmg/ddv064>
- Nover, L., Scharf, K. D., & Neumann, D. (1989). Cytoplasmic heat shock granules are formed from precursor particles and are associated with a specific set of mRNAs. *Molecular and Cellular Biology*, 9(3), 1298–1308. <https://doi.org/10.1128/mcb.9.3.1298>
- O'Brien, J. S., & Sampson, E. L. (1965). Lipid composition of the normal human brain: gray matter, white matter, and myelin. *Journal of Lipid Research*, 6(4), 537–544.
- O'Reilly, É. J., Wang, H., Weisskopf, M. G., Fitzgerald, K. C., Falcone, G., McCullough, M. L., ... Ascherio, A. (2013). Premorbid body mass index and risk of amyotrophic lateral sclerosis. *Amyotrophic Lateral Sclerosis and Frontotemporal Degeneration*, 14(3), 205–211. <https://doi.org/10.3109/21678421.2012.735240>
- O'Rourke, J. G., Bogdanik, L., Yáñez, A., Lall, D., Wolf, A. J., Muhammad, A. K. M. G., ... Baloh, R. H. (2016). C9orf72 is required for proper macrophage and microglial function in mice. *Science (New York, N.Y.)*, 351(6279), 1324–1329. <https://doi.org/10.1126/science.aaf1064>
- Ogrodnik, M., Zhu, Y., Langhi, L. G. P., Tchkonja, T., Krüger, P., Fielder, E., ... Jurk, D. (2019). Obesity-Induced Cellular Senescence Drives Anxiety and Impairs Neurogenesis. *Cell Metabolism*, 29(5), 1061-1077.e8. <https://doi.org/10.1016/j.cmet.2018.12.008>
- Olkowski, Z. L. (1998). Mutant AP endonuclease in patients with amyotrophic lateral sclerosis. *NeuroReport*, 9(2), 239–242. <https://doi.org/10.1097/00001756-199801260-00012>
- Osaka, M., Ito, D., & Suzuki, N. (2016). Disturbance of proteasomal and autophagic protein degradation pathways by amyotrophic lateral sclerosis-linked mutations in ubiquilin 2. *Biochemical and Biophysical Research Communications*, 472(2), 324–331. <https://doi.org/10.1016/j.bbrc.2016.02.107>
- Osawa, T., Kotani, T., Kawaoka, T., Hirata, E., Suzuki, K., Nakatogawa, H., ... Noda, N. N. (2019). Atg2 mediates direct lipid transfer between membranes for autophagosome formation. *Nature Structural & Molecular Biology*, 26(4), 281–288. <https://doi.org/10.1038/s41594-019-0203-4>
- Ou, S. H., Wu, F., Harrich, D., García-Martínez, L. F., & Gaynor, R. B. (1995). Cloning and characterization of a novel cellular protein, TDP-43, that binds to human immunodeficiency virus type 1 TAR DNA sequence motifs. *Journal of Virology*, 69(6), 3584–3596. Retrieved from <http://www.ncbi.nlm.nih.gov/pubmed/7745706>
- Palikaras, K., Lionaki, E., & Tavernarakis, N. (2015, September 11). Balancing mitochondrial biogenesis and mitophagy to maintain energy metabolism homeostasis. *Cell Death and Differentiation*. Nature Publishing Group. <https://doi.org/10.1038/cdd.2015.86>

## References

- Pamplona, R., Dalfó, E., Ayala, V., Bellmunt, M. J., Prat, J., Ferrer, I., & Portero-Otín, M. (2005). Proteins in human brain cortex are modified by oxidation, glycooxidation, and lipoxidation: Effects of Alzheimer disease and identification of lipoxidation targets. *Journal of Biological Chemistry*, 280(22), 21522–21530. <https://doi.org/10.1074/jbc.M502255200>
- Pamplona, R., Portero-Otín, M., Sanz, A., Ayala, V., Vasileva, E., & Barja, G. (2005). Protein and lipid oxidative damage and complex I content are lower in the brain of budgerigar and canaries than in mice. Relation to aging rate. *Age (Dordrecht, Netherlands)*, 27(4), 267–280. <https://doi.org/10.1007/s11357-005-4562-x>
- Pan, Q., Saltzman, A. L., Yoon, K. K., Misquitta, C., Shai, O., Maquat, L. E., ... Blencowe, B. J. (2006). Quantitative microarray profiling provides evidence against widespread coupling of alternative splicing with nonsense-mediated mRNA decay to control gene expression. *Genes and Development*, 20(2), 153–158. <https://doi.org/10.1101/gad.1382806>
- Pandey, S. N., Lee, Y. C., Yokota, T., & Chen, Y. W. (2014). Morpholino treatment improves muscle function and pathology of Pitx1 transgenic mice. *Molecular Therapy*, 22(2), 390–396. <https://doi.org/10.1038/mt.2013.263>
- Pankiv, S., Clausen, T. H., Lamark, T., Brech, A., Bruun, J.-A., Outzen, H., ... Johansen, T. (2007). p62/SQSTM1 binds directly to Atg8/LC3 to facilitate degradation of ubiquitinated protein aggregates by autophagy. *The Journal of Biological Chemistry*, 282(33), 24131–24145. <https://doi.org/10.1074/jbc.M702824200>
- Passoni, M., De Conti, L., Baralle, M., & Buratti, E. (2012). UG repeats/TDP-43 interactions near 5' splice sites exert unpredictable effects on splicing modulation. *Journal of Molecular Biology*, 415(1), 46–60. <https://doi.org/10.1016/j.jmb.2011.11.003>
- Patil, P., Dong, Q., Wang, D., Chang, J., Wiley, C., Demaria, M., ... Vo, N. (2019). Systemic clearance of p16INK4a-positive senescent cells mitigates age-associated intervertebral disc degeneration. *Aging Cell*, 18(3). <https://doi.org/10.1111/accel.12927>
- Petrov, D., Mansfield, C., Moussy, A., & Hermine, O. (2017). ALS Clinical Trials Review: 20 Years of Failure. Are We Any Closer to Registering a New Treatment? *Frontiers in Aging Neuroscience*, 9(MAR), 68. <https://doi.org/10.3389/fnagi.2017.00068>
- Pinarbasi, E. S., Cağatay, T., Fung, H. Y. J., Li, Y. C., Chook, Y. M., & Thomas, P. J. (2018). Active nuclear import and passive nuclear export are the primary determinants of TDP-43 localization. *Scientific Reports*, 8(1), 7083. <https://doi.org/10.1038/s41598-018-25008-4>
- Pluquet, O., & Hainaut, P. (2001, December 10). Genotoxic and non-genotoxic pathways of p53 induction. *Cancer Letters*. [https://doi.org/10.1016/S0304-3835\(01\)00698-X](https://doi.org/10.1016/S0304-3835(01)00698-X)
- Poesen, K., & Van Damme, P. (2019). Diagnostic and prognostic performance of neurofilaments in ALS. *Frontiers in Neurology*. Frontiers Media S.A. <https://doi.org/10.3389/fneur.2018.01167>
- Pokrishevsky, E., Hong, R. H., Mackenzie, I. R., & Cashman, N. R. (2017). Spinal cord homogenates from SOD1 familial amyotrophic lateral sclerosis induce SOD1 aggregation in

## References

- living cells. *PLoS One*, 12(9), e0184384. <https://doi.org/10.1371/journal.pone.0184384>
- Poorani, R., Bhatt, A. N., Dwarakanath, B. S., & Das, U. N. (2016). COX-2, aspirin and metabolism of arachidonic, eicosapentaenoic and docosahexaenoic acids and their physiological and clinical significance. *European Journal of Pharmacology*, 785, 116–132. <https://doi.org/10.1016/j.ejphar.2015.08.049>
- Porta, S., Xu, Y., Restrepo, C. R., Kwong, L. K., Zhang, B., Brown, H. J., ... Lee, V. M. Y. (2018). Patient-derived frontotemporal lobar degeneration brain extracts induce formation and spreading of TDP-43 pathology in vivo. *Nature Communications*, 9(1). <https://doi.org/10.1038/s41467-018-06548-9>
- Prinz, M., & Priller, J. (2014). Microglia and brain macrophages in the molecular age: From origin to neuropsychiatric disease. *Nature Reviews Neuroscience*. Nature Publishing Group. <https://doi.org/10.1038/nrn3722>
- Prusiner, S. B. (1982). Novel proteinaceous infectious particles cause scrapie. *Science*, 216(4542), 136–144. <https://doi.org/10.1126/science.6801762>
- Prusiner, S. B. (1991). Molecular biology of prion diseases. *Science*, 252(5012), 1515–1522. <https://doi.org/10.1126/science.1675487>
- Pytte, J., Anderton, R. S., Flynn, L. L., Theunissen, F., Jiang, L., Pitout, I., ... Akkari, P. A. (2020). Association of a structural variant within the SQSTM1 gene with amyotrophic lateral sclerosis. *Neurology Genetics*, 6(2), e406. <https://doi.org/10.1212/nxg.0000000000000406>
- Read, R., Savelieva, K., Baker, K., Hansen, G., & Vogel, P. (2011). Histopathological and neurological features of Atg4b knockout mice. *Veterinary Pathology*, 48(2), 486–494. <https://doi.org/10.1177/0300985810375810>
- Reaume, A. G., Elliott, J. L., Hoffman, E. K., Kowall, N. W., Ferrante, R. J., Siwek, D. F., ... Snider, W. D. (1996). Motor neurons in Cu/Zn superoxide dismutase-deficient mice develop normally but exhibit enhanced cell death after axonal injury. *Nature Genetics*, 13(1), 43–47. <https://doi.org/10.1038/ng0596-43>
- Renton, A. E., Majounie, E., Waite, A., Simón-Sánchez, J., Rollinson, S., Gibbs, J. R., ... Traynor, B. J. (2011). A hexanucleotide repeat expansion in C9ORF72 is the cause of chromosome 9p21-linked ALS-FTD. *Neuron*, 72(2), 257–268. <https://doi.org/10.1016/j.neuron.2011.09.010>
- Requena, J. R., Fu, M. X., Ahmed, M. U., Jenkins, A. J., Lyons, T. J., Baynes, J. W., & Thorpe, S. R. (1997). Quantification of malondialdehyde and 4-hydroxynonenal adducts to lysine residues in native and oxidized human low-density lipoprotein. *Biochemical Journal*, 322(1), 317–325. <https://doi.org/10.1042/bj3220317>
- Rifai, A., Brysch, W., Fadden, K., Clark, J., & Schlingensiepen, K. H. (1996). Clearance kinetics, biodistribution, and organ saturability of phosphorothioate oligodeoxynucleotides in mice. *American Journal of Pathology*, 149(2), 717–725. Retrieved from [/pmc/articles/PMC1865299/?report=abstract](https://pubmed.ncbi.nlm.nih.gov/1865299/)
- Rigo, F., Chun, S. J., Norris, D. A., Hung, G., Lee, S., Matson, J., ... Bennett, C. F. (2014).

## References

- Pharmacology of a central nervous system delivered 2'-O-methoxyethyl- modified survival of motor neuron splicing oligonucleotide in mice and nonhuman primates. *Journal of Pharmacology and Experimental Therapeutics*, 350(1), 46–55.  
<https://doi.org/10.1124/jpet.113.212407>
- Rinaldi, C., & Wood, M. J. A. (2018). Antisense oligonucleotides: the next frontier for treatment of neurological disorders. *Nature Reviews. Neurology*, 14(1), 9–21.  
<https://doi.org/10.1038/nrneurol.2017.148>
- Rodier, F., Campisi, J., & Bhaumik, D. (2007). Two faces of p53: aging and tumor suppression. *Nucleic Acids Research*, 35(22), 7475–7484. <https://doi.org/10.1093/nar/gkm744>
- Rodríguez-Pérez, R., Fernández, L., & Marco, S. (2018). Overoptimism in cross-validation when using partial least squares-discriminant analysis for omics data: a systematic study. *Analytical and Bioanalytical Chemistry*, 410(23), 5981–5992. <https://doi.org/10.1007/s00216-018-1217-1>
- Rogakou, E. P., Pilch, D. R., Orr, A. H., Ivanova, V. S., & Bonner, W. M. (1998). DNA double-stranded breaks induce histone H2AX phosphorylation on serine 139. *Journal of Biological Chemistry*, 273(10), 5858–5868. <https://doi.org/10.1074/jbc.273.10.5858>
- Rooney, J., Byrne, S., Heverin, M., Tobin, K., Dick, A., Donaghy, C., & Hardiman, O. (2015). A multidisciplinary clinic approach improves survival in ALS: a comparative study of ALS in Ireland and Northern Ireland. *Journal of Neurology, Neurosurgery, and Psychiatry*, 86(5), 496–501. <https://doi.org/10.1136/jnnp-2014-309601>
- Rosen, D. R., Siddique, T., Patterson, D., Figlewicz, D. A., Sapp, P., Hentati, A., ... Brown, R. H. (1993). Mutations in Cu/Zn superoxide dismutase gene are associated with familial amyotrophic lateral sclerosis. *Nature*, 362(6415), 59–62. <https://doi.org/10.1038/362059a0>
- Rot, G., Wang, Z., Huppertz, I., Modic, M., Lenče, T., Hallegger, M., ... Ule, J. (2017). High-Resolution RNA Maps Suggest Common Principles of Splicing and Polyadenylation Regulation by TDP-43. *Cell Reports*, 19(5), 1056–1067.  
<https://doi.org/10.1016/j.celrep.2017.04.028>
- Rothstein, J. D., Jin, L., Dykes-Hoberg, M., & Kuncl, R. W. (1993). Chronic inhibition of glutamate uptake produces a model of slow neurotoxicity. *Proceedings of the National Academy of Sciences of the United States of America*, 90(14), 6591–6595.  
<https://doi.org/10.1073/pnas.90.14.6591>
- Rothstein, Jeffrey D., Martin, L. J., & Kuncl, R. W. (1992). Decreased Glutamate Transport by the Brain and Spinal Cord in Amyotrophic Lateral Sclerosis. *New England Journal of Medicine*, 326(22), 1464–1468. <https://doi.org/10.1056/NEJM199205283262204>
- Rothstein, Jeffrey D., Van Kammen, M., Levey, A. I., Martin, L. J., & Kuncl, R. W. (1995). Selective loss of glial glutamate transporter GLT-1 in amyotrophic lateral sclerosis. *Annals of Neurology*, 38(1), 73–84. <https://doi.org/10.1002/ana.410380114>
- Rudnick, N. D., Griffey, C. J., Guarnieri, P., Gerbino, V., Wang, X., Piersaint, J. A., ... Maniatis, T.



## References

- (2017). Distinct roles for motor neuron autophagy early and late in the SOD1G93A mouse model of ALS. *Proceedings of the National Academy of Sciences of the United States of America*, 114(39), E8294–E8303. <https://doi.org/10.1073/pnas.1704294114>
- Rupaimoole, R., & Slack, F. J. (2017, March 1). MicroRNA therapeutics: Towards a new era for the management of cancer and other diseases. *Nature Reviews Drug Discovery*. Nature Publishing Group. <https://doi.org/10.1038/nrd.2016.246>
- Sasaki, S., Warita, H., Murakami, T., Shibata, N., Komori, T., Abe, K., ... Iwata, M. (2005). Ultrastructural study of aggregates in the spinal cord of transgenic mice with a G93A mutant SOD1 gene. *Acta Neuropathologica*, 109(3), 247–255. <https://doi.org/10.1007/s00401-004-0939-7>
- Sastry, P. S. (1985). Lipids of nervous tissue: Composition and metabolism. *Progress in Lipid Research*. [https://doi.org/10.1016/0163-7827\(85\)90011-6](https://doi.org/10.1016/0163-7827(85)90011-6)
- Scherz-Shouval, R., Shvets, E., Fass, E., Shorer, H., Gil, L., & Elazar, Z. (2007). Reactive oxygen species are essential for autophagy and specifically regulate the activity of Atg4. *The EMBO Journal*, 26(7), 1749–1760. <https://doi.org/10.1038/sj.emboj.7601623>
- Schmitt, C. A. (2007). Cellular senescence and cancer treatment. *Biochimica et Biophysica Acta*, 1775(1), 5–20. <https://doi.org/10.1016/j.bbcan.2006.08.005>
- Schopfer, F. J., Cipollina, C., & Freeman, B. A. (2011, October 12). Formation and signaling actions of electrophilic lipids. *Chemical Reviews*. <https://doi.org/10.1021/cr200131e>
- Schwab, J. M., Chiang, N., Arita, M., & Serhan, C. N. (2007). Resolvin E1 and protectin D1 activate inflammation-resolution programmes. *Nature*, 447(7146), 869–874. <https://doi.org/10.1038/nature05877>
- Selkoe, D. J., & Hardy, J. (2016). The amyloid hypothesis of Alzheimer's disease at 25 years. *EMBO Molecular Medicine*, 8(6), 595–608. <https://doi.org/10.15252/emmm.201606210>
- Sellier, C., Campanari, M., Julie Corbier, C., Gaucherot, A., Kolb-Cheynel, I., Oulad-Abdelghani, M., ... Charlet-Berguerand, N. (2016). Loss of C9 ORF 72 impairs autophagy and synergizes with polyQ Ataxin-2 to induce motor neuron dysfunction and cell death. *The EMBO Journal*, 35(12), 1276–1297. <https://doi.org/10.15252/emboj.201593350>
- Sephton, C. F., Good, S. K., Atkin, S., Dewey, C. M., Mayer, P., Herz, J., & Yu, G. (2010). TDP-43 is a developmentally regulated protein essential for early embryonic development. *The Journal of Biological Chemistry*, 285(9), 6826–6834. <https://doi.org/10.1074/jbc.M109.061846>
- Serhan, C. N., Brain, S. D., Buckley, C. D., Gilroy, D. W., Haslett, C., O'Neill, L. A. J., ... Wallace, J. L. (2007). Resolution of inflammation: state of the art, definitions and terms. *The FASEB Journal*, 21(2), 325–332. <https://doi.org/10.1096/fj.06-7227rev>
- Serhan, C. N., Hong, S., Gronert, K., Colgan, S. P., Devchand, P. R., Mirick, G., & Moussignac, R. L. (2002). Resolvins: A family of bioactive products of omega-3 fatty acid transformation

## References

- circuits initiated by aspirin treatment that counter proinflammation signals. *Journal of Experimental Medicine*, 196(8), 1025–1037. <https://doi.org/10.1084/jem.20020760>
- Serhan, C. N., & Levy, B. D. (2018). Resolvins in inflammation: emergence of the pro-resolving superfamily of mediators. *The Journal of Clinical Investigation*, 128(7), 2657–2669. <https://doi.org/10.1172/JCI97943>
- Serrano, M., Lin, A. W., McCurrach, M. E., Beach, D., & Lowe, S. W. (1997). Oncogenic ras provokes premature cell senescence associated with accumulation of p53 and p16INK4a. *Cell*, 88(5), 593–602. [https://doi.org/10.1016/S0092-8674\(00\)81902-9](https://doi.org/10.1016/S0092-8674(00)81902-9)
- Shaikh, A. Y., & Martin, L. J. (2002). DNA base-excision repair enzyme apurinic/aprimidinic endonuclease/redox factor-1 is increased and competent in the brain and spinal cord of individuals with amyotrophic lateral sclerosis. *Neuromolecular Medicine*, 2(1), 47–60. <https://doi.org/10.1007/s12017-002-0038-7>
- Shan, X., Vocadlo, D., & Krieger, C. (2009). Mislocalization of TDP-43 in the G93A mutant SOD1 transgenic mouse model of ALS. *Neuroscience Letters*, 458(2), 70–74. <https://doi.org/10.1016/j.neulet.2009.04.031>
- Shimo, T., Tachibana, K., Saito, K., Yoshida, T., Tomita, E., Waki, R., ... Obika, S. (2014). Design and evaluation of locked nucleic acid-based splice-switching oligonucleotides in vitro. *Nucleic Acids Research*, 42(12), 8174–8187. <https://doi.org/10.1093/nar/gku512>
- Sierra, A., Gottfried-Blackmore, A. C., McEwen, B. S., & Bulloch, K. (2007). Microglia derived from aging mice exhibit an altered inflammatory profile. *Glia*, 55(4), 412–424. <https://doi.org/10.1002/glia.20468>
- Singh, R., Barden, A., Mori, T., & Beilin, L. (2001). Advanced glycation end-products: A review. *Diabetologia*. <https://doi.org/10.1007/s001250051591>
- Smith, R. A., Miller, T. M., Yamanaka, K., Monia, B. P., Condon, T. P., Hung, G., ... Cleveland, D. W. (2006). Antisense oligonucleotide therapy for neurodegenerative disease. *Journal of Clinical Investigation*, 116(8), 2290–2296. <https://doi.org/10.1172/JCI25424>
- Solinger, J. A., & Spang, A. (2013). Tethering complexes in the endocytic pathway: CORVET and HOPS. *The FEBS Journal*, 280(12), 2743–2757. <https://doi.org/10.1111/febs.12151>
- Solomon, D. A., Stepto, A., Au, W. H., Adachi, Y., Diaper, D. C., Hall, R., ... Hirth, F. (2018). A feedback loop between dipeptide-repeat protein, TDP-43 and karyopherin- $\alpha$  mediates C9orf72-related neurodegeneration. *Brain*, 141(10), 2908–2924. <https://doi.org/10.1093/brain/awy241>
- Sorek, R. (2007, October). The birth of new exons: Mechanisms and evolutionary consequences. *RNA*. <https://doi.org/10.1261/rna.682507>
- Steinacker, P., Hendrich, C., Sperfeld, A. D., Jesse, S., von Arnim, C. A. F., Lehnert, S., ... Otto, M. (2008). TDP-43 in cerebrospinal fluid of patients with frontotemporal lobar degeneration and amyotrophic lateral sclerosis. *Archives of Neurology*, 65(11), 1481–1487. <https://doi.org/10.1001/archneur.65.11.1481>

## References

- Stephenson, M. L., & Zamecnik, P. C. (1978). Inhibition of Rous sarcoma viral RNA translation by a specific oligodeoxyribonucleotide. *Proceedings of the National Academy of Sciences of the United States of America*, 75(1), 285–288. <https://doi.org/10.1073/pnas.75.1.285>
- Strimbu, K., & Tavel, J. A. (2010, November). What are biomarkers? *Current Opinion in HIV and AIDS*. NIH Public Access. <https://doi.org/10.1097/COH.0b013e32833ed177>
- Summerton, J., Stein, D., Huang, S. B., Matthews, P., Weller, D., & Partridge, M. (1997). Morpholino and phosphorothioate antisense oligomers compared in cell-free and in-cell systems. *Antisense & Nucleic Acid Drug Development*, 7(2), 63–70. <https://doi.org/10.1089/oli.1.1997.7.63>
- Sun, M., Bell, W., LaClair, K. D., Ling, J. P., Han, H., Kageyama, Y., ... Chen, L. L. (2017). Cryptic exon incorporation occurs in Alzheimer's brain lacking TDP-43 inclusion but exhibiting nuclear clearance of TDP-43. *Acta Neuropathologica*, 133(6), 923–931. <https://doi.org/10.1007/s00401-017-1701-2>
- Swindell, W. R., Kruse, C. P. S., List, E. O., Berryman, D. E., & Kopchick, J. J. (2019). ALS blood expression profiling identifies new biomarkers, patient subgroups, and evidence for neutrophilia and hypoxia. *Journal of Translational Medicine*, 17(1). <https://doi.org/10.1186/s12967-019-1909-0>
- Taga, A., & Maragakis, N. J. (2018, November 2). Current and emerging ALS biomarkers: utility and potential in clinical trials. *Expert Review of Neurotherapeutics*. Taylor and Francis Ltd. <https://doi.org/10.1080/14737175.2018.1530987>
- Takahashi, T., Nau, M. M., Chiba, I., Birrer, M. J., Rosenberg, R. K., Vinocour, M., ... Minna, J. D. (1989). p53: A frequent target for genetic abnormalities in lung cancer. *Science*, 246(4929), 491–494. <https://doi.org/10.1126/science.2554494>
- Tan, C.-F., Eguchi, H., Tagawa, A., Onodera, O., Iwasaki, T., Tsujino, A., ... Takahashi, H. (2007). TDP-43 immunoreactivity in neuronal inclusions in familial amyotrophic lateral sclerosis with or without SOD1 gene mutation. *Acta Neuropathologica*, 113(5), 535–542. <https://doi.org/10.1007/s00401-007-0206-9>
- Tan, F. C. C., Hutchison, E. R., Eitan, E., & Mattson, M. P. (2014). Are there roles for brain cell senescence in aging and neurodegenerative disorders? *Biogerontology*, 15(6), 643–660. <https://doi.org/10.1007/s10522-014-9532-1>
- Tan, Q., Krishna Yalamanchili, H., Park, J., De Maio, A., Lu, H.-C., Wan, Y.-W., ... Duncan, D. (2016). Extensive cryptic splicing upon loss of RBM17 and TDP43 in neurodegeneration models. *Human Molecular Genetics*, 25(23), 5083–5093. <https://doi.org/10.1093/hmg/ddw337>
- Tandan, R., Robison, S. H., Munzer, J. S., & Bradley, W. G. (1987). Deficient DNA repair in amyotrophic lateral sclerosis cells. *Journal of the Neurological Sciences*, 79(1–2), 189–203. [https://doi.org/10.1016/0022-510X\(87\)90272-3](https://doi.org/10.1016/0022-510X(87)90272-3)
- Tanida, I., Sou, Y., Ezaki, J., Minematsu-Ikeguchi, N., Ueno, T., & Kominami, E. (2004). HsAtg4B/HsApg4B/autophagin-1 cleaves the carboxyl termini of three human Atg8

## References

- homologues and delipidates microtubule-associated protein light chain 3- and GABAA receptor-associated protein-phospholipid conjugates. *The Journal of Biological Chemistry*, 279(35), 36268–36276. <https://doi.org/10.1074/jbc.M401461200>
- Tchkonia, T., Zhu, Y., Van Deursen, J., Campisi, J., & Kirkland, J. L. (2013, March 1). Cellular senescence and the senescent secretory phenotype: Therapeutic opportunities. *Journal of Clinical Investigation*. <https://doi.org/10.1172/JCI64098>
- Termsarasab, P., Thammongkolchai, T., Gao, J., Wang, L., Liang, J., & Wang, X. (2020). Cytoplasmic mislocalization and mitochondrial colocalization of TDP-43 are common features between normal aged and young mice. *Experimental Biology and Medicine (Maywood, N.J.)*, 1535370220914253. <https://doi.org/10.1177/1535370220914253>
- Theunissen, F., Flynn, L. L., Anderton, R. S., Mastaglia, F., Pytte, J., Jiang, L., ... Akkari, P. A. (2020). Structural Variants May Be a Source of Missing Heritability in sALS. *Frontiers in Neuroscience*, 14, 47. <https://doi.org/10.3389/fnins.2020.00047>
- Thornalley, P. J., Langborg, A., & Minhas, H. S. (1999). Formation of glyoxal, methylglyoxal and 8-deoxyglucosone in the glycation of proteins by glucose. *Biochemical Journal*, 344(1), 109–116. <https://doi.org/10.1042/0264-6021:3440109>
- Titze-de-Almeida, R., David, C., & Titze-de-Almeida, S. S. (2017, July 1). The Race of 10 Synthetic RNAi-Based Drugs to the Pharmaceutical Market. *Pharmaceutical Research*. Springer New York LLC. <https://doi.org/10.1007/s11095-017-2134-2>
- Torres, P., Andrés-Benito, P., Fernández-Bernal, A., Ricart, M., Ayala, V., Pamplona, R., ... Portero-Otin, M. (2020). Selected cryptic exons accumulate in hippocampal cell nuclei in Alzheimer's disease with and without associated TDP-43 proteinopathy. *Brain : A Journal of Neurology*, 143(3), e20. <https://doi.org/10.1093/brain/awaa013>
- Torres, P., Ramírez-Núñez, O., Romero-Guevara, R., Barés, G., Granado-Serrano, A. B., Ayala, V., ... Portero-Otín, M. (2018). Cryptic exon splicing function of TARDBP interacts with autophagy in nervous tissue. *Autophagy*, 14(8), 1398–1403. <https://doi.org/10.1080/15548627.2018.1474311>
- Tóth, G., Gáspári, Z., & Jurka, J. (2000). Microsatellites in different eukaryotic genomes: Surveys and analysis. *Genome Research*, 10(7), 967–981. <https://doi.org/10.1101/gr.10.7.967>
- Touznik, A., Maruyama, R., Hosoki, K., Echigoya, Y., & Yokota, T. (2017). LNA/DNA mixmer-based antisense oligonucleotides correct alternative splicing of the SMN2 gene and restore SMN protein expression in type 1 SMA fibroblasts. *Scientific Reports*, 7(1), 3672. <https://doi.org/10.1038/s41598-017-03850-2>
- Traxinger, K., Kelly, C., Johnson, B. A., Lyles, R. H., & Glass, J. D. (2013). Prognosis and epidemiology of amyotrophic lateral sclerosis: Analysis of a clinic population, 1997-2011. *Neurology. Clinical Practice*, 3(4), 313–320. <https://doi.org/10.1212/CPJ.0b013e3182a1b8ab>
- Traynor, B. J., Codd, M. B., Corr, B., Forde, C., Frost, E., & Hardiman, O. (2000). Amyotrophic lateral sclerosis mimic syndromes: A population-based study. *Archives of Neurology*, 57(1),

## References

- 109–113. <https://doi.org/10.1001/archneur.57.1.109>
- Turco, E., & Martens, S. (2016). Insights into autophagosome biogenesis from in vitro reconstitutions. *Journal of Structural Biology*, *196*(1), 29–36. <https://doi.org/10.1016/j.jsb.2016.04.005>
- Turner, B. J., & Talbot, K. (2008, May). Transgenics, toxicity and therapeutics in rodent models of mutant SOD1-mediated familial ALS. *Progress in Neurobiology*. <https://doi.org/10.1016/j.pneurobio.2008.01.001>
- Turner, M. R., Cagnin, A., Turkheimer, F. E., Miller, C. C. J., Shaw, C. E., Brooks, D. J., ... Banati, R. B. (2004). Evidence of widespread cerebral microglial activation in amyotrophic lateral sclerosis: an [11C](R)-PK11195 positron emission tomography study. *Neurobiology of Disease*, *15*(3), 601–609. <https://doi.org/10.1016/j.nbd.2003.12.012>
- Van Blitterswijk, M., Van Es, M. A., Hennekam, E. A. M., Dooijes, D., Van Rheenen, W., Medic, J., ... van den Berg, L. H. (2012). Evidence for an oligogenic basis of amyotrophic lateral sclerosis. *Human Molecular Genetics*, *21*(17), 3776–3784. <https://doi.org/10.1093/hmg/dds199>
- Van Damme, P., Dewil, M., Robberecht, W., & Van Den Bosch, L. (2006, January). Excitotoxicity and amyotrophic lateral sclerosis. *Neurodegenerative Diseases*. <https://doi.org/10.1159/000089620>
- Van Eijk, R. P. A., Eijkemans, M. J. C., Ferguson, T. A., Nikolakopoulos, S., Veldink, J. H., & Van Den Berg, L. H. (2018). Monitoring disease progression with plasma creatinine in amyotrophic lateral sclerosis clinical trials. *Journal of Neurology, Neurosurgery and Psychiatry*, *89*(2), 156–161. <https://doi.org/10.1136/jnnp-2017-317077>
- Van Mossevelde, S., van der Zee, J., Cruts, M., & Van Broeckhoven, C. (2017, June 1). Relationship between C9orf72 repeat size and clinical phenotype. *Current Opinion in Genetics and Development*. Elsevier Ltd. <https://doi.org/10.1016/j.gde.2017.02.008>
- Van Rheenen, W., Diekstra, F. P., Harschnitz, O., Westeneng, H. J., van Eijk, K. R., Saris, C. G. J., ... van den Berg, L. H. (2018). Whole blood transcriptome analysis in amyotrophic lateral sclerosis: A biomarker study. *PLoS ONE*, *13*(6). <https://doi.org/10.1371/journal.pone.0198874>
- Van Rheenen, W., Pulit, S. L., Dekker, A. M., Al Khleifat, A., Brands, W. J., Iacoangeli, A., ... Veldink, J. H. (2018). Project MinE: study design and pilot analyses of a large-scale whole-genome sequencing study in amyotrophic lateral sclerosis. *European Journal of Human Genetics*, *26*(10), 1537–1546. <https://doi.org/10.1038/s41431-018-0177-4>
- Vandoorne, T., De Bock, K., & Van Den Bosch, L. (2018, April 1). Energy metabolism in ALS: an underappreciated opportunity? *Acta Neuropathologica*. Springer Verlag. <https://doi.org/10.1007/s00401-018-1835-x>
- Varkouhi, A. K., Scholte, M., Storm, G., & Haisma, H. J. (2011). Endosomal escape pathways for delivery of biologicals. *Journal of Controlled Release : Official Journal of the Controlled Release Society*, *151*(3), 220–228. <https://doi.org/10.1016/j.jconrel.2010.11.004>

## References

- Vazquez-Villaseñor, I., Garwood, C. J., Heath, P. R., Simpson, J. E., Ince, P. G., & Wharton, S. B. (2019). Expression of p16 and p21 in the frontal association cortex of ALS / MND brains suggest neuronal cell cycle dysregulation and astrocyte senescence in early stages of the disease. *Neuropathology and Applied Neurobiology*, nan.12559. <https://doi.org/10.1111/nan.12559>
- Vergnaud, G., & Denoed, F. (2000). Minisatellites: Mutability and genome architecture. *Genome Research*, 10(7), 899–907. <https://doi.org/10.1101/gr.10.7.899>
- Vester, B., & Wengel, J. (2004). Current Topics LNA ( Locked Nucleic Acid ): High-Affinity Targeting of Complementary. *October*, 43(42), 13233–13241. <https://doi.org/10.1021/bi0485732>
- Veyrat-Durebex, C., Bris, C., Codron, P., Bocca, C., Chupin, S., Corcia, P., ... Blasco, H. (2019). Metabo-lipidomics of Fibroblasts and Mitochondrial-Endoplasmic Reticulum Extracts from ALS Patients Shows Alterations in Purine, Pyrimidine, Energetic, and Phospholipid Metabolisms. *Molecular Neurobiology*, 56(8), 5780–5791. <https://doi.org/10.1007/s12035-019-1484-7>
- Vivekananda, U., Manjalay, Z. R., Ganesalingam, J., Simms, J., Shaw, C. E., Leigh, P. N., ... Al-Chalabi, A. (2011). Low index-to-ring finger length ratio in sporadic ALS supports prenatally defined motor neuronal vulnerability. *Journal of Neurology, Neurosurgery and Psychiatry*, 82(6), 635–637. <https://doi.org/10.1136/jnnp.2010.237412>
- Vuopala, K., Ignatius, J., & Herva, R. (1995). Lethal arthrogyriposis with anterior horn cell disease. *Human Pathology*, 26(1), 12–19. [https://doi.org/10.1016/0046-8177\(95\)90109-4](https://doi.org/10.1016/0046-8177(95)90109-4)
- Wagenaar, T. R., Tolstikh, T., Shi, C., Jiang, L., Zhang, J., Li, Z., ... Wiederschain, D. (2015). Identification of the endosomal sorting complex required for transport-I (ESCRT-I) as an important modulator of anti-miR uptake by cancer cells. *Nucleic Acids Research*, 43(2), 1204–1215. <https://doi.org/10.1093/nar/gku1367>
- Walker, A. K., Spiller, K. J., Ge, G., Zheng, A., Xu, Y., Zhou, M., ... Lee, V. M.-Y. (2015). Functional recovery in new mouse models of ALS/FTLD after clearance of pathological cytoplasmic TDP-43. *Acta Neuropathologica*, 130(5), 643–660. <https://doi.org/10.1007/s00401-015-1460-x>
- Wang, H. Y., Wang, I. F., Bose, J., & Shen, C. K. J. (2004). Structural diversity and functional implications of the eukaryotic TDP gene family. *Genomics*, 83(1), 130–139. [https://doi.org/10.1016/S0888-7543\(03\)00214-3](https://doi.org/10.1016/S0888-7543(03)00214-3)
- Wang, I.-F., Guo, B.-S., Liu, Y.-C., Wu, C.-C., Yang, C.-H., Tsai, K.-J., & Shen, C.-K. J. (2012). Autophagy activators rescue and alleviate pathogenesis of a mouse model with proteinopathies of the TAR DNA-binding protein 43. *Proceedings of the National Academy of Sciences of the United States of America*, 109(37), 15024–15029. <https://doi.org/10.1073/pnas.1206362109>

## References

- Wang, J., Yan, K., Wu, Z.-Q., Zheng, C.-Y., Xu, R.-X., Chen, L.-H., ... Ma, Q.-H. (2014). TDP-43 interaction with the intracellular domain of amyloid precursor protein induces p53-associated apoptosis. *Neuroscience Letters*, *569*, 131–136. <https://doi.org/10.1016/j.neulet.2014.03.075>
- Wang, M.-D., Gomes, J., Cashman, N. R., Little, J., & Krewski, D. (2014). A meta-analysis of observational studies of the association between chronic occupational exposure to lead and amyotrophic lateral sclerosis. *Journal of Occupational and Environmental Medicine*, *56*(12), 1235–1242. <https://doi.org/10.1097/JOM.0000000000000323>
- Wang, P., Deng, J., Dong, J., Liu, J., Bigio, E. H., Mesulam, M., ... Wu, J. Y. (2019). TDP-43 induces mitochondrial damage and activates the mitochondrial unfolded protein response. *PLoS Genetics*, *15*(5). <https://doi.org/10.1371/journal.pgen.1007947>
- Wang, W., Wang, L., Lu, J., Siedlak, S. L., Fujioka, H., Liang, J., ... Wang, X. (2016). The inhibition of TDP-43 mitochondrial localization blocks its neuronal toxicity. *Nature Medicine*, *22*(8), 869–878. <https://doi.org/10.1038/nm.4130>
- Wang, Z., & Burge, C. B. (2008, May). Splicing regulation: From a parts list of regulatory elements to an integrated splicing code. *RNA*. <https://doi.org/10.1261/rna.876308>
- Warita, H., Hayashi, T., Murakami, T., Manabe, Y., & Abe, K. (2001). Oxidative damage to mitochondrial DNA in spinal motoneurons of transgenic ALS mice. *Molecular Brain Research*, *89*(1–2), 147–152. [https://doi.org/10.1016/S0169-328X\(01\)00029-8](https://doi.org/10.1016/S0169-328X(01)00029-8)
- Westergard, T., Jensen, B. K., Wen, X., Cai, J., Kropf, E., Iacovitti, L., ... Trotti, D. (2016). Cell-to-Cell Transmission of Dipeptide Repeat Proteins Linked to C9orf72-ALS/FTD. *Cell Reports*, *17*(3), 645–652. <https://doi.org/10.1016/j.celrep.2016.09.032>
- Wilcock, G. K., & Esiri, M. M. (1982). Plaques, tangles and dementia. A quantitative study. *Journal of the Neurological Sciences*, *56*(2–3), 343–356. [https://doi.org/10.1016/0022-510X\(82\)90155-1](https://doi.org/10.1016/0022-510X(82)90155-1)
- Williams, J. R., Trias, E., Beilby, P. R., Lopez, N. I., Labut, E. M., Bradford, C. S., ... Beckman, J. S. (2016). Copper delivery to the CNS by CuATSM effectively treats motor neuron disease in SOD(G93A) mice co-expressing the Copper-Chaperone-for-SOD. *Neurobiology of Disease*, *89*, 1–9. <https://doi.org/10.1016/j.nbd.2016.01.020>
- Wills, A. M., Hubbard, J., Macklin, E. A., Glass, J., Tandan, R., Simpson, E. P., ... Cudkovicz, M. (2014). Hypercaloric enteral nutrition in patients with amyotrophic lateral sclerosis: A randomised, double-blind, placebo-controlled phase 2 trial. *The Lancet*, *383*(9934), 2065–2072. [https://doi.org/10.1016/S0140-6736\(14\)60222-1](https://doi.org/10.1016/S0140-6736(14)60222-1)
- Wilson, A. C., Dugger, B. N., Dickson, D. W., & Wang, D. S. (2011). TDP-43 in aging and Alzheimer's disease - A review. *International Journal of Clinical and Experimental Pathology*.
- Winer, L., Srinivasan, D., Chun, S., Lacomis, D., Jaffa, M., Fagan, A., ... Miller, T. M. (2013). SOD1 in cerebral spinal fluid as a pharmacodynamic marker for antisense oligonucleotide therapy. *JAMA Neurology*, *70*(2), 201–207. <https://doi.org/10.1001/jamaneurol.2013.593>
- Worley, B., & Powers, R. (2013). Multivariate Analysis in Metabolomics. *Current Metabolomics*,

## References

- 1(1), 92–107. <https://doi.org/10.2174/2213235x11301010092>
- Wright, G. S. A., Antonyuk, S. V., & Hasnain, S. S. (2016). A faulty interaction between SOD1 and hCCS in neurodegenerative disease. *Scientific Reports*, *6*, 27691. <https://doi.org/10.1038/srep27691>
- Wu, C.-H., Fallini, C., Ticozzi, N., Keagle, P. J., Sapp, P. C., Piotrowska, K., ... Landers, J. E. (2012). Mutations in the profilin 1 gene cause familial amyotrophic lateral sclerosis. *Nature*, *488*(7412), 499–503. <https://doi.org/10.1038/nature11280>
- Wu, L.-S., Cheng, W.-C., Chen, C.-Y., Wu, M.-C., Wang, Y.-C., Tseng, Y.-H., ... Shen, C.-K. J. (2019). Transcriptomopathies of pre- and post-symptomatic frontotemporal dementia-like mice with TDP-43 depletion in forebrain neurons. *Acta Neuropathologica Communications*, *7*(1), 50. <https://doi.org/10.1186/s40478-019-0674-x>
- Wu, Y., Dai, X., Ni, Z., Yan, X., He, F., & Lian, J. (2017). The downregulation of ATG4B mediated by microRNA-34a/34c-5p suppresses rapamycin-induced autophagy. *Iranian Journal of Basic Medical Sciences*, *20*(10), 1125–1130. <https://doi.org/10.22038/IJBMS.2017.9446>
- Xiao, X., Wang, Z., Jang, M., Nutiu, R., Wang, E. T., & Burge, C. B. (2009). Splice site strength-dependent activity and genetic buffering by poly-G runs. *Nature Structural and Molecular Biology*, *16*(10), 1094–1100. <https://doi.org/10.1038/nsmb.1661>
- Xie, Y., Zhou, B., Lin, M.-Y., & Sheng, Z.-H. (2015). Progressive endolysosomal deficits impair autophagic clearance beginning at early asymptomatic stages in fALS mice. *Autophagy*, *11*(10), 1934–1936. <https://doi.org/10.1080/15548627.2015.1084460>
- Xie, Z., Nair, U., & Klionsky, D. J. (2008). Atg8 controls phagophore expansion during autophagosome formation. *Molecular Biology of the Cell*, *19*(8), 3290–3298. <https://doi.org/10.1091/mbc.E07-12-1292>
- Xue, W., Zender, L., Miething, C., Dickins, R. A., Hernando, E., Krizhanovskiy, V., ... Lowe, S. W. (2007). Senescence and tumour clearance is triggered by p53 restoration in murine liver carcinomas. *Nature*, *445*(7128), 656–660. <https://doi.org/10.1038/nature05529>
- Yang, Z., Wilkie-Grantham, R. P., Yanagi, T., Shu, C.-W., Matsuzawa, S.-I., & Reed, J. C. (2015). ATG4B (Autophagin-1) phosphorylation modulates autophagy. *The Journal of Biological Chemistry*, *290*(44), 26549–26561. <https://doi.org/10.1074/jbc.M115.658088>
- Yerbury, J. J., Ooi, L., Blair, I. P., Ciryam, P., Dobson, C. M., & Vendruscolo, M. (2019). The metastability of the proteome of spinal motor neurons underlies their selective vulnerability in ALS. *Neuroscience Letters*, *704*, 89–94. <https://doi.org/10.1016/j.neulet.2019.04.001>
- Yin, H., Moulton, H. M., Seow, Y., Boyd, C., Boutilier, J., Iverson, P., & Wood, M. J. A. (2008). Cell-penetrating peptide-conjugated antisense oligonucleotides restore systemic muscle and cardiac dystrophin expression and function. *Human Molecular Genetics*, *17*(24), 3909–3918. <https://doi.org/10.1093/hmg/ddn293>
- Yip, P. K., Pizzasegola, C., Gladman, S., Biggio, M. L., Marino, M., Jayasinghe, M., ... Michael-Titus, A. (2013). The Omega-3 Fatty Acid Eicosapentaenoic Acid Accelerates Disease



## References

- Progression in a Model of Amyotrophic Lateral Sclerosis. *PLoS ONE*, 8(4).  
<https://doi.org/10.1371/journal.pone.0061626>
- Young, A. R. J., Narita, M., Ferreira, M., Kirschner, K., Sadaie, M., Darot, J. F. J., ... Narita, M. (2009). Autophagy mediates the mitotic senescence transition. *Genes & Development*, 23(7), 798–803. <https://doi.org/10.1101/gad.519709>
- Zacco, E., Graña-Montes, R., Martin, S. R., de Groot, N. S., Alfano, C., Tartaglia, G. G., & Pastore, A. (2019). RNA as a key factor in driving or preventing self-assembly of the TAR DNA-binding protein 43. *Journal of Molecular Biology*, 431(8), 1671–1688.  
<https://doi.org/10.1016/j.jmb.2019.01.028>
- Zarnack, K., König, J., Tajnik, M., Martincorena, I., Eustermann, S., Stévant, I., ... Ule, J. (2013). Direct competition between hnRNP C and U2AF65 protects the transcriptome from the exonization of Alu elements. *Cell*, 152(3), 453–466. <https://doi.org/10.1016/j.cell.2012.12.023>
- Zeineddine, R., Farrowell, N. E., Lambert-Smith, I. A., & Yerbury, J. J. (2017). Addition of exogenous SOD1 aggregates causes TDP-43 mislocalisation and aggregation. *Cell Stress and Chaperones*, 22(6), 893–902. <https://doi.org/10.1007/s12192-017-0804-y>
- Zhang, F., Ström, A.-L., Fukada, K., Lee, S., Hayward, L. J., & Zhu, H. (2007). Interaction between familial amyotrophic lateral sclerosis (ALS)-linked SOD1 mutants and the dynein complex. *The Journal of Biological Chemistry*, 282(22), 16691–16699.  
<https://doi.org/10.1074/jbc.M609743200>
- Zhang, P., Kishimoto, Y., Grammatikakis, I., Gottimukkala, K., Cutler, R. G., Zhang, S., ... Mattson, M. P. (2019). Senolytic therapy alleviates A $\beta$ -associated oligodendrocyte progenitor cell senescence and cognitive deficits in an Alzheimer's disease model. *Nature Neuroscience*, 1.  
<https://doi.org/10.1038/s41593-019-0372-9>
- Zhang, Q., Raouf, M., Chen, Y., Sumi, Y., Sursal, T., Junger, W., ... Hauser, C. J. (2010). Circulating mitochondrial DAMPs cause inflammatory responses to injury. *Nature*, 464(7285), 104–107. <https://doi.org/10.1038/nature08780>
- Zhang, X., Li, L., Chen, S., Yang, D., Wang, Y., Zhang, X., ... Le, W. (2011). Rapamycin treatment augments motor neuron degeneration in SOD1(G93A) mouse model of amyotrophic lateral sclerosis. *Autophagy*, 7(4), 412–425. <https://doi.org/10.4161/auto.7.4.14541>
- Zhang, Y. J., Gendron, T. F., Grima, J. C., Sasaguri, H., Jansen-West, K., Xu, Y. F., ... Petrucelli, L. (2016). C9ORF72 poly(GA) aggregates sequester and impair HR23 and nucleocytoplasmic transport proteins. *Nature Neuroscience*, 19(5), 668–677. <https://doi.org/10.1038/nn.4272>
- Zharikov, S., & Shiva, S. (2013). Platelet mitochondrial function: From regulation of thrombosis to biomarker of disease. In *Biochemical Society Transactions* (Vol. 41, pp. 118–123). Biochem Soc Trans. <https://doi.org/10.1042/BST20120327>
- Zhu, Y., Tchkonja, T., Fuhrmann-Stroissnigg, H., Dai, H. M., Ling, Y. Y., Stout, M. B., ... Kirkland, J. L. (2016). Identification of a novel senolytic agent, navitoclax, targeting the Bcl-2 family of anti-apoptotic factors. *Aging Cell*, 15(3), 428–435. <https://doi.org/10.1111/accel.12445>

## References

- Zhu, Y., Tchkonina, T., Pirtskhalava, T., Gower, A. C., Ding, H., Giorgadze, N., ... Kirkland, J. L. (2015). The Achilles' heel of senescent cells: From transcriptome to senolytic drugs. *Aging Cell*. <https://doi.org/10.1111/acer.12344>
- Zou, Z. Y., Zhou, Z. R., Che, C. H., Liu, C. Y., He, R. L., & Huang, H. P. (2017). Genetic epidemiology of amyotrophic lateral sclerosis: A systematic review and meta-analysis. *Journal of Neurology, Neurosurgery and Psychiatry*, *88*(7), 540–549. <https://doi.org/10.1136/jnnp-2016-315018>
- Zubiri, I., Lombardi, V., Bremang, M., Mitra, V., Nardo, G., Adiutori, R., ... Malaspina, A. (2018). Tissue-enhanced plasma proteomic analysis for disease stratification in amyotrophic lateral sclerosis. *Molecular Neurodegeneration*, *13*(1). <https://doi.org/10.1186/s13024-018-0292-2>

## **A non-canonical profile of senescence biomarkers in the spinal cord of the motor neuron disease mouse model hSOD1-G93A.**

Pascual Torres (1), Carlos Anerillas (2), Mario Encinas (2), Mònica Povedano (3), Pol Andrés-Benito (4), Isidre Ferrer (4,5), Victòria Ayala (1), Reinald Pamplona (1), Manuel Portero-Otín (1,6).

1. Metabolic Pathophysiology Research Group, Department of Experimental Medicine, University of Lleida-IRBLleida, Lleida, Spain. PT: [Pascual.torres@mex.udl.cat](mailto:Pascual.torres@mex.udl.cat), VA: [Victoria.ayala@mex.udl.cat](mailto:Victoria.ayala@mex.udl.cat), RP: [reinald.pamplona@mex.udl.cat](mailto:reinald.pamplona@mex.udl.cat), MPO: [manuel.portero@mex.udl.cat](mailto:manuel.portero@mex.udl.cat)

2. Oncogenic Signalling and Development, Department of Experimental Medicine, University of Lleida-IRBLleida, Lleida, Spain. CA: [carlos.anerillas@mex.udl.cat](mailto:carlos.anerillas@mex.udl.cat), ME: [Mario.encinas@udl.cat](mailto:Mario.encinas@udl.cat)

3. Functional Unit of Amyotrophic Lateral Sclerosis (UFELA), Service of Neurology, Bellvitge University Hospital, Hospitalet de Llobregat, Spain. MP: [30058mpp@gmail.com](mailto:30058mpp@gmail.com)

4. Department of Pathology and Experimental Therapeutics, University of Barcelona, Hospitalet de Llobregat, Spain and 5. Biomedical Network Research Center on Neurodegenerative Diseases (CIBERNED), Institute Carlos III, Hospitalet de Llobregat, Spain PAB: [pol.andres.benito@gmail.com](mailto:pol.andres.benito@gmail.com), IF: [8082ifa@gmail.com](mailto:8082ifa@gmail.com)

6. To whom correspondence should be addressed at

Manuel Portero-Otín, IRBLleida-UdL, Edifici Biomedicina I, Avda Rovira Roure 80, E25196 Lleida, Spain ([manuel.portero@mex.udl.cat](mailto:manuel.portero@mex.udl.cat)). Tel+34973702408. Fax +34973702426

## Abstract

Recent evidence demonstrates a pathological role for senescent cells in Alzheimer's and Parkinson's diseases. The present study aimed to show senescence mechanisms including senescence-associated secretory phenotype (SASP) in the familial amyotrophic lateral sclerosis (ALS) transgenic mouse model hSOD1-G93A. We evaluated, as senescence biomarkers, the expression of *p16* and *p21* with reverse-transcriptase quantitative PCR (RT-qPCR), immunofluorescence (IF), and immunohistochemistry (IHC), as well as the senescence-associated  $\beta$  galactosidase (SA- $\beta$ -gal) activity in the lumbar spinal cords (LSC) of this model. As SASP markers, we quantified the mRNA levels of *Il1a*, *Il6*, *Ifna*, and *Ifnb*. Furthermore, we explored if an alteration of alternative splicing is associated with senescence phenomena in this model. Thus, we quantified the *Adipor2* cryptic exon inclusion levels, a specific splicing variant repressed by *TAR-DNA binding of 43 kDa* (TDP-43), using RT-qPCR. Our results show an atypical senescence-profile in LSC from transgenic mice, increasing *p16* and *p21* mRNA and protein levels in glial cells with a mostly cytoplasmic pattern, without the canonical increase in SA-beta-gal activity in these cells. Consistent with enhanced SASP, there is an increase in *Il1a* and *Il6* expression. Also, TDP-43 splicing activity is compromised in this ALS model, in a direct relationship with the increase in *p16* expression. However, senolytic drug Navitoclax -with reported benefits in Alzheimer and Parkinson disease mouse models - does not alter the present model's disease progression. Navitoclax neither eliminates cells expressing senescence and nor represses the expression of SASP related genes. Globally, our findings support the existence of a non-canonical profile of senescence biomarkers in the LSC of the ALS model hSOD1-G93A.

## KEYWORDS

Amyotrophic lateral sclerosis, navitoclax, senolytic, neuroinflammation, therapy, cell cycle, cryptic exon

## Main text

Aging is a major risk factor for developing amyotrophic lateral sclerosis (ALS) (Niccoli et al. 2017). ALS is a neurodegenerative disease characterized by the loss of motor neurons with an unfavorable outcome (<5% survival at 5 years after diagnosis). Cellular senescence was first described by Hayflick in the 1960s as a limitation on division of normal cells *in vitro* (Hayflick & Moorhead 1961). The cellular mechanisms behind this phenomenon were later described, with an important role for cell cycle inhibitors, highlighting p16-INK4a as the major contributor (Serrano et al. 1997). Another hallmark of senescent cells is the increase in  $\beta$ -galactosidase, commonly known as SA- $\beta$ -gal which is associated with an increase in lysosomal biogenesis (Kurz et al. 2000). Cellular senescence has been described as a barrier against oncogenesis, with a tradeoff where these cells can develop a pro-inflammatory status known as SASP. This process reflects an attempt to induce tissue repair in which senescent cells, usually accumulating DNA damage, can stimulate its clearance by the immune system. Regarding neurodegenerative diseases, several groups have independently demonstrated the presence of senescent glial cells and SASP in the central nervous system (CNS).

Another process related to aging is the change in alternative splicing (AS), a conserved mechanism that increases the complexity of the proteome. TDP-43 regulates a large number of AS events in a complex way (Tollervey et al. 2011). Several evidence support the role of TDP-43 pathology in age-related neurodegenerative processes and physiological aging (McAleese et al. 2017). Most AS events regulated by TDP-43 involve the repression of a set of non-conserved (cryptic) exons which are abnormally incorporated into mRNA in ALS (Ling et al. 2015). In this line, we previously quantified the rate of inclusion of cryptic exons in nervous tissue from ALS donors and cellular models and found a positive correlation with age at death (Torres et al. 2018).

To clarify whether senescence-associated phenomena and TDP-43 dysfunction could be implicated in ALS, we measured the abovementioned variables in the familial ALS transgenic mouse model hSOD1-G93A at different disease stages. The senescence markers *p16* and *p21*, typical biomarkers of senescent cells (Coppé et al. 2010), were analyzed in LSC. Using two different technics (IHC and IF), we characterized the cellular expression pattern of p16. The results show that the expression of *p16* mRNA was progressively increased during disease evolution (Fig. 1A), whereas *p21* mRNA levels were

only higher at the end-stage (Fig. 1B). p16 and p21 exhibited a predominantly cytoplasmic pattern (Fig. 1C), in contrast to recent results from an ALS rat model where it was mainly nuclear (Trias et al. 2019). As shown by IF, p16 positive cells were microglia (Iba1+ cells) (Fig. 2A) and astroglia (GFAP+ cells) (Fig. 2B). These results indicate dynamic changes in cellular senescence-associated markers and SASP related to disease evolution. *p16* expression is highly expressed before the symptomatology in our transgenic mice, similarly to p16+ microglia in LSC from transgenic rats (Trias et al. 2019). Both facts suggest a role for p16 in disease initiation and progression. Interestingly, senescence-associated cell cycle arrest in an early symptomatic stage (120d) is driven exclusively by p16, whereas *p21* only increases later in this model. This may be seen as a result of the late-onset activation of p53 and the DNA damage response pathway, similar to what occurs in the senescence process in microglia (Stojiljkovic et al. 2019). In contrast to *p21* (related to reversible cell cycle arrest or quiescence), the senescence process depends heavily on prolonged p16 expression. Strictly speaking, our work and most published articles on 'senescence' do not demonstrate an always irreversible cell cycle arrest. There may be divergent processes sharing common biomarkers (Sharpless & Sherr 2015). This is the case with macrophage polarization, in which p16 expression and SA- $\beta$ -gal activity are physiological, reversible, and not associated with cellular senescence (Hall et al. 2017). In this line, cytoplasmic p16 can regulate cell migration in a manner similar to cyclin D1 (Chen et al. 2013). This evidence reflects a convergent pathway of cell cycle- and senescence-associated proteins regulating cytoskeleton functions. In the case of ALS, cytoskeleton regulators like Rac1 and Cdc42 are implicated in the disease progression and neuroinflammation (D'Ambrosi et al. 2014). Thus, we hypothesized that cytoplasmic p16 could have a similar role in ALS. Like p16 cytoplasmic functions, p21 inhibits the ROCK/LIMK/Cofilin Pathway through MAPK signaling, inducing cytoskeleton remodeling (Tanaka et al. 2002)

We also analyzed another senescence canonical biomarker: SA- $\beta$ -gal activity. The main cellular populations expressing SA- $\beta$ -gal in ventral LSC are the motor neuron cells (Nissl+ cells in the ventral horn, with a motor-neuron compatible cellular size). Neurons of other LSC locations and the vast majority of Nissl- do not show SA- $\beta$ -gal activity (Fig. 1D and S1). Interestingly, SA- $\beta$ -gal activity was reduced during disease progression in motor neurons and in a small fraction of Nissl- cells (compatible with glia). Our findings agree with previously shown data demonstrating that SA- $\beta$ -gal activity in neurons is not associated with senescence, although it is increased in aging mouse brain (Piechota et al. 2016). Our results suggest that motor neurons contain more lysosomes in cell body than other cells, and that

their biogenesis is compromised in this ALS mouse model. In this line, lysosomal mass deficit has already been described in this model, highlighting a role of hSOD1 aggregates disturbing lysosomal biogenesis (Xie et al. 2015) and potentially explaining our results from the SA- $\beta$ -gal activity assay.

Another marker commonly employed in senescence description is the increase in cytokines linked to SASP. In this case, we quantified the expression of typical SASP markers *Il1a* and *Il6*. We analyzed as well the expression of *Ifna* and *Ifnb* (corresponding to type-I IFN response) as they are postulated as late-senescence markers and could be helpful in determining senescence progression in the LSC of this model. The expression of *Ifna* was not detected in any of the analyzed samples (data not shown). We observed a different pattern of expression between *Il1a* (Fig. 3A) and *Il6* (Fig. 3B). *Il1a* is increased in the pre-symptomatic stage and is known to be the upstream regulator of IL-6 in SASP (Orjalo et al. 2009). IL-6 is increased in cerebrospinal fluid in ALS, Alzheimer's, and Parkinson's disease (Chen et al. 2018). In contrast, *Ifnb* expression (Fig. 3C) is not altered, which could indicate that senescence in this model does not evolve a late phase. Overall, this might reflect a complex interaction between senescence, SASP, and changes in reactive glial cells and neurodegeneration.

Regarding TDP-43 splicing function, in mice it controls the inclusion in *Adipor2* mRNA (Figure S2). In line with loss of TDP-43 function in this model, cryptic exon inclusion in *Adipor2* mRNA was higher in lumbar spinal cord in end-stage mice (Fig. 3D) and positively correlated with *p16* expression (Fig. 3E). The present data are the first to show specific alteration regarding splicing function in this ALS model. Notably, this process is associated with an increase in the senescence marker *p16*, and the two processes are likely to be linked in the same pathway.

We wanted to explore the potential benefits of senolytic treatment due to the higher expression of senescence related genes in this mouse model. We performed Navitoclax treatment following the protocol described for Alzheimer's disease mouse model (Bussian et al., 2018). The treatment was initiated at 90 days old and finished at end point (Figure 4A). We estimated the disease progression by weight loss. Navitoclax treatment did not prevent weight loss, neither prolonged survival (Figure 4B and 4C). Finally, we quantified senescence and SASP genes in lumbar spinal cord. None of the analyzed genes showed statistically significant differences (Figure 4D). These results suggest differences in molecular effectors between Alzheimer's and ALS.

Navitoclax is an inhibitor of antiapoptotic protein Bcl2 (Zhu et al., 2016). Senescent cells are highly dependent of different antiapoptotic members. Senolysis is achieved when this antiapoptotic protein is inhibited, promoting cell death (Zhu et al., 2015). Navitoclax treatment is not enough to slow the disease progression and does not extend the survival. In contrast with data in Alzheimer's and Parkinson's disease models, this treatment does not prevent the increase of senescence and SASP markers. It suggests that senescence phenotype is not driven by Bcl2 expression of stressed or aged cells in this model (Zhu et al., 2015). Further studies are warranted to determine whether senescence-linked phenomena are mechanistically involved in this fatal disease, clearing the pathway for therapeutic development.

In the case of ALS, we speculate that Navitoclax treatment is not efficient because Bcl2 is not overactivated in our G93A mouse model (Vukosavic, Dubois-Dauphin, Romero, & Przedborski, 1999). However, Bcl-XL, a Bcl-2 family member, is overactive in astrocytes and provides pro-survival input and may mediate the activation of toxic astroglia (Lee, Kannagi, Ferrante, Kowall, & Ryu, 2009). It suggests that an specific inhibition Bcl-XL could have greater effects on disease progression.

In conclusion, the LSC from the hSOD1-G93A mouse, a model of familial ALS, exhibits a non-canonical profile of senescence biomarkers. It is characterized by an early increase in *p16* and a late increase in *p21*, with both displaying a mainly cytoplasmic pattern in glial cells without an increase in SA- $\beta$ -gal activity. In the case of SASP, it also has a dynamic profile with increasing levels of *Il1a* from the pre-symptomatic stage onward and an acute peak of expression in end-stage transgenic mice. Regarding AS, this tissue shows a dysfunctional splicing activity of TDP-43 in end-stage ALS mice. This is the first time that senescence markers, SASP, and TDP-43-associated splicing dysfunction have been described in this ALS mouse model.

## **Experimental procedures**

### *Animal Experiments*

A colony of the strain B6.Cg-Tg(SOD1\*G93A)1Gur/J JAX catalogue stock number 004435; from now on hSOD1G93A or G93A) was purchased at The Jackson Laboratories (Bar Harbor, MN, USA). Mice were maintained in C57BL/6J background. Genotyping was performed following manufacturer's instructions. After genotyping and weaning, animals



were placed at 12:12 hours dark / light cycle, at  $22\pm 2^{\circ}\text{C}$  temperature,  $50\%\pm 10$  relative humidity, in individual cages (at 21 days). For age-related studies, we evaluated . Navitoclax (T2101, Targetmol) was diluted in 60% Phosal 50 PG (Lipoid), 30% PEG400 (Sigma, 91893) 10% EtOH. Navitoclax was administered by oral gavage at a dose of  $50\text{ mg kg}^{-1}$  body during five consecutive days followed by 16 days of rest ( $N= 5$  per group). Treatment cycles were repeated until clinical endpoint (righting reflex  $>20$  s). Spinal cords were rapidly excised, frozen in liquid  $\text{N}_2$  and stored at  $-80^{\circ}\text{C}$ . This study was approved by the Animal Research and Ethics Committee at the University of Lleida.

### *Cell culture*

3T3 cells were maintained in Dulbecco's Modified Eagle's Medium (11965, Thermo Fisher Scientific), 10% FBS (10270, Thermo Fisher Scientific), 100 U/ml Penicillin-Streptomycin (15140-122, Thermo Fisher Scientific) at  $37^{\circ}\text{C}$  and 5%  $\text{CO}_2$ . For silencing, 20 nM (final concentration) of *TARDBP* siRNA mmsiTDP-43s: 5'-AGGAAUCAGCGUGCAUAUA-3' mmsiTDP-43as: 5'-UAUAUGCACGCUGAUUCCU-3' (siTDP) or scrambled siRNA (siCTL) was mixed in 100  $\mu\text{l}$  Opti-MEM (31985062, Thermo Fisher Scientific) with 2  $\mu\text{l}$  of RNAiMAX (13778100, Thermo Fisher Scientific) on the bottom of the well and incubated for 20 minutes at room temperature. 2 ml of DMEM (11965092, Thermo Fisher Scientific) supplemented with 10% FBS containing 100000 HeLa or 3T3 cells/well were seeded onto transfection mix. After 24 hours, transfection media was removed and changed to DMEM 10% FBS media. 48 hours post-transfection, cells were collected for posterior analyses.

### *Western Blot*

Protein from platelets was extracted adding 100  $\mu\text{L}$  of radioimmunoprecipitation (RIPA) buffer with Protease Inhibitor Cocktail (1X) to the pellet. After sonication, protein quantification was performed with Bradford assay (5000006, Bio-Rad). Fifteen  $\mu\text{g}$  of protein were loaded onto a 12% acrylamide SDS-PAGE gel. Membranes were blocked with I-Block (T2015, Thermo Fisher Scientific) for 1 hour and incubated overnight with primary incubated anti-TDP-43 (10782-2-AP, Proteintech) 1:1000 in TBS-T 0.05%. After primary antibody incubation, membranes were washed 3 times with TBS-T 0.05% and incubated with secondary antibody for 1h. Immobilon™ Western Chemiluminiscent HRP Substrate (WBKLS0500, Merck Millipore) was used for immunodetection. Membranes were stained with Coomassie Brilliant Blue G (27815, Sigma) for normalization. Specific bands were quantified with ImageLab v5.2.1 (Bio-Rad).

### *RNA extraction, cDNA synthesis and RT-qPCR*

1 ml of TRIzol reagent (Thermo Fisher Scientific, AM9738) was added to 50-100 mg of tissue. The tissue was then mechanically homogenized using T 10 basic ULTRA-TURRAX® (IKA). 200 µl of chloroform was added to each sample and mixed. After 5 minutes of incubation at room temperature, the samples were centrifuged at 12,000 xg (15 mins, 4°C) to separate the phases. The aqueous phase was separated into a new tub and mixed by vortexing with 500 µl of isopropanol. After an incubation of 10 minutes at room temperature, RNA was precipitated through spun at 12,000 xg (10 mins, 4°C). The resulting supernatant was removed, and the pellet was washed with a 75% ethanol. After vortexing, the samples were centrifuged again at 12,000 xg (10 mins, 4°C). The supernatant was discarded, and the RNA pellet was allowed to air dry at room temperature. The RNA was resuspended with 50 µl of RNase-free water, quantified with Nanodrop (Nanodrop technologies, ND-1000 UV/Vis Spectofotometer) and stored at -80°C until further use. One microgram of RNA was used for retrotranscription employing TaqMan Reverse Transcription Reagent using random hexamers (Thermo Scientific, N8080234). RT-qPCR experiments were performed using a CFX96 instrument (Bio-Rad, Hercules, California, USA) with SYBR select Master mix (Thermo Fisher Scientific, 4472908). Each 20 µL of reaction contained 4µL cDNA, 10 µL SYBR Select Master Mix, 0.2 nM of forward primer and 0.2 nM of reverse primer solutions and 4 µL PCR grade water. RT-qPCR run protocol was as follows: 50 °C for 2 minutes and 95 °C for 2 minutes, with the 95 °C for 15 seconds and 60 °C for 1 minute steps repeated for 40 cycles; and a melting curve test from 65°C to 95 °C at a 0.1 °C/s measuring rate. N=3-10 mice per group were used for RT-PCR experiments. Primers employed in these experiments are listed in Supplementary Table S1. *Actb* expression was used as housekeeping to normalize the other genes. Specific *Adipor2 cryptic* mRNA (primers annealed with cryptic exon) was normalized with *Adipor2* normal transcript (the primers annealed with conserved exons).

### *Senescence-associated β-galactosidase activity*

Briefly, paraformaldehyde-fixed frozen sections were incubated with X-gal solution (20 mg/ml X-Gal (SIGMA), 5 mM K<sub>3</sub>Fe(CN)<sub>6</sub>, 5 mM K<sub>4</sub>Fe(CN)<sub>6</sub> and 2 mM MgCl<sub>2</sub>) in PBS at

pH 6.0 overnight at 37 °C. To allow comparison between specimens, all samples were assayed simultaneously. Then, neurons were stained with Green Fluorescent Nissl Stain (Thermo Fisher Scientific, N21480) diluted 1:150 in PBS and incubated 20 minutes at room temperature. The slices were then washed 3x with PBS for 10 minutes at room temperature and 1x with PBS for 2 hours at room temperature. Nuclei were stained with DAPI (SIGMA, 32670). Images of the stained sections were taken using inverted microscope (Olympus, IX71S8F-2). Eight randomly selected areas of each mouse (N=2-3 per group) of the ventral horn of lumbar spinal cord sections were photographed at 20x magnification for visual analysis. The whole section of SA- $\beta$ -Gal stained slices was photographed at 4x magnification.

### *Immunofluorescence*

One control and one transgenic lumbar spinal cord were fixed in 4% paraformaldehyde made in PBS overnight at 4°C and cryopreserved in 30% sucrose in PBS 48 hours. The lumbar spinal cord was then cut at a 16  $\mu$ m section depth and resulting seeded on a gelatin-coated slide. Samples were permeabilized with 0.3% Triton X-100 PBS for 30 min and blocked with 5% BSA in PBS for 1h at room temperature. The primary antibody 1:100 anti-p16 (abcam, ab54210) and 1:200 anti-GFAP (abcam, ab7260) were diluted in 0.3% Triton X-100 PBS and incubated overnight at 4°C. The slices were washed with PBS three times for 5 min at room temperature, followed by the secondary antibody (diluted 1:800 in PBS), goat anti-mouse Alexa Fluor 555 (Thermo Fisher Scientific, A21422) and goat anti-rabbit Alexa Fluor 488 (Thermo Fisher Scientific, A11008) incubation for 1h at room temperature in darkness. Sections were finally counterstained with 1  $\mu$ g/ml 4,6-diamidino-2-phenylindole dihydrochloride (DAPI) in PBS for 10 min at RT and mounted on slides with Fluoromount-G® (Southern Biotech, 0100). Samples were imaged using a laser scanning confocal microscope Olympus FluoView FV10.

### *Immunohistochemistry*

One control and one transgenic paraformaldehyd fixed paraffin embedded tissue slides were dried for 1h at 65° before pre-treatment procedure of deparaffinization, rehydration and epitope retrieval in the Pre-Treatment Module (Agilent Technologies-DAKO, PT-LINK) at

95°C for 20 min in 50x Tris/EDTA buffer, pH 9. For p21 immunohistochemical staining, p21WAF1/Cip1 antibody (Agilent Technologies-DAKO, clone SX118) 1:100 dilution was used. After incubation, the reaction was visualized with the EnVision™ FLEX Detection Kit (Agilent Technologies-DAKO) using diaminobenzidine chromogen as a substrate. For p16 immunohistochemical staining, p16 INK4a antibody was used using CINtec® Histology Kit (ROCHE, clone E6H4) following manufacturer's instructions. Sections were counterstained with hematoxylin.

### *Statistical Analysis*

All statistical tests and graphs were performed using GraphPad Prism 6 (GraphPad Software). Normalized mRNA expression was analyzed with ordinary Two-way ANOVA test of the variables time and genotype. For multiple comparisons between genotypes, Bonferroni's multiple comparisons test was used. In SA-beta-gal activity experiments, p-value was determined by Chi-square's test. To evaluate relationship between *p16* and *Adipor2* cryptic mRNA levels a linear regression was tested.

### **List of abbreviations**

ALS: amyotrophic lateral sclerosis

AS: Alternative splicing

CNS: Central nervous system

IF: Immunofluorescence

IHC: Immunohistochemistry

LSC: Lumbar spinal cord

RT-Qpcr: Reverse-transcriptase quantitative PCR

SASP: Senescence-associate secretory phenotype

SA- $\beta$ -gal: Senescence-associated beta galactosidase

TDP-43: TAR-dna binding of 43 kDa

## **Declarations**

### **Ethics approval and consent to participate**

This study was approved by the Animal Research and Ethics Committee at the University of Lleida.

### **Availability of data and materials**

The datasets used and/or analysed during the current study are available from the corresponding author on reasonable request.

### **Competing interests**

The authors declare that they have no competing interests

### **Funding**

Grants were received from the Instituto de Salud Carlos III (PI 17-000134, PI 20-0155) to MPO, from the Generalitat de Catalunya 2017SGR696 to RP, and from the Ministerio de Ciencia, Innovación y Universidades (BFU2017-83646-P, AEI, FEDER, UE) to ME. PT is a predoctoral fellow from the Spanish Ministry of Education [FPU16/01446]. Support was also received in the form of a FUNDELA Grant, RedELA-Plataforma Investigación and the Fundació Miquel Valls (Jack Van den Hoek donation). FEDER funds are acknowledged (“A way to make Europe”).

### **Acknowledgements**

This study was supported by the Scientific and Technical Service of Immunohistochemistry, Lleida Institute for Biomedical Research, Dr. Pifarré Foundation, IRBLleida. We thank T. Yohannan for editorial assistance.

### **Author’s contributions**

PT, PAB and IF performed IF and IHC assays; PT, CA and ME analyzed and interpreted tissue IHC slides regarding histological scores of inflammation and SA-beta-GAL staining;

MPO and RP Planned the experimental approach and performed data analyses; PT, CA and ME planned and performed RT-qPCR analyses. PT, MP and VA drafted the manuscript and analyzed immunohistochemical data. IF and MPO revised and prepared final form of the manuscript. All authors read and approved the final manuscript.

## References

- Chen X, Hu Y, Cao Z, Liu Q & Cheng Y (2018) Cerebrospinal Fluid Inflammatory Cytokine Aberrations in Alzheimer's Disease, Parkinson's Disease and Amyotrophic Lateral Sclerosis: A Systematic Review and Meta-Analysis. *Front. Immunol.* 9, 2122.
- Chen Y-W, Chu H-C, Ze-Shiang Lin, Shiah W-J, Chou C-P, Klimstra DS & Lewis BC (2013) p16 Stimulates CDC42-dependent migration of hepatocellular carcinoma cells. *PLoS One* 8, e69389.
- Coppé J-P, Desprez P-Y, Krtolica A & Campisi J (2010) The senescence-associated secretory phenotype: the dark side of tumor suppression. *Annu. Rev. Pathol.* 5, 99–118.
- D'Ambrosi N, Rossi S, Gerbino V & Cozzolino M (2014) Rac1 at the crossroad of actin dynamics and neuroinflammation in Amyotrophic Lateral Sclerosis. *Front. Cell Neurosci.* 8, 279.
- Hall BM, Balan V, Gleiberman AS, Strom E, Krasnov P, Virtuoso LP, Rydkina E, Vujcic S, Balan K, Gitlin II, Leonova KI, Consiglio CR, Gollnick SO, Chernova OB & Gudkov AV (2017) p16(Ink4a) and senescence-associated  $\beta$ -galactosidase can be induced in macrophages as part of a reversible response to physiological stimuli. *Aging (Albany, NY)* 9, 1867–1884.
- Hayflick L & Moorhead PS (1961) The serial cultivation of human diploid cell strains. *Exp. Cell Res.* 25, 585–621.
- Kurz DJ, Decary S, Hong Y & Erusalimsky JD (2000) Senescence-associated (beta)-galactosidase reflects an increase in lysosomal mass during replicative ageing of human endothelial cells. *J. Cell Sci.* 113 ( Pt 20), 3613–3622.
- Ling JP, Pletnikova O, Troncoso JC & Wong PC (2015) TDP-43 repression of nonconserved cryptic exons is compromised in ALS-FTD. *Science* 349, 650–655.
- McAleese KE, Walker L, Erskine D, Thomas AJ, McKeith IG & Attems J (2017) TDP-43 pathology in Alzheimer's disease, dementia with Lewy bodies and ageing. *Brain Pathol.* 27, 472–479.

- Niccoli T, Partridge L & Isaacs AM (2017) Ageing as a risk factor for ALS/FTD. *Hum. Mol. Genet.* 26, R105–R113.
- Orjalo AV, Bhaumik D, Gengler BK, Scott GK & Campisi J (2009) Cell surface-bound IL-1alpha is an upstream regulator of the senescence-associated IL-6/IL-8 cytokine network. *Proc. Natl. Acad. Sci. USA* 106, 17031–17036.
- Piechota M, Sunderland P, Wysocka A, Nalberczak M, Sliwinska MA, Radwanska K & Sikora E (2016) Is senescence-associated  $\beta$ -galactosidase a marker of neuronal senescence? *Oncotarget* 7, 81099–81109.
- Serrano M, Lin AW, McCurrach ME, Beach D & Lowe SW (1997) Oncogenic ras provokes premature cell senescence associated with accumulation of p53 and p16INK4a. *Cell* 88, 593–602.
- Sharpless NE & Sherr CJ (2015) Forging a signature of in vivo senescence. *Nat. Rev. Cancer* 15, 397–408.
- Stojiljkovic MR, Ain Q, Bondeva T, Heller R, Schmeer C & Witte OW (2019) Phenotypic and functional differences between senescent and aged murine microglia. *Neurobiol. Aging* 74, 56–69.
- Tanaka H, Yamashita T, Asada M, Mizutani S, Yoshikawa H & Tohyama M (2002) Cytoplasmic p21(Cip1/WAF1) regulates neurite remodeling by inhibiting Rho-kinase activity. *J. Cell Biol.* 158, 321–329.
- Tollervy JR, Curk T, Rogelj B, Briese M, Cereda M, Kayikci M, König J, Hortobágyi T, Nishimura AL, Zupunski V, Patani R, Chandran S, Rot G, Zupan B, Shaw CE & Ule J (2011) Characterizing the RNA targets and position-dependent splicing regulation by TDP-43. *Nat. Neurosci.* 14, 452–458.
- Torres P, Ramírez-Núñez O, Romero-Guevara R, Barés G, Granado-Serrano AB, Ayala V, Boada J, Fontdevila L, Povedano M, Sanchís D, Pamplona R, Ferrer I & Portero-Otín M (2018) Cryptic exon splicing function of TARDBP interacts with autophagy in nervous tissue. *Autophagy* 14, 1398–1403.
- Trias E, Beilby PR, Kovacs M, Ibarburu S, Varela V, Barreto-Núñez R, Bradford SC, Beckman JS & Barbeito L (2019) Emergence of microglia bearing senescence markers during paralysis progression in a rat model of inherited ALS. *Front. Aging Neurosci.* 11, 42.
- Xie Y, Zhou B, Lin M-Y & Sheng Z-H (2015) Progressive endolysosomal deficits impair autophagic clearance beginning at early asymptomatic stages in fALS mice. *Autophagy* 11, 1934–1936.

## Figure Legends

**Figure 1.** Increase in senescence markers in spinal cord during ALS progression. *p16* expression was progressively higher at 120 days and 150 days (a), whereas *p21* were only found to be increased at end stage (b). Both *p16* and *p21* exhibited cytoplasmic staining (c). Nissl+ cells of the ventral horn of the spinal cord (compatible with motor neurons) are the main contributor to SA-beta-gal activity in lumbar spinal cord and are almost depleted in this activity in hSOD1-G93A mice at 150 days, similarly to Nissl- (glia) cells (d). *p16* and *p21* expression are expressed as mean  $\pm$ SEM. Ns indicates  $p > 0.05$ ; \*\* $p < 0.01$ ; \*\*\* $p < 0.001$ ; \*\*\*\* $p < 0.0001$  for Student's t test or ANOVA, when appropriate. Red arrows indicate *p16* and *p21* positive cells. Green scale bar represents 100  $\mu$ m, yellow scale bar represents 500  $\mu$ m, and red scale bar represents 2500  $\mu$ m.  $n=4$  from each genotype and age.

**Figure 2.** Cytoplasmic *p16*+ microglia (*Iba1*+) (a) and astrocytes (*GFAP*+) (b) are present in lumbar spinal cord of transgenic mice and absent in controls. Scale bar represents 500  $\mu$ m. Representative images from independent experiments ( $n= 10$  slices from at least 3 different animals from each genotype and age) are shown.

**Figure 3.** SASP markers and TDP-43 dysfunction are increased in LSC from transgenic hSOD-G93A mice. *Il1a* mRNA was higher from pre-symptomatic stage onward in transgenic mice and increased in later stages (a). *Il6* expression (b) was induced in end-stage hSOD1-G93A mice, in contrast with *Ifnb* (c). Cryptic exon in *Adipor2* mRNA was more incorporated in 150-day-old transgenic mice (d). The inclusion ratio of *Adipor2* cryptic exon positively correlated with *p16* expression (e) *Il1a*, *Il6*, *Ifnb*, and cryptic *Adipor2* expression are expressed as mean  $\pm$ SEM. ns  $p > 0.05$ ; \* $p < 0.05$ ; \*\*\* $p < 0.001$ ; \*\*\*\* $p < 0.0001$ .  $n=4$  from each genotype and age.

**Figure 4.** Senolytic treatment using Navitoclax does not slow the disease progression. A chronic treatment was established with five consecutive doses followed by two weeks of resting (a). Weight loss was not different between Navitoclax and vehicle experimental groups (b). Survival time was also unaltered between groups (c), as senescence and SASP genes (d).  $n=5$  from each genotype.



**Figure S1.** SA-beta-gal activity was decreased in 90- and 120-day-old hSOD1-G93A mice. Nissl+ cells are the main contributors of this activity, which is lower in ALS mice. In contrast, Nissl- cells exhibited a slight decrease in transgenic mice. \*\*\*p < 0.001; \*\*\*\*p < 0.0001. Yellow scale bar represents 500  $\mu$ m and red scale bar represents 2500  $\mu$ m.

**Figure S2.** *Adipor2* cryptic exon splicing is increased in *Tardbp* silenced murine cells. RT-qPCR of *Adipor2* cryptic exon showed a high increase (a) and Western Blot analyses of TDP-43 confirmed the reduction of this protein in silenced 3T3 cells (b). \*p < 0.05. Shown are data representative from 3 independent experiments.

**Table 1.** SYBR Green probes used in RT-qPCR analysis.

# Figures and Tables

**Figure 1**

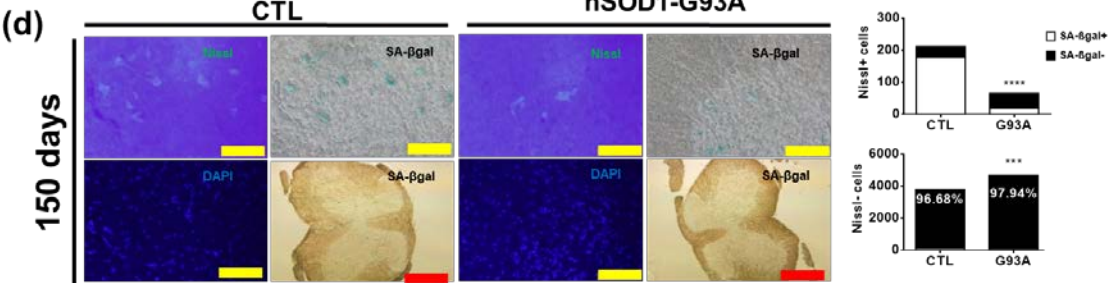
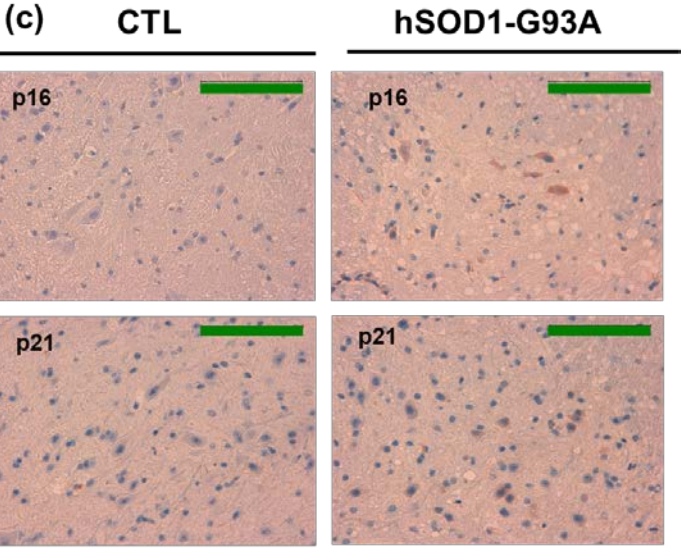
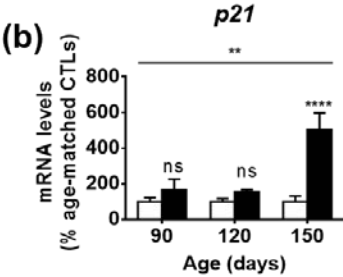
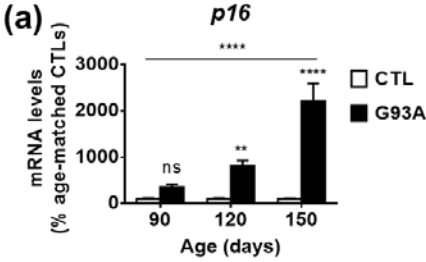
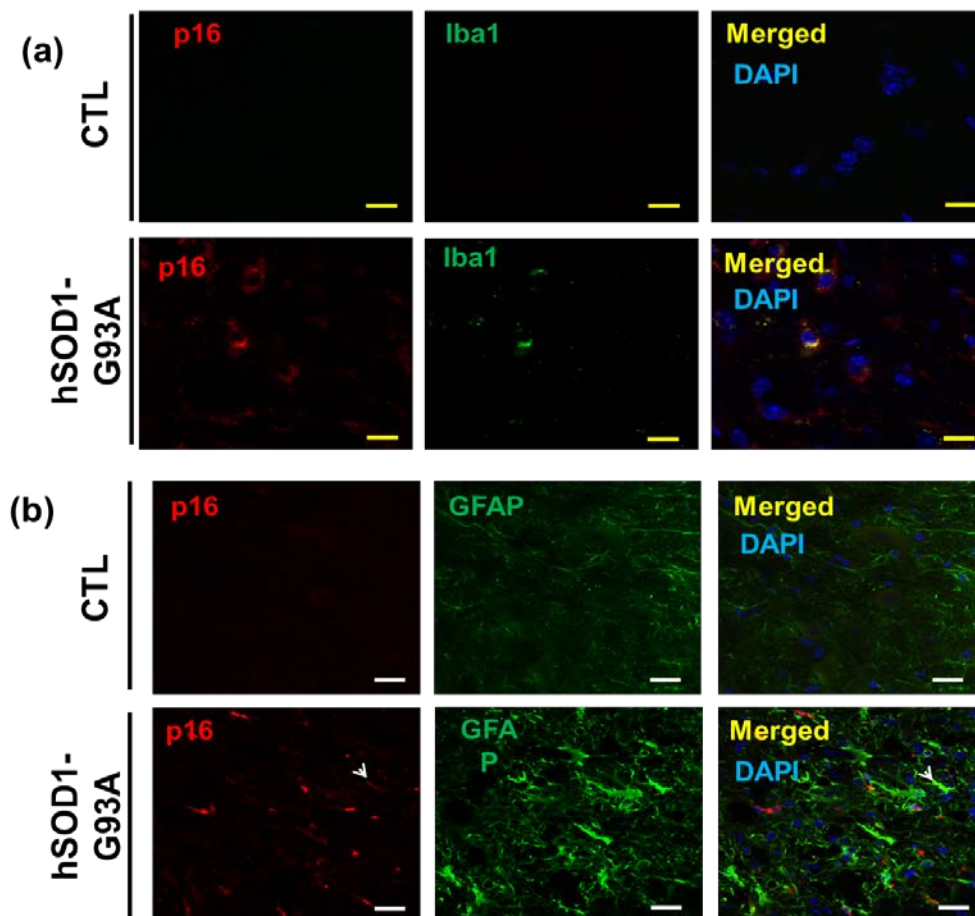
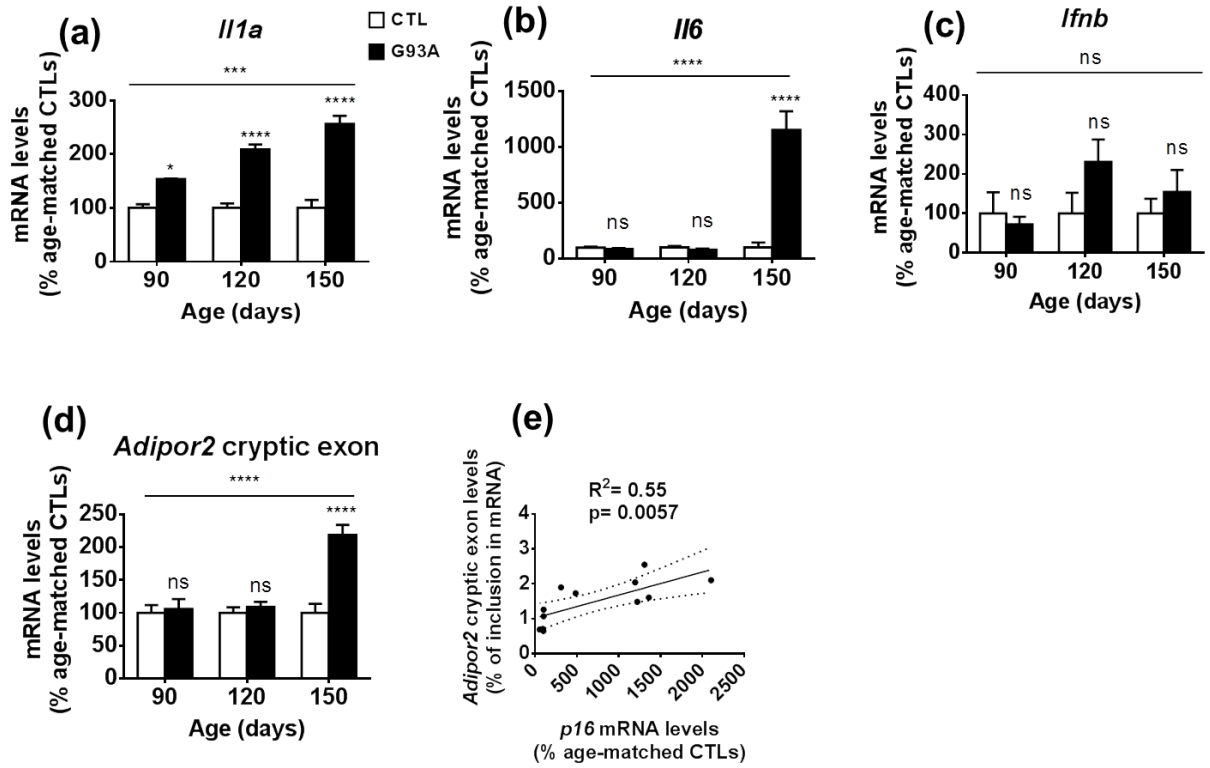


Figure 2



**Figure 3**



**Figure 4**

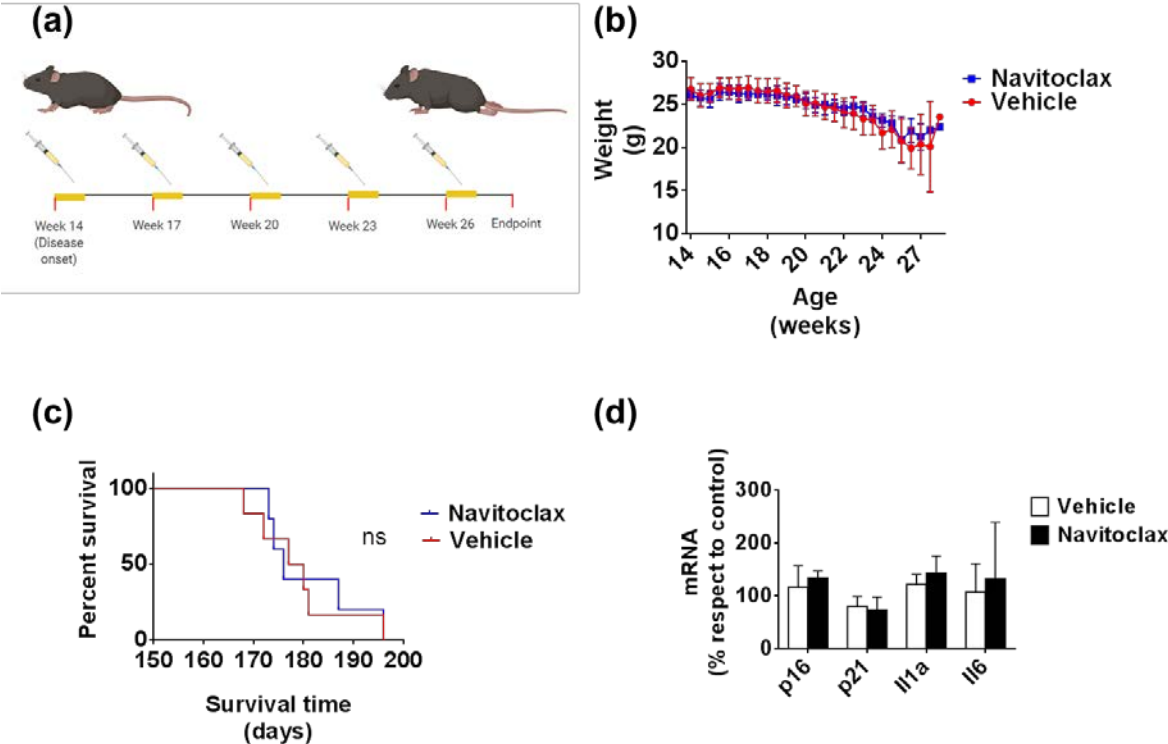


**Figure S1**

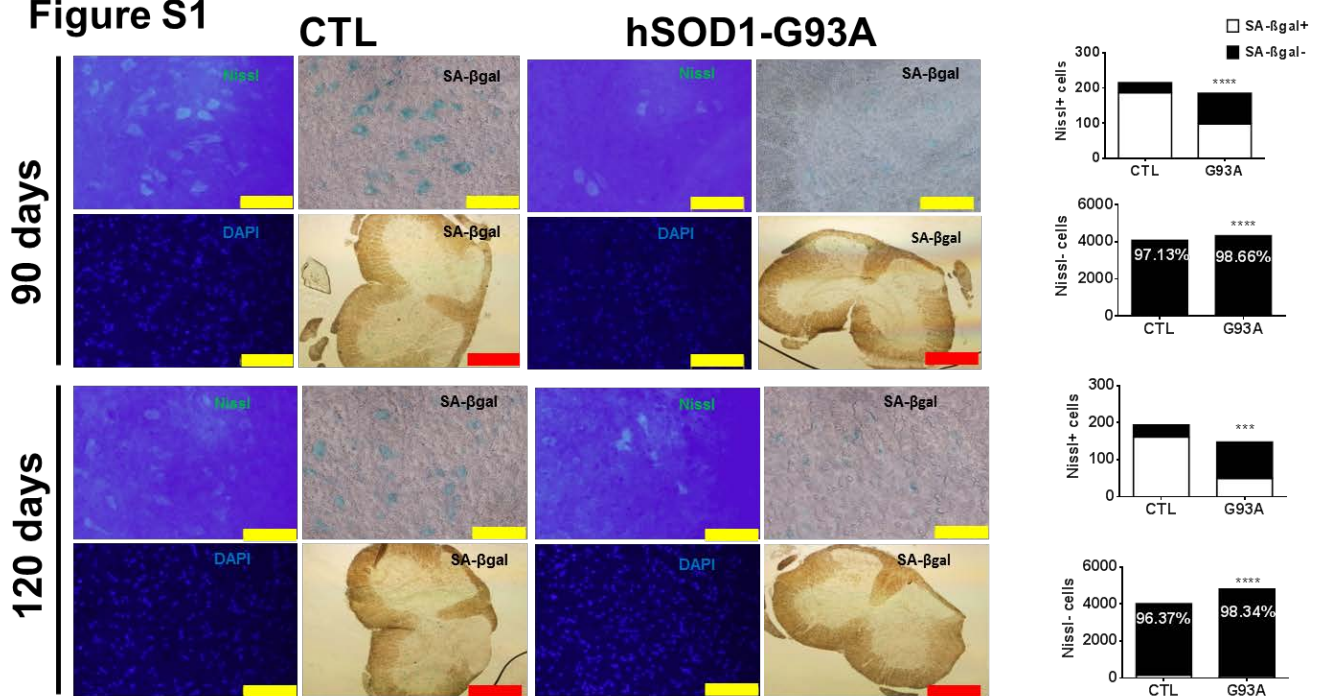


**Figure S2**

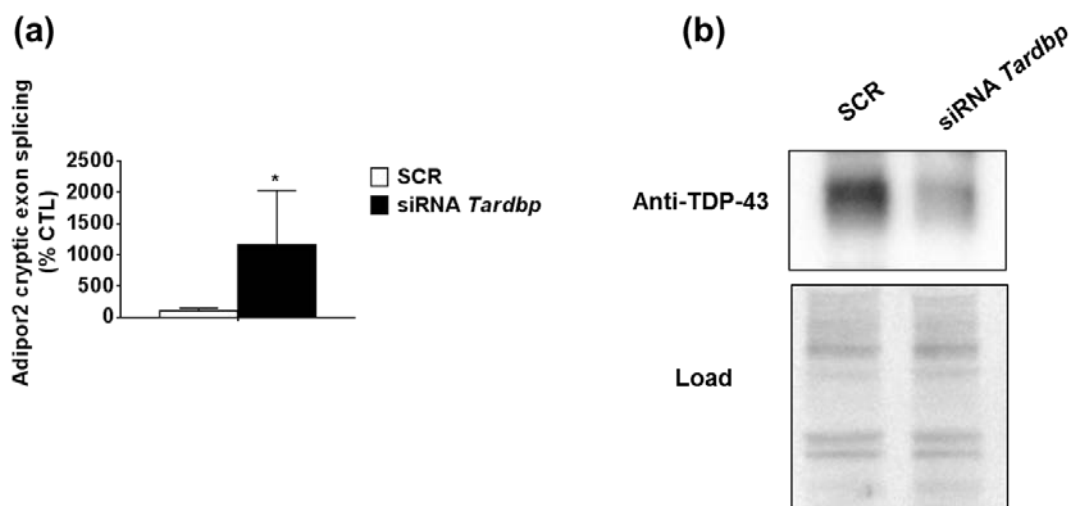


**Table 1.**

<b>Gene</b>	<b>Sequence</b>
<i>Actb</i> Fwd	GTGACGTTGACATCCGTAAAGA
<i>Actb</i> Rev	GCCGGACTCATCGTACTCC
<i>p16</i> Fwd	CCCAACGCCCCGAACT
<i>p16</i> Rev	GCAGAAGAGCTGCTACGTGAA
<i>I11a</i> Fwd	AGCGCTCAAGGAGAAGACC
<i>I11a</i> Rev	CCAGAAGAAAATGAGGTCGG
<i>I16</i> Fwd	ACCAGAGGAAATTTTCAATAGGC
<i>I16</i> Rev	TGATGCACTTGCAGAAAACA
<i>Ifna</i> Fwd	ATGGCTAGGCTCAGCACTTTC
<i>Ifna</i> Rev	CTCACTCAGACTTGCCAGCA

<i>lfnb</i> Fwd	AGCTCCAAGAAAGGACGAACA
<i>lfnb</i> Rev	GCCCTGTAGGTGAGGTTGAT
<i>Adipor2</i> Fwd	TGTTTGTAAGGTGTGGGAAGG
<i>Adipor2</i> Rev	GTTGCCCGTCTCTGTGTGTAT
<i>Adipor2</i> cryptic Fwd	AGAAGTGGAGTTACAATTGTG
<i>Adipor2</i> cryptic Rev	AAACAACTCTTCCATTCGTT
<i>p21</i> Fwd	TTGCCAGCAGAATAAAAGGTG
<i>p21</i> Rev	TTTGCTCCTGTGCGGAAC